Fate of Engineered Nanomaterials

in Wastewater Treatment Plants

by

Mehlika Ayla Kiser

A Dissertation Presented in Partial Fulfillment
of the Requirements for the Degree
Doctor of Philosophy

Approved August 2011 by the
Graduate Supervisory Committee:

Paul Westerhoff, Chair
Bruce Rittmann
Kiril Hristovski

ARIZONA STATE UNIVERSITY

December 2011

ABSTRACT

As the use of engineered nanomaterials (ENMs) in consumer products becomes more common, the amount of ENMs entering wastewater treatment plants (WWTPs) increases. Investigating the fate of ENMs in WWTPs is critical for risk assessment and pollution control. The objectives of this dissertation were to (1) quantify and characterize titanium (Ti) in full-scale wastewater treatment plants, (2) quantify sorption of different ENMs to wastewater biomass in laboratory-scale batch reactors, (3) evaluate the use of a standard, soluble-pollutant sorption test method for quantifying ENM interaction with wastewater biomass, and (4) develop a mechanistic model of a biological wastewater treatment reactor to serve as the basis for modeling nanomaterial fate in WWTPs. Using titanium (Ti) as a model material for the fate of ENMs in WWTPs, Ti concentrations were measured in 10 municipal WWTPs. Ti concentrations in pant influent ranged from 181 to 3000 μg/L, and more than 96% of Ti was removed, with effluent Ti concentrations being less than 25 μg/L. Ti removed from wastewater accumulated in solids at concentrations ranging from 1 to 6 μg Ti/mg solids. Using transmission electron microscopy, spherical titanium oxide nanoparticles with diameters ranging from 4 to 30 nm were found in WWTP effluents, evidence that some nanoscale particles will pass through WWTPs and enter aquatic systems. Batch experiments were conducted to quantify sorption of different ENM types to activated sludge. Percentages of sorption to 400 mg TSS/L biomass ranged from about 10 to 90%, depending on the ENM material and functionalization. Natural organic matter, surfactants,

and proteins had a stabilizing effect on most of the ENMs tested. The United States Environmental Protection Agency's standard sorption testing method (OPPTS 835.1110) used for soluble compounds was found to be inapplicable to ENMs, as freeze-dried activated sludge transforms ENMs into stable particles in suspension. In conjunction with experiments, we created a mechanistic model of the microbiological processes in membrane bioreactors to predict MBR, extended and modified this model to predict the fate of soluble micropollutants, and then discussed how the micropollutant fate model could be used to predict the fate of nanomaterials in wastewater treatment plants.

To my beloved Mom and Dad.

Thank you for your infinite love and for being my greatest teachers.

ACKNOWLEDGMENTS

TABLE OF CONTENTS

LIST OF TABLES

LIST OF FIGURES

Chapter 1

INTRODUCTION

Background of Engineered Nanomaterials

The principles of physics, as far as I can see, do not speak

against the possibility of maneuvering things atom by atom.

It is not an attempt to violate any laws: It is something in

principle that can be done; but in practice it has not been

done because we are too big.

Richard Feynman, 1959

Though just an idea in 1959, Feynman's vision of manipulating matter at the atomic level was realized a couple of decades later when the scanning tunneling microscope was invented in 1985 and used to move individual atoms on a substrate (Mansoori, 2005; Maynard, 2006). Advances in scanning probe microscopy, electron microscopy, and other analytical techniques enabled scientists to explore the structure of matter and then develop new materials at the nanoscale (Maynard, 2006). Nanotechnology is the design, production, and application of materials having at least one dimension between 1 and 100 nanometers (nm) (The Royal Society and The Royal Academy of Engineering, 2004).

Nanomaterials can be produced intentionally, as engineered nanomaterials (ENMs), or unintentionally from natural or anthropogenic processes. Aerosols from volcanic eruptions, forest fires, pollen fragments, and viruses are examples of natural nanomaterials, while examples of unintentional anthropogenic nanomaterials include soot or black carbon

generated from power plants, vehicles, coal combustion, and welding (Navarro et al., 2008). Nanomaterials from unintentional sources are polydisperse, irregularly shaped, and often contain sulfide, sulfate, nitrate, ammonium, organic carbon, elemental carbon, and trace metals (Navarro et al., 2008). ENMs, however, are monodisperse and regularly shaped (Navarro et al., 2008), and can be fabricated with innumerable combinations of composition, morphology, surface chemistry, and purity (Posner, 2009).

ENMs have different physicochemical properties than the same materials in larger sizes (Auffan et al., 2009). Nanoscale materials owe their unusual properties to their small size and thus large surface area, chemical composition, surface structure, solubility, and shape (Nel et al., 2006). Scientists and engineers are exploiting the unique properties of ENMs to design materials and devices that are superior to bulk-scale technologies in terms of speed, efficiency, and strength (Guzman et al., 2006). For example, the development of nanomedicine is providing more targeted treatments for cancer and other diseases, and polymer nanocomposites yield stronger, lighter materials for applications such as advanced membrane technologies (Lowry and Casman, 2009). Furthermore, nanotechnology offers the potential for more sparing use of resources, improved efficiency of energy production and use, and enhanced treatment of surface water, groundwater, and wastewater contaminated by toxic metal ions, organic and inorganic solutes, and microorganisms (Lowry and Casman, 2009; Theron et al., 2008). One study demonstrated that using 5-nm gold nanoparticles as catalysts in a biohydrogen production system increased the conversion efficiency of sucrose

to hydrogen by 15% compared to a standard system without gold

nanoparticles (Zhang and Shen, 2007). Bae and Tak (2005) demonstrated

that titanium dioxide nanoparticles deposited on ultrafiltration membranes

mitigated fouling in membrane bioreactor systems. Indeed, nanotechnology

is a highly promising and exciting frontier that spans many areas of science

and technological application (Moore, 2006).

The potential benefits of ENMs to quality of life are awesome.

However, like any new materials or technology, the possibility of negative

impacts on people and ecosystems should be considered. Escalating

production and use of ENMs will inevitably result in the release of increasing

quantities of these materials into environmental systems (Wiesner et al.,

2009). In addition, as nanotechnology progresses, variations of chemical and

physical composition will undoubtedly increase (Posner, 2009). While natural

nanomaterials have been a part of the evolution of ecosystems over billions of

years, ENMs have been in existence for only the last few decades of Earth's

history. The introduction of ENMs into the environment, which exposes

organisms to materials never before seen in nature, will present new

challenges to ecosystem adaptation and survival.

The same properties that make ENMs valuable to industry – high

specific surface area, abundant reactive surface sites, and mobility – could

also be properties that lead to health risks. Incidental nanoparticles have

been associated with negative health effects and changes in cloud properties

(Guzman et al., 2006). A growing number of toxicity studies suggest that

ENMs are not inherently benign and can affect organisms at cellular,

3

subcellular, and protein levels (Nel et al., 2006). According to Nel et al., (2006), some ENMs "readily travel throughout the body, deposit in target organs, penetrate cell membranes, lodge in mitochondria, and may trigger injurious responses." Research has demonstrated ENM interaction with and toxicity to various organisms, such as bacteria, daphnia, algae, plants, fungi, fish, and rodents (Oberdorster, 2004; Lyon et al., 2005; Lovern and Klaper, 2006; Navarro et al., 2008), as well as diverse mammalian cell types, including human colon cells, brain microglia, osteoblasts, endothelia, epithelia, skin fibroblast, and liver (Colvin, 2003; Sayes et al., 2004; Long et al., 2007).

Municipal WWTPs are particularly important point sources of contaminant release into the environment, as they provide potential pollutant pathways into surface waters, soils, and air through treated effluent, biosolids, and plant-generated aerosols (Handy et al.,2008; Limbach et al., 2008; Mueller and Nowack, 2008). Approximately 16,000 municipal wastewater treatment plants (WWTPs) are in operation in the United States, serving about 75% of the nation's population (Tiemann, 2008). These plants were designed to remove nutrients, pathogens, and other contaminants from wastewater. However, as technologies become more advanced and the products that we dispose of more chemically or physically complex, new challenges in wastewater treatment will arise. While WWTPs successfully remove most nutrients, pathogens, and readily biodegradable or sorbable contaminants from wastewater, some compounds are difficult to treat. They pass through the treatment train unaltered and are released into the

environment with treated plant effluent. More recently in the field of environmental engineering and science, the release of pharmaceuticals and personal care products (PPCPs) from wastewater treatment plants has become a critical issue of interest, as many of these compounds are poorly removed from WWTPs and their effects in the environment are cause for concern.

Industrial and consumer use of ENM-containing products and their disposal into sewage are already occurring (Benn and Westerhoff, 2008; Kaegi et al., 2008; Mueller and Nowack, 2008; Kiser et al., 2009). As manufactured nanomaterials become increasingly common ingredients in a gamut of consumer products, the release of increasing quantities of ENMs into sewage and the environment is inevitable (PEN, 2010; Roco, 2005; Aitken et al., 2006; Nowack and Bucheli, 2007). A recent risk assessment study of engineered silver nanoparticles found that municipal wastewater treatment plants are "considered to be key intermediate stations that control the most prominent flows of silver between anthropogenic and environmental compartments" (Kim et al., 2010). As with PPCPs, the spatial distribution of ENMs in the environment may be determined in part by their passage through WWTPs.

Once nanomaterials in sewage enter a wastewater treatment plant, several pathways of release into the environment are possible. Figure 1.1 shows potential pathways of ENMs from consumers to wastewater treatment plants to environmental compartments. Figure 1.2 is a schematic of a typical conventional activated sludge wastewater treatment plant. Nanoparticles in

a wastewater treatment plant will be either sorbed to solids or suspended in the liquid phase. The term "sorption" is used throughout this dissertation to generally represent either nanomaterial absorption into or adsorption onto wastewater solids. In this context, absorption refers to the uptake of nanoparticles into a structure or across a membrane (Burau and Zasoski, 2002). Adsorption is the accumulation of nanomaterials at the solid-solution interface due to either physical or chemical interactions with the surfaces of the solids (Burau and Zasoski, 2002). Physical adsorption is caused by nonspecific binding mechanisms, such as electrostatic or van der Waal forces, and is the most common mechanism of adsorbate removal in water treatment (Crittenden, 2005). Chemical adsorption (or chemisorption) is a chemical reaction that involves the transfer of electrons between adsorbate and adsorbent, such as ionic or covalent bonding (Crittenden, 2005). The surface coatings of nanoparticles may undergo chemical bonding with surfaces. Adsorption occurs when a particle comes in close contact with a surface and then, with attractive forces or chemical bonding being greater than repulsive forces, adheres to the surface. Nanoparticles may adsorb to each other, known as homoaggregation, or they may adsorb to other types of solids during heteroaggregation. Henceforth, the terms "interaction," "aggregation," and "affinity" are used synonymously with "sorption."

In the liquid phase, nanoparticles may sorb to the thin film of bubbles in the aeration tank and be released into the atmosphere as the bubbles break at the surface of the water. Plant operators may be exposed to nanoparticles through inhalation of nanoparticle-containing water aerosols.

If not removed from volatilization, stable nanoparticles will be discharged

from the plant with treated effluent into surface waters. In this case, aquatic

ecosystems and people who use the surface water will be exposed to

nanomaterials either in the water column, while nanoparticles are in

suspension or settling after aggregation, or in sediments, after aggregates

have settled.
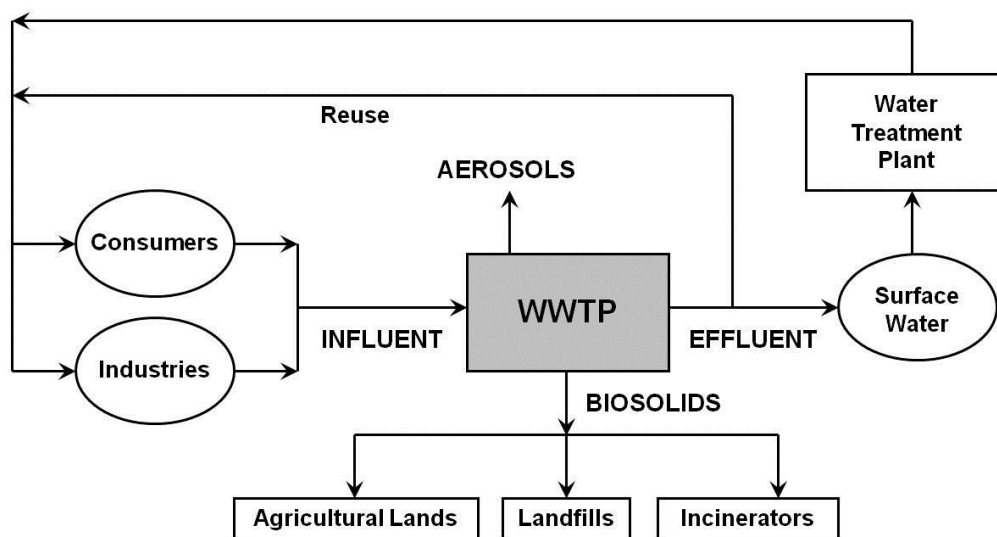
Figure 1.1. Potential fate pathways of engineered nanomaterials from
consumers into the environment.
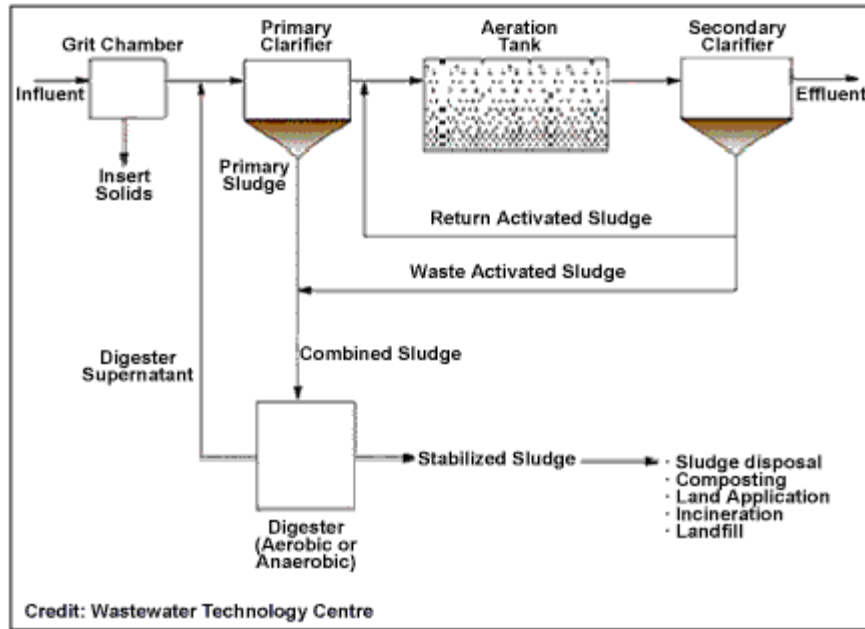
Figure 1.2. Schematic of a typical conventional activated sludge wastewater treatment plant.

In the solid phase, nanoparticles may be biodegraded or wasted from the plant with primary and secondary solids. Primary and secondary solids are processed into biosolids. Biosolids are applied to agricultural soils as soil conditioners, disposed of in landfills, or incinerated in thermal waste treatment plants (Blaser et al., 2008). If applied to soils, nanoparticles could be transported with irrigation water into aquifers or with surface runoff into surface waters, or they may adsorb to matter in soil. Silver was found to stay mostly in the top layer of soils when applied to fields (Hou et al., 2005; Blaser et al., 2008). A recent study showed that earthworms ingested copper nanoparticles from soil, indicating that nanoparticles in soil could enter the food chain (Unrine et al., 2010). Landfilling biosolids may result in the pollution of soil and groundwater via leachate (Blaser et al., 2008). Incineration seems to pose the most minor exposure potential, as emissions of

silver were found to account for only 1% of the emissions leaving thermal waste treatment plants, instead mostly ending up in slag and bottom and fly ashes (Blaser et al., 2008). Blaser et al. (2008) suggest that the most immediate releases to the environment arises from WWTP effluents, untreated wastewater, and from nanomaterials in biosolids that are spread out on agricultural fields.

Research Objectives

Nanomaterials have both benefits and risks. In order to minimize risks (i.e., exposure to potentially harmful ENMs), scientific studies of ENM fate in the environment must be conducted. The work in this research focuses on the fate of ENMs in wastewater treatment plants. WWTPs are dynamic and complex biological reservoirs that collect society's wastes and either degrade them or distribute them into the environment. We attempted to answer the following fundamental question through the work presented in this dissertation: Where will nanomaterials go once they enter a wastewater treatment plant? We used two approaches to answer this question: (1) full-scale wastewater treatment plant analyses and (2) laboratory-scale experimentation. We also began development of a mechanistic model to predict the fate of nanomaterials during biological wastewater treatment. The objectives of this dissertation were to:

1. Characterize nanomaterials in each unit operation, in biosolids, and in treated effluent of a full-scale conventional activated sludge wastewater treatment plant.

2. Measure, characterize, and compare nanomaterial removal and release from several different types of full-scale wastewater treatment plants: conventional activated sludge, activated sludge with advanced tertiary treatment, membrane bioreactor, and trickling filter plants).

3. Quantify the sorption of various types of nanomaterials to wastewater biomass in laboratory-scale batch experiments.

4. Compare fresh and freeze-dried activated sludge as sorbents in laboratory-scale batch experiments to test nanomaterial sorption to wastewater biomass.

5. Develop a comprehensive, mechanistic model of a biological wastewater treatment reactor to predict basic reactor performance and to serve as the basis of a model to predict nanomaterial fate during treatment.

Dissertation Organization

The research done to accomplish each objective is presented as a chapter in this dissertation. Table 1.1 outlines each objective, its corresponding chapter, and chapter citation information. At present, Chapters 3, 4, 5, and 7 have already been published in peer-reviewed journals, Chapter 6 has been submitted to a journal for review, and the nanoparticle fate modeling described in Chapter 8 is underway for future publication. In its entirety, Chapter 8 synthesizes the research chapters and outlines approaches for fusing experimental data with modeling to predict nanomaterial fate in wastewater treatment plants.

Table 1.1

Dissertation Organization

Objective 1 *Characterize nanomaterials in each unit operation, in biosolids, and in treated effluent of a full-scale conventional activated sludge wastewater treatment plant* 　▪ Dissertation Chapter 3 　▪ Published: Kiser, M.A., Westerhoff, P., Benn, T., Wang, Y., Perez-Rivera, J., Hristovski, K., 2009. Titanium nanomaterial removal and release from wastewater treatment plants. *Environmental Science and Technology* 43 (17), 6757-6763.
Objective 2 *Measure, characterize, and compare nanomaterial removal and release from several different types of full-scale wastewater treatment plants: conventional activated sludge, activated sludge with advanced tertiary treatment, membrane bioreactor, and trickling filter plants.* 　▪ Dissertation Chapter 4 　▪ Published: Westerhoff, P.K., Song, G.X., Hristovski, K., Kiser, M.A., 2011. Occurrence and removal of titanium at full-scale wastewater treatment plants: implications for TiO_2 nanomaterials. *Journal of Environmental Monitoring* 13 (5), 1195-1203.
Objective 3 *Quantify the sorption of various types of nanomaterials to wastewater biomass in laboratory-scale batch experiments.* 　▪ Dissertation Chapter 5 　▪ Published: Kiser, M.A., Ryu, H., Jang, H., Hristovski, K., Westerhoff, P., 2010. Biosorption of nanoparticles to heterotrophic wastewater biomass. *Water Research* 44 (14), 4105-4114.
Objective 4 *Compare fresh and freeze-dried activated sludge as sorbents in laboratory-scale batch experiments to test nanomaterial sorption to wastewater biomass.* 　▪ Dissertation Chapter 6 　▪ Submitted: Kiser, M.A., Ladner, D., Hristovski, K.D., Westerhoff, P., 2011. Nanomaterial transformation and interaction with fresh and freeze-dried wastewater biomass. *Environmental Science and Technology*.
Objective 5 *Develop a comprehensive, mechanistic model of a biological wastewater treatment reactor to predict basic reactor performance and to serve as the basis of a model to predict nanomaterial fate during treatment.* 　▪ Dissertation Chapter 7 　▪ Published: Kiser, M.A., Oppenheimer, J., DeCarolis, J., Hirani, Z.M., Rittmann, B.E., 2010. Quantitatively understanding the performance of membrane bioreactors. *Separation Science and Technology* 45 (7), 1003-1013.

Chapter 2

BACKGROUND OF NANOMATERIALS IN

WASTEWATER TREATMENT PLANTS

Types and Sources of Nanomaterials Entering Wastewater Treatment Plants

Because of the technological sophistication conferred by

nanomaterials, nanotechnology is predicted (expected) to revolutionize a

diverse array of industries (Guzman et al., 2006). Though at present

nanotechnology is still in its infancy, nanoscale materials and devices have

not gone unnoticed by these industries. Over 1,000 allegedly nanotechnology-

based consumer products are currently on the global market (PEN, 2010),

including electronics, optics, textiles, medical devices, cosmetics, food

packaging, and catalysts (Handy et al., 2008). By 2014, more than 15% of all

products on the global market are likely to be produced using some form of

nanotechnology (Bystrzejewska-Piotrowska et al., 2009). The total global

investment in nanotechnologies was around US$10 billion in 2005 (Navarro

et al., 2008) and is projected to become a US$1 trillion market by 2015 (Nel et

al., 2006). In terms of mass, one estimate for the global production of

engineered nanomaterials was 2,000 tons in 2004, which is expected to

increase to 58,000 tons from 2011 through 2020 (Nowack and Bucheli, 2007).

Nanomaterials can be generally categorized into three major product

types: (i) materials where the bulk is made of nanostructure, (ii) materials

with nanostructures on the surface (e.g. coatings), and (iii) materials

containing nanoparticles (Handy and Shaw, 2007). All of these types of

nanomaterial products are being developed, if not even already used in

society. For instance, nanomedicine (product type i) is being created to treat diseases such as cancer in a targeted and efficient manner than traditional medicine. Researchers are developing nanoparticle-coated membranes (product type ii) to decrease fouling in water and wastewater treatment systems. Cosmetics and fabrics are being created that contain nanoparticles (product type iii).

The materials used to produce these products are essentially custom made for a particular application, and so a wide variety of nanomaterials and nanoparticles exist (Handy and Shaw, 2007). Table 2.1 shows many of the types of nanomaterials being produced and their applications. In general, ENMs can be classified as carbon-based materials (fullerenes, carbon nanotubes, etc.) and as inorganic ENMs, including those based on metal oxides (titanium dioxide, cerium oxide, silicon dioxide, iron oxide, etc.), metals (gold, silver, etc.), and semiconductor nanoparticles like quantum dots (cadmium sulfide, cadmium selenide) (Fadeel and Garcia-Bennett, 2010). Composite or multilayer nanoparticles, like platinum core-silica shell nanoparticles, are also manufactured (Handy et al., 2008). Many ENM applications require surface functionalization, achieved with organic or inorganic surface coatings or capping agents, in order to stabilize the particles against aggregation, provide specific functionality, and make them biocompatible (Lowry and Casman, 2009). As technology progresses, the variety of nanomaterials produced will greatly multiply (Lowry and Casman, 2009).

Table 2.1

Types of nanomaterials produced and applications (Brar et al., 2010)

Class	Type	Quantity used in terms of tons	Application – Product
Metals and alkaline earth metals	Ag	High	Antimicrobials, paints, coatings, medical use, food packaging
	Fe	High	Water treatment
	Pt group metals	High	Catalysts
	Sn	Unknown	Paints
	Al	High	Metallic coating/plating
	Cu	Unknown	Microelectronics
	Zr	High	
	Se	Low	Nutraceuticals, health supplements
	Ca	Low	Nutraceuticals, health supplements
	Mg	Low	Nutraceuticals, health supplements
Metal oxides	TiO_2	High	Cosmetics, paints, coatings
	ZnO	Low	Cosmetics, paints, coatings
	CeO_2	High	Fuel catalysts
	SiO_2	High	Paints, coatings
	Al_2O_3	Low	Usually substrate bound, paintings
Carbon materials	Carbon black	High	Substrate bound, but released with tire wear
	Carbon nanotubes	Medium-High	Used in a variety of composite materials
	Fullerenes (C_{60} – C_{80})	Medium-High	Medical and cosmetics use
Miscellaneous	Nanoclay	High	Plastic packaging
	Ceramic	High	Coatings
	Quantum dots	Low	Different compositions
	Organic nanoparticles	Low	Vitamins, medicines, carriers for medicines and cosmetics, food additives and ingredients

At present, the two most common nanomaterials used in consumer goods are nanoscale silver (nano-Ag) and titanium dioxide (nano-TiO_2) (Lowry and Casman, 2009). Because silver is antibacterial, silver nanomaterials are being used in humidifiers, washing machines, cutting boards, and food packaging, among other products. Benn et al. (2010) measured the silver content in several consumer products – a shirt, medical mask and cloth, toothpaste, shampoo, detergent, towel, toy teddy bear, and two humidifiers. Silver concentrations ranged from 1.4 to 270,000 micrograms per gram of product, the lowest concentration having been found in shampoo and one of the humidifiers and the highest in the medical mask and cloth. Titanium dioxide is probably the most prevalent manufactured nanomaterial (Lowry and Casman, 2009), found in cosmetics, paint, and batteries (Lowry and Casman, 2009).

Kaegi et al. (2008) showed for the first time that TiO_2 particles are released in significant amounts from painted exterior facades into the aquatic environment. The authors traced TiO_2 particles from exterior façade paints to the discharge into surface waters. The spatial distribution and size of TiO_2 particles in a newly-painted exterior façade were investigated by SEM. The particles were homogeneously spread over the façade, loosely attached to the surface, and ranged in size (diameter) from about 50 to 200 nm. Through analytical electron microscopy (TEM-EDX) and ICP-MS, the authors found that TiO_2 particles detach from new and aged façade paints by natural weather conditions and are then transported by façade runoff and discharged into receiving waters. The concentration of TiO_2 nanoparticles (< 300 nm) in

urban runoff samples were determined to be 3.5 x 10^8 particles/L, of which about 10% or 3.5 x 10^7 particles/L are less than 100 nm in diameter. The authors conclude that other exterior applications, such as nanosilver in paints, exposed to natural weather conditions may release nanoparticles in a similar way.

Benn et al. (2010) investigated the potential of various consumer products to release nanosilver into water, air, or soil. Release of silver was quantified from a shirt, medical mask and cloth, toothpaste, shampoo, detergent, towel, toy teddy bear, and two humidifiers. Mist from the humidifiers was collected, and the other products were washed with 500 mL of tap water. Silver in the mist and wash water were measured by ICP-OES. Silver was released in quantities up to 45 µg/L, with the highest release being from the medical cloth. Size fractions of the released particles were both larger and smaller than 100 nm. The authors suggest that most of the silver from these products will probably be released into wastewater from domiciles that will enter municipal and septic sewage systems.

WWTP Biomass Components

The activated sludge process is the most widely used biological process for treatment of wastewater (Rittmann and McCarty, 2001). The components of this process are the aeration basin, a settling tank, solids recycle from the settler to the aeration basin, and a sludge wasting line. The settling tank serves the purpose of separating solids from treated wastewater. A more advanced and effective method of solid separation is the use of membranes in membrane bioreactors (MBRs). The objectives of activated sludge treatment

are to (1) oxidize dissolved and particulate biodegradable matter into acceptable end products, (2) capture and incorporate suspended colloidal solids into floc, (3) transform or remove nutrients, and (4) if possible, remove specific trace organic constituents and compounds (Metcalf and Eddy, 2003). These objectives are accomplished because of two central characteristics of activated sludge. First, activated sludge is comprised of a wide variety of microorganisms, including bacteria, protozoa, crustacea, nematodes, and rotifers. Bacteria are the simplest and most numerous life form in activated sludge with respect to number of species and total biomass (Gerardi, 2006). Second, these microorganisms exist as floc, aggregates of organisms held together by organic polymers and electrostatic forces (Rittmann and McCarty, 2001). Floc formation packages a large and diverse population of microorganisms into aggregates that can be separated from the waste stream in the secondary clarifier and then recycled as needed.

Floc formation occurs naturally with increasing solids retention time and is initiated by floc-forming bacteria, which are able to produce three cellular components that enable them to agglutinate – pili or fimbriae, EPS, and poly-beta-hydroxybutyrate (PHB) granules. In floc formation, pili or fimbriae contain key functional groups, such as carboxyl (-COOH) and hydroxyl (-OH) groups that become ionized with the loss of hydrogen atoms. Bacterial cells become joined together when bivalent cations in solution, such as Ca^{2+}, bridge fibrils together. Ionized fibrils not joined together remain exposed to the bulk solution and act like wisps of a broom as they sweep and remove fine solids and heavy metals from the bulk solution (Gerardi, 2006).

Nanomaterials in WWTPs

Because ENMs have only recently (within the last decade) been introduced into consumer products, only a few studies have been published that experimentally or theoretically (through modeling) investigate the fate of ENMs in wastewater treatment plants. With the exception of our research group's publications, which are presented as chapters in this dissertation, publication on nanomaterials in wastewater treatment plants are summarized below.

Farré et al. (2010) described the development, optimization, and validation of a novel method for analyzing C_{60}, C_{70}, and N-methylfulleropyrrolidine C_{60} in wastewater effluent solids. Wastewater effluents from 22 municipal WWTPs in the Catalonia region of Spain were collected. All of the plants that were sampled from treat mainly municipal sewage with about 10% of inflows from industries, including food and textile plants. All of the plants utilized biological and chemical processes, with five of these plants using nitrification-denitrification processes and one plant equipped with tertiary treatment. Effluent samples were filtered through 0.45-micrometer nylon membranes. The solid-lined membranes were submerged in toluene and sonicated for 15 minutes, the toluene was rotoevaporated to a small volume, and then methanol was added to obtain a toluene-methanol mixture of 2:1 v/v. The extracts were analyzed by liquid chromatography coupled to hybrid triple quadrupole linear ion trap mass spectrometry (QqLIT-MS) for trace quantification. The method was validated by spiking ultrapure water, river water, and effluent wastewater matrices

with 0.5, 1.0, and 1.5 µg/L of C_{60}. Recovery percentages were generally

greater than 60%, and overall variability of the method was below 15%. The

method was found to have a lower detection limit ranging from 0.2 to 1 ng/L.

Fullerenes were detected in more than half of the WWTP effluents sampled,

with nine of them in the µg/L concentration range. Effluent fullerene

concentrations ranged from about 10 to 70,000 ng/L. The paper did not make

any connections between the types of treatment plants sampled from (extent

of treatment) and effluent C_{60} concentrations.

Limbach et al. (2008) investigated the removal of cerium oxide

nanoparticles in a model WWTP. 100 mg/L of cerium oxide dispersion was

continuously fed into a sludge-containing reactor. Though the majority of

nanoparticles adhered to sludge, up to 6% of the input cerium oxide

nanoparticles remained in the exit stream. Scanning electron micrographs

showed aggregates of nanoparticles and microorganisms. Cerium oxide

nanoparticles were primarily positioned around cells, indicating preferred

bonding to the sludge. The authors postulate that the fraction of

nanoparticles that did not adhere to sludge was stabilized by constituents of

wastewater, such as by the adsorption of peptides.

Tiede et al. (2010) evaluated the application of hydrodynamic

chromatography (HDC-ICP-MS) to investigate the fate of silver nanoparticles

in activated sludge. They conducted batch sorption experiments with 2,000

mg/L TSS activated sludge and 0.5, 5, and 10 mg/L of silver nanoparticles.

After 6 hours of shaking and 30 minutes of settling, supernatant samples

were collected. Silver remaining in the supernatant was measured by ICP-

MS, and the size distribution analyzed by HDC-ICP-MS. The authors state that more than 90% of the silver nanoparticles partitioned to activated sludge, though no evidence of partitioning versus aggregation is presented. HDC-ICP-MS verified that silver nanoparticles less than 100-nm in diameter were in the supernatant.

Using analytical high-resolution transmission electron microscopy, Kim et al. (2010) identified and characterized nano-sized silver sulfide particles in final stage sewage sludge materials of a full-scale municipal WWTP. The silver sulfide nanocrystals found in the sludge were ellipsoidal in shape, had sizes ranging from 5 to 20 nm, and formed very small, loosely-packed aggregates. Some of the silver sulfide nanoparticles were found to have excess sulfur on their surface, resulting in a ratio of Ag to S close to 1. The authors suggest that nano-sized silver sulfide particles are formed in situ in wastewater treatment plants when silver nanoparticles or soluble silver species react with reduced sulfur present under anaerobic conditions. Anaerobic portions of WWTPs can be sulfur-rich environments, and the formation of silver sulfide during anaerobic sludge digestion has been experimentally demonstrated in lab stories. The types and sources of silver that enter wastewater treatment plants may vary, but most are likely to form thermodynamically-favorable silver sulfide in the presence of reduced sulfur species. Thus, nanoparticles may undergo physicochemical transformations during treatment, such that the characteristics of the nanoparticles leaving a wastewater treatment plant (in effluent or biosolids) may be very different than the original form of the nanoparticles entering the plant.

Ganesh et al. (2010) performed bench-scale studies to evaluate the removal of copper nanoparticles (Cu NPs) and copper ions in activated sludge biomass. Two sets of batch experiments were conducted. In the first set of experiments, flasks with 650 mg/L total suspended solids of activated sludge were spiked with 2 to 10 mg/L of copper, added as Cu NPs or ionic copper from $CuCl_2$ salt, and shaken for 20 hours. The second set of experiments used flasks of activated sludge filtrates (from 0.45-micrometer filters) that were spiked with the same concentrations of copper NPs or ions as in the first experiment and shaken for 20 hours. From these two experiments, the authors sought to identify the fraction of copper removed without biosorption. Cu NPs were removed more effectively (about 95% for all Cu concentrations) than Cu ions (35 to 70%) in the presence of biomass. Even in the absence of biomass, copper nanoparticles were removed more effectively than ionic copper; nearly 75 to 80% of Cu NPs and 25 to 55% of Cu ions were removed in the biomass-free filtrate solution. Comparing the results of these two experiments, the authors concluded that only about 15 to 35% of copper is removed in the presence of biomass due to adsorption of copper to activated sludge biomass, since the copper removed in the biomass-free filtrate is 65 to 85% of the amount removed in the presence of biomass. The authors suggest that the predominant mechanisms of copper removal appear to be aggregation and settling of nanoparticles or precipitation of ions rather than biosorption.

Chang et al. (2007) observed that the biological stage of wastewater treatment for Hsinchu Science-based Industrial Park (HSIP) is almost

entirely ineffective in removing silicate nanoparticles. HSIP is Taiwan's manufacturing hub of high-technology products. Wastewater from the park contains nano-sized silicate particles whose size distributions peak at 2 and 90 nm. The WWTP of the park consists of bar screen, aerated grit chamber, equalization tank, contact aerated biological stage, and chemical coagulation-sedimentation basins. The biological unit removes only 9% of Si, mostly from the suspended particle fraction (> 0.45 micrometer). Following biological treatment, the chemical coagulation unit effectively removed most of the suspended particles, but the removal rate of the colloidal fraction (< 0.45 micrometer) was limited. Even with the addition of 3 to 5 mg/L as Al of polyaluminum chloride (PACl), only 9% of colloidal Si particles were removed. Thus, the wastewater treatment process of HSIP exhibits a very low removal efficiency of Si-based nanoparticles.

Jarvie et al. (2009) found results similar to the Chang study of silica-based nanoparticle removal during wastewater treatment. Jarvie et al. examined the fate of silicon dioxide nanoparticles in primary wastewater treatment microcosms using small-angle neutron scattering (SANS). SANS is a technique that quantifies concentration, size, shape, and floc structure of nanoparticles in aqueous dispersions. Through the use of SANS, the authors compared the stability of nonfunctionalized (uncoated or bare) and Tween-coated synthetic silicon dioxide (SiO_2) nanoparticles in wastewater matrices, ultrapure water, and electrolyte solutions. Quartz cuvettes containing raw wastewater (with 293 mg/L total suspended solids), filtered wastewater (without solids), ultrapure water, or 0.01 M $La(NO_3)_3$ electrolyte solution

22

(equivalent to 10 mM NaCl) were spiked with 2,470 mg/L SiO_2 nanoparticles. Though it is highly unlikely that such high nanoparticle concentrations will enter municipal WWTPs, the authors chose this concentration to produce a statistically significant scattering signal during SANS analysis while ensuring that colloidal behavior of SiO_2 nanoparticles was not subject to interference from interparticle interactions.

In nanopure water, both nonfunctionalized and Tween-coated SiO_2 nanoparticles were completely stable for over 24 hours. Nonfunctionalized SiO_2 nanoparticles were also very stable in both raw and filtered wastewater, with no sedimentation occurring over a period of 24 hours. On the other hand, Tween-coated SiO_2 nanoparticles were much less stable in both raw and filtered wastewater – up to 90% of these coated nanoparticles were removed from suspension, more so in filtered than in raw wastewater. The greater removal of Tween-coated SiO_2 nanoparticles in filtered wastewater indicates that the presence of solids is of minor significance for SiO_2 nanoparticle sedimentation. In 0.01 M $La(NO_3)_3$ solution, uncoated SiO_2 nanoparticles flocculated within 30 minutes, whereas Tween-coated SiO_2 nanoparticles flocculated much more gradually. The results in electrolyte solution indicate that rapid flocculation of Tween-coated SiO_2 nanoparticles in wastewater is not an electrolyte effect and must be due to interactions between adsorbed Tween molecules and sewage constituents. Conversely, the long-term stability of nonfunctionalized SiO_2 nanoparticles in raw and filtered wastewater demonstrates that sewage organic matter did not induce aggregation of the bare nanoparticles. The authors conclude that Tween-

coated nanoparticles will flocculate and produce aggregates that will settle out during primary treatment, thereby removing them from the effluent stream and instead incorporating them into sewage sludge. Nonfunctionalized SiO_2 nanoparticles, however, are likely to pass through primary treatment and continue in the effluent stream into secondary (biological) treatment.

Chapter 3

TITANIUM NANOMATERIAL REMOVAL AND RELEASE FROM

WASTEWATER TREATMENT PLANTS*

Abstract

Titanium (Ti) occurs naturally in soils and as highly purified nano-scale titanium dioxide (TiO_2) in many commercial products that have been used for decades. We report for the first time the occurrence, characterization and removal of Ti at wastewater treatment plants (WWTP). At one WWTP studied in detail, raw sewage contained 100 to nearly 3000 µg Ti/L with < 50 µg Ti/L in the size fraction that passed through a 0.7 µm nominal glass fiber filter. Ti larger than 0.7 µm was well removed during primary clarification, secondary activated sludge treatment, and clarification and tertiary filtration. Ti concentrations in wastewater effluents from several other WWTPs ranged from <5 to 15 µg/L. As Ti was removed, it accumulated in settled solids at concentrations ranging from 1 to 6 µg Ti/mg. Ti is insoluble in water; using a newly developed hydrogen peroxide-based pretreatment system, we were able to image Ti-containing solids in sewage, biosolids, and liquid effluent as well as in commercial products containing the engineered nanomaterial (ENM) TiO_2. Spherical aggregates (50 to a few hundred nm in size) comprised of sub-50 nm spheres of Ti and oxygen only (presumably TiO_2) were observed in all samples. Significantly larger silicate particles containing a mixture of TI and other metal atoms were also

---

observed in the samples. To support this field work, laboratory adsorption batch and sequencing batch reactor experiments using TiO_2 and activated sludge bacteria were conducted. These experiments verified that adsorption of TiO_2 onto activated sludge biomass played an important role in removing this ENM from wastewater. This research is significant, as it is the first report of data on ENM release into the environment for a material that has significant annual production volume and reports of potential adverse ecosystem responses. For this reason we hypothesize that TiO_2 ENMs can serve as a model, or *sentinel*, ENM for the behavior or fate of other ENMs that are and will be manufactured and used in commercial products.

Introduction

Titanium (Ti) is the ninth most abundant element and the seventh most abundant metal in the Earth's crust (Barksdale, 1968). With significant worldwide reserves in excess of 600 million tons, the estimated annual production of Ti metal is 90,000 tons, while the annual production of titanium dioxide (TiO_2) is approximately 4.3 million tons (Emsley, 2001). While Ti has numerous industrial applications, from metal alloying to aerospace applications to biomedical devices, approximately 95% of mined Ti is refined into nearly pure TiO_2 through the treatment of Ti-bearing ores with carbon, chlorine, oxygen or sulfuric acid (USGS, 2009). Because it is inert, somewhat opaque, and resists fading, TiO_2 is used in an extensive array of consumer products, including paints, paper, plastics, sunscreens and even food (USGS, 2009; Robichaud et al., 2009; Lomer et al., 2000; Popov et al., 2005; Contado and Pagnoni, 2008; Nohynek et al., 2007). TiO_2 is commercially available in

the form of dry powder or an aqueous suspension, and in food products it is used to whiten, increase opacity, or modify texture (Reijnders, 2006). Typical food products containing TiO_2 include confectioneries, white-colored sauces and dressings, non-dairy creamers, and mozzarella and cottage cheeses (Mattigod et al., 2005; Lomer et al., 2002). Food-grade TiO_2 ranges in size from tens to hundreds of nanometers, the common mean diameter being approximately 200 nm (Robichaud et al., 2009). The daily human intake of TiO_2 (average size < 200 nm) has been estimated to exceed 5.4 mg/day (Lomer et al., 2002). Consumption of TiO_2 leads to negligible accumulation in people, although Ti is present in human bones (Schroeder et al., 1963). Thus, humans should excrete ingested TiO_2, which will then be transported in sewage to wastewater treatment plants (WWTPs). Surprisingly, the only reports of Ti in feces are from rangeland animals and aquaculture fish (Myers et al., 2006; Vandenberg and de la Noue, 2001; Weatherup and McCracken, 1998; Mayland et al., 1975). Currently, no publications report on the removal of nano-sized Ti or TiO_2 in WWTPs.

TiO_2 is among the most frequently reported engineered materials used in nanotechnology-based consumer products (Aitken et al., 2006). Direct and indirect uses of consumer products containing nanomaterials (e.g., food additives, pharmaceuticals, and clothing) will lead to the release of engineered nanomaterials (ENMs) into domestic sewage (Benn and Westerhoff, 2008; Nowack and Bucheli, 2007). A recent study presented evidence of the release of synthetic TiO_2 nanoparticles (NPs) from paints on building facades and measured a significant amount of TiO_2 NPs in urban

runoff after a rainstorm (Kaegi et al., 2008). Therefore, in addition to excretion from humans, TiO_2 in sunscreens and paints is likely to be washed or disposed into sewage systems. Serving more than 80% of the U.S. population, municipal WWTPs generally utilize biological treatment, in which dense bacterial communities (activated sludge) sorb and degrade pollutants (Rittmann and McCarty, 2001). Recent life-cycle predictions of nanomaterial loadings in the environment indicate an important role for WWTPs in nanomaterial removal. The analysis suggested that of the three types of nanoparticles studied – nano silver, nano-TiO_2, and carbon nanotubes – only the predicted concentrations of nano-TiO_2 in WWTP effluents (0.7 – 16 µg/L) were close to or higher than the predicted no-effect concentration level (1 µg/L) (Mueller and Nowack, 2008). For that reason, more information is required on the sources, occurrence, and morphology of Ti in wastewater effluents and the factors affecting Ti removal in WWTPs. Furthermore, because TiO_2 has been used for decades, it may serve as a *sentinel* for other nanomaterials, especially those that are of similar size and aggregate like TiO_2, by indicating where these nanomaterials may occur or accumulate in the environment as they become used in larger quantities.

The objectives of this study were to 1) quantify Ti concentrations in a full-scale municipal WWTP; 2) characterize the morphology and composition of Ti-based solids in consumer products plus wastewater effluents and biosolids; 3) quantify Ti concentrations in lab-scale treatment reactors and the sorption capacity of wastewater biomass for TiO_2 NPs. Wastewater biomass is a mixture of active bacterial cells, inert or residual biomass,

extracellular polymeric substances (EPS), protozoa and other higher life forms, mineral precipitates, and influent refractory solids (Rittmann and McCarty, 2001), which we hypothesize included Ti solids. Through the accomplishment of these goals, we develop a more lucid understanding of the potential fate and transport of TiO_2 NPs in WWTPs.

Materials and Methods

Wastewater Treatment Plant Site Description and Sample Collection

Most of this research was conducted at a wastewater reclamation facility in central Arizona (USA) that uses activated sludge process and tertiary filtration treatment (Figure 3.1). This facility uses the following unit processes: headwork screening, primary clarification, activated sludge treatment with aerobic and anoxic zones to achieve nitrification and partial denitrification, secondary clarification, and tertiary anthracite filtration. At four different times (7:00, 11:00, 15:00, and 18:00) on each day in June 2008, effluent samples from each unit process, activated sludge from the aeration basins (except at 7:00), wasted solids from the primary and secondary
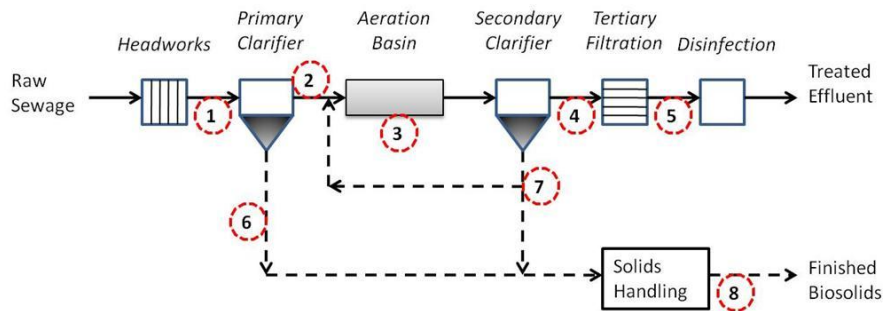
Figure 3.1. Schematic of advanced WWTP including sampling locations (circles): 1) influent, 2) primary effluent, 3) aeration basin, 4) secondary effluent, 5) tertiary effluent, 6) primary solids, 7) secondary solids, and 8) finished biosolids. Solid lines indicate direction of water flow. Dashed lines represent direction of flow of solids.

clarifiers, and finished biosolids were collected from the facility. To investigate possible seasonal variations, effluent samples were also collected from each unit process at the same facility once around noon (during peak flow) on a day in January 2009. Approximately 15% of the June samples were collected in replicate, while 100% of the January samples were collected in triplicate. For quality control, field and trip blanks of ultrapure water (< 1.5 µS/cm) were included in the sampling. Samples were stored on ice (< 4 °C) until return to the laboratory. Portions of each sample were used for suspended solids analysis, nonfiltered analysis, and filtered (GF/F-grade glass microfiber filter, Whatman Inc.) sample analysis. Settled solids from the primary and secondary clarifiers were also collected and analyzed. Activated sludge from aeration basins was collected and used in sorption experiments (described below).

Additional final liquid effluent and biosolids samples were collected from confidential WWTPs in Arizona, California, Colorado, Iowa, Maryland, and three facilities in New York. Samples were shipped to our laboratories by overnight courier.

Laboratory-Scale Experimental Approach

A nano-scale TiO_2 suspension was prepared by adding TiO_2 (Hombikat, Sigma-Aldrich) to ultrapure water, sonicating for 1 hour (200 W/L), and centrifuging at $F = 1000$ G for 30 minutes. Following centrifugation, the supernatant containing suspended TiO_2 was removed and used as stock solution. Hombikat TiO_2 was selected because of its low isoelectric point (approximately 2.5), which prevented aggregation of the

nanoparticles in pH-neutral water environments. Phase analysis light

scattering (90 Plus, Brookhaven Instruments Corp., Holtsville, NY)

measurement indicated a mean particle size of 40 nm (number distribution).

Periodic particle size measurements indicated a stable TiO_2 suspension.

Batch Adsorption Isotherm Experiment

A TiO_2 test solution (2 mg Ti/L from the TiO_2 stock solution; 1 mM

$NaHCO_3$; pH 7.2) was mixed continuously and equilibrated for 10 hours. A

wastewater bacteria biomass stock solution was prepared by rinsing the

activated sludge three times with a 1-mM $NaHCO_3$ solution and then

resuspending the sludge in the rinsing solution. A series of 60-mL glass vials

containing a fixed volume of TiO_2 test solution were spiked with varying

amounts of biomass stock solution and then agitated for 3 hours. After

agitation, the biomass was allowed to settle by gravity (about 30 minutes),

and then 20 mL of supernatant was collected from each sample and analyzed

for Ti. Fifteen percent of the samples were conducted in triplicate.

Sequencing Batch Reactor Experiment

Sequencing batch reactors (SBRs) were used to represent the full scale

WWTP operations of aeration and settling. SBRs were constructed using 2-L

reactors supplied with compressed air and mechanical mixing units. The

SBR contained heterotrophic bacteria acclimated to a feed solution (668 mg/L

$C_5H_8NO_4Na$, 44 mg/L KH_2PO_4, 90mg/L $MgSO_4 \cdot 7H_2O$, 14 mg/L $CaCl_2 \cdot 2H_2O$,

10 mg/L yeast extract, and 0.3 mL/L nutrient solution) and was operated to

maintain a total volume of 1.6 L, a hydraulic residence time (HRT) of 10

hours, and a solids retention time (SRT) of 6 days, which is typical of aerobic

WWTPs. The SBR cycle involved 8 hours of aeration plus mixing, followed by

2 hours of settling time. SRT and HRT were managed by removing a total of

0.25 L of completely mixed solution plus 0.75 L of settled supernatant once

per day. During a separate operating cycle, an additional 1 L of settled

supernatant was removed per day. Removed solutions were analyzed for

concentrations of Ti and suspended solids, and were replaced with the same

volumes of feed solution.

Analytical Methods

Because TiO_2 has very low solubility (Antignano and Manning, 2008),

Ti in wastewater is expected to occur solely in solid phases, not in ionic forms.

For the quantification method used in this investigation, these solid phases

must be transformed into ionic forms by acid digestion. Liquid and solid

samples were acid digested using the HNO_3/H_2SO_4 digestion method for Ti as

described by Standard Method 3030 G for water and wastewater analysis

(Eaton et al., 2005). The digested samples were analyzed by Inductively

Coupled Plasma Optical Emission Spectroscopy (ICP-OES) (iCAP 6000

Series, Thermo Scientific, Cambridge, UK). Suspended solids measurements

were made following Standard Method 2540 D (Eaton et al., 2005).

Visual characterization of the Ti-bearing solids was conducted using

the Scanning Electron Microscopy/Electron Dispersive X-Ray microanalysis

(SEM/EDX) technique (FEI XL-30 equipped with EDAX system). To

minimize potential interferences from organic biomass constituents, we

employed a new approach for biosolids examination in which samples were

digested with 30% hydrogen peroxide (H_2O_2) at 90° C until foaming ceased

(Carter, 1995). Hydrogen peroxide oxidized the organic matter and facilitated the solubilization of inorganic constituents. TiO_2 is chemically inert under these conditions and does not dissolve or change shape, as verified in control experiments using commercial TiO_2. Oxidized samples were centrifuged (F = 1000 G) on a SEM stub, air dried, and then analyzed by SEM/EDX. A backscatter detector was used to differentiate between heavier elements such as Ti, which appeared white, and lighter elements, which appeared darker.

Results and Discussion

Titanium Occurrence and Fate in Wastewater Treatment Plants

Figure 3.2 presents the results of the June 2008 WWTP sampling campaign. During the 11:00 am sample set, representative of peak plant flow conditions, the Ti concentration at the headworks (plant influent) was 185 µg/L; this decreased to 17 µg/L in the tertiary effluent. Thus, approximately 91% of the Ti that entered the treatment plant was removed from wastewater. The removed Ti accumulated in plant solids – primary solids, activated sludge biomass, and secondary solids. Samples collected at other times of the day exhibited similar removal and solids-accumulation trends across the WWTP, with the exception of the 18:00 sample from the headworks. This sample had elevated Ti levels (2800 µg Ti/L) that were statistically different from other samples at that location ($p < 0.01$), perhaps due to an industrial source (e.g., paint, polishers, semiconductor wastes) discharged into the sewers during the day. The average overall removal of Ti for the four different sampling times in June 2008 was 79% ± 23%.
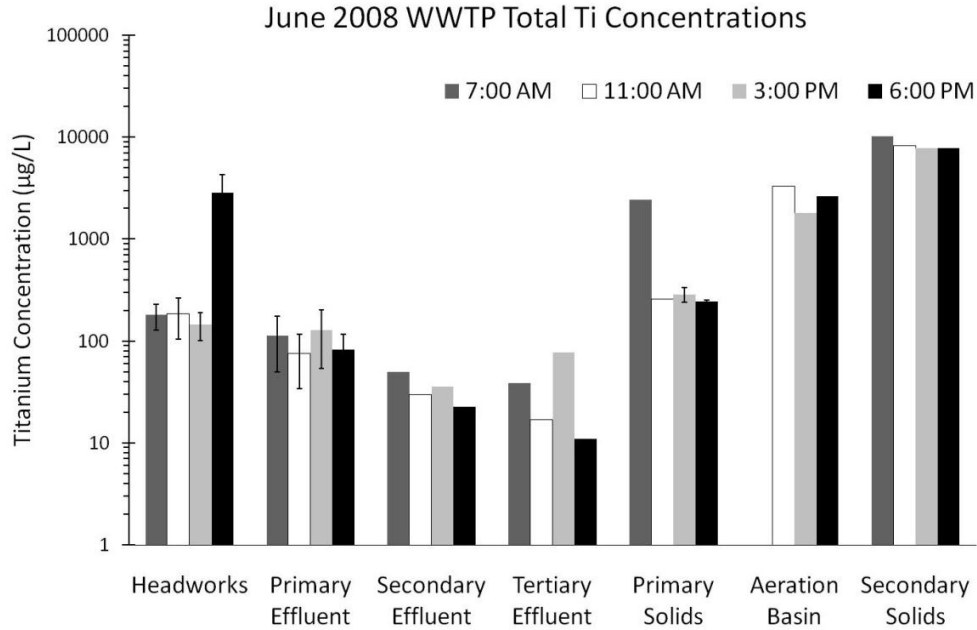
Figure 3.2. June 2008 Ti concentrations for four sampling periods at an Arizona WWTP. Sampling points are as identified in Figure 3.1.

Figure 3.3 compares Ti concentrations in filtered (nominal filter pore size of 0.7 μm) and non-filtered samples at 11:00 am in June 2008. In general, Ti concentrations in filtered samples were lower than those in non-filtered samples. The difference between Ti levels in filtered and non-filtered samples is particularly obvious for samples containing relatively higher concentrations of total suspended solids, such as plant influent and primary effluent, which contained 221 and 76 mg/L TSS, respectively. For the tertiary effluent, which had only 4 mg/L TSS, the Ti concentrations in the filtered and non-filtered samples are approximately the same. The distinction between Ti concentrations in filtered and non-filtered samples of relatively high TSS suggests that the majority of Ti associated with suspended organic matter of a size larger than the pore size and/or that the

Ti formed aggregates greater than 0.7 µm in size. Thus, spectroscopic

analysis was carried out to determine the morphology and composition of the

Ti in wastewater tertiary effluent (see next section).
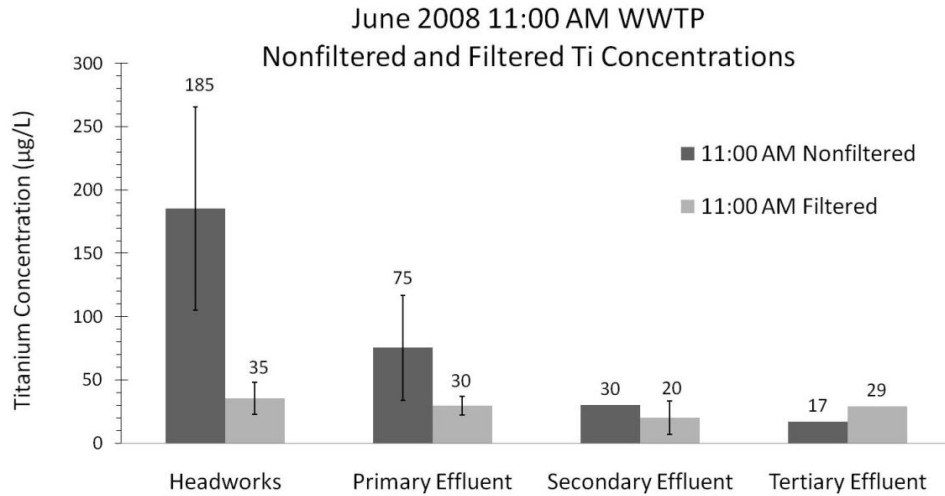
Figure 3.3. June 2008 Ti concentrations of 11:00 AM Arizona WWTP filtered
and nonfiltered headworks and process effluent samples.

Ti concentrations in filtered samples exhibited less variability during

the day across the treatment processes compared to the total (non-filtered)

samples collected (Table 3.1). The average tertiary treated Ti concentration

for the four sampling times was 36 µg/L (20±9 µg/L in filtered samples),

compared to 843 µg/L (34±3 µg/L in filtered) at the headworks. These

concentrations were at the low end of our detection capabilities, but were

verified through Ti spike-addition and recovery tests.

Table 3.1

June 2008 average concentrations for four sampling periods

Sample Description	Filtrate Ti (µg/L)	Total Ti (µg/L)	Total Suspended Solids (mg/L)	Total Ti Normalized to Solids (mgTi/g TSS)
Headworks	34±3.2	843	336	1.6±0.4
Primary Effluent	66±51	99	97	1.0±0.1
Aeration Basin	14±9	2572	2220	0.9±0.3
Secondary Effluent	40±48	35	7	—[a]
Tertiary Effluent	20±9	36	6	—[a]
Primary Solids	—[b]	803	1220	0.7±0.2
Secondary Solids	—[b]	8464	7542	1.1±0.1

[a] indicates samples where TSS was too low to accurately quantify normalized Ti concentrations; [b] solid samples were not further filtered.

While total Ti removal was 79%±23%, removal of filterable Ti was only 42%±22%. Thus large sized Ti, which may include larger naturally occurring Ti-silicate minerals or large titanium oxide ENM aggregates (see later discussion of Figure 3.5), were removed more efficiently than smaller sized Ti that passed through the 0.7 µm filter. Other factors may also be associated with this size dependency. For example, some of the smaller Ti particles could be coated, functionalized or have surfaces that were otherwise organically modified such that their stability / removability is affected.

Compared to other locations along the treatment train, the highest total Ti concentrations (2572 µg/L) were found within the activated sludge system (i.e., aeration basin) (Table 3.1), with the exception of secondary solids, which contain dewatered activated sludge materials. In an activated sludge system, a portion of the settled secondary solids are recirculated back to the head of the aeration basin (Figure 3.1) to maintain a sludge residence time (SRT) longer than the hydraulic residence time (HRT), resulting in a dense biological community with a relatively stable concentration (2220 mg TSS/L). Because of this recirculation, the biosolids are repeatedly exposed to inorganics, such as Ti-bearing solids, in the WWTP flowstream. Because the concentrations of Ti associated with particulate phases are quite high in activated sludge systems, it appears that Ti has a tendency to adsorb into the biosolids. Biosolids contain activated bacteria, inert or residual biomass, extracellular polymeric substances, protozoa and other higher life forms, mineral precipitates, and influent refractory solids (Laspidou and Rittmann, 2002a; Metcalf and Eddy, 2003). As the biomass grows through consumption of soluble carbon and other nutrients, the new biomass also appears to accumulate Ti. The secondary clarification system efficiently settled the biosolids, as shown by the difference in TSS levels between the aeration basin and secondary effluent samples (Table 3.1). These WWTP basics explain how and why Ti-bearing materials accumulate in activated sludge biosolids and secondary clarifier settled solids.

To reiterate, association of nano-scale Ti with biosolids must also be critical for their removal during wastewater treatment. Stokes settling rates

$$v_s = \frac{g(\rho_p - \rho)d_p^2}{18\,\mu}$$

$(\qquad)$ (3.1)

are extremely slow for sub-micron particles. Even for TiO_2, which has a density of 4.2 g/cm^3, 10, 100, and 500 nm diameter aggregates require 59 days, 14 hours, or 34 minutes, respectively, to settle only one mm in 25 ^{o}C water.
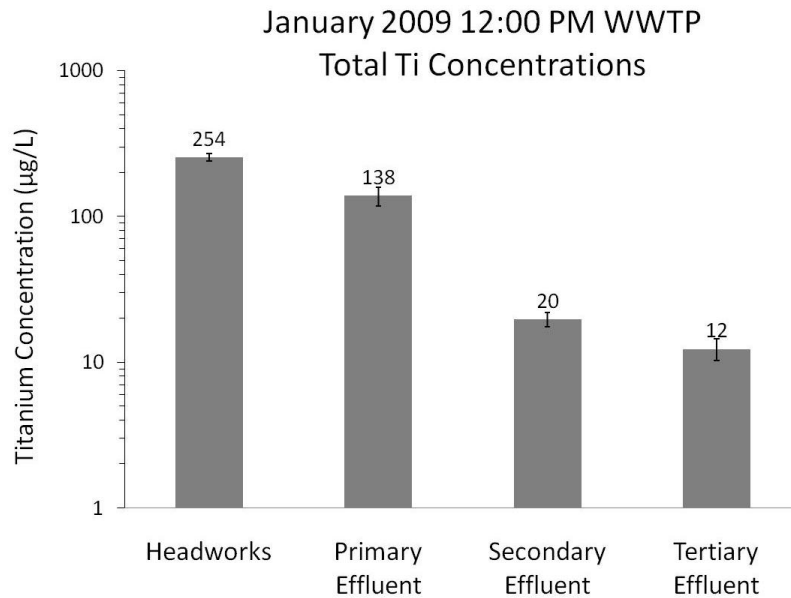
Figure 3.4. January 2009 Ti concentrations of 12:00 PM Arizona WWTP headworks and process effluent samples.

Figure 3.4 shows the January 2009 WWTP sampling results, which exhibit the same trends as those seen in June 2008. The Ti concentrations in the plant influent and tertiary effluent were 254±15 µg/L and 12±2 µg/L, respectively, equating to a 95% removal of Ti from wastewater. This sample

set also supports the conclusion from the summer experiment that the majority of Ti associates with solids in wastewater. The average overall removal of Ti for the June 2008 and January 2009 sampling experiments was 82%±21%.

During the June 2008 sampling campaign at the Arizona WWTP, finished biosolids were also collected, digested, and analyzed. Ti concentrations in the biosolids ranged from 0.6 to 1.4 mg Ti/g SS, with an average of 1.1±0.42 mg Ti/g SS. In separate measurements from eight other WWTPs around the United States with varying types of unit processes, the Ti associated with biosolids ranged from 1.8 to 6.4 mg Ti/g SS, averaging 2.8±1.5 mg Ti/g SS. Triplicate analysis of one biosolids sample showed a high degree of reproducibility (1.79±0.02 mg Ti/g SS). The WWTP effluents contained 8 to 31 μg Ti/L (average 16±7 μg/L), which is also consistent with the results from the more intensive study at the Arizona WWTP. The facility with the highest level of Ti in the biosolids also had the highest level in the liquid effluent. A national USEPA study of 83 WWTP biosolid samples observed a range of Ti from 0.018 to 7.02 mg Ti/g SS (USEPA, 2009). Overall, these additional points of reference indicate that the WWTP in which we conducted intensive sampling is likely representative of many WWTPs across the United States. Ti levels in biosolids are important because they are land applied as fertilizers, incinerated, disposed to landfills, and used in other applications. A significant fraction of the TiO_2 used in commercial products that enter the sewer system appears likely to accumulate in biosolids and enter the

environment via these routes. A smaller fraction of TiO_2 appears to be present in the liquid effluent that enters rivers, lakes and oceans.

Spectroscopic Analysis of Ti in Wastewater

After the oxidation of organics in biosolids via hydrogen peroxide, SEM in backscatter mode easily detected Ti in biosolids and various commercial products (Figure 3.5). SEM and EDX analysis confirmed the presence of various sizes, shapes and compositions of Ti-containing solids. Based on EDX analysis at various locations in the SEM image, primary particles of nearly pure titanium and oxygen solids (TiO_x), were observed to occur in small aggregates (3.5A and 3.5C), while larger, single crystal structures (3.5B) were also present. Ti (3.5D) was also found to co-occur in other solids with iron, calcium, silica and oxygen atoms, suggesting a type of silicate or other mineral. Many consumer products contain Ti (Robichaud et al., 2009), and several were examined by SEM. For example, in hydrogen peroxide-digested toothpaste, TiO_x was easily identified (3.5E) and appeared to be in aggregates of nearly spherical primary nanoparticles. This interpretation is similar to that employed in a study by Powell et al. to analyze aluminum, silicon, and Ti in human gut samples. Three distinct types of microparticles were found to be related to macrophages at the base of gut-associated lymphoid tissue (Powell et al., 1996): type I - spheres of TiO_2, 100-200 nm diameter, characterized as the synthetic food additive polymorph anatase; type II - aluminosilicates, < 100-400 nm in length, generally of flaky appearance, often with adsorbed surface iron, and mostly characteristic of the natural clay mineral kaolinite; and type III - mixed environmental silicates

without aluminum, 100-700 nm in length and of variable morphology. The study concluded that the TiO_2 was partly derived from food additives and partly from the environment. Beyond the image analysis similarities of the gut and biosolid samples, the Powell study suggests that the metals associated with collagen fibers and plasma cells. This finding is of significance to the investigation of Ti in wastewater because wastewater biomass also contains collagen fibers, suggesting at least one important component of biomass is potentially related to its interaction with Ti solids.

Ti oxides were also present in WWTP effluents (e.g., Figure 3.5F). These were not always easily found in the WWTP effluent samples, which contained relatively low concentrations of Ti, but those observed were often aggregates of a few hundred nanometers comprised of several primary particles of a size less than 100 nm that were made solely of TiO_x. The primary particles were often spherical in shape, as illustrated by the SEM image shown in Figure 3.5F. The shape and size of these Ti materials are consistent with TiO_2 synthesized for industrial / food applications. To our knowledge, this is the first report of Ti in wastewater effluents or biosolids.
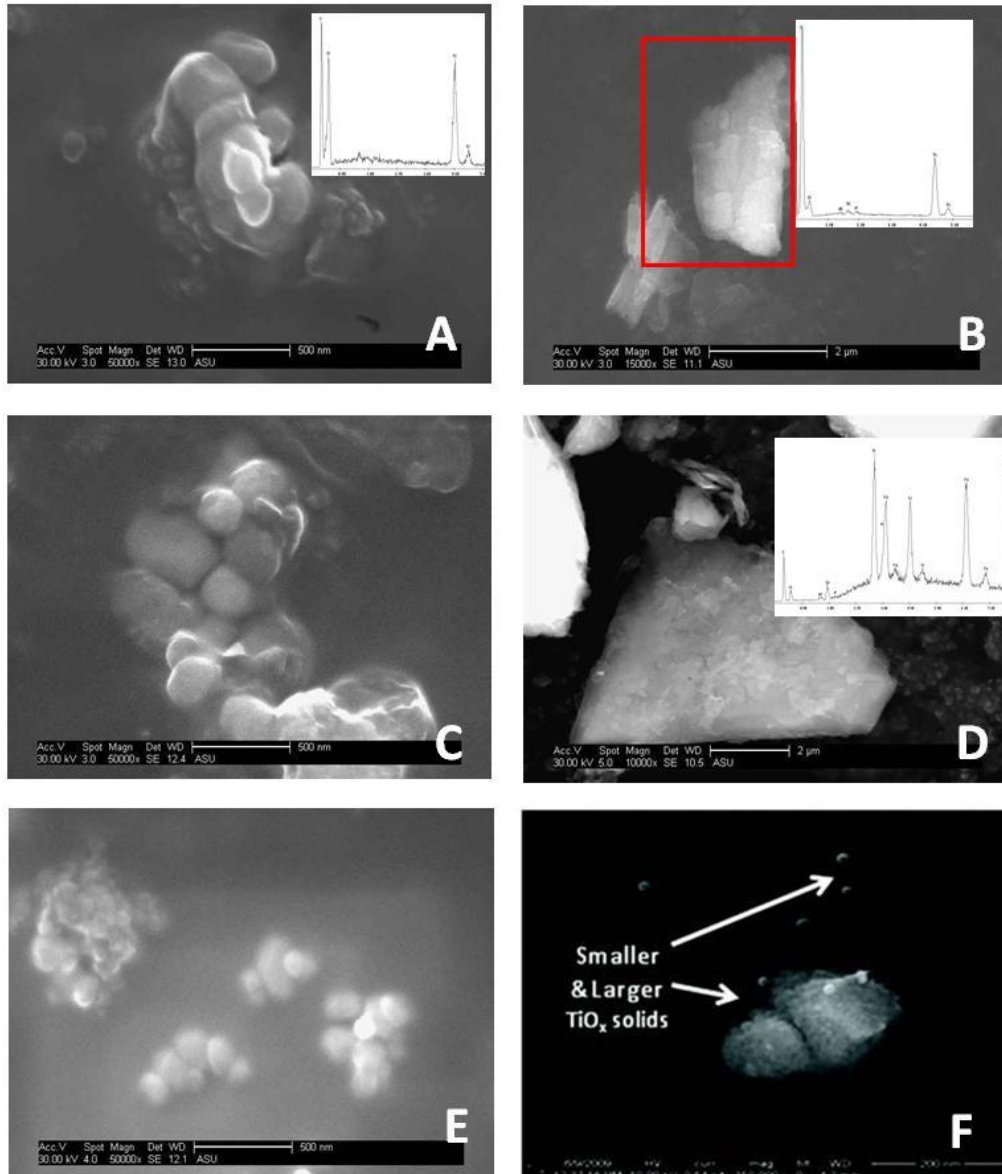
Figure 3.5. SEM analysis of A) nanoscale TiO₂, B) microscale TiO₂, C) an aggregate of primary TiO₂ material, D) mineral-containing Ti in a biosolid sample, E) TiO₂ in toothpaste as a representative consume product, and F) nanoscale TiO₂ in WWTP tertiary effluent. EDX inserts were provided for some images, but all solids shown were confirmed to contain Ti and O.

Adsorption of Titanium Dioxide with Wastewater Biomass

Bacterial cells can uptake or attach to nanoparticles (Thill et al., 2006; Brayner et al., 2006; Arias and Yang, 2009). The mechanisms responsible for these observations are poorly understood. To investigate the potential for TiO_2 to sorb onto wastewater biomass, a batch adsorption experiment was performed (Figure 3.6). A control sample (no biomass) contained 0.8 mg/L Ti. As increasing dosages of biomass (in solutions of the same ionic strength) were added to the samples, more TiO_2 was removed from the supernatant. A comparison of the Ti concentrations in the control and the sample containing 2250 mg/L TSS shows that approximately 85% of the Ti was removed from suspension. Removal data were fit by a Freundlich Isotherm ($q = 0.025 \ C^{0.53}$; $R^2=0.90$) (inset of Figure 3.6). Biomass-TiO_2 interactions may be viewed as discrete particle-particle aggregation or as more similar to molecular sorption. While a mature literature exists on settling analyses of wastewater biomass, we have almost no mechanistic understanding of how submicron particles (even virus particles) actually interact with complex biomass because the biomass is not a discrete homogeneous solid but rather a heterogeneous gel-like phase. Wastewater biomass is a mixture of active bacterial cells, inert or residual biomass, extracellular polymeric substances (EPS), protozoa and other higher life forms, mineral precipitates, and influent refractory solids (Laspidou and Rittmann, 2002a; Metcalf and Eddy, 2003), including Ti solids.
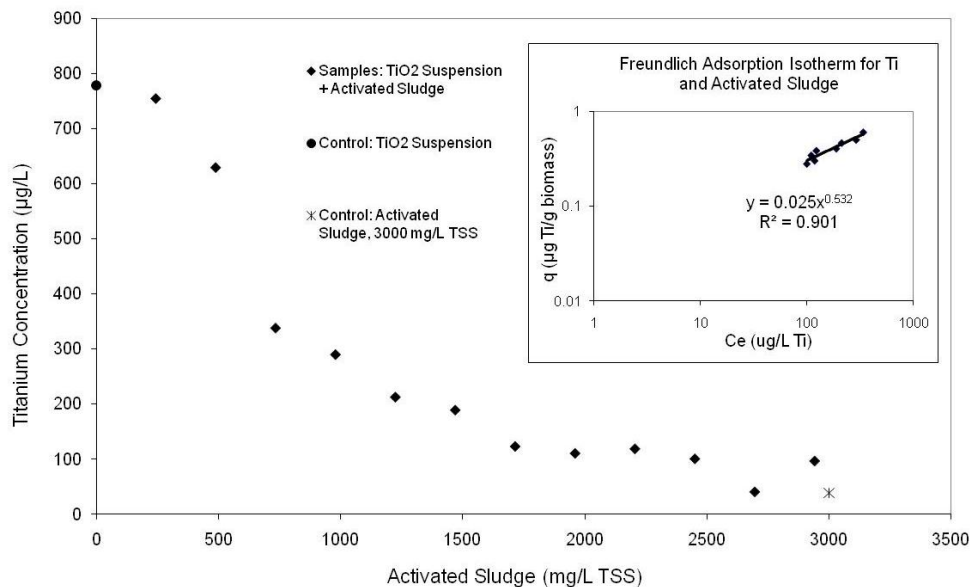
Figure 3.6. Removal of Ti (as Hombikat TiO_2 NPs) from suspension by wastewater biomass. The * sample represents Ti in the supernatant that was "released" when 3000 mg/L of biosolids was added to water without Hombikat TiO_2 present. The inset shows the adsorption isotherm generated from the removal data.

Titanium in Lab-Scale Reactors

To evaluate the effects of TiO_2 on wastewater biomass and assess

sustained TiO_2 removal over time in an actively growing wastewater bacteria

culture, continuously operated SBRs containing a feed solution only (no

biomass) or feed solution plus biomass (TSS = 3300 mg/L) were supplied with

2.9 ± 0.3 mgTi/L during each liquid exchange for 9 days (18 exchanges) to

manage the HRT and SRT; this equated to adding 4.4 ± 1.0 mgTi/gTSS. This

was followed by an input of feed solution without TiO_2 to evaluate the

"washout" of TiO_2 from the reactor. SBRs represent the full scale WWTP

operations of aeration and settling. Over the course of the experiment, a mass

balance closure on Ti was maintained (Figure 3.7). The added Ti

44

concentration (2.9±0.3 mgTi/L) was always greater than that of the settled

supernatant (0.28±0.22 mgTi/L; range 0.03 to 0.73 mgTi/L) (Figure 3.8) and

less than that of the suspended solids (13.2±3.0 mgTi/g TSS; not shown). Ti

outflow was, therefore, significantly higher during SRT control (i.e., removal

of biosolids from the completely mixed reactor) compared to Ti outflow during

HRT control (i.e., removal of settled supernatant). After stopping the TiO_2

feed to the reactor, a gradual washout of Ti from the system was observed

(exchanges 12 through 18).
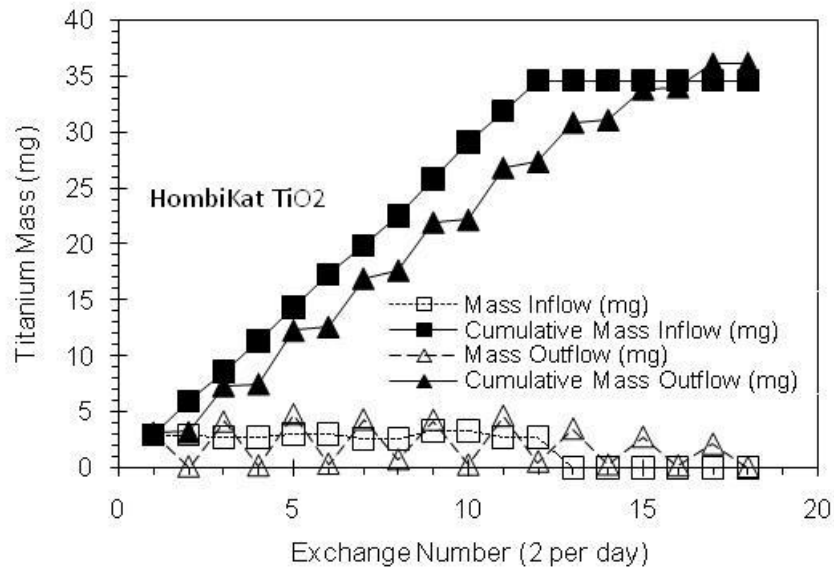
Figure 3.7. SBR experiment using Hombikat TiO_2 with heterotrophic biomass. Plot shows cumulative (mass balance) Ti data.
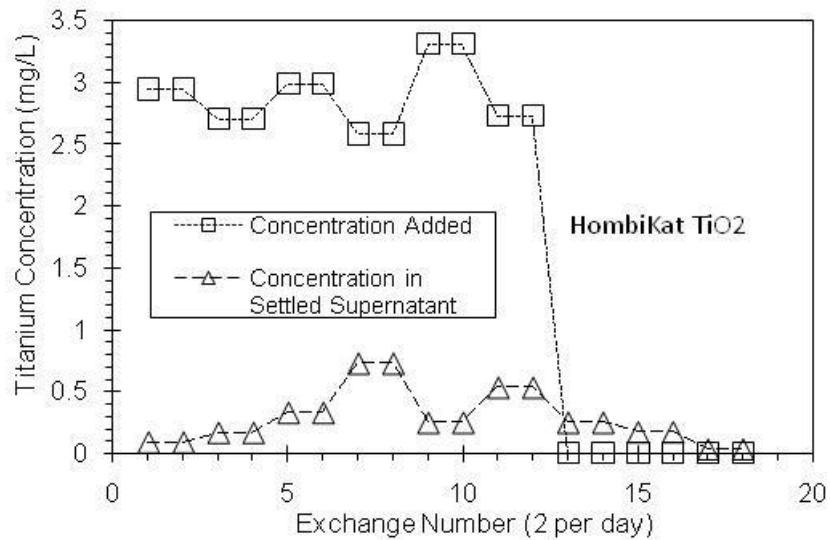
Figure 3.8. SBR experiment using Hombikat TiO₂ with heterotrophic biomass.

Overall, only 12% of the Ti passed through the SBR in the supernatant, while 88% was associated with the biosolids fraction. These experimental results further reveal the high affinity of TiO₂ for biomass. Based on the data presented in Figures 3.2 and 3.3, these two full-scale unit processes achieved roughly 69% removal of Ti. The lower degree of Ti removal in the full-scale WWTP compared to that in the SBRs may be due to the more complex wastewater matrix in WWTPs. For example, wastewater contains surfactants and natural organic matter, which have been shown to hinder the removal of some nanoparticles from water (Hyung et al, 2007; Christian et al., 2008; Yang et al., 2009; Domingos et al., 2009). Though not completely equivalent, both systems lead to the conclusion that while significant fractions of Ti will associate with biomass and be present in

46

finished biosolids, a portion of the Ti will also be present in WWTP effluents that enter the aquatic environment.

Conclusions and Implications

To the best of our knowledge, this study is the first to provide evidence of the quantities, physical characteristics, and fate of Ti in a municipal WWTP. Given that nano-scale TiO_2 has been used by industry for decades, is currently one of the most utilized nanomaterials in consumer products, and is relatively easy to measure and image in complex biological matrices, TiO_2 is a prime candidate to serve as a *sentinel* for other nanomaterials, especially those of similar size and aggregation behavior, by indicating the possible fate of nanomaterials in a WWTP. Furthermore, monitoring the presence of TiO_2 in the environment may serve to identify locations where other ENMs may occur or accumulate in the future.

Through our field-scale investigation at a municipal WWTP, the concentrations of Ti at each point along the WWTP process train were quantified, thereby revealing the pathways of TiO_2 NPs into the environment as well as their relative significance. Although the majority of Ti sorbed to biomass, we found that 10 to 100 µg/L Ti still remained in effluents. This study, therefore, defines environmentally relevant concentrations for studying the toxicity of TiO_2 NPs to organisms.

Results of the lab-scale experiments indicated that TiO_2 particles have an affinity for solids, and the majority of TiO_2 in water – on the order of 70 to 85% – will be removed by wastewater biomass concentrations of around 2,000 to 3,000 mg/L TSS. In addition, data obtained from lab experiments were

valuable for substantiating the Ti removal observed in the full scale WWTPs (both scales achieved comparable percentage Ti removals). This provides evidence that SBR experiments should be appropriate for evaluating the fate of other ENMs in cases where field-scale work is currently not possible, such as the many ENMs that occur in very low, difficult to detect concentrations because products containing these nanomaterials are not yet in widespread use.

While wastewater effluents are discharged primarily to surface waters (lakes, rivers, streams, oceans) and represent a significant potential point source for ENMs into the environment, the presence of TiO_2 and other ENMs is likely to be much higher in wastewater biosolids. Biosolids are usually used as agricultural land amendments (fertilizers), placed in landfills, incinerated, or dumped into oceans. Thus, biosolids may represent another point or non-point source of ENM release into the environment that is very different from WWTP liquid discharge, and these biosolid releases and resulting ecosystem exposures remain poorly understood.

Chapter 4

OCCURRENCE AND REMOVAL OF TITANIUM AT FULL-SCALE

WASTEWATER TREATMENT PLANTS: IMPLICATIONS FOR TIO₂

NANOMATERIALS[*]

Abstract

Titanium dioxide nanoparticles increasingly will be used in

commercial products and have a high likelihood of entering municipal sewage

that flows to centralized wastewater treatment plants (WWTPs). Treated

water (effluent) from WWTPs flows into rivers and lakes where nanoparticles

may pose an ecological risk. To provide exposure data for risk assessment,

titanium concentrations in raw sewage and treated effluent were determined

for 10 representative WWTPs that use a range of unit processes. Raw sewage

titanium concentrations ranged from 181 to 1233 µg/L (median of 26 samples

was 321 µg/L). The WWTPs removed more than 96% of the influent

titanium, and all WWTPs had effluent titanium concentrations of less than

25 µg/L. To characterize the morphology and presence of titanium oxide

nanoparticles in the effluent, colloidal materials were isolated via rota-

evaporation, dialysis and lyophilization. High resolution transmission

electron microscopy and energy dispersive x-ray analysis indicated the

presence of spherical titanium oxide nanoparticles (crystalline and

amorphous) on the order of 4 to 30 nm in diameter in WWTP effluents. This

research provides clear evidence that some nanoscale particles will pass

---

through WWTPs and enter aquatic systems and offers a methodological framework for collecting and analyzing titanium-based nanomaterials in complex wastewater matrices.

Introduction

Engineered nanomaterials may pose an ecological risk to aquatic organisms (Ziccardi et al., 2008; Scown et al., 2010; Yang et al., 2010; Crosera et al., 2009; Morimoto et al., 2010; Zhu et al., 2010; Baun et al., 2009; Kahru and Dubourguier, 2010; Koeneman et al., 2010). Risk assessment and management requires information on both toxicity and exposure. Hundreds of studies now exist on the potential toxicity of nanomaterials, but only a few exposure modeling papers and even fewer actual exposure sampling studies have been reported. This paper aims to expand our knowledge regarding release of nanomaterials, specifically titanium-based nanoparticles, from municipal wastewater treatment plants (WWTPs) into receiving waters (lakes, rivers, streams). WWTPs have been identified as a major point source for engineered nanomaterials entering into aquatic systems (O'Brien and Cummins, 2010; Gottschalk et al., 2010a; Stone et al., 2010; Gottschalk et al., 2010b; Gottschalk et al., 2009; Nowack and Bucheli, 2007). Research to determine the potential removal mechanisms for engineered nanomaterials during wastewater treatment has only recently begun (Brar et al., 2010; Yin et al., 2009; Kiser et al., 2009; Kang et al., 2009; Choi and Hu, 2009; Nyberg et al., 2008; Limbach et al., 2008; Westerhoff et al., 2007; Chin et al., 2006; Bae and Tak, 2005). These studies suggest that among different types of

nanomaterials, titanium dioxide (TiO_2) should occur at the highest concentration, and therefore TiO_2 is the focus herein.

Titanium (Ti) is the ninth most abundant element and the seventh most abundant metal in the Earth's crust (Barksdale, 1968). With significant worldwide reserves in excess of 600 million tons, the estimated annual production of Ti metal is 90,000 tons, and the annual production of titanium dioxide (TiO_2) is approximately 4.3 million tons (Emsley, 2001). Although Ti has numerous industrial applications, from metal alloys to aerospace technologies to biomedical devices, approximately 95% of mined Ti is refined into nearly pure TiO_2 through the treatment of Ti-bearing ores with carbon, chlorine, oxygen or sulfuric acid (USGS, 2009). Titanium dioxide is widely used in industry, commercial, residential and personal care products from paint to paper to toothpaste (Braun, 1997). Much of the TiO_2 used today is in the form of nanoparticle aggregates or micron-sized materials (i.e., bulk TiO_2 products), but industry trends suggest much higher usage of nano-TiO_2 in the near future (Robichaud et al., 2009). Titanium dioxide is one of the most common nanomaterials used in nano-based products (PEN, 2010). Recent analyses suggest that nanoscale TiO_2 will begin to dominate the bulk TiO_2 market because the nanoscale materials are transparent to visible light, are highly UV absorbent, have an iridescent quality, and are photocatalysts (Robichaud et al., 2009; Auffan et al., 2010b). The surface properties of TiO_2 are often modified to improve its dispersion in products or to suppress undesirable toxic effects (Auffan et al., 2010b), and it has been shown that surface properties affect the fate and toxicity of nanomaterials in WWTPs

and aquatic systems (Kiser et al., 2010; Labille et al., 2010; Auffan et al., 2010 a; Keller et al., 2010; Sharma, 2009; Zhang et al., 2008a; Zhang et al., 2008b). Despite a wide number of analytical techniques capable of size separating nanomaterials (e.g., field flow fractionation, hydrodynamic separation, centrifugation, ultrafiltration) prior to quantification, few have actually been applied to full-scale WWTP samples. Likewise, the ability to isolate titanium oxide nanomaterials from WWTP effluent samples for electron microscopy characterization remains a significant technical challenge.

Previously, we monitored for titanium over time and between unit processes at one WWTP. To assess the representative nature of that facility, we now report titanium concentrations at the same facility along with nine other WWTPs representing a broad spectrum of different types of unit processes. Raw sewage and effluent samples were collected and analyzed for titanium. Because of low titanium concentrations in the effluents and a desire to obtain solid-state (lyophilized) samples from the effluents for electron microscopy characterization, large volume samples (20 to 30 liters) were collected, concentrated via rota-evaporation, and purified via dialysis prior to freeze drying (lyophilization). Titanium concentrations in the solids after lyophilization were quantified by ICP, and solids were analyzed by transition electron microscopy (TEM) with energy dispersive x-ray (EDX) analysis to confirm the presence of titanium oxide (TiO_x) nanoparticles. We also discuss removal mechanisms for nanoscale titanium dioxide across the different types of unit processes at the 10 WWTPs sampled.

Materials and Methods

Description of Field Sites and Sampling Protocol

Samples were collected between April and August 2009 from 10 full-scale municipal WWTPs from southern to central Arizona. The facilities ranged in size, with flows from 0.1 to 7 m³/s. The WWTPs employed a range of different biological treatment processes (Figure 4.1 and Table 4.2): conventional activated sludge, trickling filter, microfiltration (~0.1 μm), membrane bioreactor (MBR), nitrification and denitrification, or various
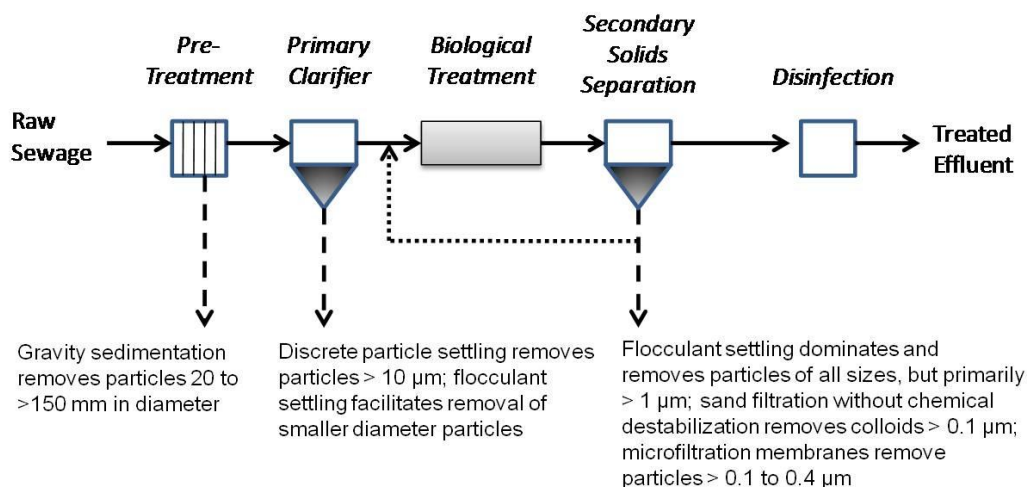
Figure 4.1. General wastewater treatment process flow diagram indicating removal mechanisms for titanium nanoparticles.
combinations of these processes.

The water quality of each effluent was determined using methods reported elsewhere (Song et al., 2010) (Table 4.1). Grab samples were collected from the headworks and effluent (prior to disinfection) at each WWTP. Samples for titanium detection were collected in acid washed 250-mL Nalgene bottles. Samples for colloidal separation were collected in clean 20-liter carboys.

Table 4.1

Sample identification and bulk water quality characteristics from 10 WWTPs

WWTP ID	Bulk Water Quality of Wastewater Effluents					
	COD mg/L O_2	DOC mg/L C	TDN mg/L N	Ammonia mg/L N	Nitrate-N mg/L N	Nitrite-N mg/L N
1	19	6.7	3.0	0.1	2.9	0.1
2	9	8.6	5.9	<0.1	5.3	<0.1
3	19	8.6	4.8	1.5	1.7	0.4
4	16	8.0	5.6	0.3	4.1	0.1
5	18	7.3	15.5	1.0	11.6	0.4
6	40	10.7	36.7	20.6	9.3	12.8
7	34	8.6	3.4	0.2	3.1	0.1
8	29	9.8	34.3	25.6	3.6	0.6
9	18	7.2	5.2	0.4	3.9	0.1
10	21	6.7	4.8	1.3	4.1	0.1

Table 4.2

Occurrence of titanium in WWTP headworks and treated effluent

WWTP ID	Primary Sediment.	Biological Treatment	Secondary Sediment.	Other Separation Processes	Eff. COD (TDN), mg/L	Titanium Content of Water (µg Ti/L)		
						Headworks[1]	Treated Effluent[1]	Treated Eff. (HCl-Colloid Separation)[2]
1	✓	AS	✓	—	19 (3)	615 ± 538	5 ± 3	3.8
				MF			< 2	
				RO			< 2	
2	✓	AS	✓	TertF	9 (5.3)	180 ± 30	7 ± 7	0.6
3	✓	AS	✓		19 (4.8)	363 ± 119	3 ± 1	1.1
4	✓	AS	✓		16 (5.6)	141 ± 28	2 ± 2	0.4
5	✓	AS & lagoons	✓		18 (15)	581 ± 125	18 ± 3	2

Ti after digestion of [1]water samples (MDL of 0.5 µgTi/L) or [2]lyophilized HCl-colloid separation samples (detection limit < 0.1 µg/L because large mass could be used); [3] TSS concentration of activated sludge in MBR is 3 to 5 times larger than activated sludge in WWTPs with secondary gravity separation. AS: activated sludge, MF: microfiltration, RO: reverse osmosis, TF: trickling filter, TertF: tertiary filtration, SMM: submerged MF membrane

Table 4.2, Continued

Occurrence of titanium in WWTP headworks and treated effluent

WWTP ID	Primary Sediment.	Biological Treatment	Secondary Sediment.	Other Separation Processes	Eff. COD (TDN), mg/L	Titanium Content of Water (µg Ti/L)		
						Headworks[1]	Treated Effluent[1]	Treated Eff. (HCl-Colloid Separation)[2]
6	✓	Pure O$_2$ AS	✓		40 (37)	NA	8 ± 4	5.4
7	✓	AS	✓		34 (3.4)	233 ± 57	2 ± 1	6.2
8	✓	TF	✓		29 (34)	549 ± 57	13 ± 3	7.1
9	✓	AS[3]		SMM	18 (5.2)	310 ± 23	< 2	0.2
10	✓	AS[3]		SMM	21 (4.8)	422 ± 40	4 ± 2	0.8

Ti after digestion of [1]water samples (MDL of 0.5 µgTi/L) or [2]lyophilized HCl-colloid separation samples (detection limit < 0.1 µg/L because large mass could be used); [3] TSS concentration of activated sludge in MBR is 3 to 5 times larger than activated sludge in WWTPs with secondary gravity separation. AS: activated sludge, MF: microfiltration, RO: reverse osmosis, TF: trickling filter, TertF: tertiary filtration, SMM: submerged MF membrane

Colloid Isolation

Two types of colloids were isolated using rota-evaporation followed by dialysis using established methodologies (Song et al., 2010; Leenheer et al., 2007; Leenheer, 2009): (1) inorganic plus organic colloids (HCl colloids) isolated by dialysis against hydrochloric acid (HCl), which removed carbonate and acid-soluble salts (Leenheer et al., 2004), and (2) HCl-HF-colloids isolated by dialysis of HCl colloids with hydrofluoric acid (HF) to remove silica and other inorganics. Effluent samples (20 to 30 L) were filtered immediately after delivery to the laboratory through a Balston inline glass-fiber filtration system (100-25-AH, nominal pore size 0.9 µm). The filtrate was kept at 4°C before rota-evaporation. The sample was adjusted with 6 M HCl to pH 4 and concentrated using a Buchi Rotavapor 220 to a salt slurry (200 to 500 mL). The slurry was loaded in a 3,500 Da dialysis tube and dialyzed against 4-L of 0.1 M HCl until all salts were visually dissolved and the color of the permeate solution was negligible; the permeate was then discarded. The HCl-treated colloids were then dialyzed against deionized water (DI) until the permeate solution conductivity was less than 100 µS cm^{-1}. The isolated colloids were separated into two parts. One half was freeze-dried; this is termed HCl-treated colloids. The other half was dialyzed for at least 24 hours against 4-L of 0.2 M HF to remove silica or silicates and then dialyzed repeatedly against DI water until the permeate conductivity was less than 10 µS cm^{-1}. This half of the colloids, after HF dialysis, was freeze-dried and is henceforth referred to as HCl-HF colloids. A complete

description of this separation method and subsequent characterization of nanoscale material is available elsewhere (Song et al., 2010).

Control studies were difficult to develop to evaluate potential artifacts arising from the isolation procedure. Distilled water was processed through the roto-evaporation step to determine if atmospheric dust or other contaminants would affect titanium content of solids. Minimal solids formed and titanium was not present. Titanium dioxide nanomaterials were observed to be stable against the dialysis liquids used above at room temperature. Because titanium has an extremely low solubility, precipitation of titanium solids from titanium ions during roto-evaporation was unlikely. However, for other inorganic materials (silver, silica, etc.) such precipitation concerns would exist. Therefore, the method employed here may only be suitable for materials such as titanium dioxide. Overall, the best validation of the roto-evaporation and dialysis method was determined to be a comparison of titanium content before and after roto-evaporation and dialysis. Closure of the mass balance could demonstrate that there was no loss or addition of titanium during the process.

Analytical Methods

Because TiO_2 has very low solubility (Antignano and Manning, 2008), Ti in wastewater is expected to occur solely in solid phases, not in ionic forms. For the quantification method used in this investigation, these solid phases must be transformed into ionic forms by acid digestion. Liquid and solid samples were acid digested using the HNO_3/H_2SO_4 digestion method for Ti as described by Standard Method 3030 G for water and wastewater analysis

(APHA et al., 2005). The digested samples were analyzed by Inductively

Coupled Plasma Optical Emission Spectroscopy (ICP-OES) (iCAP 6000

Series, Thermo Scientific, Cambridge, UK). The method detection limit

(MDL) is 0.5 µgTi/L based upon running 10 replicates of 2 and 5 µgTi/L

(USEPA, 2011). DOC was measured by a Shimadzu TOC-V$_{CSH}$ total organic

carbon analyzer. Total dissolved nitrogen (TDN), chemical oxygen demand

(COD), ammonia, nitrate, and nitrite were measured by HACH DR5000

using the following HACH kits of TNT 828, method 8000, TNT 831, TNT-

836/835, and TNT 839.

Nanoparticle images were obtained using high resolution transmission

electron microscopy (HR-STEM Phillips CM200/FEG equipped with an

energy dispersion X-ray microanalysis system (EDS)).

Results

Titanium Removal at Full-Scale WWTPs

Samples were collected from headworks and treated effluent of ten

full-scale WWTPs and analyzed for titanium after acid digestion. The

influent titanium concentration averaged 377 µg/L (median of 321 µg/L; 26

samples) and ranged from 181 to 1233 µg/L. On a percentile distribution, the

90th-, 75th-, 25th- and 10th-percentile influent titanium concentrations were

579, 463, 215 and 163 µg/L (n = 26). Overall, the concentration range is

similar to that which we previously reported for a single plant sampled

several times between 7 am and 5 pm on a single day (Kiser et al., 2009). We

also demonstrated that the morphology of titanium in water and settled

biosolids falls into one of three categories, which were similar to those used to

categorize titanium in foods (Kiser et al., 2009; Powell et al., 1996): type I -
spheres of TiO_2, 100-200 nm in diameter, characterized as the synthetic food
additive polymorph anatase; type II - aluminosilicates, <100-400 nm in
length, generally of flaky appearance, often with adsorbed surface iron, and
mostly characteristic of the natural clay mineral kaolinite; and type III -
mixed environmental silicates without aluminum, 100 to >700 nm in length
and of variable morphology.

Titanium concentrations in treated effluent were significantly lower
than those at the headworks (Table 4.1). Only two facilities (#5, #8) had Ti
concentrations greater than 10 μg/L, and these systems achieved nitrification
(i.e., most of the total dissolved nitrogen (TDN) present as nitrate) but not
denitrification. It may be that the denitrification step has biosolids surfaces
suitable for removing titanium bearing colloids or nanoparticles. The other
facilities had low Ti concentrations in treated effluent. Whereas the titanium
concentrations at the headworks exhibited large variations among duplicate
samples, presumably due to variable loading, sources and size of Ti-bearing
materials, the effluent samples had low variability and usually differed by
<10 μg/L among replicate samples. On a percentile distribution, the 90th-,
75th-, 25th- and 10th-percentile effluent titanium concentrations were 16, 10, 4,
3 and 0.7 μg/L (n = 30). Although the effluent concentrations were near our
MDL for titanium in water (0.5 μg/L), treated effluent from microfiltration
membrane systems consistently exhibited the lowest Ti concentrations.
Microfiltration membrane systems have pore sizes of 100 to a few hundred
nanometers.

Titanium in Colloidal Fraction from WWTP Effluents

Because effluent titanium concentrations were low and near the detection limits of the ICP-OES, a technique was developed to separate and concentrate colloidal material, including titanium, from the effluent. Rota-evaporation reduced the sample volume by approximately 250- to 500-fold. These rota-evaporated samples underwent dialysis against HCl, or HCl and then HF, prior to freeze drying. A freeze-dried sample (70 to 200 mg) was then weighed and acid digested. Titanium concentrations in the acid matrix ranged from 7.2 to 180 µg/L (average was 61 µg/L); duplicate digestions on three samples had less than 15% variation. These concentrations are well above the detection limit of the ICP-OES. The mass of HCl colloids separated from the water ranged from 11 to 80 mg/L (average 34 mg/L; Table 4.3), as indicated on the x-axis in Figure 4.2. The total mass of HCl colloids separated from the water, multiplied by the Ti content of the HCl colloids after acid digestion, divided by the initial volume of water from which the colloids were separated, yields an estimate of the titanium content present in the wastewater effluent. These values are expressed on the y-axis in Figure 4.2. The trend line in Figure 4.2 suggests that effluent samples from across Arizona with different types of treatment exhibit similar titanium content per unit colloid mass present in the wastewater effluent. The slope of the line (95 µgTi/mg colloid) provides a reasonable estimate for the titanium content of WWTP effluents in Arizona, and the arithmetic average dry mass content of the HCl colloids was 66 µgTi/mg dry weight of HCl colloids. The

61

sample from Facility #1 appeared to be an outlier and is discussed further in the microscopy section.

Table 4.3

Analysis of HCl colloids and HCl-HF colloids

WWTP ID	HCl Colloids				HCl-HF Colloids			
	Isolated mass mg	Yield mg/L	Moisture %	Ash %	Isolated mass mg	Yield mg/L	Moisture %	Ash %
1	354.5	15.3	6.3	73.3	50.0	2.2	5.4	13.5
2	655.3	24.9	5.0	89.2	30.6	1.2	7.3	5.2
3	669.1	26.6	36.7	50.6	54.1	2.2	5.4	10.8
4	620.0	23.0	10.1	66.9	103.6	3.8	4.0	36.4
5	862.1	34.4	1.9	76.1	229.1	9.1	4.2	22.8
6	1522.2	57.4	6.2	65.5	286.4	10.8	3.3	33.8
7	2547.5	79.6	12.8	78.8	744.5	23.3	2.7	80.1
8	1364.1	51.1	4.5	77.5	299.6	11.2	2.9	29.8
9	291.7	11.4	3.4	82.2	24.6	1.0	19.4	0.0
10	433.2	14.0	12.3	79.9	24.3	0.8	7.6	31.8
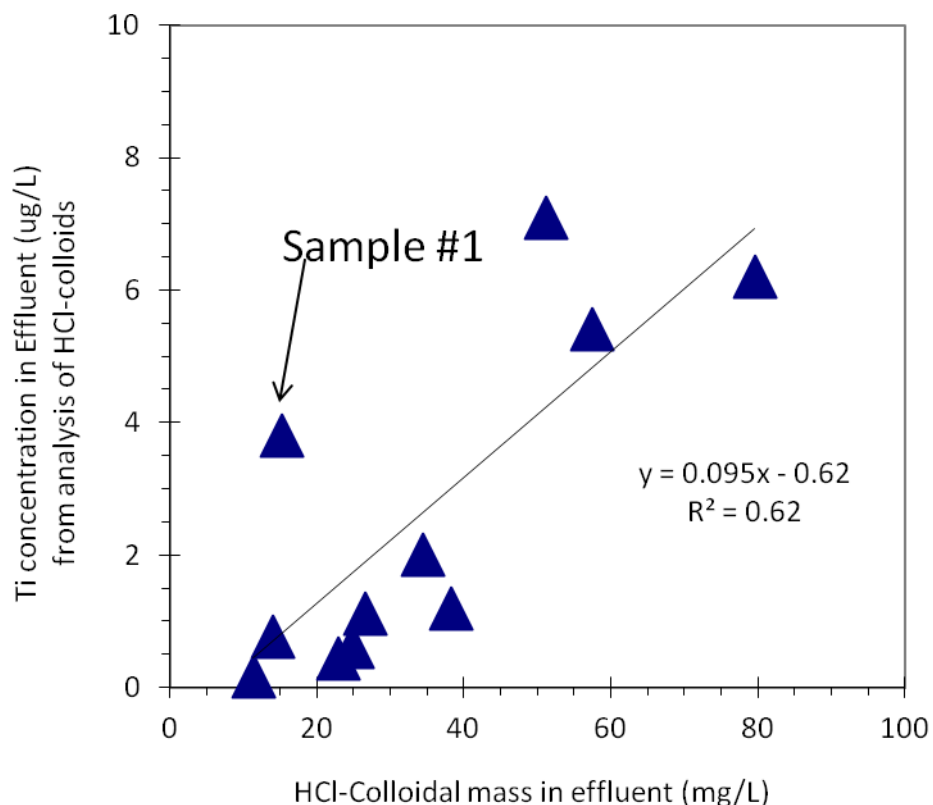
Figure 4.2. Comparison of titanium content in HCl colloids relative to the total colloidal concentration separated from the WWTP effluent.

While the roto-evaporation and dialysis methods were primarily designed to obtain samples for electron microscopy analysis, comparison of titanium content of the isolated samples to the bulk water samples was considered important to validate the procedure. Titanium concentrations calculated from the separation method ranged from 0.2 to 7.1 µg/L for the WWTP effluents (Table 4.2). The difference between the direct measurement of titanium in the treated effluent and the calculation of titanium content from the separated and acid-digested HCl colloids was relatively small. That is, the separation technique gave the same order of magnitude titanium

concentration as the direct measurement of titanium in the treated effluent. The membrane bioreactor plants had among the lowest titanium concentrations. The largest variation was observed in sample ID#5, which was one of the three samples run in duplicate. The small discrepancies between the two approaches for obtaining titanium data can be attributed mainly to obtaining the entire dry mass of HCl colloids accurately and assuring complete digestion of some Ti-containing silicates. Overall, we deemed the rota-evaporation and dialysis technique acceptable for separating and concentrating Ti-bearing colloids from large volume and dilute water samples.

Electron Microscopy Characterization of Colloids from WWTP Effluents

Electron microscopy was conducted on most of the colloidal samples, including samples from the same location both before and after HCl or subsequent HF treatment. Select samples are presented that represent the overall trends observed. HCl treatment removes most of the carbonates and hydroxides, whereas additional HF-HCl treatment dissolves most of the silicates. The most significant finding is that TiO_x nanoparticles are present in treated wastewater effluent. Clusters of TiO_x nanoparticles in the HCl-HF treated colloid WWTP effluent sample from Facility #2 are shown in Figure 4.3.
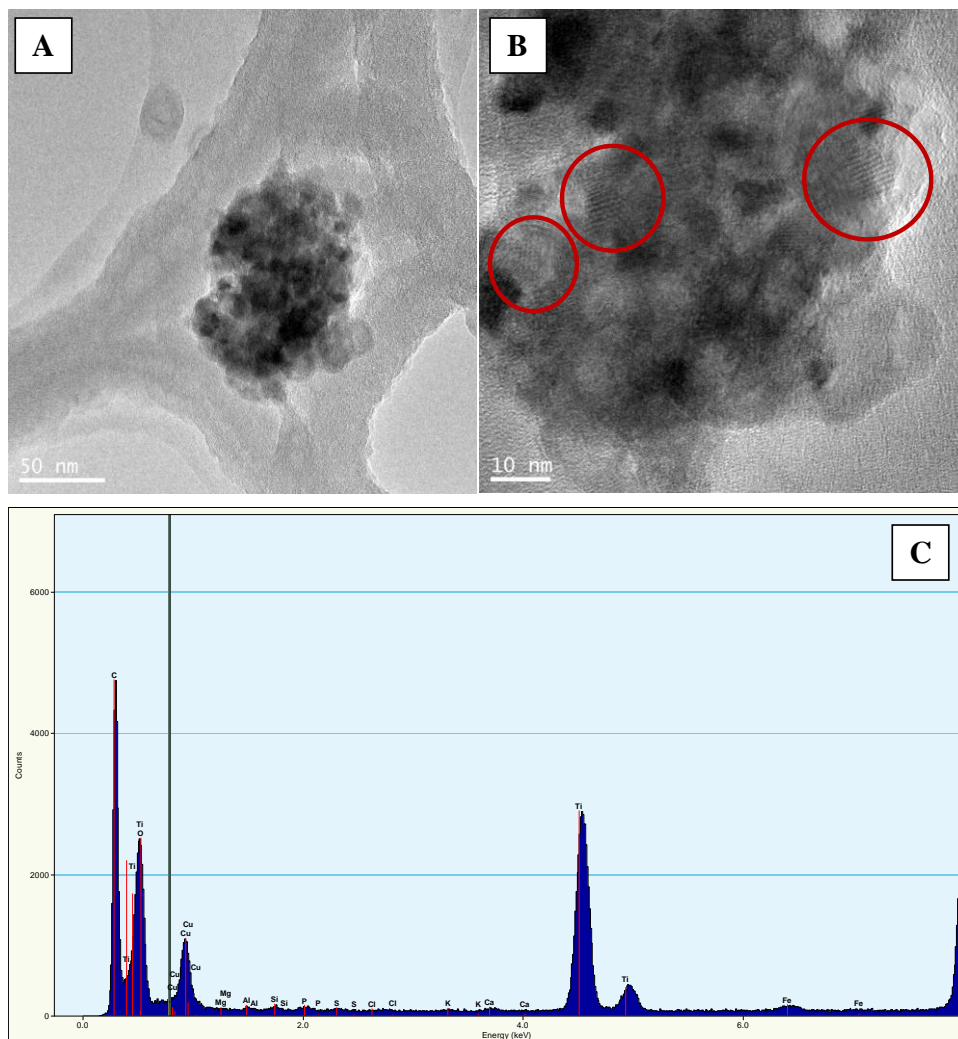
Figure 4.3. TEM images of (A) clusters of nanoparticles in the HCl-HF treated colloid WWTP effluent sample from facility #2; (B) high resolution TEM image of the cluster indicates the presence of nanoparticles with diameters of approximately 10 nm that have crystalline lattices (inside circles); (C) EDS of cluster indicating elemental composition.

A high-resolution TEM image of the cluster indicates the presence of nanoparticles with diameters of approximately 10 nm that have crystalline lattices. EDS of the cluster indicated the presence of primarily Ti, O, Cu and C, with trace amounts of other elements. Copper and carbon are present in the TEM grid. Carbon, and some oxygen, is present in the sample as colloidal

65

organic material (Song et al., 2010). The crystalline lattice, dominant Ti and O peaks, and lack of silica support the conclusion that TiO_x nanoparticles are present in the sample. The TiO_x nanoparticles also appear to be fused together; this could represent the morphology of the TiO_x as used in society or may have occurred during colloid isolation and preparation.

TiO_x nanoparticles from the same site (Facility #2) could not be identified in HCl-colloid samples. On the basis of EDS analysis, the HCl-treated samples contained high concentrations of silicon dioxide nanoparticles, which formed large clusters of discrete nanoparticles (Figure 4.4); titanium was present in these samples but at very low elemental mass ratios due to the large amount of silica present. High resolution TEM indicates that the discrete nanoparticles were approximately 20 to 30 nm in diameter (Figure 4.4B), larger than the TiO_x nanoparticles observed after HCl-HF treatment (Figure 4.3). Figure 4.4B indicates that the nanoparticles are amorphous, unlike the more crystalline TiO_x nanoparticles shown in Figure 4.3B. The amorphous silica-based nanoparticles may be present in the WWTP effluent or may form during colloid isolation. In the HCl-treated sample from Facility #1 (not shown) silica particles were non-spherical structures, rather elongated and planar with sharp edges. Additional research is underway to address the presence of silica nano-structures, but is important to note because titanium is often substituted for silica with silicate minerals.
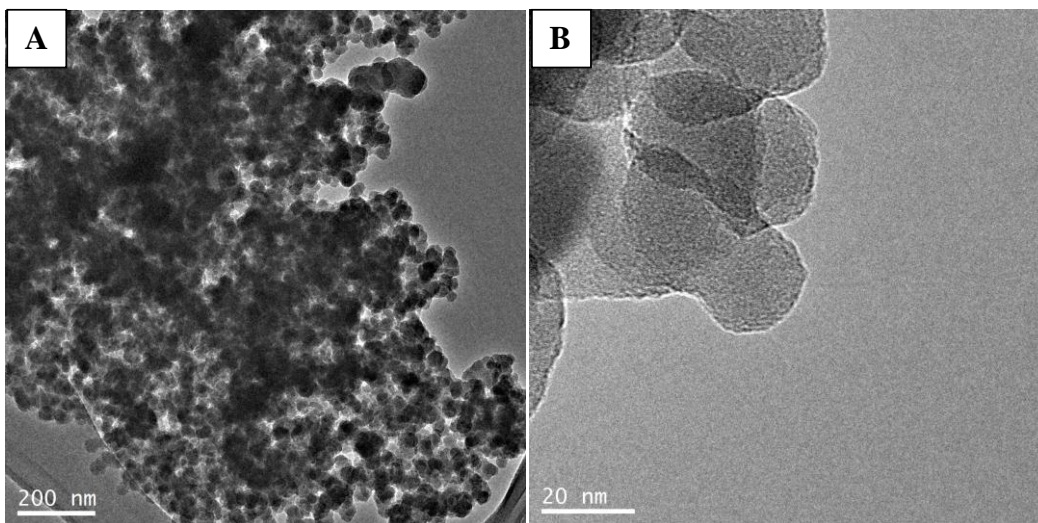
Figure 4.4. TEM images showing (A) primarily silicon dioxide nanoparticles in HCl treated sample from Facility #3; (B) high resolution image showing amorphous minerals.

A few additional examples of the different types of titanium structures present after HCl-HF treatment are illustrated in Figure 4.5. Samples from Facility #8, which contained the second largest mass concentration of titanium in the WWTP effluent (Table 4.2), indicate the presence of very small (~ 4-5 nm diameter) nanoparticles (dark spheres) embedded in an amorphous matrix of colloidal organic matter and some silica. High resolution TEM could not determine if these small spheres were crystalline, but EDS confirmed high levels of titanium and oxygen with lower amounts of carbon, copper and silica. The high abundance of TiO_x nanoparticles in samples from Facility #8 meant that they could be imaged after only HCl treatment (not shown); larger crystalline structures (20 to 30 nm) were observed in these images. In addition, larger titanium-containing particles were found in HCl-treated samples from Facility #6. These particles were

aggregated with silica nanoparticles in large clusters with sizes of several micrometers, as illustrated in Figure 4.5B. Based on EDS analysis (not shown), the particles were composed of iron phosphate in addition to magnesium and titanium. Samples from Facility #1 differed from those from Facilities #3, #6 or #8 described above. TiO_x nanoparticles with sizes of 4 to 5 nm were present in HCl-HF treated colloids from Facility #1. However, these nanoparticles (Figure 4.5D) appeared to be encased in large particles containing iron, aluminum, chloride phosphate, and sulfate (Figure 4.5C). These mineral differences as well as the differences in silica morphology noted above in the Ti-bearing material from Facility #1 may shed light on why this site is somewhat of an outlier in Figure 4.2.
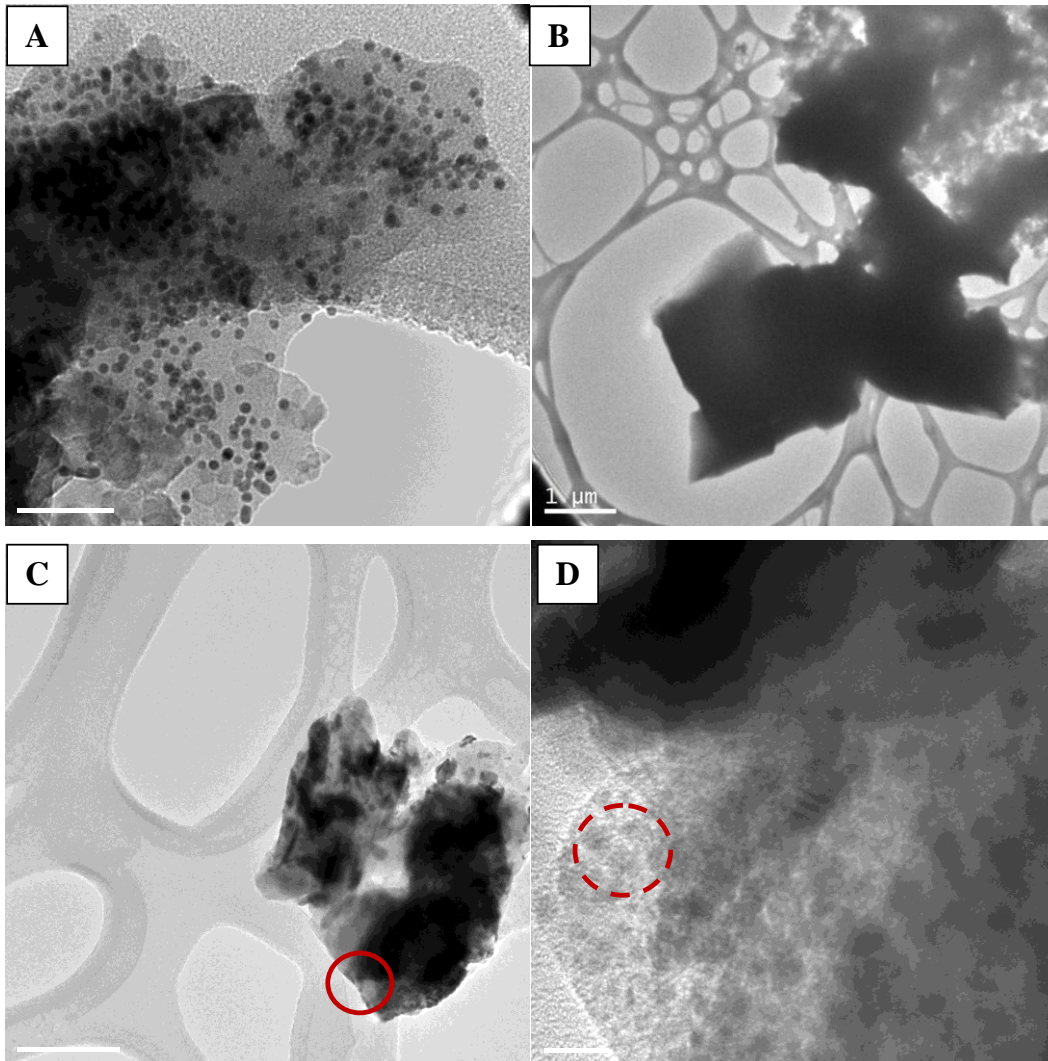
Figure 4.5. TEM images of samples after HCl-HF treatment from (A) Facility #8; (B) Facility #6; (C) Facility #1; (D) high resolution image of the circled region in (C) in which the dashed circle shows the presence of Ti-based nanoparticles that appear embedded in a larger mineral.

Discussion

Removal of the colloid-sized material in treated wastewater is affected by the design and operational efficiency of each unit process (sedimentation, granular media and/or membrane separation). Previous mass flow modeling of nanomaterials during wastewater treatment considered fixed removal

efficiencies (97%) of particles based solely on their size <100 nm or uniform removal distributions (90.6% to 99.5%) as determined by bench-scale studies in the presence of biomass (Gottschalk et al., 2009; Mueller and Nowack, 2008). Based on Table 4.2, the overall removal efficiency of titanium is quite high (96.1% to 99.4% with an average removal of 98.3%). However, previous research in which we conducted size fractionation of titanium across one of the facilities included in this paper indicated quite low removal (<30%) of titanium that passed through a 0.7 μm nominal size glass fiber filter (Kiser et al., 2009). Several observations may reconcile these apparent differences.

First, not all titanium present in wastewater is of a nano- or colloidal size of <100 nm. In fact, as Figures 4.3-4.5 indicate, the TiO_x nanoparticles we detect in wastewater effluents appear to be 4 to 30 nm in diameter. Typical WWTP sedimentation processes are designed with surface loading rates on the order of 30 m/day. On the basis of discrete particle settling (i.e., Stokes settling velocities), these loading rates are suitable only for removing particles larger than 5 to 10 μm and particles with densities of 1.5 to 4.5 g/cm^3 at 20°C ; TiO_2 has a density of ~ 4.2 g/cm^3. Thus sedimentation (primary or secondary, Figure 4.1) cannot remove discrete and stable NPs with sizes < 0.1 μm. Titanium-containing particles (e.g., clays), aggregates and clusters of TiO_2, or TiO_2 sorbed to biomass could be large enough to settle. Actual removals and minimal size removed are difficult to calculate due to a process called flocculant settling in which aggregating particles continually change in size, shape, and specific gravity (Davis and Cornwell, 1991). Thus the size distribution of titanium in WWTP influent and across

70

WWTP unit processes strongly influences its potential for removal by sedimentation processes.

Second, biological treatment processes designed to decompose domestic and industrial compounds through metabolic processes and cellular growth can affect nanoparticle removals. Two basic means of biological treatment were included in our sampling campaign. Suspended biomass in activated sludge processes was the most common, whereas attached biofilms were used only at Facility #8, which employed trickling filters. Diffusion governs the movement of nanoscale particles, including nano-TiO_2, near and within biofilms and suspended biomass (Brar et al., 2010). Many types of nanoparticles, including TiO_2, readily sorb to suspended biomass from WWTPs (Kiser et al., 2010). Once attached, the removal of the NP becomes connected to the management and removal of the suspended biomass. WWTP secondary sedimentation unit processes are very effective at settling biomass and thus would remove sorbed NPs. This explains the high removals reported in the batch experiments that served as the basis for mass flow modeling of NPs (Gottschalk et al., 2010a; Limbach et al., 2008). Furthermore, NPs undoubtedly sorb to attached biomass (i.e., biofilms in trickling filters), although no data specifically related to WWTPs is yet available. However, filter media coated with biofilm extracellular polymers retained more NPs than uncoated filter media to an extent unaccountable for simply by electrostatic attraction (Tong et al., 2010). Carboxylated and PEG-coated quantum dots also accumulated in biofilms (Morrow et al., 2010). In the presence of high concentrations of NPs, biofilm sloughing due to silver

NPs was observed, whereas carbon nanotubes affect biofilm attachment and exhibit potential NP-biofilm interactions (Fabrega et al., 2009; Upadhyayula and Gadhamshetty, 2010).

Third, although filtration processes are common in some European countries, most WWTPs in the USA do not include them (Mueller and Nowack, 2008). However, submerged and pressurized microfiltration membrane systems are becoming an increasingly common means of achieving secondary solids separation (Figure 4.1) and are part of two sampled facilities (Table 4.1). These membranes commonly have 0.1- to 0.4-µm pore sizes and achieve very high levels of colloid removal (Meng et al., 2009). Although the beneficial use of nanoparticles in conjunction with innovate membrane treatment systems have been identified, few reports specifically on rejection (i.e., removal) of engineered nanoparticles from wastewater by membranes currently exist (Chin et al., 2006; Bae and Tak, 2005; Guo et al., 2010; Jassby et al., 2010; Lippa et al., 2009; Theron et al., 2008). In one study, ultrafiltration membranes were observed to remove polystyrene or magnetic nanoparticles (20 to 250 nm) better than microfiltration membranes did. The removal mechanisms for colloids and membranes are complex and involve not only size exclusion but also colloid surface charge interactions with bare membrane or membrane foulants; the mechanisms are also affected by water movement (dead-end versus cross-flow membrane designs). Based on the TSS, COD and NP data presented in Table 4.2, the membrane bioreactor facilities (#9 and 10) achieved among the highest water quality. These facilities use microfiltration membranes to separate activated sludge

suspended biomass from the water. In contrast, Facility #1 processes

secondary settled water (biomass separation process) through microfiltration

as a pretreatment for reverse osmosis. The microfiltration removes greater

than 60% of the titanium-bearing nanoparticles present in the secondary

settled water (Table 4.2). Overall, micro- or ultrafiltration membrane

processes appear capable of achieving the highest levels of NP removal as

compared with trickling filter or activated sludge systems with conventional

gravity secondary sedimentation.

Summary and Conclusions

Titanium oxide (TiO_x) nanoparticles were detected in wastewater

effluents from 10 municipal facilities at concentrations ranging from <2 to 20

µg/L, which is consistent with our previously reported findings from a single

WWTP (Kiser et al., 2009). The biological wastewater treatment facilities

removed, on average, 98.3% of the incoming titanium, although the size and

composition of materials containing titanium in the influent wastewater

sewage was not characterized. Attached (trickling filters) and suspended

(activated sludge) biological treatment processes play an important role in

"trapping" NPs in biomass, which can then be settled or removed via

membrane filtration.

This paper is the first to identify TiO_x nanoparticles in WWTP

effluents by high resolution TEM, which indicates that they are 4 to 30 nm in

diameter and roughly spherical. WWTP effluents commonly discharge

treated water into lakes, rivers and streams, and this work clearly documents

that the release of nanoscale TiO_x into the environment is possible. It

appears that microfiltration-treated wastewaters contain fewer nanoparticles than conventionally settled wastewater, and this additional benefit to the use of membranes in wastewater treatment should be explored. Although beyond the scope of this titanium-focused paper, our findings suggest the presence of silica nanoparticles in wastewater effluents at far higher concentrations than TiO_x. Our study was not designed to quantify silica nanoparticles, which would require working with non-silica-based sampling equipment, filters, and separation techniques that could avoid potential precipitation of silica colloids, but this is the focus of ongoing research.

Chapter 5

BIOSORPTION OF NANOPARTICLES TO HETEROTROPHIC

WASTEWATER BIOMASS*

Abstract

Sorption onto activated sludge is a major removal mechanism for pollutants, including manufactured nanoparticles (NPs), in conventional activated sludge wastewater treatment plants. The objectives of this work were to (1) image sorption of fluorescent NPs to wastewater biomass; (2) quantify and compare biosorption of different types of NPs exposed to wastewater biomass; (3) quantify the effects of natural organic matter (NOM), extracellular polymeric substances (EPS), surfactants, and salt on NP biosorption; and (4) explore how different surface functionalities for fullerenes affect biosorption. Batch sorption isotherm experiments were conducted with activated sludge as sorbent and a total of eight types of NPs as sorbates. Epifluorescence images clearly show the biosorption of fluorescent silica NPs; the greater the concentration of NPs exposed to biomass, the greater the quantity of NPs that biosorb. Furthermore, biosorption removes different types of NPs from water to different extents. Upon exposure to 400 mg/L TSS of wastewater biomass, 97% of silver nanoparticles were removed, probably in part by aggregation and sedimentation, whereas biosorption was predominantly responsible for the removal of 88% of aqueous fullerenes, 39% of functionalized silver NPs, 23% of nanoscale titanium dioxide, and 13% of fullerol NPs. Of the NP types

investigated, only aq-nC$_{60}$ showed a change in the degree of removal when the NP suspension was equilibrated with NOM or when EPS was extracted from the biomass. Further study of carbonaceous NPs showed that different surface functionalities affect biosorption. Thus, the production and transformations in NP surface properties will be key factors in determining their fate in the environment.

Introduction

With the number of consumer products that contain manufactured nanoparticles (NPs) steadily rising, the release of increasing quantities of NPs into sewage and the environment is inevitable (PEN, 2009 ; Roco, 2005; Aitken et al., 2006; Nowack and Bucheli, 2007). This is cause for concern, as mounting evidence from toxicology studies points toward possible negative impacts of NPs on the human and ecosystem health (Nel et al., 2006; Handy and Shaw, 2007). Industrial and consumer use of NP-containing products and their disposal into sewage are already occurring (Benn and Westerhoff, 2008; Kaegi et al., 2008; Mueller and Nowack, 2008; Kiser et al., 2009). Municipal WWTPs are particularly important sources of contaminant release into the environment, as they provide potential pollutant pathways into surface waters, soils, and air through treated effluent, biosolids, and plant-generated aerosols (Handy et al., 2008; Limbach et al., 2008; Mueller and Nowack, 2008). Thus, the spatial distribution of NPs in the environment may be determined in part by their passage through WWTPs. However, very little information is available on factors affecting NP removal in WWTPs.

Sorption on organic and inorganic solids is one of the primary physical removal mechanisms of pollutants in conventional activated sludge (CAS) WWTPs, resulting in accumulations of these compounds in biosolids at concentrations several orders of magnitude higher than in plant influents (Dobbs et al., 1989; Jacobsen et al., 1993). The highest concentration of solids along the treatment train in CAS WWTPs is found in the aeration basins, where concentrations typically range from 1,000 – 5,000 mg/L of total suspended solids (TSS) (Metcalf and Eddy, 2003). Activated sludge is used to reduce concentrations of nutrients, suspended solids, metals, synthetic organic chemicals, and pathogens in wastewater. Inert and active heterotrophic bacteria and extracellular polymeric substances (EPS), the main constituents of activated sludge, play a significant role in the sorption of contaminants (Sheng et al., 2008). In this paper, we use the term biosorption to refer to the net effect of all biomass-particle sorption mechanisms that remove NPs from water, including adsorption to cell surfaces, adsorption to EPS, and uptake into cells (absorption) through active or passive transport across the cytoplasmic membrane or through membrane disruption (Kloepfer et al., 2005). Wasted sludge from the treatment train is thickened and then applied to land as soil conditioners, land-filled, or incinerated (Kinney et al., 2006; Sabourin et al., 2009). These methods of handling biosolids could introduce relatively high concentrations of contaminants, including NPs, into the environment (Mueller and Nowack, 2008).

The overall aim of this study was to qualitatively and quantitatively describe biosorption of different types of NPs to wastewater biomass. More specifically, our main objectives were to (1) image biosorption of fluorescent NPs to wastewater biomass; (2) quantify and compare degrees of biosorption of different types of NPs; (3) quantify the effects of natural organic matter (NOM), extracellular polymeric substances (EPS), surfactants, and salt – common components in surface and wastewaters – on NP biosorption; and (4) explore how different surface functionalities of fullerenes affect their removal from water. The accomplishment of these objectives will begin to elucidate potential pathways of different types of NPs from WWTPs to the environment.

Materials and Methods

Nanoparticle Suspension Preparation

Silica NPs doped with fluorescein isothiocyanate (SiO_2-FITC) were used to image biosorption. For other sorption experiments, we used seven NP suspensions: two types of nonfunctionalized fullerenes (aq-nC_{60} and tol-nC_{60}), two types of functionalized fullerenes ($nC_{60}(OH)_x$ and nC_{60}-PVP), titanium dioxide (TiO_2), silver (Ag), and functionalized silver (f-Ag). These NPs were chosen because they are amongst the NPs produced in the greatest quantities, are found in a wide range of commercial products, and exhibit unique sizes and surface chemistries (PEN, 2009; Aitken et al., 2006; Benn and Westerhoff, 2008; Rebecca et al., 2009). Table 5.1 provides the measured properties of the NPs used in this study.

Table 5.1

Measured properties of NP stock suspensions

	Diameter (nm) Measured by PALS	Zeta Potential at pH ~7 (mV)	Functional Group Reported by Manufacturer	Mass Quantification Method
SiO_2-FITC	85	-50[a]	FITC	Fluor. Microscopy
aq-nC_{60}	88	-52	None	DOC
tol-nC_{60}	56	-23	None	DOC
$nC_{60}(OH)_x$	48	-21	Hydroxyl	UV/Vis, DOC
nC_{60}-PVP	100	-2	Polyvinylpyrrolidone	UV/Vis
TiO_2	40	-30	None	ICP-OES
Ag	13	-40	None	ICP-OES
f-Ag	3	-6	Carboxyl	ICP-OES

[a]Hegde and Babu (2004)

The SiO_2-FITC suspension was provided by the Center for Nano-Bio Sensors at the University of Florida. SiO_2-FITC NPs were prepared via the sol gel method using water-in-oil microemulsions (Bagwe et al., 2004).

Two types of nonfunctionalized fullerene (nC_{60}) suspensions were prepared. One suspension was made following the solvent exchange method with toluene (tol-nC_{60}) developed by Andrievsky et al. (Andrievsky et al., 1995), and the other was made using only water (aq-nC_{60}), without an organic solvent medium (Lyon et al., 2006). To make the tol-nC_{60} suspension, 99.9% C_{60} powder (MER Corporation; Tucson, AZ) was added to HPLC-grade toluene and magnetically stirred for 1 h. The characteristic purple-colored toluene-C_{60} solution was then added to ultrapure water and sonicated (2000U, Ultrasonic Power Corporation; Freeport, IL) at 200 W/L for 4.5 h.

Following sonication, the amber-colored suspension was vacuum filtered through a 0.7-µm GF/F filter (Whatman; Maidstone, UK) to remove larger aggregates. The aq-nC$_{60}$ suspension was prepared by adding 99.9% C$_{60}$ powder (MER Corporation; Tucson, AZ) directly to ultrapure water and sonicating at 200 W/L for 4.5 h. The suspension was filtered through a 0.7-µm GF/F filter.

Two types of functionalized nC$_{60}$ suspensions were prepared. The -fullerol (nC$_{60}$(OH)$_x$) suspension was prepared by adding C$_{60}$(OH)$_x$ powder (MER Corporation; Tucson, AZ) to ultrapure water, sonicating at 200 W/L for 1 h, and filtering the suspension with a 0.7-µm GF/F filter. The nC$_{60}$-PVP suspension was prepared following the procedure developed by Xiao et al. (2006). A C$_{60}$-toluene stock suspension was made by adding C$_{60}$ powder to toluene and sonicating in a water bath for 15 min. Following sonication, the C$_{60}$-toluene suspension was mixed with polyvinylpyrrolidone (PVP) solution (K30, Sigma Aldrich; St. Louis, MO) in chloroform (Mallinckrodt; Phillipsburg, NJ). Solvents were evaporated under purified nitrogen, and the residual solid was sonicated in ultrapure water and filtered through a GF/F filter.

The TiO$_2$ suspension was prepared by adding nanoscale ~ 99% TiO$_2$ (Hombikat, Sigma-Aldrich; St. Louis, MO) to ultrapure water and sonicating for 1 h at 200 W/L. Following sonication, the suspension was centrifuged at F = 1000 G for 30 min. The supernatant, which contained suspended TiO$_2$, was collected and used as stock solution. Ag and f-Ag suspensions were prepared in the same way as the TiO$_2$ suspension using 99% nano Ag powder (Sigma-

Aldrich) and concentrated citrate-functionalized Ag suspension (Vive; Ontario, Canada).

Portions of aq-nC_{60}, tol-nC_{60}, $nC_{60}(OH)_x$, TiO_2, Ag, and f-Ag suspensions were equilibrated with natural organic matter (NOM). For the NOM, a stock solution of Suwannee River fulvic acid (SR-NOM) (Standard 1S101F, International Humic Substances Society; pH ~ 7) was prepared from powdered solid by equilibrating 1,350 mg SR-NOM/L for several days to completely hydrate the material. Stock solution was added to the NP suspensions, the pH was adjusted to ~7 using HCl and NaOH, and the suspensions were allowed to equilibrate overnight before use. In one set of experiments, tol-nC_{60} was equilibrated with sodium dodecyl sulfate (SDS) (Sigma-Aldrich), a synthetic surfactant.

Biomass Collection and Preparation

For all experiments, activated sludge was collected from a full-scale, conventional activated sludge WWTP serving a metropolitan area in central Arizona, USA. Collected sludge was stored on ice at 4 °C until arrival in the laboratory. To minimize the amount of nutrients and other extraneous compounds from the matrix solution, the sludge was prepared as described below.

For experiments comparing the association of five different NPs (aq-nC_{60}, $nC_{60}(OH)_x$, TiO_2, Ag, and f-Ag) with biomass, activated sludge was rinsed three times with a buffer solution (10 mM NaCl, 4 mM $NaHCO_3$) and then centrifuged ($F = 350$ G) for 15 min; the centrifuged supernatant was discarded. The rinsed, dewatered activated sludge (referred to as wastewater

biomass) was divided into two portions. One portion (whole biomass) was stored at 4 °C without further processing. The other portion (EPS-extracted biomass) was processed as described by Esparza-Soto and Westerhoff (2001) to extract EPS from the biomass. The rinsed and dewatered sludge was resuspended in a pH 11 extraction solution (10 mM NaOH, 10 mM NaCl), such that the sludge-to-solution ratio was 1:4 by weight. Resuspended sludge was mixed on a shaker for 15 min and then centrifuged for 15 min ($F = 350$ G). The centrifuged supernatant containing separated and suspended EPS was decanted and discarded. The EPS-extracted wastewater biomass was washed once with buffer solution and stored at 4 °C until used in experiments.

For all other experiments, collected activated sludge was rinsed three times with and resuspended in 1- or 2-mM $NaHCO_3$ buffer solution. The pH of the buffer solution and biomass were adjusted to ~7 with HCl and NaOH. Only whole biomass was used for these experiments.

Batch Sorption Experiments

A series of glass vials containing NP suspension and buffer solution were spiked with biomass and agitated for a specified contact period. After agitation, biomass was gravitationally settled (approximately 30 min) to simulate settling in WWTP secondary clarifiers, and supernatant was collected from each sample and analyzed. Controls (no NPs; no biomass) were also made with the samples and agitated for the same duration. Table 5.2 lists the NP and biomass concentrations and the contact time used for each experiment. A range of biomass concentrations were chosen to

demonstrate sorption sensitivity (lower concentrations) and to approach the

solids concentrations found in aeration basins (higher concentrations).

Table 5.2

Sorbent and sorbate concentrations and contact times used in experiments

Experiment	NP	NP Initial Concentration(s) (mg/L)	Biomass Concentration(s) (mg/L TSS)	Contact Time (h)
SiO_2-FITC sorption and imaging	SiO_2-FITC	$1 - 50$	2,000	3
Comparison of NP biosorption	aq-nC_{60} $nC_{60}(OH)_x$ TiO_2 Ag f-Ag	4 (as C) 12 (as C) 0.5 (as Ti) 0.6 (as Ag) 0.5 (as Ag)	$50 - 1,000$	3
Effect of salt, SDS, and NOM on tol-nC_{60} biosorption	tol-nC_{60}	13 (as C)	1,500	1
Fullerene biosorption comparison	tol-nC_{60} aq-nC_{60} $nC_{60}(OH)_x$ nC_{60}-PVP	3 (as C) 3 (as C) 14 (as C) 2 (as C)	$50 - 2,000$	3

Short contact times of 1 and 3 h were chosen to minimize NP

aggregation and biodegradation, as well as growth or other changes in

biomass that would obscure effects due to biosorption. Furthermore, a 3-h

contact time falls within the range of typical hydraulic retention times for

conventional activated sludge WWTPs (Metcalf and Eddy, 2003). For SiO_2-

FITC, the solids of each sample were vacuum filtered with 0.7-μm GF/F filters and stored at 4° C until used for imaging. To increase ionic strength in the experiment focusing on tol-nC$_{60}$, sodium chloride (NaCl) (Sigma-Aldrich) was added to the buffer solution.

Analytical Methods

Biosorption of SiO$_2$-FITC NPs with biomass was imaged using fluorescence microscopy. Solid samples were applied with ultrapure water to a glass slide, which was observed using an epifluorescence microscope (Nikon Eclipse TE 300; Melville, NY) with a 20x objective lens (Nikon ELWD Plan Fluor/0.45 NA) and an illumination system (770 Opti Quip Model 1600 with a xenon bulb; Highland Mills, NY). Both bright-field and fluorescence images were captured for each slide. For fluorescence imaging, the excitation/emission wavelengths (nm) were set to 485/20 and 530/25, respectively, to observe the green light emitted by FITC molecules. Images were captured by a Quantix 12-bit CCD camera (Photometrics/QImaging Corp.; Blaine, WA).

The hydrodynamic diameters of nanoparticle suspensions were measured using phase analysis light scattering (PALS) (90 Plus, Brookhaven Instruments Corp.; Holtsville, NY). The SiO$_2$-FITC concentration was determined by measuring fluorescence at 408 nm with a luminescence spectrometer (LS 50 B, Perkin Elmer; Waltham, Massachusetts). The carbon concentration of the tol-nC$_{60}$ stock solution was determined by gravimetric analysis and UV/Vis absorbance measurement at 347 nm (MultiSpec-1501, Shimadzu; Kyoto, Japan) (Fortner et al., 2005). nC$_{60}$-PVP concentration was

determined by measuring UV/Vis absorbance at 340 nm and using a

published molar absorption coefficient of 49,000 (Yamakoshi et al., 1994).

Concentrations of carbon in aq-nC$_{60}$ and nC$_{60}$(OH)$_x$ stock suspensions and

samples were determined by measurement of dissolved organic carbon (DOC)

(TOC-V$_{CSH}$, Shimadzu). Samples containing Ag were digested in nitric acid

and those containing TiO$_2$ in sulfuric and nitric acids (Eaton et al., 2005),

followed by analysis with inductively-coupled plasma optical emission

spectroscopy (ICP-OES) (Icap 6000 Series, Thermo Scientific; Cambridge,

UK).

Total and volatile suspended solids measurements of wastewater

biomass were made (Eaton et al., 2005). Extracted EPS was characterized by

DOC and total dissolved nitrogen (TDN) analysis. DOC and TDN were

measured using a TOC-V$_{CSH}$ with a TNM-1TN unit (Shimadzu) (Eaton et al.,

2005). EPS extracted for these experiments had a DOC content of 413.0 mg

C/L and TDN of 137.5 mg N/L. Although the percentage of EPS extracted

from biomass stock could not be directly ascertained, the carbon content of

the supernatant from 400 mg/L TSS of whole wastewater biomass was found

to be 1.08 mg/L DOC, while the same solids concentration of EPS-extracted

biomass contained only 0.79 mg/L DOC – a 27% reduction in DOC resulting

from EPS extraction.

Results and Discussion

Imaging Biosorption of Fluorescent Silica Nanoparticles

"Seeing is believing" is a particularly relevant adage for the study of

nanoparticles. The series of fluorescent microscopy images in Figure 5.1
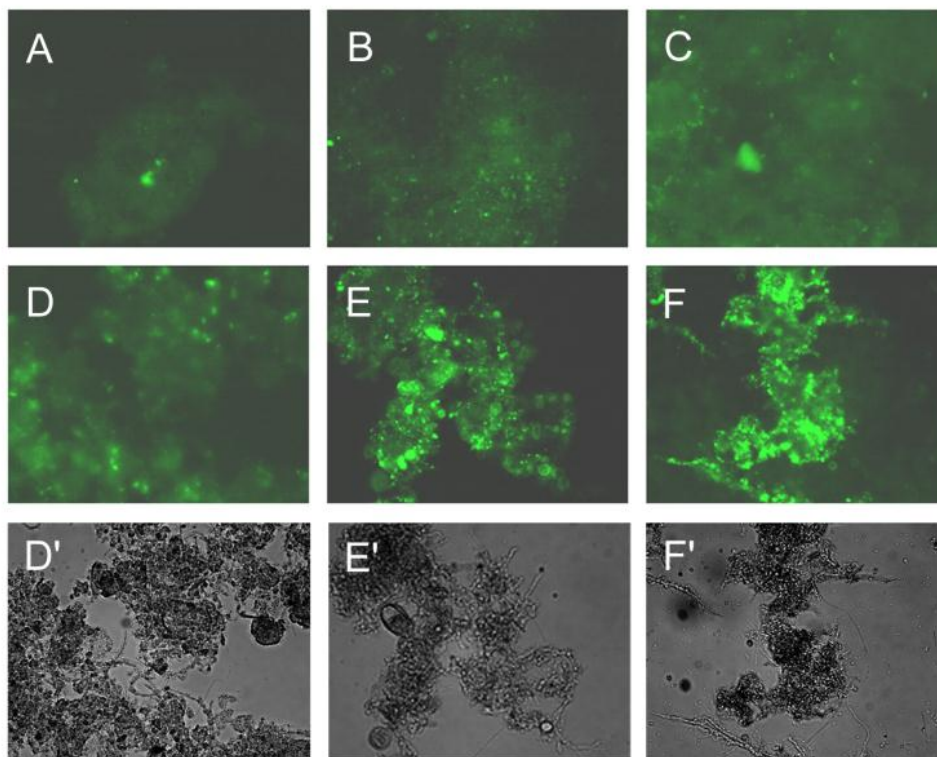
Figure 5.1. Epifluorescence images of wastewater biomass exposure to (A) no nanoparticles (control – biomass only); (B) 1 mg/L SiO_2-FITC; (C) 5 mg/L SiO_2-FITC; (D) 10 mg/L SiO_2-FITC; (E) 20 mg/L SiO_2-FITC; (F) 50 mg/L SiO_2-FITC. Light areas in these images indicate fluorescence primarily from SiO_2-FITC nanoparticles; some background fluorescence from biomass, as seen in the control, was induced from the imaging process. Brighter spots indicate regions with greater nanoparticle concentration. Dark areas contain no detectable nanoparticles. Images (D′), (E′), and (F′) are bright-field images corresponding to epifluorescence images (D), (E), and (F).

shows that SiO_2-FITC NPs sorb to wastewater biomass. Figure 5.1A is an

image of the control (biomass only, without any exposure to SiO_2-FITC NPs)

that shows a very low level of background fluorescence plus a few specks of

higher-intensity fluorescence, which are probably due to a green-fluorescing

compound that sorbed to the activated sludge during treatment at the

WWTP. After exposure to 1 mg/L SiO_2-FITC NPs (Figure 5.1B), the overall

86

fluorescence of the biomass is greater than that of the control, with numerous spots of concentrated fluorescence speckling the terrain of solids. Successive images (Figures 5.1B – 5.1F) show a general trend of increasing fluorescence as biomass is exposed to higher NP concentrations.

Figure 5.2 is a quantitative representation of SiO_2-FITC biosorption. The adsorption isotherm shows near-linear partitioning (Freundlich intensity parameter, $1/n = 1.1$). Percent removal was approximately the same across the range of NP dosages used, averaging $21 \pm 4\%$. Although less than a quarter of the NPs were removed from suspension, the sorbed NPs cover the majority of the biomass surface, as can be seen by superimposing Figures 5.1D through 5.1F on their corresponding bright-field images (Figures 5.1D′ – 5.1F′). More specifically, most of the biomass is dotted with small spots of fluorescence, while some regions bear more concentrated accumulations of NPs, as indicated by bright spots of significantly greater intensities. When biomass is exposed to higher SiO_2-FITC concentrations (20 and 50 mg/L in Figures 5.1E and 5.1F), not only does the overall fluorescence across the biomass increase, but the bright spots become considerably larger and of higher intensity than those in images of lower NP concentrations.
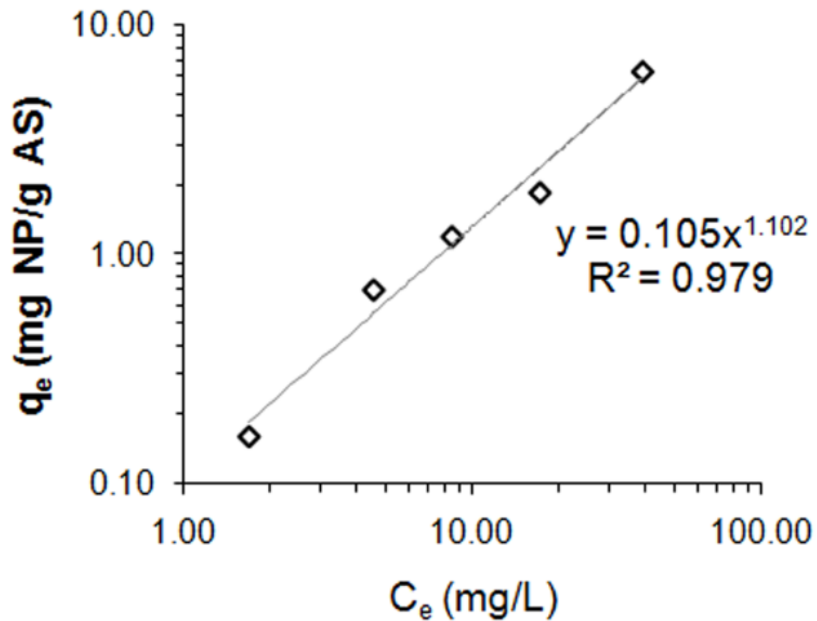
Figure 5.2. Freundlich adsorption isotherm of SiO_2-FITC nanoparticles.

In all of the fluorescence images of SiO_2-FITC biosorption, distinct bright regions are discernable from the surrounding broad fluorescence. Higher-intensity fluorescence indicates areas of biomass to which a greater number of NPs sorbed. These high-intensity spots may be explained as large (secondary) aggregates of NPs whose random spatial arrangement on biomass surfaces was due to indiscriminate adsorption. Another plausible explanation is that fluorescent silica NPs may have greater affinity for particular regions of biomass than for others and, therefore, selectively adsorbed in greater number (as primary or secondary aggregates) to higher-affinity regions. Because biomass contains a wide array of components with different surface chemistries, such as Gram-positive, Gram-negative, and filamentous bacteria, a range of sorption potentials must also be present.

Sorption potential is defined in this context as the potential degree of interaction between sorbent and sorbate surfaces, which is determined by the surface properties of the two materials. SiO_2-FITC NPs are, therefore, likely to have different degrees of affinity for various components of biomass. Although the images do not provide concrete proof, selective adsorption of NPs to specific biomass regions – those with relatively higher sorption potential for the given NPs than other areas – may explain the distinct concentration differences seen over biomass surfaces. Lyon et al. (2005) found that fullerenes associated more strongly with Gram-negative *Escherichia coli* than with Gram-positive *Bacillus subtilis*, suggesting differences in sorption potential due to differences in surface chemistries of these two types of bacteria. In a study of the interaction of silver NPs with HIV-1 viruses, high angle annular dark field scanning transmission electron microscopy images revealed a very regular spatial arrangement of silver nanoparticles sorbed to the surface of a virus; Elechiguerra and his colleagues (2005) suggest that preferential binding occurs between silver NPs and glycoprotein knobs that protrude from the viral lipid membrane.

Comparison of Biosorption of Different Types of Nanoparticles

Figure 5.3 presents the percent removals of aq-nC_{60}, $nC_{60}(OH)_x$, TiO_2, Ag and f-Ag from the liquid phase after exposure to 50 and 400 mg/L TSS of whole wastewater biomass relative to controls without biomass. All five types of NPs were removed from the liquid phase to some degree when exposed to 400 mg/L TSS of solids. Even exposure to only 50 mg/L TSS yielded more than 10% removal of all NP types except fullerol ($nC_{60}(OH)_x$). A

comparison of the percent removals of the NPs tested in this experiment clearly indicates varying extents of removal. $nC_{60}(OH)_x$ had the lowest percent removal, followed by TiO_2, f-Ag, aq-nC_{60}, and Ag, respectively.
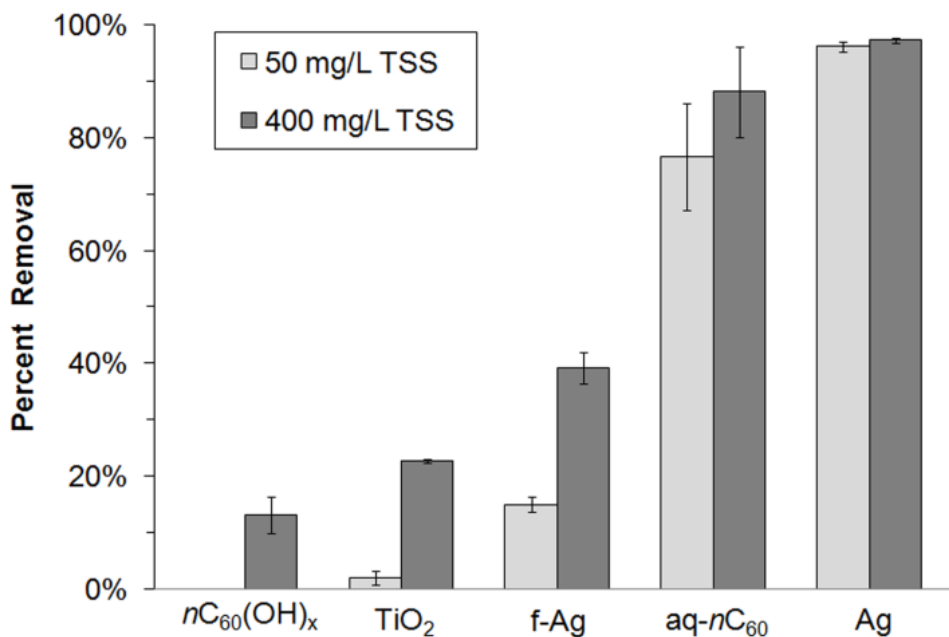
Figure 5.3. Percent removal of five types of nanoparticles from the liquid phase after exposure to 50 and 400 mg/L TSS of whole wastewater biomass. Error bars represent ± standard deviation of triplicate samples.

With exposure to only 50 mg/L TSS, 96 ± 1% of Ag NPs were removed from suspension. A high degree of silver removal was observed in a study that surveyed the partitioning and fate of silver and other metals in WWTPs (Shafer et al., 1998). The study found that of the 17 metals examined in several different WWTPs, silver had the greatest overall removal (>94%) across the treatment train. Nonfunctionalized Ag NPs have a tendency to aggregate in electrolytic solutions (Doty et al., 2005). In our study,

aggregation and sedimentation upon exposure to the biomass matrix may have contributed to the removal of Ag from suspension. We observed a linear relationship between biomass concentration and conductivity of the liquid, which is described by the equation Conductivity, $\mu S = 0.14*(\text{Biomass, mg/L TSS}) + 106$, ($R^2 = 0.999$). Thus, the addition of biomass to the matrix raises the ionic strength of the mixture, which may increase electric double layer suppression and destabilization, making Ag NPs susceptible to aggregation.

Although no trends were discernable between percent removal and NP size or zeta potential, the overall results show that functionalized NPs were less effectively removed by biomass than non-functionalized NPs. While the connection between NP properties and removal, as well as the mechanisms involved in removal, remain vague, the data provide a good comparison of biomass-induced removal of different NP types and suggest that surface properties play a significant role in the fate of NPs in the environment.

Effect of NOM, EPS, SDS, and Salt on Biosorption of Different Nanoparticles

NOM may play an important role in the fate of NPs in the environment. Composed primarily of humic substances and ubiquitous in the environment (Becker et al. 2004), research has shown that NOM has a stabilizing effect on NPs in the aqueous phase (Chen and Elimelech, 2007; Hyung et al., 2007; Diegoli et al., 2008; Domingos et al., 2009; Zhang et al., 2009). Bacterial biomass is itself a source of organic matter. EPS are polysaccharide-rich materials that form the outermost layers surrounding bacterial cells and that mediate contact and exchange processes with the cells' environments (Wingender et al., 1999). The production of EPS involves

active secretion from bacterial cells, sloughing of cell surface material, cell degradation, and adsorption of matter from the environment (Wingender et al., 1999; Li et al., 2004). Humic substances have been found to be important EPS components, comprising as much as 40% of the total organic matter in EPS (Baker and Dudley, 1998; Esparza-Soto and Westerhoff, 2001; Lyko et al., 2007; Ouyang et al., 2009). A portion of bound EPS is hydrolysable to form soluble biomass-associated products (Laspidou and Rittmann, 2002a), which may further contribute to the stabilization of NPs by organic matter.

Samples were equilibrated with 0.5 mg/L DOC of NOM, which is on the order of the NOM concentrations found to reduce the aggregation propensity of metal-based NPs, including TiO_2 (Zhang et al., 2009). The addition of NOM and partial extraction of EPS only affected the degree of removal of aq-nC$_{60}$ (Figure 5.4); no noticeable effect was observed for any other NP type investigated (not shown). NOM and EPS inhibited the removal of aq-nC$_{60}$ from the bulk water phase when exposed to wastewater biomass. Sorption samples containing NOM-equilibrated aq-nC$_{60}$ suspension had about 0.8 mg/L more DOC than samples containing the standard fullerene suspension. Moreover, the use of 400 mg/L TSS of whole biomass contributed approximately 0.3 mg/L more DOC than the same concentration of EPS-extracted biomass. The following trend is based upon data presented in Figure 5.4 and represents conditions yielding greatest-to-least percent removal of fullerene in the presence of 400 mg/L TSS: 1) standard aq-nC$_{60}$ suspension with EPS-extracted biomass – 95% removal, 2) standard suspension with whole biomass – 88% removal, 3) NOM-equilibrated

suspension with EPS-extracted biomass – 81% removal, and 4) NOM-equilibrated suspension with whole biomass – 55% removal. These sorbate-sorbent combinations are also listed in order of least-to-greatest DOC content, indicating that NOM and EPS hinder interaction between aq-nC$_{60}$ NPs and bacterial cells and therefore reduce the percent removal of fullerenes from the bulk water phase. The mechanisms by which organic matter impedes NP-cell interactions are likely to be the same as those thought to stabilize colloids: increasing electrical repulsion, decreasing van der Waals forces of attraction, and/or introducing steric repulsion between particles (Becker et al., 2004).
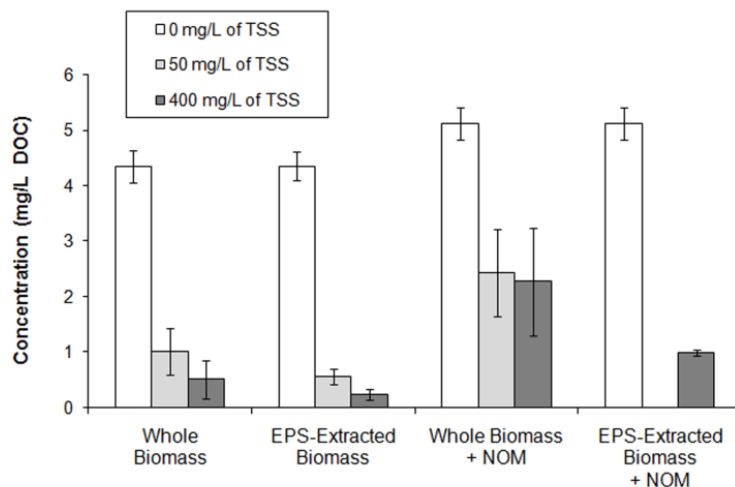
Figure 5.4. Comparison of the effect of EPS extraction and NOM addition on the association of aq-nC$_{60}$ nanoparticles with biomass. The y axis of the plots is the concentration of nanoparticles in the supernatant after exposure to 0, 50, and 400 mg/L TSS of biomass. The x axis shows the sorbents used in the experiment – whole or EPS-extracted biomass, with or without the addition of 0.5 mg/L DOC of NOM. Error bars represent ± standard deviation of triplicate samples.

In another experiment, we investigated the effect of NOM, sodium dodecyl sulfate (SDS), and salt on the biosorption of tol-nC$_{60}$ (Figure 5.5). In a standard sorption experiment utilizing 1500 mg/L TSS of biomass in a 2-mM NaHCO$_3$ matrix (baseline case), about 50% of tol-nC$_{60}$ NPs were removed from the liquid phase. When the suspension was equilibrated with 1% SDS, the percent removal was only 33%. Even in a 10-mM NaCl matrix, only 35% of tol-nC$_{60}$ was removed in the presence of SDS. Clearly, SDS has a stabilizing effect upon tol-nC$_{60}$, decreasing its sorption onto wastewater biomass. However, an experiment with 25 mg/L DOC of NOM in the 2-mM NaCl matrix did not result in any noticeable change in the degree of removal of tol-nC$_{60}$. Only in the higher ionic strength matrix did the stabilizing effect of NOM become apparent.
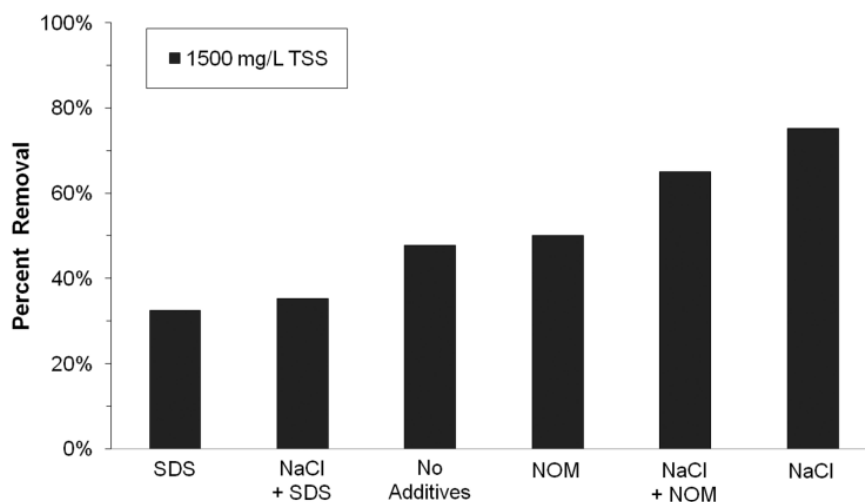
Figure 5.5. Effect of salt, SDS, and NOM on the percent removal of tol-nC$_{60}$ nanoparticles exposed to 1500 mg/L TSS of whole wastewater biomass. The concentrations used were: 10 mM NaCl, 1% SDS, and 25 mg/L DOC of NOM.

Effect of Fullerene Production Method on Biosorption

Sorption experiments with four types of fullerenes (tol-nC$_{60}$, aq-nC$_{60}$, C$_{60}$(OH)$_x$, and nC$_{60}$-PVP) were carried out to investigate the effect of suspension preparation methods and functionalization on the association of carbonaceous NPs with wastewater biomass. Several studies have found that size, structure, and charge of C$_{60}$ aggregates vary as a function of the method employed to produce nC$_{60}$ suspensions, particularly the use or lack of organic solvent in the suspension process (Brant et al., 2006; Lyon et al., 2006; Duncan et al., 2008). In addition, functionalization of C$_{60}$ NPs with hydroxyl groups to form nC$_{60}$(OH)$_x$ results in NPs with different properties than nonfunctionalized C$_{60}$, such as a considerable increase in water solubility (Brant et al., 2006).
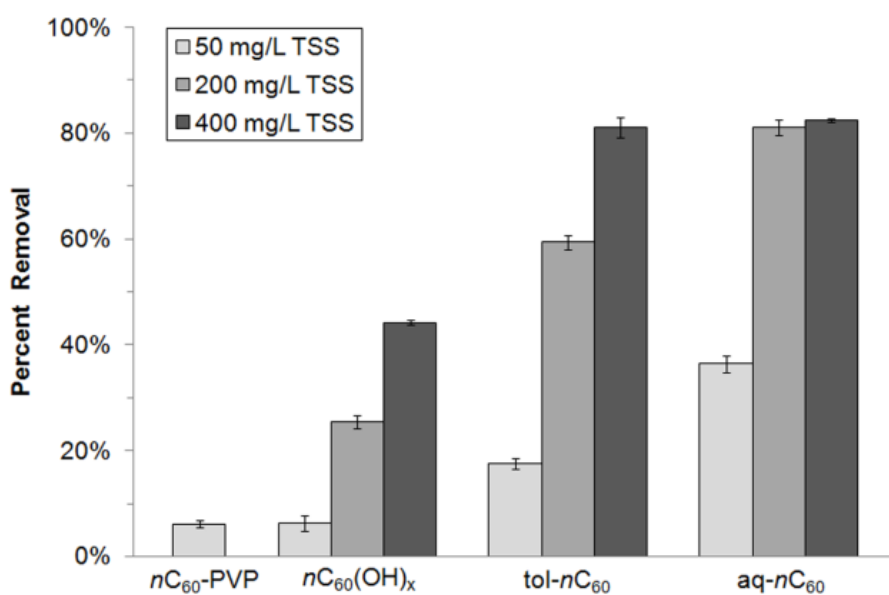
Figure 5.6. Percent removal of fullerenes from the bulk water phase by whole wastewater biomass. Error bars represent ± standard deviation of triplicate samples.

Figure 5.6 shows the percent removals of tol-nC_{60}, aq-nC_{60}, $nC_{60}(OH)_x$, and nC_{60}-PVP by exposure to wastewater biomass. After exposure to 50 mg/L TSS, only $6 \pm 0.7\%$ and $6 \pm 1.5\%$ of nC_{60}-PVP and $nC_{60}(OH)_x$, respectively, were removed, while $18 \pm 1.0\%$ of tol-nC_{60} and $36 \pm 1.6\%$ of aq-nC_{60} were removed from suspension. Of the three fullerene types exposed to 400 mg/L TSS of biomass ($nC_{60}(OH)_x$, aq-nC_{60}, and tol-nC_{60}), fullerol had the lowest degree of removal, with only $44 \pm 0.4\%$ sorption of $nC_{60}(OH)_x$ to biomass. tol-nC_{60} and aq-nC_{60} have approximately the same percent removal by 400 mg/L TSS ($81 \pm 2\%$ and $82 \pm 0.3\%$, respectively).

The results of the comparative fullerene sorption experiment support the findings in the experiment represented by Figure 5.3: functionalized C_{60} is less readily removed from suspension than nonfunctionalized C_{60}, which suggests that functionalized fullerenes may be more persistent in the environment. Due to a different biomass preparation method, samples in the comparative sorption experiment (Figure 5.3) had greater ionic strength than those in the fullerene experiment described in this section, which is why the former resulted in greater percent removal of aq-nC_{60} with 50 mg/L TSS of whole biomass. Furthermore, a comparison of NOM stabilization of aq-nC_{60} and tol-nC_{60} (Figures 5.4 and 5.5) indicates that the stabilizing effect of NOM is less significant on tol-nC_{60} than on aq-nC_{60}. At solids concentrations found in wastewater treatment plants, the majority of fullerenes made by either production method will most likely be sorbed to biomass. A scanning transmission electron micrograph of tol-nC_{60} NPs sorbed to *Escherichia coli* is shown in Figure 5.7.
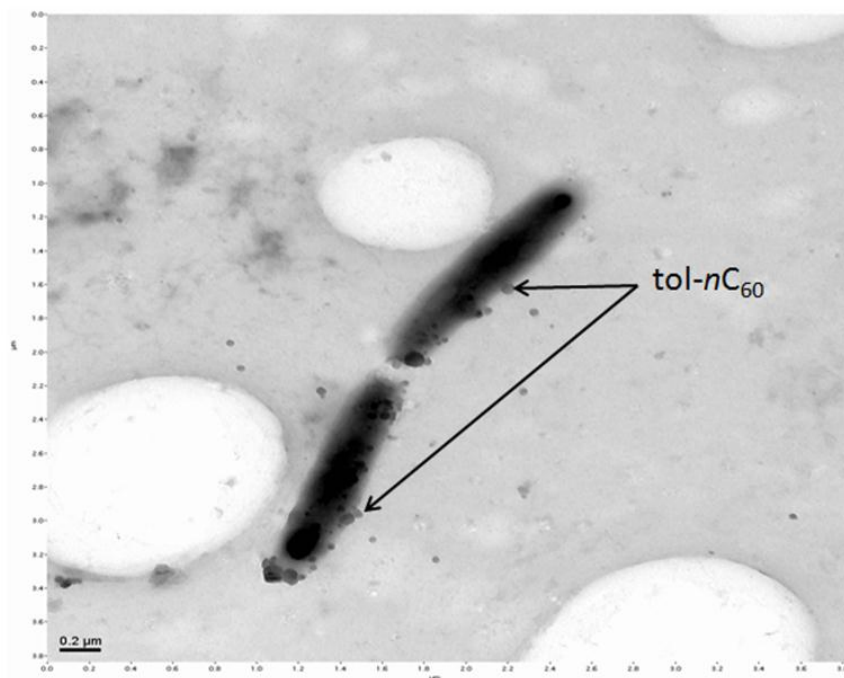
Figure 5.7. Scanning transmission electron micrograph (STEM) (CM 12S, Philips-FEI; Hillsboro, Oregon) of tol-nC$_{60}$ nanoparticle sorption to rod-shaped *Escherichia coli.* 300-mesh, formvar-coated copper grids were incubated in drops of 50 μg/mL bacitracin for 2 min and dried. The grids were then incubated in sample for 2 min and dried, and then incubated in stain (0.5% aqueous uranyl acetate, pH ~5) for 1 min and completely dried. The grids were observed in the STEM at 80 keV.

Possible Mechanisms of Nanoparticle Biosorption

The images and data demonstrate that most of the NPs used in our experiments interact with wastewater biomass. NP association with biomass is likely to occur in one or two general steps. The first step is adsorption of NPs to EPS or the cell surface. The specific mechanism(s) responsible for adsorption of NPs to bacterial surfaces is still unknown, though some studies suggest that the phenomenon is driven by electrostatic attraction (Sondi and Salopek-Sondi, 2004; Morones et al., 2005; Thill et al., 2006). If adsorption to the cell surface occurs, then a second step – uptake into the cell – could

97

potentially follow. Several mechanisms may be responsible for the cellular

uptake of nanoparticles, such as passive diffusion or facilitated transport

across an intact membrane, or diffusion across a disrupted membrane. The

difference between passive diffusion and facilitated transport is that the

latter employs channel-like transmembrane proteins to transport ions and

molecules across the membrane (Madigan and Martinko, 2006). The largest

globular proteins known to passively diffuse across intact membranes of

Bacilis subtilis have radii of about 2 nm (Demchick and Koch, 1996). In

contrast, bacterial transmembrane porins have been shown to have openings

up to approximately 6 nm (Wang et al., 2003). Given the estimated size of

bacterial porins, it is not surprising that NPs 10 nm or less in diameter have

been found to penetrate bacterial cells, whereas larger NPs do not (Kloepfer

et al., 2005; Morones et al., 2005; Choi and Hu, 2008). Morones et al. (2005)

exposed *Escherichia coli* to silver nanoparticles with an average size of 21 ±

18 nm, but the Ag NPs found inside the cells were only 5 ± 2 nm. With the

exception of functionalized silver, the NPs used in our study had mean

hydraulic diameters greater than 10 nm. Smaller size fractions of each NP

type may have been absorbed into cells, but since the majority of NPs were

larger than 10 nm, removal likely was dominated by adsorption without

uptake. The functionalized silver we used in our study, which had a mean

diameter of 3 nm, could have been transported across bacterial cell

membranes if adsorption to the surface occurred. However, functionalization

seems to have hindered the NPs' interaction with biomass surfaces, as

indicated by the relatively low percent removals of f-Ag NPs. Disruption of

the membrane upon exposure to NPs is also possible. After treating *E. coli* with silver nanoparticles, Sondi and Salopek-Sondi (2004) noted the formation of pits on the cell surfaces, an indication of damage. Damaged membranes exhibit considerable increases in permeability (Sondi and Salopek-Sondi, 2004), which may provide NPs easier access to the cell interior and ultimately lead to cell lysis and death.

Conclusions

Epifluorescence imaging showed fluorescent silica NP biosorption on wastewater biomass, and sorption experiments showed that different types of NPs biosorb to differing degrees, although the high removal of Ag NPs from suspension may have been due partly to aggregation and settling. For all types of NPs investigated, increasing the biomass concentration to which NPs were exposed increased NP removal. We used low concentrations of biomass (50 – 400 mg/L TSS) in order to clearly observe differences in removal amongst different types of NPs. The majority of nonfunctionalized carbonaceous and silver NPs that enter a WWTP will most likely associate with solids, while functionalized NPs may persist to a greater degree in effluent. Of the NP types investigated, NOM and EPS had the most significant effect on fullerene biosorption, decreasing aq-nC$_{60}$ removal from water. Furthermore, fullerene suspension preparation methods were shown to impact NP removal from water. The work presented in this paper serves as a starting point for more thorough investigation of NP biosorption, including the relative roles of cell membranes and EPS in NP removal from water. Future research is necessary to uncover the specific sorption

mechanisms involved. A better understanding of NP sorption to wastewater

biomass is essential for improving predictions of the fate and transport of

NPs in the environment.

Chapter 6

NANOMATERIAL TRANSFORMATION AND INTERACTION WITH

FRESH AND FREEZE-DRIED WASTEWATER BIOMASS*

Abstract

Engineered nanomaterials (ENMs) are being used with increasing

frequency in consumer products and are an emerging class of contaminants

entering wastewater treatment plants (WWTPs). Standardized testing

protocols are needed by industry and regulators to assess the fate of ENMs,

including their potential removal in WWTPs. A standardized EPA protocol

(OPPTS 835.1110) for screening removal of chemical pollutants in WWTPs

has been suggested for ENMs without any detailed studies. The goal of this

study was to evaluate freeze-dried, heat-treated (FDH) biomass used in the

OPPTS method for quantifying nanomaterial removal from suspension by

activated sludge. While soluble pollutants sorbed equally to fresh and FDH

biomass, fullerene, silver, gold, and polystyrene nanoparticles' interactions

with FDH biomass was approximately 60 to 100 percent less than with fresh

activated sludge. Freeze drying and heat inactivation denatured proteins

and affected bacterial membrane integrity, resulting in the release of

surfactant-like cellular material into suspension. These biosurfactants

transformed ENMs into more stable materials, which interacted less with

biomass and hence significantly underestimates ENM removal efficiencies in

WWTPs. Therefore, FDH biomass is not a suitable sorbent for quantifying

---

nanoparticle removal by wastewater activated sludge, while fresh biomass has been shown to reasonably predict full-scale performance for titanium removal. Furthermore, this study indicates that natural or engineered processes (e.g. anaerobic digestion, biosolids application and decomposition in soils) that result in biomass degradation and matrices rich in surfactant-like materials (natural organic matter, proteins, phospholipids, etc.) may transform nanoparticle surfaces and significantly alter their fate in the environment.

Introduction

Conventional wastewater treatment plants (WWTPs) and membrane bioreactor treatment plants use activated sludge to remove nutrients, metals, organic chemicals, pathogens, and suspended particles from wastewater. Activated sludge, herein also referred to as wastewater biomass or solids, is produced as a mixed population of microorganisms converts organic matter into cellular material. Various strains of bacteria and their extracellular products, rotifers, protozoa, and fungi are constituents of activated sludge (Rittmann and McCarty, 2001). If a pollutant readily adsorbs to or otherwise interacts with solids, it will be removed from the plant during primary or secondary solids separation. Approximately one-half of biosolids generated by WWTPs in the US are applied to agricultural land as soil conditioner, and the remaining fraction is either landfilled or incinerated (Agyin-Birikorang et al., 2010). If a pollutant has low affinity for solids and is not degraded or volatilized during treatment, it will remain mostly in the aqueous phase and be released with treated effluent into surface water. Quantifying a

pollutant's affinity for wastewater biomass is an essential step towards predicting its fate in the environment and assessing exposure risks.

One of the most fundamental methods for quantifying pollutant affinity for solids has been the batch adsorption isotherm experiment. The United States Environmental Protection Agency (USEPA) standardized the method for testing soluble pollutant sorption to wastewater biomass with the publication of the OPPTS 835.1110 Activated Sludge Sorption Isotherm test guideline (USEPA, 1998). The experimental method outlined in this guideline has become standard industry and research practice for predicting chemical removal from wastewater during biological treatment in WWTPs (Andersen et al., 2005; Yu et al., 2006; Agyin-Birikorang et al., 2010; Oakes et al., 2010; Parrott et al., 2010; Yao et al., 2010). OPPTS 835.1110 calls for the use of freeze-dried and heat-inactivated (FDH) wastewater biomass as sorbent. Unlike fresh biomass, which must be collected, processed, and used daily, FDH biomass can be stored for several months, allowing for a convenient and uniform supply of sorbent for batch experiments.

As the production of consumer products containing engineered nanomaterials (ENMs) grows, nanomaterials are entering WWTPs in increasing amounts and have been detected in WWTP solids and effluent (Kiser et al., 2009; Kim et al., 2010; Westerhoff et al., 2011). Studies have shown that ENMs interact with wastewater biomass and that ENM removal during wastewater treatment is controlled by their affinity for biomass (Limbach et al., 2008; Jarvie et al., 2009; Kiser et al., 2009; Kiser et al., 2010). A standardized method of quantifying nanomaterial affinity for

103

wastewater biomass does not currently exist. The USEPA recently published an interim technical guide for evaluating the environmental fate of nanomaterials using OPPTS 835.1110 with the hope that "experienced scientists will find it helpful and will contribute to the further development and validation of this approach" (USEPA, 2010). However, the OPPTS guideline for testing soluble compounds was not developed nor validated for use with nanomaterials.

The goal of this study was to evaluate the use of FDH biomass, the standard sorbent in batch experiments for chemicals, for quantifying ENM removal by activated sludge. We compared nanomaterial affinity for fresh and FDH wastewater biomass by conducting batch experiments with fresh biomass following protocol we developed in previous work (Kiser et al., 2010) and with FDH biomass following the method outlined in OPPTS 835.1110 (USEPA, 1998).   Furthermore, we studied the effect of FDH biomass processing steps (freeze drying, heat inactivation) on ENM removal from wastewater. Biomass degradation and the resulting release of soluble biosurfactants were investigated as a mechanism for transforming ENM surface properties. This study contributes to the development of a reliable standard method for evaluating nanoparticle adsorption to activated sludge and has important implications for the transformation and fate of nanomaterials in the environment.

Materials and Methods

Chemical Solutions and Nanomaterial Suspensions

We used three compounds to serve as model soluble contaminants to test in our adsorption experiments. Methylene blue (MB) (Fisher Scientific; Pittsburgh, USA) is an organic, cationic dye that readily stains bacteria because of its affinity for negatively-charged cellular constituents such as acidic polysaccharides and nucleic acids (Madigan and Martinko, 2006). Used as a dye in material industries and as a biological stain, MB has also been widely employed for several decades as a model sorbate in adsorption (Barton, 1987; Rozada et al., 2007). 17α-ethinylestradiol (EE2) (Sigma-Aldrich; St. Louis, USA), a synthetic steroid estrogen and the active ingredient in contraceptive pills, is only partially removed in conventional activated sludge WWTPs and is implicated in the endocrine disruption of aquatic organisms (Andersen et al., 2005; Clouzot et al., 2010). Ionic silver (Ag^+) from silver nitrate ($AgNO_3$) (Sigma-Aldrich; St. Louis, USA) is antimicrobial and used as a biological stain for scanning electron microscopy and protein demonstration in PAGE gels. Ag^+ readily binds to thiol groups in membrane proteins and disrupts protein function (Klueh et al., 2000). Silver has been quantified along the treatment train of WWTPs and found to strongly associate with solids, resulting in more than 94% removal of silver over the course of treatment (Shafer et al., 1998).

We used nine nanomaterial suspensions to compare affinity to fresh and FDH biomass and expose relationships between nanomaterial properties and interaction with solids. Non-functionalized fullerene (aq-nC_{60})

suspension was prepared by magnetically stirring 99.9% C_{60} powder (MER

Corporation; Tucson, AZ, USA) in ultrapure water for several months and

then filtering the golden-brown suspension through 0.7-µm glass-fiber filters

(Whatman; Maidstone, UK). We purchased suspensions of tannic-acid-

capped nanogold (TA-Au) in a range of sizes (NanoComposix; San Diego, CA,

USA), PVP-coated gold (PVP-Au) (NanoComposix), carboxylate- and sulfate-

functionalized yellow-green fluorescent microspheres (Car-PS and Sulf-PS,

respectively) (FluoSpheres, Invitrogen; Eugene, OR, USA), and carboxylate-

functionalized silver (Car-Ag) (Vive Nano; Toronto, ON, Canada). Dr. Mark

Wiesner of Duke University's Center for Environmental Implications of

Nanotechnology (CEINT) provided us with three different nanosilver

suspensions: polyvinylpyrrolidone-coated (PVP-Ag) (NanoAmor, Los Alamos,

New Mexico, USA), citrate-coated (Cit-Ag) (prepared at Duke University),

and gum-arabic-coated (GA-Ag) (prepared at Duke University).

Characterization data of nanoparticles used in this study are shown in Tables

6.1 and 6.2.

Table 6.1

Hydrodynamic diameters and zeta potentials of nanoparticle stock suspensions in ultrapure water; all measurements were taken at sample pH 7.0 ± 0.1

ENM	Hydrodynamic Diameter (nm)	Zeta Potential (mV)
TA-Au, 10-nm	9.3	-32.3 ± 1.4
PVP-Au	10.0	-39.8 ± 1.4
Sulf-PS	22.7	-39.6 ± 2.0
Car-PS	22.0	-51.5 ± 2.8
Aq-nC$_{60}$	85.9	Not Measured
Car-Ag	36.4	-52.1 ± 2.1
Cit-Ag	26.8	-41.3 ± 0.5
GA-Ag	178.2	-42.2 ± 1.6
PVP-Ag	106.0	-21.5 ± 1.1

Table 6.2

Hydrodynamic diameters and zeta potentials of selected nanoparticle stock suspensions in ultrapure water, 0.45-μm filtered supernatant of 800 mg/L TSS fresh biomass, and 0.45-μm filtered supernatant of 800 mg/L TSS FDH biomass; all measurements were taken at sample pH 7.0 ± 0.1

	Hydrodynamic Diameter (nm)			Zeta Potential (mV)		
ENM	H_2O	Fresh Biomass Matrix	FDH-14d Biomass Matrix	H_2O	Fresh Biomass Matrix	FDH-14d Biomass Matrix
TA-Au, 10-nm	9.3	3.5	4.3	-32.3 ± 1.4	-12.5 ± 4.0	-26.9 ± 4.0
PVP-Au	10.0	14.4	8.7	-39.8 ± 1.4	-14.8 ± 0.8	-19.1 ± 1.3
Sulf-PS	22.7	25.2	23.4	-39.6 ± 2.0	-22.1 ± 1.8	-25.7 ± 1.6
Car-PS	22.0	22.8	25.2	-51.5 ± 2.8	-15.9 ± 0.4	-21.1 ± 0.1
Car-Ag	36.4	44.4	88.4	-52.1 ± 2.1	-20.7 ± 0.7	-24.8 ± 0.9

Activated Sludge Collection and Preparation

Return activated sludge was collected from a municipal conventional activated sludge wastewater treatment plant in central Arizona, USA. The sludge was kept at 4 °C during transport and storage in the laboratory. Within 48 hours of collection, we prepared the sludge for experimentation. To prepare FDH biomass, we followed the procedure detailed in OPPTS

835.1110. Briefly, activated sludge was rinsed three times with ultrapure water by centrifuging at RCF = 2000 G for 5 min (IEC Multi, Thermo IEC; Waltham, MA, USA) and decanting. Rinsed sludge was freeze dried following manufacturer instructions (FreeZone 6 Liter, Labconco; Kansas City, MO, USA), passed through a No. 30 (600-µm aperture) sieve (SoilTest, Inc.; Evanston, IL, USA), and finally heat dried at 104 ^{o}C for a fixed length of time. The resulting powder-like FDH biomass was cooled to room temperature in a desiccator. We also prepared freeze-dried biomass without the final heat-drying step (FD biomass). The day before an experiment, we made biomass suspensions by mixing desiccated biomass powder in buffered (1 mM $NaHCO_3$) ultrapure water and storing the suspension overnight (4 ^{o}C) to rehydrate the biomass. Fresh biomass suspensions were prepared by rinsing activated sludge three times with buffered water as described above and then resuspending the rinsed sludge in buffered water. Fresh biomass was stored at 4 ^{o}C for a maximum of 24 hours before being used in experiments.

Batch Affinity Experiments

Glass vials containing biomass suspension and buffer solution (1 mM $NaHCO_3$) were spiked with nanoparticle suspension. Sample concentrations of sorbents and sorbates are listed in Table 6.3. We chose concentrations of sorbent (800 mg/L TSS) and sorbates (~30 µg/L – 6 mg/L for soluble compounds; ~0.1 – 3 mg/L for nanoparticles) at which differences could be distinguished in the affinities of the various ENM types for fresh and FDH biomass.

Table 6.3

Sorbent and sorbate types and concentrations used in experiments

Experiment Type	Biomass Type (800 mg TSS/L)	Sorbate Type and Dosage	
Comparison of Sorption to Fresh and FDH Biomass	Fresh FDH– 14d	Methylene Blue	5.6 mg/L
		EE2	26.8 ± 0.2 µg/L
		$AgNO_3$	2.3 ± 0.003 mg/L
		Car-Ag	2.1 ± 0.05 mg/L
		Cit-Ag	0.4 mg/L
		PVP-Ag	0.1 mg/L
		GA-Ag	0.5 mg/L
		TA-Au, 10-nm	2.2 ± 0.3 mg/L
		PVP-Au	0.9 mg/L
		Car-PS	2.0 mg/L
		Sulf-PS	2.0 mg/L
		aq-nC$_{60}$	3.4 ± 0.04 mg/L
Comparison of Desorption from Fresh and FDH Biomass	Fresh FDH-3h	$AgNO_3$	2.3 ± 0.003 mg/L
		Car-Ag	2.0 ± 0.05 mg/L
		Sulf-PS	2.0 mg/L
Effect of Biomass Processing on Sorption	Fresh FD (not heat-dried) FDH-3h FDH-12h FDH-24h FDH-3d FDH-7d FDH-14d	$AgNO_3$	2.3 ± 0.003 mg/L
		Vive-Ag	2.1 ± 0.05 mg/L
		Car-PS	2.0 mg/L
		Sulf-PS	2.0 mg/L
Effect of NP Diameter on NP Sorption	Fresh FDH-14d	TA-Au, 5-nm	2.0 ± 0.01 mg/L
		TA-Au, 10-nm	2.2 ± 0.3 mg/L
		TA-Au, 20-nm	2.0 ± 0.05 mg/L
		TA-Au, 50-nm	1.9 ± 0.01 mg/L
		TA-Au, 70-nm	1.8 ± 0.05 mg/L
		TA-Au, 100-nm	1.9 ± 0.05 mg/L

Samples were agitated for 3 h on a platform shaker (C1, New Brunswick Scientific; Edison, NJ) and then stood upright for 2 h to simulate mixing in aeration basins and sedimentation in secondary clarifiers, respectively (Wang et al., 1993; Metcalf and Eddy, 2003). After

sedimentation, supernatant was collected from each sample and analyzed.

To quantify reversibility of nanoparticle interaction with biomass, we

discarded the volume of liquid remaining over the settled solids and replaced

the volume with fresh buffer solution. These samples were agitated for 3 h

and settled for 2 h, and then supernatants were collected and analyzed. For

all experiments, controls (without NPs; without biomass) were made and

analyzed alongside samples. At least 15% of samples were conducted in

replicate. Assuming that volatilization and biodegradation were negligible,

we quantified sorbate affinity to sorbent in terms of percent removal of the

sorbate from suspension in the bulk liquid phase. Percent removals in

samples were calculated from differences between measured sorbate

concentrations in controls and samples. Detailed protocol for batch affinity

experiments are given in Appendix A.

Analytical Methods

        Nanoparticle hydrodynamic diameters were measured using phase

analysis light scattering (PALS) (90 Plus, Brookhaven Instruments Corp.;

Holtsville, NY, USA). Zeta potentials were determined on a dynamic light

scattering (DLS) particle sizer (NICOMP 380 ZLS, Particle Sizing Systems;

Santa Barbara, CA, USA). We digested samples with nanosilver and

nanogold with nitric acid and aqua regia, respectively, and measured the

concentrations of these metals using inductively-coupled plasma optical

emission spectroscopy (ICP-OES) (Icap 6000 Series, Thermo Scientific;

Cambridge, UK). We indirectly measured concentrations of yellow-green

fluorescent Car- and Sulf-PS NPs by measuring sample fluorescence

(excitation/emission maxima = 505/515 nm) (LS 50 B Luminescence Spectrophotometer, PerkinElmer; Waltham, MA, USA). For aq-nC$_{60}$, we prepared samples for analysis using liquid-liquid extraction (LLE). The optimal LLE condition was selected as follows: 10ml sample, 10 ml toluene, and 25 ml glacial acetic acid (GAA). After 2 h of agitation, vials were stood upright for 60 minutes, during which time toluene separated from the rest of the mixture and formed a layer on top. 0.5 ml of toluene of each LLE sample was collected in an HPLC vial and then evaporated under a nitrogen stream. After evaporation to dryness, the sample was reconstituted with 0.5 ml of toluene and then sonicated in an ultrasonication bath (100W) for 5 min. The vial was filled with 0.5 ml of acetonitrile for HPLC analysis. HPLC analysis using a wavelength of 336 nm was performed on a Water Alliance Separate Module and a UV/vis detector (Waters 2475, 2695, and 2996; Milford, MA, USA). The analytical column was a Discovery C18, 150mm x 4.6mm, packed with 5 um particles (Supelco, USA). The chromatographic separation was performed at a constant flow rate of 1 ml/min with a mobile phase of 50% acetonitrile and 50% toluene.

Biomass stocks were characterized by measurement of total suspended solids (TSS) (Eaton et al., 2005) and chemical oxygen demand (COD) (Hach, USA). Filtered (0.45-µm polysulfone) biomass supernatants were also characterized by measuring COD, UV/Vis absorbance at 280 nm (MultiSpec-1501, Shimadzu; Kyoto, Japan), surface tension (Tensiomate 21, Fisher Scientific; Waltham, MA, USA), and protein concentration (BCA Protein Assay Kit, Thermo Scientific; Waltham, MA, USA). Solid samples

were imaged after exposure to fluorescent Sulf-PS microspheres using both bright-field and epifluorescence microscopy, as described by Kiser et al (2010).

Results and Discussion

Comparison of Nanomaterial Affinity for Fresh and FDH Biomass

Figure 6.1 shows sorption percentages of MB, EE2, and Ag^+ to 800 mg/L total suspended solids (TSS) of fresh and FDH activated sludge. EE2 sorption to the two biomass types were similar: $48 \pm 4\%$ of EE2 sorbed to fresh biomass, and $43 \pm 14\%$ sorbed to FDH biomass. Ag^+ sorption to FDH biomass also reasonably represented the extent of sorption to fresh biomass. $95 \pm 1\%$ and $91 \pm 1\%$ of Ag^+ sorbed to fresh and FDH biomass, respectively.
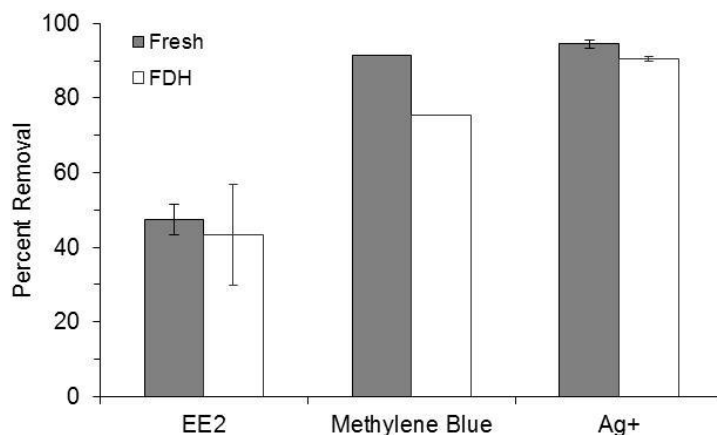
Figure 6.1. Percent removal of soluble organic and inorganic compounds after exposure to 800 mg/L TSS fresh or FDH-14d biomass; error bars represent ± standard deviation of duplicate samples.

Levels of EE2 and Ag^+ sorption to activated sludge are similar to values reported in other studies (Shafer et al., 1998; Andersen et al., 2005). MB

sorbed about 15% less to FDH biomass than to fresh biomass. Overall,

sorption percentages of the model soluble contaminants to fresh and FDH

biomass were comparable. Thus, the widely-used OPPTS protocol using FDH

biomass is demonstrated as a viable sorbent for quantifying soluble

compound sorption to activated sludge.

Figure 6.2 shows removal results for nine different types of ENMs by

the two biomass types. For fresh biomass, two groups of nanomaterials exist.

Nanomaterial removal in Group I (CIT-Ag, PVP-Ag, PVP-Au, Car-Ag, and

GA-Ag) ranged from 39 to 62%. Nanomaterials in Group II (TA-Au, Car-PS,

Sulf-PS, and aq-nC_{60}) had higher removal (92 to 94%) by fresh biomass. All

of the nanomaterial types in our study had significantly lower affinity for

FDH biomass than for fresh biomass. We detected no removal of Cit-Ag,

PVP-Ag, PVP-Au, or TA-Au with FDH biomass. For those nanomaterials

that did interact with FDH biomass, removal ranged from 7 to 24%, which

was significantly less than their removal by fresh biomass.
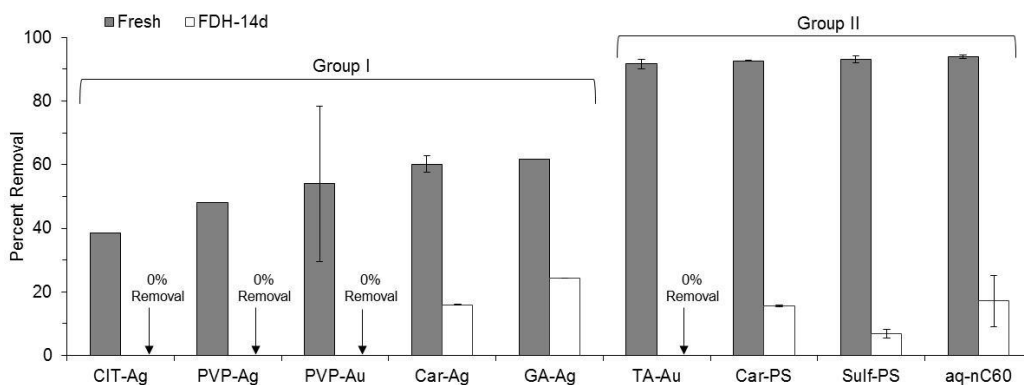
Figure 6.2. Percent removal of nanoparticles after exposure to 800 mg/L TSS
fresh or FDH-14d biomass; error bars represent ± standard deviation of
duplicate samples.

The range of removals by fresh biomass is attributed to differences in ENM surface properties, size, density, and number concentrations. Group I includes surface functionalizations (Figure 6.3) resulting in lower biomass affinities. Carboxyl groups are low molecular weight polar molecules that make colloids they attach to more hydrophilic. PVP is a hydrophilic synthetic polymer that has been used as a coating to make membrane filters hydrophilic and as a carrier matrix to improve dissolution of hydrophobic drugs (Dahlberg et al., 2010). Gum arabic, a natural polysaccharide with hydroxyl and carboxyl functional groups, is used to stabilize nanoparticles in aqueous solutions; the hydrophilicity of polysaccharides has been shown to increase nanoparticle residence time in blood and inhibit particle coating by plasma components (Dias et al., 2011).
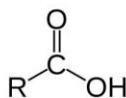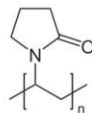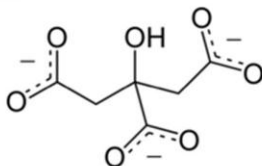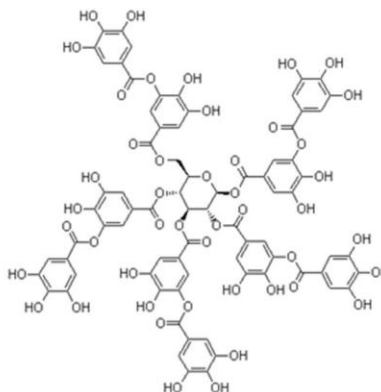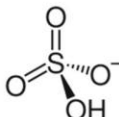
Figure 6.3. Chemical structures of carboxylate, citrate, sulfate, polyvinylpyrrolidone, and tannic acid ENM coatings.

ENMs in Group II have properties that favor association with fresh biomass. Tannic acid (TA) (Fig. 6.3) is a hydrolysable tannin. Tannins, high-molecular-weight polyphenols produced by plants, strongly bind to proteins and other macromolecules to form insoluble complexes (Bossi et al., 2007). Numerous studies have found that tannins bind to bacterial cell membranes and extracellular structures such as fimbriae (Smith et al., 2005; Bossi et al., 2007). Polystyrene nanoparticles used in this study are hydrophobic and will passively and nearly irreversibly interact with almost any type of protein, according to the manufacturer's description. Though stabilized in water through long-term stirring, aq-nC$_{60}$ aggregates are also relatively hydrophobic (Brant et al., 2005) and have been shown to amass around bacterial cells (Lyon et al., 2005; Kiser et al., 2010). After simulating the translocation of C$_{60}$ across a lipid bilayer, Qiao et al. (2007) suggest that C$_{60}$ sorption into the lipid bilayer is driven by hydrophobic interactions between C$_{60}$ and the lipid tails of the bilayer.

We wanted to test the effect of particle size on ENM removal while keeping other nanoparticle properties constant. We quantified removals of 5-, 10-, 20-, 50-, 70-, and 100-nm TA-Au gold nanoparticles with fresh biomass in terms of mass and number of nanoparticles removed per gram TSS of biomass (Fig. 6.4). Nanoparticle removal by fresh biomass expressed as the number of particles removed per gram biomass shows the relationship between size and removal. For a given initial mass concentration of a particular nanoparticle type and fixed contact time, the smaller the hydrodynamic diameter, the greater the number of particles that were

removed by wastewater biomass. Aggregation of biomass and nanomaterials

is logically a function of particle numbers. Zhang et al. (2011) investigated

the effect of size on the sorption of hematite nanoparticles on *E. coli* cells and

found that, in terms of the number of hematite nanoparticles sorbed per unit

cell surface area per unit time, sorption rates were faster for smaller

nanoparticles than those for larger nanoparticles. The faster rate for smaller

nanoparticles was attributed to faster particle mobility and lower energy

barriers in the total interaction energy. No removal of nanoparticles of any

size was detected with FDH biomass (not shown), which is consistent with

Fig. 6.2.
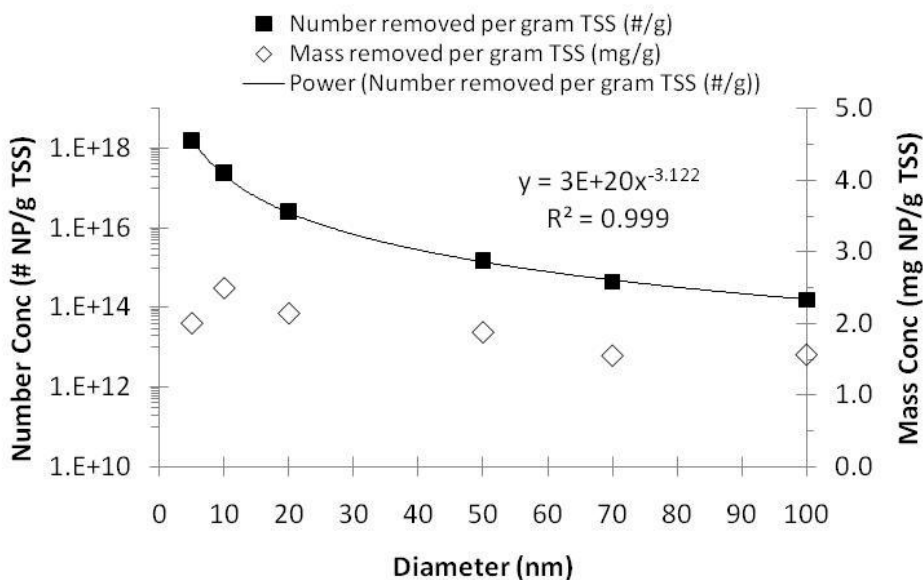
Figure 6.4. Effect of size on TA-Au removal by 800 mg/L TSS fresh biomass.

In additional experiments, we used bright-field and epifluorescence

microscopy to qualitatively compare fresh and FDH biomass (Fig. 6.5). Well-

defined components of activated sludge are visible in fresh biomass samples,

such as spheres and filaments of different sizes and densities. In contrast,

FDH biomass lacks distinct features and instead appears as thick,

amorphous clumps of matter. The epifluorescence images show the fresh

biomass sample as noticeably more fluorescent than the FDH sample,

indicating greater association of fluorescent Sulf-PS nanoparticles with fresh

biomass. Although fluorescence can be seen in the FDH sample, this is due

to biomass autofluorescence from light exposure; a biomass-only control

(without exposure to nanoparticles) showed similar background color

intensity as the FDH sample. The results of our batch sorption experiments

and imaging indicate that nanomaterials sorb less to FDH biomass than to

fresh activated sludge. Therefore, the OPPTS 835.1110 method is unlikely to

provide reliable data to predict nanomaterial fate in an activated sludge

treatment system. In a previous study, we demonstrated that fresh

wastewater biomass in batch experiments yielded comparable results to

titanium removal in a full-scale wastewater treatment plant (Kiser et al.,

2009).
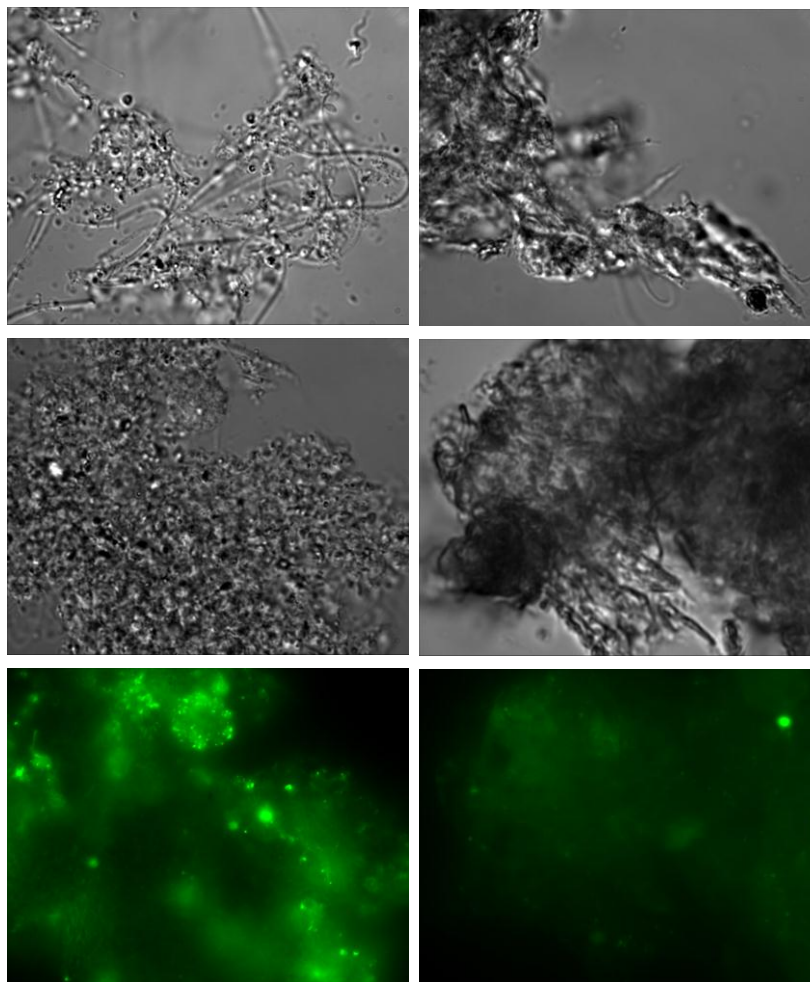
Figure 6.5. Bright-field and epifluorescence images of 800 mg/L TSS fresh (left-hand column) and FDH-14d (right-hand column) biomass. Epifluorescence images in the bottom row correspond to the bright-field images in the preceding row. Biomass was exposed to 5 mg/L 20-nm sulfate-functionalized polystyrene nanoparticles.

Effect of FDH Biomass Processing on Nanomaterial Interaction with Solids

We quantified the effect of each processing step in the OPPTS 835.1110

method on the removal of Ag^+, Sulf-PS, Car-PS, and Car-Ag nanoparticles

(Fig. 6.6). Biomass processing had little effect on Ag^+ removal.

Nanomaterials removal was 25 to 35% less with freeze-dried and sieved (FD)

biomass than with fresh biomass. Heat drying further reduced nanomaterial

removal, particularly for PS nanoparticles. Sulf-PS, Car-PS, and Car-Ag nanoparticle removals were 62%, 59%, and 28% less, respectively, with biomass dried at 104 °C for 3 h (FDH-3h) than with fresh biomass. Heat drying biomass for more than 12 h resulted in nonsignificant differences in nanomaterial removal. The maximum effect of heat drying on biomass, and consequently particle affinity with solids, was reached between 3 and 12 h of exposure to 104-°C heat. Sulf-PS, Car-PS, and Car-Ag nanoparticle removal with biomass heat dried for 14 days (FDH-14d) was 77%, 69%, and 44% lower than with fresh biomass, respectively.
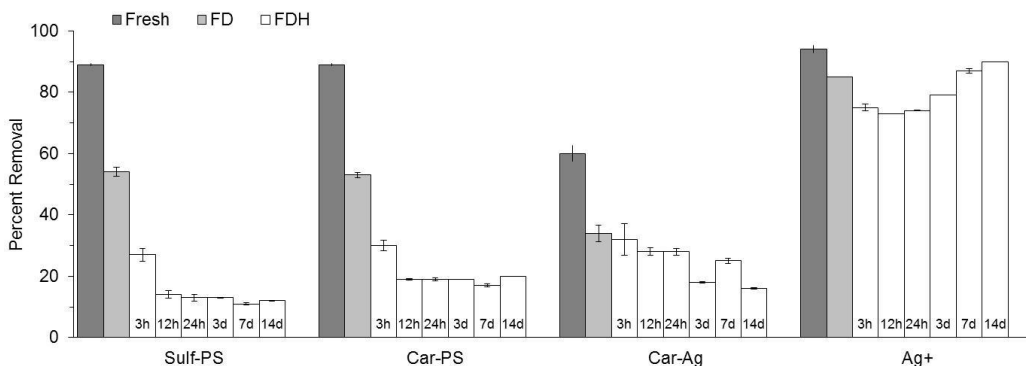
Figure 6.6. Effect of biomass processing (freeze drying and heat drying) on nanoparticle removal. Notations within the FDH columns indicate duration of heat drying. Columns for each NP type are ordered from least to greatest degree of processing. Error bars represent ± standard deviation of duplicate samples.

Freeze drying is a common technique to preserve bacteria for long-term storage. However, freeze drying is usually accompanied by some decline in cell viability because of osmotic shock and loss of membrane integrity from intracellular ice formation and recrystallization (Schwab et al., 2007). The extent of bacterial death from freeze drying depends on strain properties as

well as growth conditions and growth state (Schwab et al., 2007). When we freeze dried activated sludge, membranes of some fraction of cells were probably damaged. Loss of membrane integrity would result in the release of membrane and intracellular components into solution. Furthermore, heat drying bacteria at temperatures above optimum-growth temperatures alters cell morphology (Lepock et al., 1990). Bacteria in the activated sludge process at WWTPs are mesophiles, whose optimum growth temperatures range from about 25 to 45 ^{o}C (Lepock et al., 1990; Gerardi, 2006). At 104 ^{o}C, bacterial membranes become excessively fluid and proteins are irreversibly denatured (Lepock et al., 1990; Madigan and Martinko, 2006). Therefore, heat drying destroys membrane integrity loss and causes the release of membrane and intracellular components, such as proteins, into solution. 0.45-µm-filtered supernatant of 1600 mg/L TSS of FDH biomass contained 59 ± 0.7 µg protein/mL and 185 mg COD/L, while supernatant of the same concentration of fresh biomass only had 1.6 ± 0.4 µg protein/mL and 22 mg/L COD, evidence that freeze drying and heat exposure result in the release of proteins into suspension.

Nanomaterial Transformation By Biosurfactants

Proteins released into solution after membrane disintegration are amphiphiles – molecules that possess both hydrophilic and hydrophobic regions. Along with proteins, phospholipids are likely to be released into solution when bacterial membranes are destroyed. Phospholipids, the primary component of biological membranes, are amphiphiles, containing both hydrophobic fatty acid and hydrophilic glycerol-phosphate components.

Amphiphilic proteins and phospholipids released into solution behave like surfactants. Samples containing FDH biomass visibly produced foam after being agitated, whereas fresh biomass did not (Fig. 6.7). In addition, we measured the surface tension of fresh and FDH biomass supernatants. Fresh biomass supernatant had a surface tension of 74.5 dyne/cm – similar to the surface tension of pure water. On the other hand, FDH biomass supernatant had a surface tension of only 55.4 dyne/cm. Foaming and decreased surface tension indicate the presence of surface-active agents in FDH biomass supernatant. The hydrophobic portions of surfactant molecules are not stable in an aqueous environment and consequently associate with other surfaces (McGraw-Hill, 2011). Therefore, biosurfactants (proteins and phospholipids) in solution of FDH biomass samples probably coated nanoparticles. Numerous studies have shown that natural and synthetic surfactants, such as natural organic matter and sodium dodecyl sulfate, respectively, stabilize natural colloids, carbon nanotubes, fullerenes, quantum dots, and various metal and metal-oxide nanoparticles in water (Hyung et al., 2007; Chen and Elimelech, 2008; Zhang et al., 2009; Kiser et al., 2010; Lee et al., 2011; Stankus et al., 2011). Furthermore, Cedervall et al. (2007) found that when human serum albumin was introduced to nanoparticle suspensions, the proteins formed a coating around the nanoparticles; the number of proteins bound to nanoparticle surfaces increased with particle hydrophobicity.
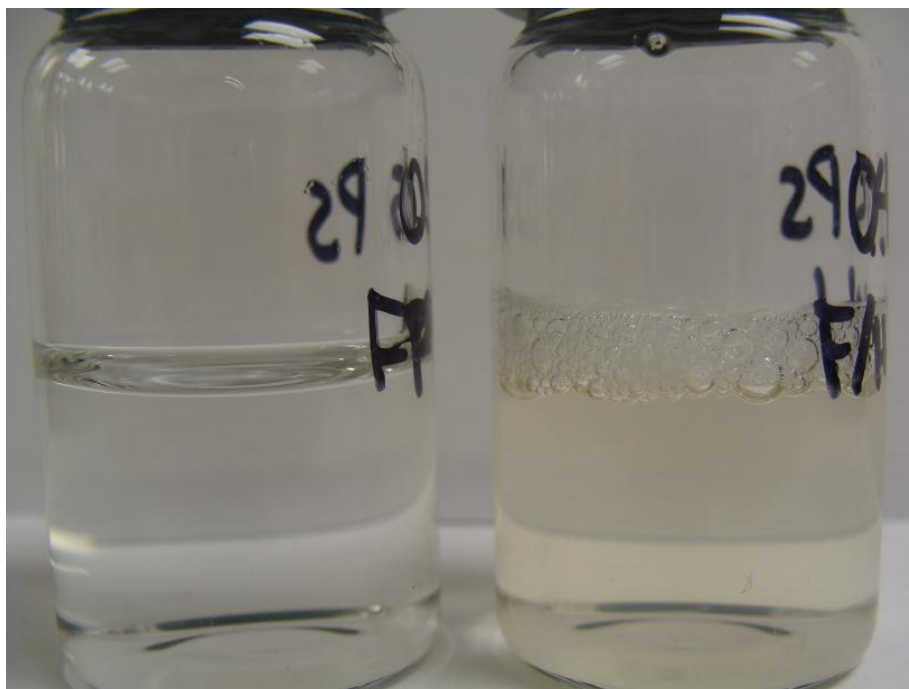
Figure 6.7. 0.45-µm-polysulfone-filtered supernatants of fresh (left) and FDH-14d (right) biomass.

Though we did not directly measure hydrophobicities of the various nanoparticles used in our experiments, we can safely make a general statement based on known bulk properties of the materials: sulfate-functionalized polystyrene is relatively more hydrophobic than carboxylate-functionalized silver. Given our experimental results along with Cedervall's findings, the more hydrophobic Sulf-PS nanoparticles were probably transformed by biosurfactants to a greater extent than Car-Ag nanoparticles.

Figure 6.8 compares the removal and release of Sulf-PS and Car-Ag nanoparticles to both fresh and FDH biomass. With fresh biomass, whose low-COD matrix would not result in extensively transformed nanoparticles, the more hydrophobic Sulf-PS particles were removed about 30% more than Car-Ag nanoparticles. In contrast, with FDH biomass, Sulf-PS removal was

similar to the removal of Car-Ag nanoparticles. The difference in removal between fresh and FDH biomass was approximately 70% for Sulf-PS and 45% for Car-Ag. These results suggest that, in FDH biomass samples, the initially more hydrophobic Sulf-PS nanoparticles were transformed by biosurfactants to a greater extent than Car-Ag particles. The hydrophobicity of polystyrene surfaces decreases after protein adsorption (van Loosdrecht et al., 1990). The enhanced stability of Sulf-PS nanoparticles that we observed in the FDH biomass samples probably resulted from a decrease in hydrophobicity and/or increase in steric hindrance from biosurfactant coating.
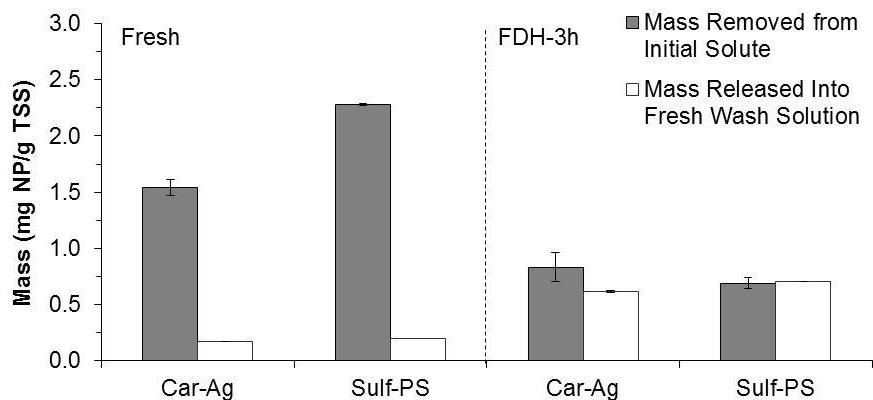
Figure 6.8. Mass concentrations removed by and released from Car-Ag and Sulf-PS nanoparticles (initial dosage of 2 mg/L ENM) after exposure to 0.8 g/L TSS fresh or FDH-3h biomass.

The release of ENMs from biomass was investigated as an indicator of the strength of affinity between the particles and solids (Fig. 6.8). Of the mass of Car-Ag and Sulf-PS nanoparticles that associated with fresh biomass, approximately 11% and 9%, respectively, were released from the solids. For FDH biomass, about 74% of Car-Ag and 100% of Sulf-PS

124

nanoparticles were released. Higher ENM release values from FDH biomass than fresh biomass is evidence that, after surface transformation in the protein-rich FDH biomass matrix, nanoparticle affinity for solids is weak, particularly for the more hydrophobic Sulf-PS nanoparticles.

Conclusions and Implications

The use of FDH biomass is inappropriate for quantifying nanoparticle removal by activated sludge. The preparation of FDH biomass involves freeze drying and heat inactivation, steps that denature proteins and disintegrate bacterial membranes, processes that cause the release of proteins and other cellular materials into suspension. While this cellular matter minimally affects soluble compounds, they transform nanoparticles, ultimately defining particle surface properties. The biosurfactant-induced transformation stabilizes nanoparticles in the liquid phase, thereby significantly decreasing nanoparticle association with wastewater biomass. Thus, fate-and-transport testing protocol established for soluble contaminants cannot be applied to nanoparticles; instead, new standard methods must be developed for the latter.

The biomass degradation processes and nanomaterial transformations observed in our study have important implications for the fate and transport of ENMs in the environment. Activated sludge wasted by WWTPs is introduced to various engineered and natural systems in which heat- and microorganism-induced decomposition of biomass occurs (e.g. anaerobic digesters, compost piles, soils, and landfills). Within each of these compartments, the decomposition of biosolids will result in the release of

biosurfactants that have the potential to transform and mobilize

nanoparticles in the aqueous phase. Thus, further research emphasis is

needed on nanomaterial transformation mechanisms and the fate and

transport of transformed nanoparticles in the environment.

Chapter 7

QUANTITATIVELY UNDERSTANDING THE PERFORMANCE OF

MEMBRANE BIOREACTORS[*]

Abstract

The membrane bioreactor (MBR) is a special form of activated sludge in which a membrane separator allows perfect solids retention. This offers obvious benefits for effluent COD and attaining a large ratio of solids retention time to hydraulic retention time (SRT/HRT). However, these benefits come with trade-offs. This work explores the trade-offs with a mechanistic model based on the unified theory for the biomass and soluble components in microbiological processes and adapted for the special features of MBRs. In particular, only large biomass-associated products (BAP_L) are retained by the membrane, while a high concentration of mixed liquor suspended solids (MLSS) lowers the oxygen-transfer rate and the critical trans-membrane flux. According to the model results, effluent COD is sensitive to the influent COD and to the ability of the membrane to retain BAP_L. While the ability of an MBR to achieve high MLSS and volumetric loading has cost benefits, high MLSS increases the required aeration power and decreases the trans-membrane flux. These strong trends point out the areas in which MBR research ought to yield a large benefit.

127

Introduction

Membrane bioreactors (MBRs), a marriage of microbiology and membrane technologies, are taking an increasingly large share of the wastewater-treatment market. A survey of the eight major MBR vendors shows that the number of MBRs in operation worldwide increased from 6 in 2000 to 166 in 2011, while the treatment capacity increased from about 38,000 to 250,000 m³/day (10 MGD to 650 MGD) (Oppenheimer et al., 2010). These represent average growth rates of 30% and 38% per year for number and capacity, respectively.

Although the MBR is a normal activated sludge process in most ways, utilizing low-pressure membranes to replace the gravity settler in activated sludge offers significant advantages in terms of operations simplicity, economics, and performance (Oppenheimer et al., 2010; Daigger et al., 2005). The greater reliability of membrane separation allows MBRs to be operated with higher solids retention time (SRT), but lower hydraulic retention time (HRT), compared with conventional activated sludge. This advantage leads to a smaller footprint and capital-cost savings. Operations flexibility, automation capability, and the potential for retrofits and expansion also are enhanced with the MBR. Furthermore, membrane filtration improves effluent quality, since the membrane consistently provides an effluent with no suspended solids. In addition, some of the larger soluble macromolecules are removed from the effluent (de Silva et al., 1998; Jang et al., 2006), which enhances effluent quality further, particularly if the retained molecules are more completely biodegraded.

While the MBR offers many benefits, they come with a set of trade-offs. For example, the membranes add significant capital cost and also operating cost for keeping them from fouling (Oppenheimer et al., 2010; Water Environment Federation, 2006). Operation with a higher SRT, lower HRT, or both increases the concentrations of mixed liquor volatile suspended solids (MLVSS) and mixed liquor suspended solids (MLSS), and this can reduce aeration efficiency and increase the trans-membrane pressure needed to produce the effluent flow (Oppenheimer et al., 2010; Schwarz et al., 2006).

Our focus is on the performance aspects of MBRs. We take advantage of a series of recent advances in the quantitative modeling of microbiological processes immediately relevant to MBRs.

1. A unified model of active biomass, inert biomass, soluble microbial products (SMP), and extracellular polymeric substances (EPS) (Laspidou and Rittmann, 2002a,b) makes it possible to sub-divide the biomass into its basic components, which behave quite distinctly with SRT. This allows an accurate description of the biomass concentration, its components, and its wasting rate.

2. A meta-analysis of MBR performance data (Schwarz et al., 2006) quantifies when and how the MLVSS concentration affects aeration efficiency and the trans-membrane flux.

In this work, we create and utilize a comprehensive, mechanistic model of the microbiological phenomena that affect effluent water quality, aeration efficiency, excess solids wasting, and trans-membrane flux in MBRs. The specific goals are:

1. Develop a mechanistic model that incorporates the new advancements for the MBR setting.

2. Use the model to predict MBR performance in terms of effluent chemical oxygen demand (COD), MLVSS, excess sludge production, O_2 supply required, aeration power needed, and trans-membrane flux.

3. Define trends in MBR performance with controllable or variable design/operation factors: e.g., SRT, HRT, influent COD, and membrane removal of organic macromolecules.

To the degree possible, we compare model results with measurements in field-scale and pilot-scale MBRs to interpret why we see experimental results and to identify when fundamental modeling advances are needed.

Modeling Methods

Model Overview

The framework of our model is based upon the analysis and design of a conventional activated sludge (CAS) process by Rittmann and McCarty (2001). Because MBRs replace gravitational settling with membrane separation, the CAS design was modified to accurately represent processes of an MBR. Four important changes were made from the basic CAS model:

1. The membrane accomplishes perfect retention of solids in the system. Thus, MBR effluent contains no active biomass, residual inert biomass, or EPS. Solids are removed from the system only by sludge wasting.

130

2. Active and inert biomass, EPS, and SMP (i.e., utilization-associated products (UAP) and biomass-associated products (BAP)) are described by a set of nonsteady-state mass balance equations that represent the unified theory of Laspidou and Rittmann (2002a,b), who made the pathways of electron flow from the donor substrate to the range of microbial products consistent and comprehensive.

3. BAP are composed of macromolecules that range in size (Namkung and Rittmann, 1986), and the larger molecules cannot pass through the membrane. In the model, the large-BAP fraction (BAP_L) is wasted with solids, but does not pass through the membrane to the effluent. The small-BAP fraction (BAP_S) passes through the membrane, leaving the system in effluent and waste streams. Also passing through the membrane are the original substrate (S) and UAP.

4. Membrane separation allows MBRs to operate at much higher MLSS concentrations than those used in conventional activated sludge reactors. Because increasing MLSS affects the oxygen transfer efficiency and trans-membrane flux within a system, the model includes MLSS-specific adjustments to these parameters based on the analysis of MBR performance by Schwarz et al (2006).

The model contains seven nonsteady-state equations to quantify relationships among three solid and four soluble species according to the

unified theory as modified for the MBR setting. Active biomass (X_a), residual inert biomass (X_{res}), and EPS are the solid species; soluble species are S, UAP, BAP_L, and BAP_S. Figure 7.1 summarizes all electron flows in the model.
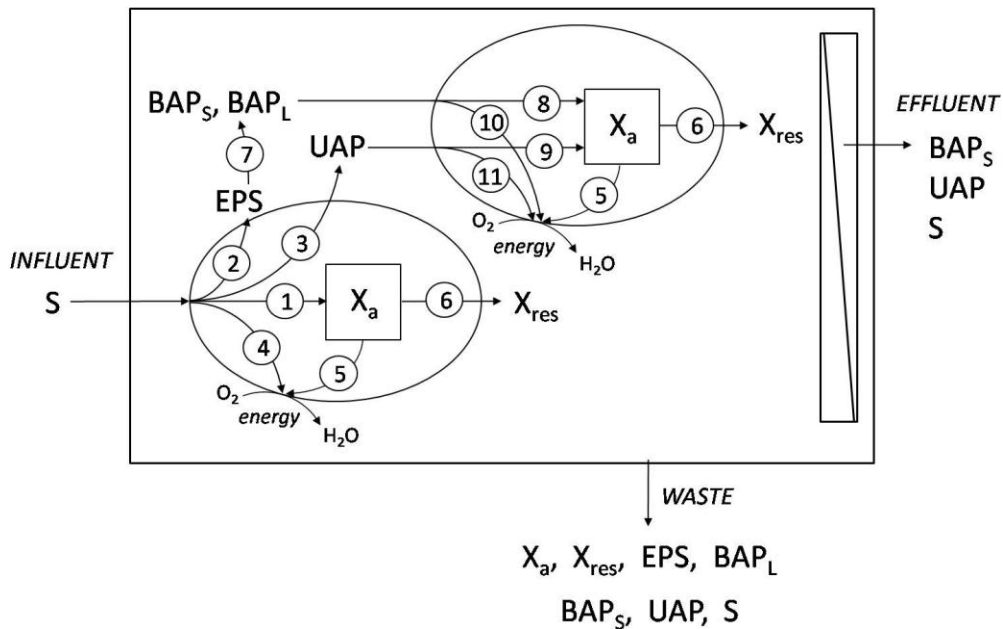
Figure 7.1. Primary electron pathways in an MBR. The numbered pathways for electron flow represent (1) biomass synthesis, (2) EPS formation, (3) UAP formation, (4) substrate respiration, (5) endogenous biomass respiration, (6) formation of inert biomass from decay, (7) BAP formation from EPS hydrolysis, (8) biomass synthesis by utilization of donor substrate BAP, (9) biomass synthesis by utilization of donor substrate UAP, (10) donor substrate BAP respiration, and (11) donor substrate UAP respiration.

Donor electrons from original substrate are used to synthesize active biomass, manufacture UAP and EPS, and respire an electron acceptor (O_2) to generate energy (Laspidou and Rittmann, 2002a). When active biomass is oxidized through endogenous respiration, energy is generated for cell maintenance, and residual inert biomass is generated. When UAP is

132

produced, it is released directly into the aqueous solution. BAP is produced

from the hydrolysis of EPS. Because UAP and BAP are biodegradable, a

portion of their electrons can be used as "recycled" substrate by bacteria for

biomass synthesis, while the remainder of electrons is devoted to the acceptor

for energy generation. The model is constructed such that electrons from

UAP and BAP can only be used for synthesis or energy generation, not for the

formation of new UAP or EPS. Substrate, UAP, and BAP$_S$ are the only

components of the system that can permeate the membrane and affect the

quality of effluent. The remaining species (X_a, X_{res}, EPS, and BAP$_L$)

constitute wasted sludge, as they are too large to pass through the

membrane. The model also relates the concentrations of these components to

performance parameters commonly measured in an activated sludge process:

effluent COD, MLVSS, MLSS, aeration power required, and trans-membrane

flux.

Jang et al. (2006) published an MBR model that captures some of the

features of the unified model. In particular, it determines X_a, X_{res}, EPS, UAP,

and fractions of BAP that will and will not permeate the membrane. In

addition, the model calculates a modified fouling index used to predict

biofouling potentials. It does not include effects of MLSS on trans-membrane

flux and $k_L a$. Furthermore, Jang et al. (2006) define MLSS and MLVSS

differently from the definitions used in our model.

Mass Balance Equations

The seven mass balance equations (Eqns. 2 and $4 - 9$) described in

this section are patterned after those developed by Laspidou and Rittmann

133

(2002b), but with adaptations made for an MBR. Each mass-balance
equation is composed of rate and advection terms. The underlying bases for
each rate term are provided in Laspidou and Rittmann (2002b). The
definitions, values, and units of each parameter used in the mass balance
equations are given in Table 7.1. Parameter values were taken from the
literature (Laspidou and Rittmann, 2002b; Furumai and Rittmann, 1992;
Rittmann and McCarty, 2001). The complete Fortran code of the model is
given in Appendix B.

The advection term is of the form

$$\frac{Q^0 Z^0}{V} - \frac{Q^e Z}{V} - \frac{Q^w Z}{V} \qquad (7.1)$$

Q^0, Q^e, and Q^w represent the influent, effluent, and waste-biosolids flow rates,
respectively (L/d). Z^0 and Z are the influent and reactor concentrations of the
species of interest (mg/L), and V is the liquid volume (L). All concentrations
are in units of mg COD/L, and terms are in mg COD/L-d. When a species is
not present in a stream, i.e., X_a in the membrane permeate, its Z value is
zero.

Original donor substrate (S). The first term in Eq. (7.2) is the rate at
which substrate is consumed by active biomass.

$$\frac{dS}{dt} = -\hat{q}_s \left(\frac{S}{K_S + S} \right) X_a + \frac{Q^0 S^0}{V} - \frac{Q^e S}{V} - \frac{Q^w S}{V} \qquad (7.2)$$

The specific rate of utilization, r_s, is part of the consumption term:

$$r_s = -\hat{q}_s \left(\frac{S}{K_S + S} \right) \qquad (7.3)$$

Table 7.1

Parameters for nonsteady-state mass balance and aeration equations in the

MBR model

Variable	Definition	Value and Units
b	First-order endogenous decay rate coefficient	0.10 d^{-1}
f_d	Biodegradable fraction of active biomass	0.80 [unitless]
k_1	UAP formation rate constant	0.05 mg COD$_P$/mg COD$_S$
k_{EPS}	EPS formation coefficient	0.18 mg COD$_P$/mg COD$_S$
k_{hyd}	First-order hydrolysis rate coefficient	0.17 d^{-1}
K_{BAP}	Half-maximum-rate concentration for BAP utilization	85 mg COD$_P$/L
K_s	Half-maximum-rate concentration for utilization of original substrate	10.0 mg COD$_S$/L
K_{UAP}	Half-maximum-rate concentration for UAP utilization	100 mg COD$_P$/L
q_s	Maximum specific substrate utilization rate for original substrate	10 mg COD$_S$/mg COD$_x$-d
q_{BAP}	Maximum specific BAP utilization rate	0.07 mg COD$_P$/mg COD$_x$-d
q_{UAP}	Maximum specific UAP utilization rate	1.27 mg COD$_P$/mg COD$_x$-d
x_{BAPS}	Fraction of small BAP produced	0.5 [unitless]
Y_s	True yield for substrate utilizations	0.4 mg$_x$/mg$_S$
Y_P	True yield for SMP utilization	0.45 mg$_x$/mg$_P$
β	Wastewater oxygen solubility correction factor	0.95 [unitless]
c_1^*	Liquid phase equilibrium oxygen concentration	8.70 mg O$_2$/L
c_1	Liquid phase bulk oxygen concentration	2.0 mg O$_2$/L
$SOTE$	Standard oxygen transfer efficiency	2.0 kg O$_2$/kWh

Active biomass (X_a). In Eq. (4), the first term describes the synthesis rate of new active biomass from utilization of original substrate. The second term represents the synthesis rate of active biomass using electrons from UAP and BAP. Endogenous decay of active biomass is given by the third term. Because active biomass is a solid, it is retained by the membrane and has a concentration of 0 mg COD/L in the effluent. Thus, the effluent concentration rate term for X_a disappears from the advection equation.

$$\frac{dX_a}{dt} = Y_S r_S \left(1 - k_1 - k_{EPS}\right) X_a + Y_p \left(\frac{\hat{q}_{UAP} UAP}{K_{UAP} + UAP} + \frac{\hat{q}_{BAP} BAP}{K_{BAP} + BAP} \right) X_a$$

$$- b X_a + \frac{Q^0 X_a^0}{V} - \frac{Q^w X_a}{V} \tag{7.4}$$

True residual inert biomass (X_{res}). The rate of formation of residual inert biomass is described by the first term in Equation 7.5. Like active biomass, inert biomass does not permeate the membrane and only leaves the system in the waste-solids stream.

$$\frac{dX_{res}}{dt} = b\left(1 - f_d\right) X_a + \frac{Q^0 X_{res}^0}{V} - \frac{Q^w X_{res}}{V} \tag{7.5}$$

Extracellular polymeric substances (*EPS*). The first term in Equation 7.6 is the rate at which a fraction of substrate electrons are used for EPS formation. The second term provides the rate of EPS loss due to hydrolysis, which forms BAP. EPS advects out only in the waste-solids stream.

$$\frac{dEPS}{dt} = k_{EPS} r_S X_a - k_{hyd} EPS + \frac{Q^0 EPS^0}{V} - \frac{Q^w EPS}{V} \tag{7.6}$$

Small biomass-associated products (*BAP$_s$*). The formation of small BAP from the hydrolysis of bound EPS is given by the first term in Equation

7.7. The fraction of total BAP formed that is small, x_{BAPS}, is a variable input in the model. Biodegradation of BAP_S is given by the second term. BAP_S is present in waste-solids and effluent streams.

$$\frac{dBAP_S}{dt} = x_{BAPS}\, k_{hyd}\, EPS - \frac{\hat{q}_{BAP}\, BAP_S}{K_{BAP} + BAP_S}\, X_a + \frac{Q^0 BAP_S^{\ 0}}{V}$$

$$- \frac{Q^e BAP_S}{V} - \frac{Q^w BAP_S}{V} \tag{7.7}$$

Large biomass-associated products (BAP_L). The terms for BAP_L are the same as those for BAP_S, except that $(1\text{-}x_{BAPS})$ of total BAP produced is too large to pass through the membrane and is, therefore, not in the effluent stream.

$$\frac{dBAP_L}{dt} = (1 - x_{BAPS})k_{hyd} EPS - \frac{\hat{q}_{BAP}\, BAP_L}{K_{BAP} + BAP_L}\, X_a + \frac{Q^0 BAP_L^{\ 0}}{V} - \frac{Q^w BAP_L}{V} \tag{7.8}$$

Utilization-associated products (UAP). The rates of UAP formation and degradation are given in the first and second terms, respectively, of Equation 7.9. UAP is soluble and, like substrate and BAP_S, affects effluent quality.

$$\frac{dUAP}{dt} = k_1 r_s X_a - \frac{\hat{q}_{UAP} UAP}{K_{UAP} + UAP}\, X_a + \frac{Q^0 UAP^0}{V} - \frac{Q^e UAP}{V} - \frac{Q^w UAP}{V} \tag{7.9}$$

Model Solution and Performance Parameters

We made three assumptions to simplify the model solution without sacrificing important phenomena.

1. All influent soluble COD is biodegradable; it contains no refractory soluble COD.

2. Any particulate COD entering the reactor is either biodegradable or refractory. The biodegradable fraction is completely hydrolyzed to soluble COD in the MBR, and the soluble COD is utilized by the active biomass. The refractory COD passes through the system unchanged.

3. The reactor is completely mixed, which means that concentrations of all species are uniform and mass transport resistances are not considered.

We discretized the set of nonsteady-state mass balance equations and, using a small time step and constant input, solved the equations until the results reached steady-state values. Mass balance verification was completed following the verification method of de Silva and Rittmann (2000), and the model gave near-perfect (< 0.1% difference) mass balance closures for all COD. Steady-state values of S, X_a, X_{res}, EPS, BAP_L, BAP_S, and UAP were subsequently used as input for the remainder of model calculations.

MLVSS is the sum of the steady-state values of X_a, X_{res}, and EPS determined by solving the discretized equations. MLSS, estimated following the method given by Rittmann and McCarty (2001), is the sum of MLVSS, inorganic solids associated with MLVSS, and input inorganic solids. We assumed 10 parts inorganics per 90 parts organics in the MLVSS; thus, inorganic solids associated with MLSS are (10/90)MLVSS. Since only S, BAP_S, and UAP permeate the membrane, we computed effluent COD as the sum of these values.

Along with effluent water quality, the required aeration power and trans-membrane flux are key indicators of MBR performance. The required aeration power was determined by first calculating the oxygen supply rate (kg O_2/d), which is the difference between the input and output oxygen demand of the reactor.

$$O_2^{in} = Q^0\left(O_2^0 + S^0 + X_a^0 + X_{res}^0 + EPS^0 + UAP^0 + BAP_S^0 + BAP_L^0\right) \tag{7.10}$$

$$O_2^{out} = \left(Q^e + Q^w\right)\left(S + UAP + BAP_S\right) + \frac{\left(X_a + X_{res} + EPS + BAP_L\right)V}{\theta_x} \tag{7.11}$$

To determine the aeration power requirement of an MBR in kilowatts (kW), the oxygen supply rate was divided by the field oxygen transfer efficiency (FOTE) (kg O_2/kWh):

$$FOTE = SOTE \times 1.035^{T-20} \times \frac{\alpha\left(\beta c_1^* - c_1\right)}{9.2} \tag{7.12}$$

where $SOTE$ is the standard oxygen transfer efficiency (kg O_2/kWh), T is the reactor temperature (C), c_1^* is the liquid phase oxygen concentration (mg/L) in equilibrium with the bulk gas phase, c_1 is the liquid phase bulk oxygen concentration (mg/L), β is a correction factor to better represent wastewater oxygen solubility, and α is a correction factor to better describe the aeration capacity in a volume of wastewater (Rittmann and McCarty, 2001). Pilot- and full-scale studies of MBR aeration have shown that α decreases as the MLSS concentration increases (Schwarz et al., 2006). The following equation, developed from a pilot-scale study of internal and external MBRs, describes the relationship between α and MLSS (Schwarz et al., 2006):

$$\alpha = e^{-0.088\,MLSS} \tag{7.13}$$

where *MLSS* is in units of grams per liter (g/L). Values of the other factors in the *FOTE* equation, given in Table 7.1, were selected for typical wastewater conditions and do not vary with MLSS. Once a was determined and *FOTE* calculated, we computed the power requirement by dividing the oxygen supply rate by *FOTE*.

Trans-membrane flux is the water throughput capacity of a membrane, expressed in units of volume of permeate passing through a unit of membrane surface area per day. Critical permeate flux (J_c) is the flux value above which the deposition of microbial aggregates begins, forming a "cake layer." For steady-state operation, flux should be maintained at or below the critical flux to reduce fouling from cake layer formation. Based on findings of how critical flux is affected by hydrodynamics and MLSS concentration, Schwarz et al. (2006) developed relationships to quantify flux for given MLSS and cross-flow velocities (CFVs). Because the majority of MBRs currently in full-scale operation are internal MBRs (Oppenheimer et al., 2010), we used the equation for the critical flux of internal MBRs (IMBRs):

$$J_c = 31.85 MLSS^{-0.17} \qquad\qquad (7.14)$$

Modeling Strategy

In order to define trends in MBR performance with respect to operational parameters, we ran numerous scenarios with different combinations of values of S^0, SRT, and HRT. We first defined a range of values for each parameter. For S^0, the minimum value of the range was 100

mg COD/L, the maximum was 1000 mg COD/L, and the typical value was defined as being 550 mg COD/L. SRT ranged from 2 to 60 days, with a typical value of 12.5 days. HRT varied from 1 to 10 hours, and we chose 5.5 hours as the typical HRT. Oppenheimer et al. (2010) surveyed the operating conditions and performance of full-scale MBR facilities. They found that the influent COD ranged from 110 to 600 mg COD/L, the SRT was from 3 to 50 days, and the HRT was from 3 to 20 hours. Thus, the ranges of values we selected are consistent with current practice. The fraction of small biomass produced, x_{BAPS}, also was a variable parameter. The range for x_{BAPS} is 0 to 1.0, and we used 0.35 as a typical value, as this is close to what de Silva et al. (1999) found to be appropriate for modeling MBR results.

Each individual input was varied across its designated range of values, while the other inputs were fixed at either minimum, typical, or maximum values of their ranges. We present combinations of inputs that yield a comprehensive array of operation scenarios and provide insight into relationships between different features of MBR performance and S^0, SRT, HRT, and x_{BAPS}. The performance features include effluent COD, MLVSS, solids wasting rate, required aeration power, and critical trans-membrane flux.

Results and Discussion

Effluent COD

Figure 7.2 shows the effect of influent donor substrate (S^0), SRT, and HRT on effluent COD. This figure illustrates the format in which we

141

highlight the results and main trends. We show three curves to create a "performance envelope" for the range of parameter combinations we tested. The top and bottom curves are the highest and lowest values for the output parameter (y-axis), and the legend indicates what combinations of parameters give those curves. The middle curve is for the typical values of the parameter ranges. A significant slope to a curve means that the dependent parameter (the x-axis) has a strong impact on the output parameter. Having the curves close together indicates that the other input parameters have little impact.
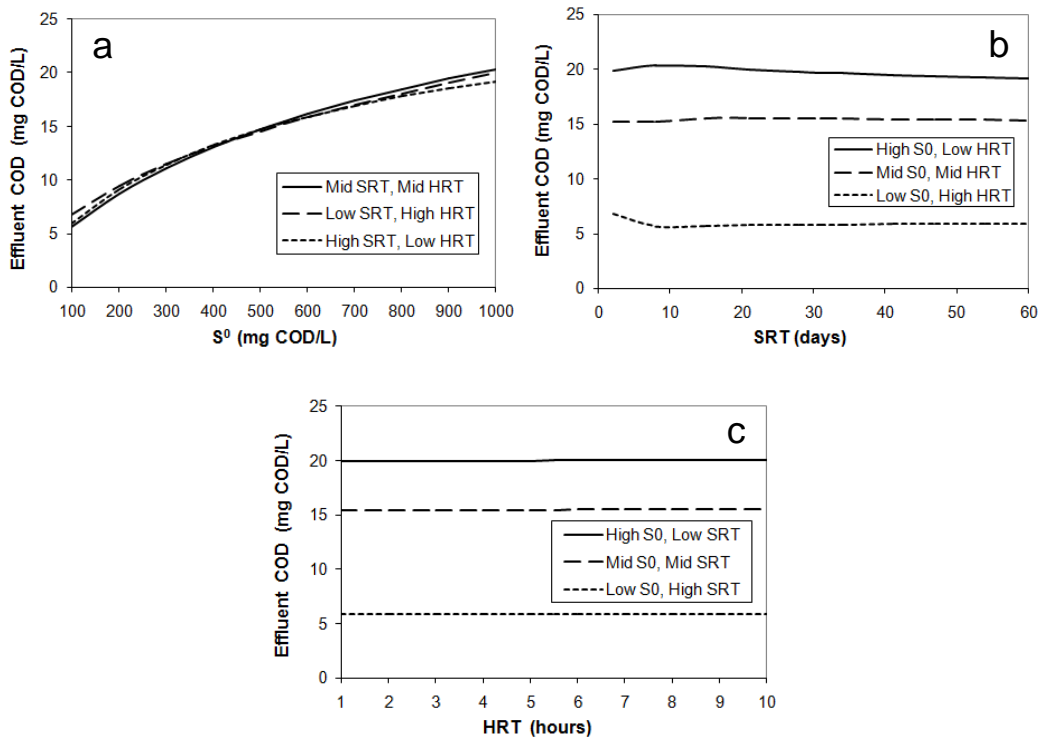
Figure 7.2. Effect of (a) S^0, (b) SRT, and (c) HRT on effluent COD.

Figure 7.2a shows that S^0 has a pronounced impact on effluent COD, but HRT and SRT have minimal effects. COD in the effluent rises steadily when the influent COD concentration increases: from ~ 6 mg COD/L for S^0 = 100 mg COD/L to ~ 20 mg/L for S^0 = 1,000 mg COD/L. However, the increase in effluent COD is not proportional to the increase in S^0, and the percentage COD removal goes from ~ 94% to ~ 98%. The very narrow band of curves, reflecting small differences in effluent COD concentrations despite very different operation regimes for SRT and HRT, means that effluent COD is not sensitive to SRT or HRT, which is confirmed by the flat slopes in Figs. 7.2b and 7.2c.

The components comprising effluent COD are shown in Fig. 7.3. Plots of effluent COD against S^0 and SRT highlight that BAPs dominates the effluent COD for SRT greater than about 8 days (81 to 91%), which is in good agreement with the experimental finding by Jang et al. (2007) that SMP accounts for 83-91% of COD in MBR effluents. In Fig. 7.3, UAP comprises 7 to 15%, while S is only 2 to 4% of COD in the effluent. BAPs makes up a larger fraction of the effluent COD as S^0 increases, but it becomes a smaller fraction of S^0. This explains why the percentage removal of COD goes up as S^0 is larger.
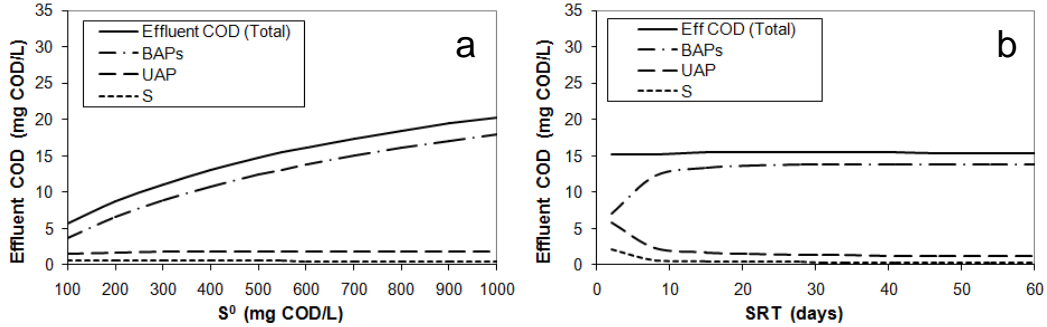
Figure 7.3. Constituents of effluent COD with respect to (a) influent COD and (b) SRT. Non-varied parameters are fixed at typical values (S^0 = 550 mg COD/L; SRT = 12.5 days; HRT = 5.5 hours; x_{BAPS} = 0.35).

Since BAPs controls effluent COD, effluent quality is changed if the membrane retains more or less BAP. In the model, this is reflected by the ratio of BAPs to total BAP (i.e., x_{BAPS}). We used a typical value of x_{BAPS} = 0.35 (de Silva et al., 1998; Jang et al., 2007) to generate the results in Figs. 7.2 and 7.3. Having x_{BAPS} = 1 is the same as having activated sludge with a settler instead of a membrane, and a value of 0 reflects retention of all BAP. Figure 7.4 quantifies the importance of x_{BAPS} on effluent COD. The effluent COD could decline to as low as 2 mg COD/L if all BAP were retained by the membrane. The value for achieving our typical retention of BAP_L (x_{BAPS} = 0.35) is apparent, since the effluent COD (~ 15 mg COD/L) is only about 35% of that for no BAP retention.
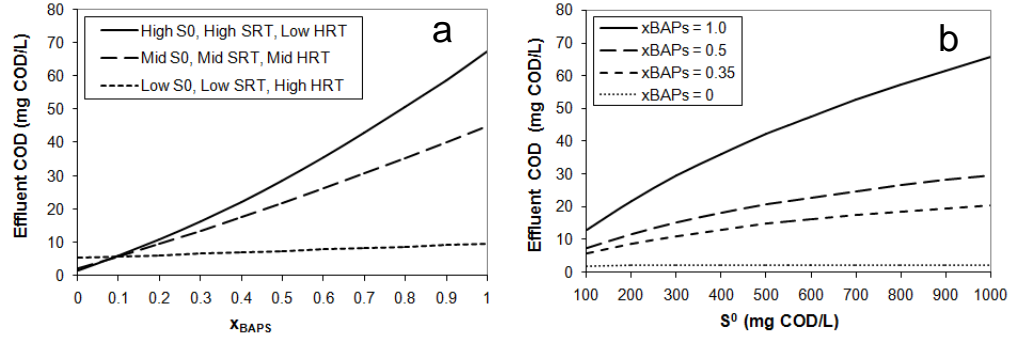
Figure 7.4. (a) Effect of varying x_{BAPS} of three different scenarios on effluent COD. (b) Effluent COD as a function of S^0 and x_{BAPS}; SRT and HRT are typical values (12.5 days and 5.5 hours, respectively).

Oppenheimer et al. (2010) tabulated the effluent COD values from the full-scale MBR facilities and found that the range was 8 – 30 mg COD/L. The modeling results in Figs. 7.2 and 7.3 correspond to the observed values. Seeing some observed values well above 15 mg COD/L suggests that x_{BAPS} may have been larger than 0.35 in some cases. Since x_{BAPS} is poorly understood, but has a strong impact on effluent quality, it deserves attention as a means to characterize membranes used in MBRs.

Mixed Liquor Volatile Suspended Solids

Figure 7.5 illustrates the impact of S^0, SRT, and HRT on MLVSS. Note that the concentrations are plotted logarithmically. As is well known for all activated sludge processes (Rittmann and McCarty, 2001), MLVSS increases when the influent substrate increases (Fig. 7.5a), the SRT increases (Fig. 7.5b), and the HRT decreases (Fig. 7.5c). The fact that the top curve in Fig. 7.5a has MLVSS concentrations so much higher than the other curves demonstrates that the combination of high SRT and low HRT can allow a

145

very high MLVSS. This is reflected by the bioconcentration factor, SRT/HRT, which is 1,440 for the top curve in Fig. 7.5a, but only 55 for the intermediate curve. In the high-extreme case, the MLVSS curve extends from about 20,000 to about 220,000 mg VSS/L, making volumetric loading $4 - 25$ kg COD/m^3-d, which is much higher than typical MBR loading rates ($1.2 - 3.6$ kg COD/m^3-d) (Metcalf and Eddy 2003; Oppenheimer et al. 2010). Clearly, the MLVSS and volumetric loading values for the high-extreme case are unrealistic, and it is not feasible to have an SRT/HRT ratio close to 1,400. For the typical case, the MLVSS is in the range of 1,300 to 13,000 mg/L, which corresponds reasonably well to the values tabulated by Oppenheimer et al. (2010) in their survey of full-scale MBR facilities: 4,200 to 20,000 mg/L. The generally higher values from the field survey probably reflect that SRT/HRT ratios were somewhat larger than the value for our intermediate case (55).

As shown in Fig. 7.5b, the MLVSS concentration changes most rapidly when SRT increases from 2 to 10 days. In Fig. 7.5c, the slopes of the curves are steepest with a 1- to 2-hour HRT, when small decreases in HRT yield significant increases in MLVSS concentration.
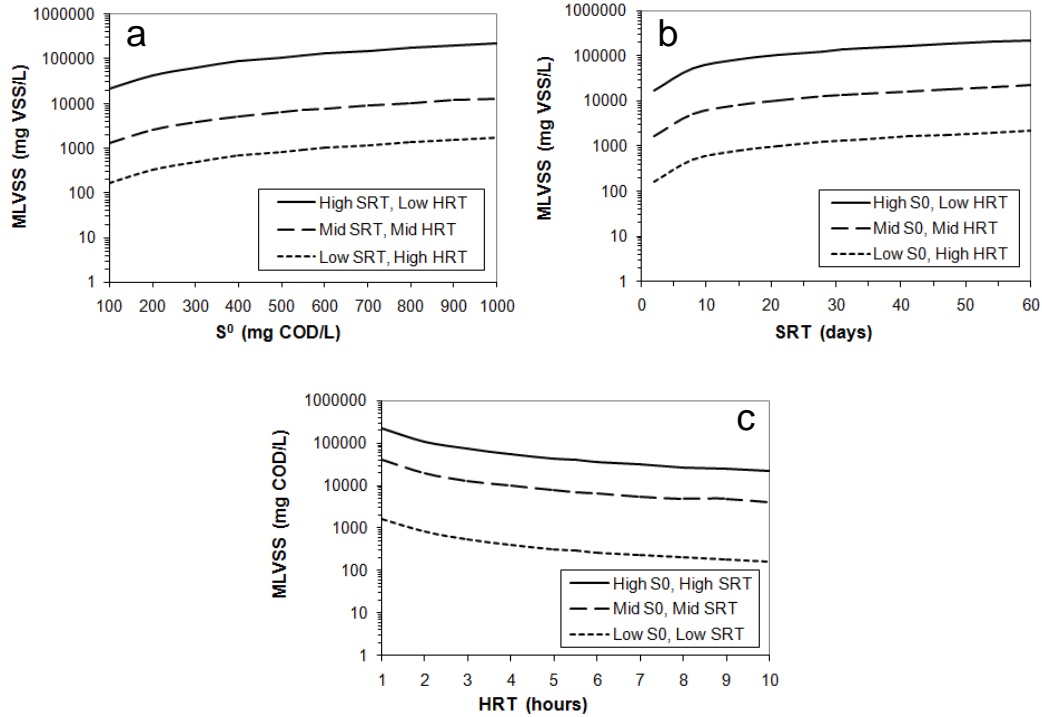
Figure 7.5. Effect of (a) S^0, (b) SRT, and (c) HRT on MLVSS. Note that the MLVSS concentrations are plotted on a logarithmic scale due to the very large range of values.

The trends in Fig. 7.5a underscore the potential to achieve high values of MLVSS and volumetric loading in an MBR by achieving a large bioconcentration factor. The advantages in terms of capital costs and areal footprint are obvious, but they come with trade-offs that we quantify in upcoming sections.

Figure 7.6 shows quantitatively how X_a, X_{res}, and EPS contribute uniquely to MLVSS as S^0 and SRT vary. The rate of change of all biomass concentrations is greatest for SRT less than about 10 days. All components increase with increasing S^0 (Fig. 7.6a) and increasing SRT (Fig. 7.6b), since they are solids. X_a increases relatively more strongly with S^0, because it is

147

the direct result of substrate utilization. In contrast, X_{res} increases relatively more with SRT, since it is the result of biomass decay. X_a makes up the largest portion of MLVSS only until an SRT of about 20 days, beyond which X_{res} becomes the dominant fraction. For an SRT of 60 days, X_{res} is 67% of the MLVSS, while X_a is only 25%. EPS generally follows X_a, but is more important at lower SRT: 48% of X_a at a SRT of 2 days versus 29% at 60 days.
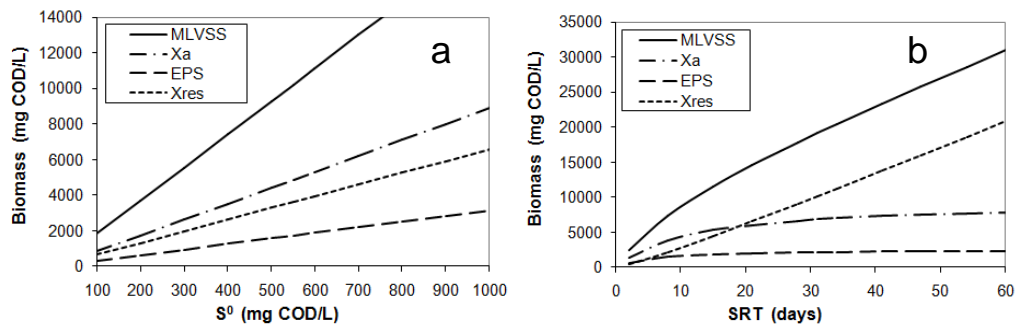
Figure 7.6. Effect of (a) S^0 and (b) SRT on biomass components. Non-varied parameters are fixed at typical values ($S^0 = 550$ mg COD/L; SRT = 12.5 days; HRT = 5.5 hours; $x_{BAPS} = 0.35$).

Solids Wasting

Figure 7.7 presents the influences of S^0, HRT, and SRT on the rate of MLVSS wasting, expressed as kg COD/d. As is the case for any activated sludge process, increasing S^0 or decreasing the SRT requires more sludge wasting, while HRT has no effect.

148
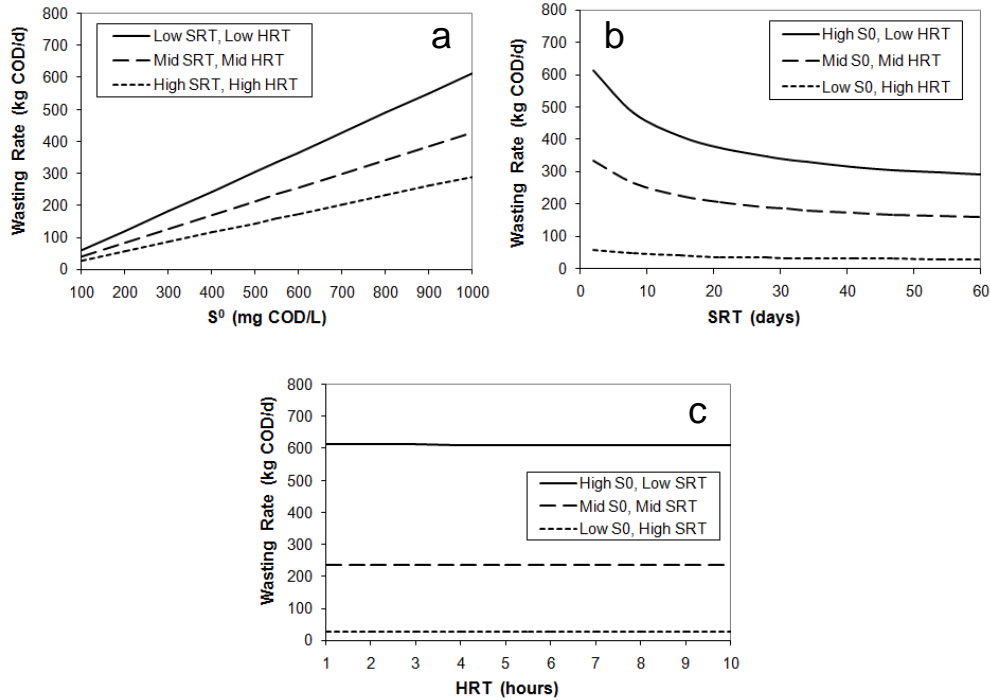
Figure 7.7. Effect of (a) S⁰, (b) SRT, and (c) HRT on sludge wasting rate.

Aeration Power

Figure 7.8 illustrates strong impacts of S^0, SRT, and HRT on required aeration power. The results reflect an interaction between the oxygen demand that must be met and the effect of MLSS on aeration efficiency. For a given reactor volume, the influent substrate loading is increased when S^0 goes up or HRT goes down. Thus, part of the strong trends in Figs. 7.8a and 7.8c are due to this loading effect. Likewise, a longer SRT allows more endogenous respiration of biomass components, and part of the rise in aeration power in Fig. 7.8b is from this effect.

149
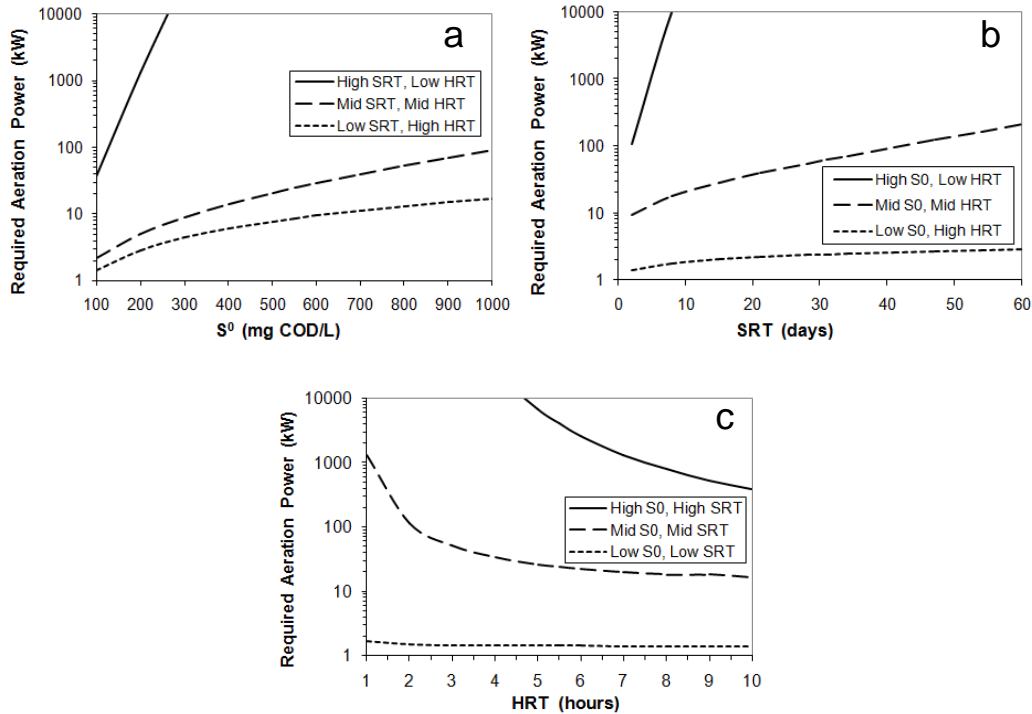
Figure 7.8. Effect of (a) S^0, (b) SRT, and (c) HRT on required aeration power.

The impacts of MLSS on aeration efficiency are even stronger than those from oxygen demand. High MLSS concentration decreases the efficiency of oxygen transfer in wastewater (Schwartz et al., 2006), and this is reflected by the way in which the a factor is affected by MLSS in Eqn. 7.13. When a decreases, Eqn. 7.12 shows that the field oxygen transfer efficiency (FOTE) declines proportionally, and more aeration power is required for the same oxygen demand. Thus, the power requirements for the top curve are unrealistically high, another reason why operation with such a high SRT/HRT ratio is impractical. For the intermediate curve, the aeration power requirement is 1.2 to 5.2 kWh/kg COD removed, or 0.05 to 2.2 kWh/m^3 of wastewater treated. Oppenheimer et al. (2010) found that full-scale MBR

facilities reported energy-use rates of $0.5 - 1.8$ kWh/m^3. The negative impact of a low α value is so profound that research needs to be focused intensely on this topic.

Trans-Membrane Flux

High MLSS also results in greater membrane fouling, which decreases trans-membrane flux (Schwartz et al., 2006). Figure 7.9 shows how increasing S^0 or SRT/HRT ratio, both of which increase the MLVSS (Fig. 7.5) and MLSS (Fig. 7.9d), causes the critical flux to decline. The critical flux for the intermediate case is around 22 L/m^2-h, but the range is from 12 to 41 L/m^2-h. Oppenheimer et al. (2010) found a range of 12 to 42 L/m^2-h for operating fluxes, which is an amazing correspondence. The strong sensitivity of critical flux to MLSS presented here underscores that better quantification of the relationship could have an important impact on defining the trade-off inherent to MBRs.

Conclusions

While the MBR behaves like any activated sludge process in most ways, the membrane separator changes some factors that improve effluent quality and the ability to accumulate a high MLSS concentration. Based on the unified model for the key biomass and soluble components in all activated sludge processes, we created a mechanistic model that is directly relevant to the unique conditions of MBRs. Specifically, we divided the BAP into a large fraction that is retained by the membrane separator and a small fraction that passes through the membrane, included relationships for how high MLSS
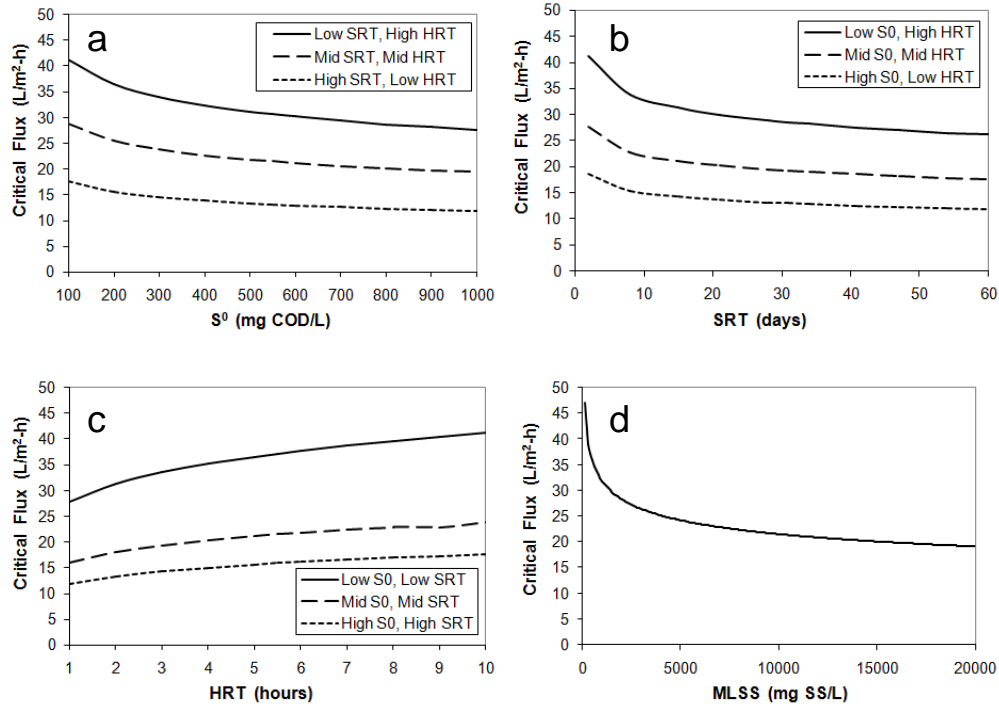
Figure 7.9. Effect of (a) S^0, (b) SRT, (c) HRT, and (d) MLSS concentration on critical trans-membrane flux.

concentration lowers the oxygen-transfer rate and the trans-membrane flux, and solved the model for ranges of S^0, SRT, and HRT relevant to MBR operation.

The effluent COD is most sensitive to the influent COD concentration and to the ability of the membrane to retain BAP_L. High influent COD or a membrane that is relatively permeable to BAP (i.e., has a large x_{BAPS}) results in larger effluent COD. The ability of the membrane to retain biomass makes it possible to operate an MBR with a high SRT/HRT ratio, and that can make the MLVSS and MLSS quite high. The volumetric loading also increases proportionally. While high MLSS has obvious benefits in terms of lowering capital costs and land-area requirements, it leads to trade-offs, since high

MLSS increases the aeration power required per unit COD and decreases the trans-membrane flux.

Several factors that strongly affect MBR performance are poorly understood. High marginal benefits should be obtained by research focused on quantifying how membranes retain BAP (i.e., what is x_{BAPS}?) and how α and the critical trans-membrane flux are affected by MLSS or a particular component of the mixed liquor (e.g., EPS or BAP_L). The components included in our model and the trends shown by it should help guide the MBR field towards the most productive areas for research and development.

Chapter 8

DISSERTATION SYNTHESIS

Introduction

The use of engineered nanomaterials (ENMs) in consumer products
has increased exponentially over the past decade. As nanotechnology
improves and applications become even broader, the variety of ENMs
produced and used will also grow. The combinations of materials,
functionalizations, sizes, and shapes of ENMs are seemingly innumerable.
Mechanistic models will be useful tools for predicting the fate of these
materials in the environment. While models have been developed to predict
the fate of soluble compounds in wastewater treatment plants (WWTPs),
such models for nanomaterials currently do not exist. The purpose of this
chapter is to outline approaches for synthesizing experimental knowledge
presented in this dissertation with models to predict ENM fate in WWTPs.

Chemicals are removed during municipal wastewater treatment by
three main processes: (1) volatilization, (2) biodegradation, and (3) sorption
(Lee et al., 1998). For the sake of simplicity, volatilization and
biodegradation are assumed to be negligible, and sorption is the only removal
mechanism included in the model scenarios. In an activated sludge basin,
most viruses, which can be considered biological nanoparticles, are removed
by sorption to sludge floc (Kim et al., 1995). Sorption is defined here as
consisting of two phenomena: (1) adsorption of a nanoparticle from the bulk
liquid onto the surface of sludge, and (2) partitioning of a nanoparticle from
the aqueous phase into the organic phase of sludge (Wang et al., 1993). Thus,

154

nanoparticles will either be in the liquid phase of wastewater, or they will be associated with wastewater biomass.

ENM Sorption to Wastewater Biomass: Insight from Bacterial Adhesion to Surfaces

While exploration of nanoparticle adhesion to bacteria has only recently begun, bacterial adhesion to various surfaces has been studied in detail for several decades. Researchers have qualitatively and quantitatively described mechanisms of bacterial attachment to surfaces such as iron oxide, titanium, silver, and polystyrene (van Loosdrecht et al., 1990; Wassall et al., 1997; Li and Logan, 2004; Scarano et al., 2004). In the past few years, several studies have been published on the attachment of iron oxide, titanium, silver, and polystyrene nanoparticles to bacteria (Zita and Hermansson, 1997a; Kiser et al., 2010; Wigginton et al., 2010; Zhang et al., 2011). Thus, the materials in these two types of studies are the same, but the scales of the sorbents and sorbates are reversed (e.g., bacterial attachment to polystyrene surfaces, versus polystyrene nanoparticle attachment to bacterial surfaces). Reviewing insight gleaned from past studies of bacterial attachment to surfaces may shed light on results obtained from recent nanoparticle-bacteria sorption experiments. Furthermore, bacterial adhesion studies may provide direction for formulating experiments and models to improve our comprehension of nanoparticle attachment to biological surfaces.

Bacteria generally prefer to be sessile (attached to surfaces that provide favorable conditions for growth) rather than planktonic (suspended as individual cells in aqueous environments) (An et al., 2000). In nature,

bacteria ubiquitously grow in biofilms by attaching to solid surfaces and proliferating (Rittmann and McCarty, 2001). Biofilms often endow bacteria with greater resistance to enzymes, antibodies, antibiotics, disinfectants, and other bacteriostatic or bactericidal agents. Furthermore, adherent bacteria can sometimes be superior competitors for nutrients than planktonic bacteria (An et al., 2000). Biofilms are used to reduce nutrients, pathogens, and organic and inorganic compounds in many wastewater treatment systems, such as trickling filters, rotating biological contactors, and anaerobic filters (Rittmann and McCarty, 2001). Bacteria can also adhere to each other in the form of floc. Conventional activated sludge and membrane bioreactors use suspended bacterial floc to treat wastewater. For both biofilm and floc formation, the ability of bacteria to adhere to surfaces is of fundamental importance. Bacterial cell surface hydrophobicity is widely accepted as one of the most important factors that govern bacterial adhesion to various surfaces, such as the air-water interface, the oil-water interface, biomaterials, teeth, animal cells, and activated sludge (Paul and Jeffrey, 1985; Zita and Hermansson, 1997a; Dickinson, 2006).

A bacterium changes from a planktonic to a sessile state through a series of steps. First, the bacterium must approach a surface via fluid convection or motility. Next, the bacterium must cross the quiescent layer of fluid near the surface via Brownian motion (Dickinson, 2006). Furthermore, a relatively hydrophobic microorganism or particle suspended in water is likely to concentrate at air-water and solid-water interfaces as polar water molecules associate strongly with themselves and exclude nonpolar molecules

(Maier et al., 2000). Initial, reversible attachment occurs when the bacterium reaches a separation distance where attractive interaction forces between the bacterium and surface become greater than thermal forces driving Brownian motion and repulsive forces between the two objects. In general, van der Waals forces and hydrophobic interactions are attractive, and electrostatic interactions are repulsive since both cell and particle surfaces are usually negatively charged (Maier et al., 2000). Many bacteria and most surfaces are hydrophobic to some degree, and attractive hydrophobic interactions tend to overcome repulsion (Gristina, 1987). Studies show that hydrophobic forces are exerted at distances as great as 15 nm; at 8 to 10 nm, hydrophobic forces are 10 to 100 times greater than van der Waals forces (Gristina, 1987). When a bacterium is within 1 nm or less of a surface, short-range chemical interactions (ionic, hydrogen, and covalent bonding) may occur (Gristina, 1987). These general steps of bacterial attachment to a surface may represent the steps of nanoparticle adhesion to bacterial surfaces – convection, which includes advection and diffusion, through the bulk fluid, Brownian motion in the quiescent fluid layer above a surface, and the dominance of attractive forces over repulsion.

While bacterial surface charge has been attributed to carboxyl groups (-COOH), hydrophobicity has been linked with hydrocarbons (C-(C,H)) and surface proteins (van Loosdrecht et al., 1987a; Hamadi et al., 2008). Bacterial surface projections, such as fimbriae and pili, may improve chances of adhesion. Surface proteins that impart cell surface hydrophobicity and promote adhesion are often packaged onto these structures (Paul and Jeffrey,

157

1985). In bacteria without surface projections, hydrophobic proteins may be distributed uniformly in a layer over the cell surface (Paul and Jeffrey, 1985). Some researchers have found that "bald" bacteria, lacking surface appendages, have a lower tendency to adhere to various surfaces (An et al., 2000).

Bacillus subtilis is an example of a bacterium without surface projections and with little tendency to bind to animal tissue; *B. subtilis* spores, however, bind to various surfaces because the spores are hydrophobic (An et al., 2000). Li and Logan (2004) also demonstrated that *B. subtilis* had low adhesion to glass, sand, and various metal oxide surfaces, while *Escherichia coli* showed stronger adhesion to these surfaces. In experiments evaluating fullerene association with *B. subtilis* and *E. coli* cells, C_{60} aggregates associated only slightly to *B. subtilis* and significantly more to *E. coli* (Lyon et al., 2005). Though the authors did not measure cell surface hydrophobicity or charge, the *E. coli* strain used in these experiments (DH5α) are fimbriaeted (Chart et al., 2000), which may be why the hydrophobic C_{60} nanoparticles sorbed more to *E. coli* than to *B. subtilis*.

Over time, initial and reversible bacterial attachment to a surface can become irreversible – resistant to any subsequent dislodging forces, such as shear forces from the fluid medium (Maier et al., 2000). Irreversible attachment is initiated when reversibly-attached bacteria excrete extracellular polymeric substances (EPS) (Maier et al., 2000). EPS forms a matrix that surrounds the cell and creates a strong chemical bridge to a surface. Although EPS are a component of microbial assemblages, these

polymers are unlikely to be involved in the initial adhesion process because EPS are often hydrophilic, loosely attached to cells, and have been found to decrease adhesiveness. Instead, EPS production is likely to be a later feature in the development of such assemblages (Wrangstadh et al., 1986; Paul and Jeffrey, 1985). Hydrophobic surface proteins are probably responsible for initial adhesion, while hydrophilic extracellular polymers and proteins coat bacterial surfaces and offer protection from hydrolytic enzymes and other compounds that might negatively impact bacteria (Bar-Or, 1990). In an experiment described in Chapter 5 (Kiser et al., 2010), we found that when some portion of EPS (hydrophilic) was extracted from wastewater biomass, sorption of C_{60} aggregates (hydrophobic) to the biomass increased.

The same factors involved with bacterial attachment to surfaces are also key for floc formation in activated sludge systems, such as conventional or membrane bioreactor wastewater treatment systems. Floc formation occurs naturally with increasing solids retention time and is initiated by floc-forming bacteria, which are able to produce three cellular components that enable them to agglutinate – pili or fimbriae, EPS, and poly-beta-hydroxybutyrate (PHB) granules. Bacterial cells become joined together when bivalent cations in solution, such as Ca^{2+}, bridge fimbriae together. Ionized fimbriae not joined together remain exposed to the bulk solution and act like wisps of a broom as they sweep and remove fine solids and heavy metals from the bulk solution (Gerardi, 2006). Adhesion of WWTP bacteria to activated sludge floc was found to be dependent on overall cell surface hydrophobicity; free-living cells had low levels of cell surface hydrophobicity

159

and escaped sedimentation in secondary clarifiers (Zita and Hermansson, 1997b).

Researchers have shown that as substrate hydrophobicity increases, microbial adhesion tends to increase (Fletcher and Loeb, 1979; Paul and Jeffrey, 1985; Klotz, 1990). For example, Fletcher and Loeb found a direct correlation between substrate hydrophobicity and the number of marine pseudomonads adhering to the substrate. *Propionibacterium acnes*, a relatively hydrophobic strain of bacteria known to infect patients with implanted plastic medical devices, adhere best to low-surface-energy (i.e., hydrophobic) substrates (acrylic > Plexiglas >> glass) (Klotz, 1990). Holgers and Ljungh (1999) found greater microbial adhesion to polymer percutaneous medical implants than to metal implants. Metals have relatively hydrophilic surfaces whereas polymers are typically hydrophobic, and the sorption of bacterial proteins to hydrophobic surfaces is more energetically favorable than sorption to metal surfaces (Holgers and Ljungh, 1999). Similarly, in our experiments described in Chapters 3, 5, and 6 (Kiser et al., 2009, 2010, 2011), we found that the more hydrophobic nanomaterials (polystyrene, C_{60}) generally sorb more than relatively less hydrophobic metal nanomaterials (silver, titanium dioxide) to fresh activated sludge.

Another research group found that the affinity of *P. aeruginosa* fimbriae for polystyrene was approximately 60 times greater than the measured affinity for stainless steel (Irvin, 1990). Ong et al. (1999) used atomic force microscopy (AFM) to measure forces between *E. coli* strains D21 and D21f2. The D21f2 strain was determined to be relatively more

hydrophobic than D21. The authors found that the attractive force for the more hydrophobic D21f2 strain increases with respect to hydrophobicity of the substrate (mica < glass < polystyrene < Teflon). D21, the more hydrophilic strain, displayed the opposite behavior of D21f2 and adhered to a greater extent to the more hydrophilic substrates (mica and glass) than polystyrene and Teflon.

Along with substrate hydrophobicity, cell surface hydrophobicity affects bacterial adhesion. Van Loosdrecht et al. (1987a,b) found that bacteria with hydrophobic cell walls adhered to a sulfated polystyrene surface to a greater extent than hydrophilic cells. Likewise, a recent study found that diffusion of polystyrene nanoparticles in biofilms is altered by bacterial cell wall hydrophobicity (Habimana et al., 2011). To explore the influence of bacterial surface properties on intrabiofilm nanoparticle mobility, the authors used genetically-engineered hydrophilic and hydrophobic cells of *Lactococcus lactis* yielding similar biofilm architectures to study the diffusion of 50-nm fluorescent carboxylate-modified polystyrene nanoparticles inside these two types of biofilms. They found that a lower fraction of polystyrene nanoparticles freely diffuse in the biofilm of the hydrophobic strain than in the more hydrophilic biofilm due to greater interaction of the particles with the hydrophobic bacterial cell walls.

Bales et al. (1993) conducted a study on the transport of two bacteriophages (viruses that attach to and infect bacteria) with different surface characteristics through silica bead columns. At pH 5.5, PRD-1, an icosahedral lipid-containing phage with a diameter of 62-nm, adhered to the

beads to a much greater extent than MS-2, an icosahedral, 26-nm phage with both hydrophobic and hydrophilic moieties on its coat. Phage adhesion is very dependent on pH. However, for a very hydrophobic phage, such as PRD-1, pH has less effect on adhesion. Although the authors increased pH to 7.6, a significant amount of PRD-1 still remained attached to the beads, suggesting that hydrophobic effects are dominant over electrostatic interactions for PRD-1. The results of this experiment are directly relevant to the study of nanoparticle-bacteria association, since viruses can be considered as biological nanoparticles or colloids.

The dominance of hydrophobic interactions over electrostatic forces for surface attachment of the more hydrophobic virus is also seen on the scale of bacterial surface attachment. Van Loosdrecht et al. (1990) examined adhesion of a range of bacteria with different cell surface properties (hydrophobicities and charge) to two surfaces – one hydrophilic (glass) and one hydrophobic (polystyrene). The effects of both hydrophobicity and charge on bacterial adhesion were considered. Cell surface hydrophobicity was found to be the dominant force in adhesion to the hydrophobic polystyrene surface. For bacteria with high surface hydrophobicities, adhesion was strong regardless of cell surface charge, which is similar to the results of PRD-1 transport found by Bales et al. For bacteria with low cell surface hydrophobicities, cell surface charge played a greater role in adhesion. For the case of adhesion to the hydrophilic surface (glass), cells with high surface charge did not adhere well, and hydrophobicity had little impact. For cells with low surface charge, hydrophobicity became more important for cell

adhesion: as hydrophobicity increased, adhesion increased. Thus, two general trends of bacterial adhesion were demonstrated in van Loosdrecht's study that could be useful for predicting initial adhesion of a particular microbe: (1) adhesion typically increases with increasing hydrophobicity of either the substrate or the cell surface, and (2) adhesion generally increases with decreasing surface charge.

If bacterial adhesion to a surface is any indication of nanoparticle adhesion to bacteria, then van Loosdrecht's study provides interesting clues about mechanisms that might dictate nanoparticle sorption to solids. To test the contributions of surface hydrophobicity and charge in nanoparticle adhesion, the van Loosdrecht study could be used as a blueprint for experimental methodology. A wide range of well-characterized (surface hydrophobicity, charge, size) nanoparticles could be used in sorption studies with a wide range of biotic (e.g., bacteria) and abiotic (e.g., filters and membranes) surfaces with various hydrophobicities and charge. Correlations between nanoparticle and solid surface properties for predicting nanoparticle sorption could be exposed. While the measurement of nanoparticle surface charge is well-established, a method of reliably measuring nanoparticle surface hydrophobicity needs to be developed.

Natural organic matter, proteins, and/or synthetic surfactants are abundant in natural surface waters, mammalian blood, and water and wastewater treatment systems. Surface-active compounds, such as fatty acids or Tween 80, usually reduce bacterial adhesion, particularly when the original surfaces are hydrophobic (van Loosdrecht et al., 1990). Paul and

163

Jeffrey (1985) studied the effect of Triton X-100 on adhesion of *Vibrio proteolytica*, a strain of marine bacteria, to hydrophilic and hydrophobic (polystyrene) substrata. Triton X-100 is a nonionic surfactant with a hydrophilic polyethylene oxide group and a hydrophobic (or lipophilic) hydrocarbon group. Triton X-100 at concentrations ranging from approximately 0.0025% to 0.1% completely (>99%) inhibited attachment of *V. proteolytica* to polystyrene but had no effect on attachment to the hydrophilic surface. This difference implies that either *V. proteolytica* has separate mechanisms of adhesion to hydrophilic and hydrophobic substrata and/or that the surfactant adsorbed to the hydrophobic surface, thereby inhibiting bacterial adhesion, but did not sorb as much to the hydrophilic surface.

In addition, coating bacteria and/or solid surfaces with protein dramatically diminishes bacterial adhesion (van Loosdrecht, 1990). Bovine serum albumin, gelatin, fibrinogen, and pepsin inhibited adhesion of a marine pseudomonad to polystyrene whether the proteins were added simultaneously with the bacteria or by precoating the polystyrene with the proteins (Fletcher, 1976). Van Loosdrecht et al. (1990) found that a variety of proteins readily adsorb to polystyrene surfaces and tend to change the surface characteristics of polystyrene by reducing hydrophobicity and charge to various extents. The result of protein adsorption to polystyrene was a marked decrease in adhesion for most, but not all, of the strains of bacteria tested. Our experimental results, described in Chapter 6, revealed the same effect (but on reversed sorbent-sorbate scales) as that observed in van

164

Loosdrecht's study: in the high-protein FDH matrix, the sorption of

polystyrene nanoparticles to solids is greatly reduced.

In general, experimental results that we or other research groups

have produced on nanomaterial sorption to bacteria reflect similar results as

experiments on bacterial adhesion to surfaces. Because both cell and

substrate hydrophobicities play important roles in bacteria-surface

interactions, we can expect that nanoparticle surface hydrophobicity may be

an important property that should be considered in the study of the

environmental fate of nanomaterials. While a few studies have pointed

toward the role of hydrophobicity in nanoparticle-surface interactions, no

published studies to date address this property for predicting the

environmental fate of nanomaterials and, instead, place more emphasis on

zeta potential measurements, which may not be a reliable measurement for

predicting nanoparticle-surface interactions, especially if the type of

nanomaterial being observed is hydrophobic. Experiments should be

conducted from which mathematical relationships between nanoparticle

properties, such as hydrophobicity, zeta potential, and size, and sorption to

surfaces can be developed. Such mathematical relationships could then be

incorporated into fate models in which sorption is a removal mechanism.

Flocculant Settling of Nonsorbed Nanoparticles

As demonstrated in previous chapters of this dissertation, not all

nanomaterials sorb to solids – some particles were found to be stable in the

aqueous phase. In analyses of full-scale wastewater treatment plants,

nanoscale titanium oxide was identified in plant effluents. When samples

collected from the treatment train of a municipal WWTP were filtered, we saw that titanium in the filtrate was poorly removed across the treatment train; the bulk of titanium mass removed during treatment was from the larger, nonfilterable fraction. From our batch sorption experiments, we showed that for all of the nanoparticle types we tested, some fraction of dosed NPs remained in the liquid phase. The nonsorbed fraction was small (~ 7%) for the more hydrophobic particles (e.g., fullerenes, polystyrene nanoparticles) and larger (~ 40 – 60%) for functionalized nanoparticles (e.g. PVP-coated gold, gum-arabic-coated silver NPs). For NPs that do not sorb to sludge, the only other possible removal mechanism, assuming no volatilization, is flocculant settling. From calculating the settling velocity of a nanoparticle with some diameter, the likelihood of removal by flocculant settling can be assessed. Settling (terminal) velocity can be calculated using Stoke's Law:

$$v_S = \frac{2}{9} \frac{\left(\rho_p - \rho_f\right)}{\mu} gR^2 \tag{8.1}$$

where v_S is the particle's settling velocity (m/s), ρ_p is the particle density (kg/m^3), ρ_f is the fluid density (kg/m^3), μ is the dynamic viscosity (N-s/m^2), g is gravitational acceleration (9.81 m/s^2), and R is the radius of the spherical particle (m). Figure 8.1 shows particle settling velocities for a range of sizes of nanoparticles or nanoparticle aggregates that were used in our experimental work. For a particle to be removed during sedimentation, its settling velocity (v_S) must be equal to or greater than the critical settling

velocity (also known as the overflow rate), v_o, for the basin (Masters and Ela, 2008).

$$v_o = \frac{h}{\theta} = \frac{Q}{A_b} \qquad (8.2)$$

where h is the depth of the sedimentation basin (m), θ is the hydraulic retention time (d), Q is the volumetric flow rate of wastewater through the basin, and A_b is the surface area of the basin.
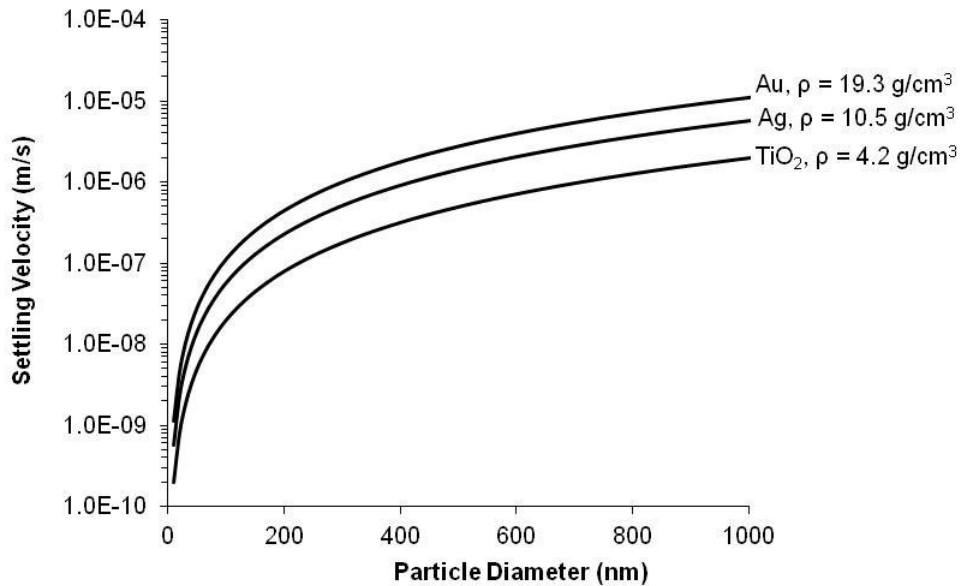
Figure 8.1. Settling velocities with respect to diameter of gold, silver, and titanium dioxide nanoparticles. ρ is the material's density.

Average overflow rates for settling following activated sludge are from 16 to 28 m/d (1.85×10^{-4} to 3.24×10^{-4} m/s, respectively). The settling velocities for nanoparticle suspensions we used in our experiments (all with diameters less than 100 nm) are much smaller than the over flow rates; thus, these particles will not settle out during sedimentation. For particle removal by

167

settling to occur, nanoparticle aggregates would have to be at least about 4, 5.5, and 10 µm for gold, silver, and TiO_2 NPs, respectively. The nanosuspensions that we used were stable (nonsignificant homoaggregation) during the time scales used in our experiments. Our findings of nanoscale titanium oxides particles and aggregates (50 to a few hundred nm) in WWTP effluents is evidence of the lack of removal of NPs by flocculant settling. Thus, nanoparticles in the liquid phase will leave the plant with treated effluent.

Models for Predicting ENM Fate During Biological Wastewater Treatment

Batch sorption experiments are important for quantifying contaminant affinity to activated sludge. Data generated from batch sorption experiments can be effectively used to predict the fate of ENMs in wastewater treatment plants when combined with mathematical modeling. Our approach to modeling is based on several stages of model development. First, we built a basic water quality model for membrane bioreactors based on Rittmann and McCarty's (2001) activated sludge model, and then updated the mathematical representation of microbiological processes following the Unified Theory model (Laspidou and Rittmann, 2002a). The development of this basic MBR model is discussed in Chapter 7. We then extended the basic model with Lee et al.'s (1998) advanced steady-state model for the fate of hydrophobic and volatile compounds in activated sludge, resulting in a robust MBR model to predict both effluent water quality and micropollutant fate. We also developed a water quality and fate model to represent a conventional

168

activated sludge (CAS) reactor (aeration basin and secondary clarifier).

Fortran codes for these models are included in Appendix B.

Though originally intended for fate prediction of soluble organic

compounds, the water quality and fate model could potentially be used for

ENMs. The models for soluble contaminant fate employ surface and bubble

volatilization, linear sorption, and biodegradation as contaminant removal

mechanisms from wastewater. At this time, we assume that sorption is the

dominant removal mechanism of ENMs in wastewater treatment plants and

neglect volatilization and biodegradation. If in future experimental work

other removal mechanisms are found to be important, they can be added to

the model. Two possible scenarios for simulating ENMS fate in WWTPs with

our model are presented here. The first scenario is the simplest – the

assumption of linear sorption of ENMs on sludge. The second scenario

represents nonlinear sorption of ENMs to activated sludge.

Scenario I: Linear Sorption

We make three assumptions for this scenario. First, we assume

aerobic, completely-mixed reactors. The batch sorption and SBR experiments

that we conducted in the lab (Chapters 3, 5, and 6) were done with aerobic

biomass. Using anaerobic biomass as sorbent may yield different results.

Though we focus on sorption in the aeration basin, the model could easily be

modified to represent primary clarifier, whose output would be the input to

an aeration basin. Second, we assume linear sorption. This assumption may

be justifiable when nanoparticle concentrations are low and solids

concentrations are high, which is likely to be the case in activated sludge

basins of municipal WWTPs. Finally, for MBRs, we assume perfect retention

of solids by the membrane, so that no solids are present in the reactor

effluent. For the CAS system, we assume a certain concentration of solids in

the secondary effluent to represent a fixed efficiency for the secondary

clarifier.

Nanoparticle sorption to solids can be described through a partition

(or distribution) coefficient, K_D. K_D is a factor representing the ratio of the

mass of adsorbate sorbed per mass of solid to the mass of adsorbate

remaining in solution at equilibrium. The partition coefficient is an

empirically-determined factor that roughly accounts for various

physicochemical mechanisms that are influenced by a myriad of variables.

Physicochemical mechanisms include van der Waals attractive forces,

hydrophobic bonding, hydrogen bonding, ligand exchange, ion exchange, and

chemisorption.

Partition coefficients can be determined experimentally through batch

sorption experiments like those described in Chapters 3, 5, and 6. We can

input data generated from these experiments into the Freundlich isotherm

model to describe sorption:

$$q_e = \mathrm{m/x} = K_D\, C_e^{1/n} \tag{8.3}$$

where q_e is the mass of nanoparticles sorbed per unit mass of bulk solid (mg

ENM/g biomass), m is the mass of adsorbent (mg biomass/L), x is the mass of

adsorbate (mg ENM/L), K_D is the Freundlich unit-capacity coefficient (L/g

biomass), C_e is the equilibrium concentration of ENM (mg ENM/L), and n is a

joint measure of both the relative magnitude and diversity of energies

associated with a particular sorption process (Weber et al., 1992). When $1/n$ is approximately 1, K_D is constant; thus, partitioning can be described as linear. Linear partitioning is generally described as the product of the linear sorption coefficient, $K_{D,L}$, and the equilibrium concentration of nanoparticles in the liquid phase.

$$q_e = K_{D,L} C_e \qquad (8.4)$$

For example, using data from sorption experiments with SiO_2-FITC NPs, we generated a Freundlich sorption isotherm. The equation to describe the plotted data was $q_e = 0.105 C_e^{1.102}$. Since the exponent is approximately 1, SiO_2-FITC sorption to wastewater biomass can be considered linear. With $q_e = 0.105 * C_e$, $K_{D,L} = 0.105$ L/g biomass. This sorption coefficient can then be used as a parameter in the water quality and fate model. In the context of our wastewater treatment models, the mass of sorbed nanoparticles per unit time is

$$M_{sorbed} = q_e X_v Q = K_{D,L} C_e X_v Q \qquad (8.5)$$

where X_v is the mixed liquor suspended solids (MLVSS) concentration (mg VSS/L), and Q is the reactor flow rate (L/d). MLVSS is the sum of active bacteria, inert (residual) bacteria, and extracellular polymeric substances (EPS). We can use this sorption term within our MBR and CAS models to calculate the concentration of nanoparticles remaining in the effluent, assuming sorption is the only removal mechanism. In general terms, (NP mass/time)effluent = (NP mass/time)influent − (NP mass/time)sorbed. For the MBR, we can calculate the liquid-phase equilibrium ENM concentration using the following equation:

171

$$C_{e,MBR} = \frac{Q^0 C_e^0}{Q^e + Q^w + K_{D,L} X_V^w Q^w} \quad (8.6)$$

where C_e is the equilibrium concentration of adsorbate (mg ENM/L) in the

liquid phase, Q^0 and C^0 are the influent volumetric flow rate (L/d) and

adsorbate concentration (mg ENM/L), respectively, X_V^w is the MLVSS

concentration in the waste stream, Q^e is the effluent volumetric flow rate

(L/d), and Q^w (L/d) is the flow rate of the waste stream. For the CAS system,

liquid-phase ENM concentration is described as follows:

$$C_{e,CAS} = \frac{Q^0 C_e^0}{Q^e + Q^w + K_{D,L} X_V^e Q^e + K_{D,L} X_V^w Q^w} \quad (8.7)$$

where X_V^e and X_V^w are MLVSS concentrations in the effluent and waste

streams, respectively. The derivations of Eqs. 8.6 and 8.7 are shown in

Appendix C. If other removal mechanisms were involved, they would be

included in Eqs. 8.6 and 8.7.

Scenario II: Nonlinear Sorption

If data collected from a sorption experiment were analyzed following

the Freundlich model and $1/n$ did not approach 1, then sorption could not be

considered linear. For example, in Chapter 3, we did batch sorption

experiments with Hombikat TiO_2 and wastewater biomass. The data were fit

with a nonlinear Freundlich isotherm: $q_e = 0.025 C_e^{0.53}$. Nonlinear sorption

would be represented in the wastewater models as follows:

$$M_{sorbed} = K_{D,NL} C_e^{1/n} X_V\, Q \quad (8.8)$$

where $K_{D,NL}$ is the nonlinear sorption coefficient (L/g biomass). To solve for

C_e with the nonlinear sorption term in the MBR model, Eq. 8.6 would become:

$$C_{e,MBR} = \frac{Q^0 C^0 - K_{D,NL} C_e^{1/n} X_v^w Q^w}{Q^e + Q^w} \tag{8.9}$$

For the CAS model, the following equation would be used to solve for the liquid-phase equilibrium ENM concentration:

$$C_{e,CAS} = \frac{Q^0 C^0 - K_{D,NL} C_e^{1/n} \left(X_v^e Q^e + X_v^w Q^w \right)}{Q^e + Q^w} \tag{8.10}$$

The derivations of Eqs. 8.9 and 8.10 are shown in Appendix C. Finding the solutions to Eqs. 8.9 and 8.10 requires an iterative numerical approach, such as simple fixed-point iteration or the Newton-Raphson method. An iteration method can be included in the code of the model. A stability analysis should be performed to ensure convergence on the root.

Multiple Sorption Coefficients

In Scenarios I and II, we discussed the use of experimentally-determined linear or nonlinear sorption coefficients in our models. Though wastewater biomass is a complex mixture of biotic and abiotic materials and has surface regions of various sorption potentials, the sorption coefficients determined from batch experiments represent the overall or composite association of nanoparticles with wastewater biomass. While an overall sorption coefficient may be sufficient for modeling the fate of ENMs during biological wastewater treatment, there may be interest in representing ENM sorption to a collection of different surface types in some natural or engineered treatment system, such as in soils or multi-media filters used for tertiary wastewater treatment.

Once the partition coefficients for each of the different surface types in a system are experimentally determined, they can be incorporated into the sorption term of a fate model. Weber et al. (1992) developed the distributed reactivity model (DRM) after observing that most natural soils and sediments are intrinsically heterogeneous in composition and structure at both interparticle and intraparticle scales. Physicochemical and structural heterogeneities of soils and sediments give rise to energetic differences between or within individual particles, which result in different combinations of linear and nonlinear "local" sorptions. The DRM describes contributing sorption reactions as a composite isotherm and could be applied to systems containing solid surfaces with different sorption potentials. For natural systems, the authors suggest that composite isotherm behavior is the result of a series of linear absorption (partitioning) reactions and nonlinear adsorption reactions. Composite linear absorption can be described as follows:

$$q_{e,r} = \sum_{i=1}^{m} x_i K_{D,Li} C_e = \left(\sum_{i=1}^{m} x_i K_{D,Li} \right) C_e = x_l K_{D,Lr} C_e \qquad (8.11)$$

where $q_{e,r}$ is the total adsorbate mass sorbed per unit mass of bulk solid, x_i is the mass fraction of the solid comprising reaction region or component i, $K_{D,Li}$ is the linear partition coefficient for reaction i expressed on a per mass of component i basis, x_l is the summed mass fraction of solid phase exhibiting linear sorptions, and $K_{D,Lr}$ is the mass-averaged linear partition coefficient (Weber et al., 1992).

Composite nonlinear sorption is expressed in the form of a Freundlich isotherm.

$$q_{e,r} = \sum_{i=1}^{m} (x_{nl})_i K_{D,NLi} C_e^{1/n,i}$$ (8.12)

where $(x_{nl})_i$ is the mass fraction of the ith nonlinearly sorbing component, $K_{D,NLi}$ is the nonlinear sorption coefficient for reaction i expressed on a per mass of component i basis, and $C_e^{1/n,i}$ is the adsorbate concentration resulting from reaction i (Weber et al., 1992). The authors use the Freundlich model because it assumes neither homogeneous site energies nor limited levels of sorption, unlike the constant-energy, limited-surface Langmuir model. The complete expression, including both linear absorption and nonlinear adsorption, becomes:

$$q_{e,r} = x_l K_{D,Lr} C_e + \sum_{i=1}^{m} (x_{nl})_i K_{D,NLi} C_e^{1/n,i}$$ (8.13)

ENM Fate Modeling Strategy

After incorporating the nanoparticle-fate equations described above into CAS or MBR treatment models, we can run the models as detailed in Chapter 7 – using ranges of influent substrate concentration, solids retention time, and hydraulic retention time that are relevant to plant operation. In doing so, we could gauge the effects of fundamental operational parameters on the fate of nanomaterials in wastewater treatment plants. The performance of MBR and CAS systems in terms of nanomaterial removal could be compared, and we could use the model to optimize the operation of each system for maximum nanomaterial removal from wastewater.

Conclusions

Experimental results that we or other research groups have produced on nanomaterial sorption to bacteria reflect similar results as experiments on bacterial adhesion to surfaces. Surface hydrophobicity and the presence of natural organic matter, proteins, and surfactants have been established as important factors for bacterial adhesion, and current studies indicate that these factors may also be important for controlling nanoparticle interaction with solids. Experiments should be conducted from which mathematical relationships between nanoparticle properties, such as hydrophobicity, zeta potential, and size, and sorption to surfaces can be developed. Such mathematical relationships could then be incorporated into fate models in which sorption is a removal mechanism. By coupling the basic wastewater treatment water quality model presented in Chapter 7 with a micropollutant fate model, we can begin to develop a model to predict the fate of nanomaterials during biological wastewater treatment. The fate model should include a nonlinear sorption term if experimental results indicate nonlinear sorption, and the sorption coefficient values for each nanoparticle type would have to be determined through batch sorption experiments. Through running the model with a range of parameter values, such as low to high values of solids retention times, the effect of operation on the fate of nanomaterials during treatment can be gauged.

Chapter 9

SUMMARY AND CONCLUSIONS

The main goal of this research was to gain insight into the fate of

nanomaterials in a wastewater treatment plant. The objectives of this

dissertation were to:

1. Characterize nanomaterials in each unit operation, in biosolids, and in

    treated effluent of a full-scale conventional activated sludge

    wastewater treatment plant..

2. Measure, characterize, and compare nanomaterial removal and

    release from several different types of full-scale wastewater treatment

    plants: conventional activated sludge, activated sludge with advanced

    tertiary treatment, membrane bioreactor, and trickling filter plants).

3. Quantify the sorption of various types of nanomaterials to wastewater

    biomass in laboratory-scale batch experiments.

4. Compare fresh and freeze-dried activated sludge as sorbents in

    laboratory-scale batch experiments to test nanomaterial sorption to

    wastewater biomass.

5. Develop a comprehensive, mechanistic model of a biological

    wastewater treatment reactor to predict basic reactor performance

    and to serve as the basis of a model to predict nanomaterial fate

    during treatment.

Each of the main chapters in this dissertation (Chapters 3 through 7)

presented research that was designed to accomplish an objective. A summary

of the main findings from each chapter is provided here.

177

Summary of Observations

Chapter 3: Titanium Nanomaterial Removal and Release from Wastewater
Treatment Plants

- At a full-scale conventional activated sludge WWTP, raw sewage
  collected from headworks contained 100 to almost 3000 µg Ti/L with <
  50 µg Ti/L in the size fraction that passed through a 0.7-µm nominal
  glass fiber filter.

- For June 2008 11:00 a.m. samples, 60% of influent total Ti (185 µg
  Ti/L) was removed during primary treatment, about 60% of primary
  effluent total Ti was removed after activated sludge and secondary
  clarification, and approximately 40% of secondary effluent was
  removed during tertiary treatment.

- As Ti was removed, it accumulated in settled solids at concentrations
  ranging from 1 to 6 µg Ti/mg solids.

- The average overall removal of Ti for June 2008 and January 2009
  sampling experiments was $82 \pm 21\%$.

- About 10 to 100 µg Ti/L was measured in finished effluent samples.

- Ti-containing solids were imaged in sewage, biosolids, and WWTP
  liquid effluent, as well as in commercial products containing
  engineered nanoscale TiO_2. Spherical aggregates (50 to a few hundred
  nm in size) comprised of sub-50 nm spheres of only Ti and oxygen
  (presumably TiO_2) were observed in all samples.

- Lab-scale experiments showed that TiO_2 particles have an affinity for
  solids, and the majority of TiO_2 in water – on the order of 70 to 85% -

will be removed by wastewater biomass concentrations of around 2,000 to 3,000 mg/L TSS.

- Results from lab-scale experiments substantiated Ti removal observed in the full-scale WWTP (both scales achieved comparable percentage Ti removals).

Chapter 4: Occurrence and Removal of Titanium and Full-Scale Wastewater Treatment Plants: Implications for TiO_2 Nanomaterials

- Raw sewage titanium concentrations for 10 representative WWTPs using various unit processes ranged from 181 to 1233 µg Ti/L.

- WWTPs removed more than 96% of the influent titanium and all WWTPs had effluent titanium concentrations of less than 25 µg Ti/L, which is consistent with findings described in the previous chapter.

- Attached (trickling filters) and suspended (activated sludge) biological treatment processes play an important role in "trapping" NPs in biomass, which can then be settled or removed via membrane filtration.

- Using high-resolution TEM, TiO_x nanoparticles with diameters ranging from 4 to 30 nm were identified in WWTP effluents.

- Microfiltration-treated wastewaters contain fewer nanoparticles than conventionally settled wastewater.

- Though beyond the scope of the research presented in this chapter, silica nanoparticles were detected in wastewater effluents at far higher concentrations than TiO_x.

Chapter 5: Biosorption of Nanoparticles to Heterotrophic Wastewater Biomass

- Epifluorescence images showed fluorescent SiO_2-FITC nanoparticles sorbed to the surface of biomass.

- 88% of aqueous fullerenes, 39% of carboxylate-functionalized nanosilver, 23% of nanoscale titanium dioxide, and 13% of fullerol (hydroxylated fullerene) sorbed to 400 mg/L TSS of wastewater biomass.

- Of all of the NP types investigated, aq-nC_{60} showed the greatest decrease in sorption when equilibrated with 0.5 mg/L NOM or when some portion of EPS was extracted from biomass.

- Fullerene sorption decreased when samples contained 1% SDS.

- Functionalizing fullerenes (hydroxyl groups or polyvinylpyrrolidone) increased their stability in the liquid phase and thus decreased their sorption to wastewater biomass.

Chapter 6: Nanomaterial Transformation and Interaction with Fresh and Freeze-Dried Wastewater Biomass

- Model soluble compounds (methylene blue, 17α-ethinylestradiol, and ionic silver) sorbed similarly to fresh and freeze-dried-and-heated (FDH) activated sludge.

- Nanoparticle sorption to FDH biomass was approximately 60 to 100 percent less than to fresh biomass.

- Freeze-drying and heat-treating activated sludge denatures proteins.

- Supernatant of 1600 mg/L TSS of FDH biomass contained 59 ± 0.7 µg protein/mL and 185 mg COD/L, while supernatant of the same concentration of fresh biomass only had 1.6 ± 0.4 µg protein/mL and 22 mg/L COD, evidence that freeze drying and heat exposure result in the release of proteins into suspension.

- The high concentration of protein and COD, foaming after agitation, and decreased surface tension in FDH biomass supernatant are evidence of denatured proteins being amphiphilic and behaving like surfactants.

- Surfactants are known to stabilize nanoparticles, and nanoparticles in FDH biomass samples were significantly more stable in the liquid phase than in fresh biomass samples.

- FDH is not a suitable sorbent for quantifying nanoparticle sorption to activated sludge.

Chapter 7: Quantitatively Understanding the Performance of Membrane Bioreactors

- Effluent water quality is sensitive to influent COD and the ability of the membrane to retain large biomass-associated products, but is unaffected by HRT and SRT.

- Membrane bioreactors can be operated with a high HRT/SRT ratio, which yields high MLVSS and MLSS concentrations in the reactor.

- A high HRT/SRT ratio reduces the reactor's aerial footprint and, thus, capital costs.

- Though capital costs may be reduced as the HRT/SRT ratio increases, operational costs rise due to an increase in the aeration power required and a decrease in the trans-membrane flux.

Chapter 8: Dissertation Synthesis

- The greater the hydrophobicity of bacteria and/or a solid surface, the greater the adhesion of the bacteria to the surface. Likewise, studies indicate that nanoparticle association with a solid increases with increasing nanoparticle and/or solid surface hydrophobicity.

- Natural organic matter, proteins, and surfactants reduce bacterial adhesion to surfaces; the same is true for nanoparticle sorption to solids.

- Bacterial adhesion studies may provide insight into methods to study ENM sorption to solids.

- Nanoparticles that do not sorb to biomass in an activated sludge reactor will not settle out during sedimentation, as the particles are too small to be gravitationally settled during the typical retention time of a secondary clarifier.

- The basic wastewater treatment water quality model presented in Chapter 7 can be coupled with a modified basic fate model to predict the fate of nanoparticles.

- Modification of the basic fate model for nanoparticles includes using a nonlinear sorption term and nanoparticle sorption coefficient values determined through batch sorption experiments.

Conclusions

Because titanium dioxide has been used by industries for decades, is currently one of the most utilized nanomaterials in consumer products, and is relatively easy to measure and image in complex biological matrices, TiO_2 is a good candidate to serve as a model nanomaterial for tracking the fate of nanomaterials of similar properties in wastewater treatment plants. Our full-scale analyses of titanium in wastewater treatment plants indicate that while wastewater effluents are important potential point sources of engineered nanomaterials into the environment, nanoscale TiO_2 and other nanomaterials are likely to be found in significantly higher amounts in wastewater biosolids. Biosolids are usually applied to land as soil amendments, landfilled, or incinerated. Therefore, biosolids will probably be important vehicles for nanomaterial release into the environment.

Our laboratory-scale batch sorption experiments showed that functionalized nanomaterials, such as nanoscale PVP-coated gold and fullerol (functionalized C_{60}), are significantly more stable in water and sorb less to biomass than TiO_2. Hence, functionalized nanomaterials will be found in conventional activated sludge effluents to a greater extent. WWTPs that use microfiltration – either as membrane bioreactors or as tertiary treatment in conventional activated sludge plants – will have fewer nanoparticles in their effluents than conventional activated sludge plants with gravitational solids separation. Even nanoparticles made to be stable in the aqueous phase will probably be retained by membranes.

Data collected from full-scale analyses and from laboratory-scale experiments were comparable. This provides evidence that lab-scale experiments are valuable for substantiating full-scale experiments. Furthermore, batch sorption and sequencing batch reactor experiments are useful for evaluating the fate of ENMs in cases where field-scale work is impossible due to low ENM concentrations that cannot be quantified. As more and more varieties of nanomaterials are produced, lab-scale experimentation will become important for predicting the fate of various nanomaterials in a wastewater treatment plant and in the environment. Fate-and-transport-testing protocol established for soluble contaminants cannot be applied to nanoparticles. Instead, new standard methods must be developed uniquely for nanomaterials in order to accurately predict their fate and transport in the environment. The batch sorption method presented in this dissertation, using fresh activated rinsed with 1 mM $NaHCO_3$, does not drastically alter the properties of activated sludge and is relatively simple to execute.

The common method of freeze-drying and heat-treating activated sludge for use as sorbent creates changes in suspension composition that have a transformative effect on nanoparticles. While this method was found to be inappropriate for quantifying nanomaterial sorption to activated sludge, testing FDH biomass revealed important factors of nanomaterial fate. First, nanoparticle sorption to solids is probably based on a combination of properties, including particle surface hydrophobicity, charge, and size. Second, nanoparticles, especially more hydrophobic particles, will become

coated in environments rich in natural organic matter, proteins, phospholipids, surfactants and other such biological and synthetic matter. Processes that cause protein denaturation, such as high-temperature biosolids treatment like composting, will be rich in biosurfactants that will bind with nanoparticles. Surface waters, soils, and blood are natural NOM- or protein-rich environments with components that will coat nanoparticles. Coatings transform overall nanoparticle properties and ultimately define nanoparticle behavior in the environment.

As for future work, developing a sound model to predict nanoparticle fate in different types of wastewater treatment systems would be an important contribution to the field of nanomaterial risk assessment. The activated sludge modeling work presented in this dissertation highlights important mechanisms of nanomaterial removal in wastewater treatment plants. In general, the separation of solids in conventional activated sludge systems is less efficient than in membrane bioreactors, which have near-perfect solids retention due to the replacement of the secondary clarifier with a membrane. Therefore, nanoparticles that are associated with floc will be completely removed from effluent in membrane bioreactors. The removal of floc-bound nanoparticles from effluent in conventional activated sludge systems will be a function of the solids-settling characteristics of the secondary clarifier. Developing a useful model to predict nanoparticle fate during wastewater treatment will require accurate representations of nanoparticle sorption to solids and of the separation of solids.

REFERENCES

Agyin-Birikorang, S., Miller, M., O'Conner, G.A., 2010. Retention-release characteristics of triclocarban and triclosan in biosolids, soils, and biosolids-amended soils. Environmental Toxicology and Chemistry 29 (9), 1925-1933.

Aitken, R.J., Chaudhry, M.Q., Boxall, A.B.A., Hull, M., 2006. Manufacture and use of nanomaterials: current status in the UK and global trends. Occupational Medicine-Oxford 56 (5), 300-306.

An, Y.H., Dickinson, R.B., Doyle, R.J., 2000. Mechanisms of bacterial adhesion and pathogenesis of implant and tissue infections. Handbook of Bacterial Adhesion: Principles, Methods, and Applications. Ed. by Y.H. An and R.J Friedman, Humana Press: Totowa, NJ.

Andersen, H.R., Hansen, M., Kjølholt, J., Stuer-Lauridsen, F., Ternes, T., Halling-Sørensen, B., 2005. Assessment of the importance of sorption for steroid estrogens removal during activated sludge treatment 61 (1), 139-146.

Andrievsky, G.V., Kosevich, M.V., Vovk, O.M., Shelkovsky, V.S., Vashchenko, L.A., 1995. On the production of an aqueous colloidal solution of fullerenes. Journal of the Chemical Society - Chemical Communications (12), 1281-1282.

Antignano, A., Manning, C. E., 2008. Rutile solubility in H_2O, H_2O-SiO_2, and H_2O-$NaAlSi_3O_8$ fluids at 0.7-2.0 GPa and 700-1000 degrees C: Implications for mobility of nominally insoluble elements. Chemical Geology 255 (1-2), 283-293.

APHA, AWWA, WEF, 2005. Standard Methods for the Examination of Water And Wastewater (21st Edition). American Public Health Association: Washington, DC.

Arias, L. R., Yang, L. J., 2009. Inactivation of Bacterial Pathogens by Carbon Nanotubes in Suspensions. Langmuir 25 (5), 3003-3012.

Auffan, M., Rose, J., Bottero, J.Y., Lowry, G.V., Jolivet, J.P., Wiesner, M.R., 2009. Towards a definition of inorganic nanoparticles from an environmental, health and safety perspective. Nature Nanotechnology 4 (10), 634-641.

Auffan, M., Bottero, J. Y., Chaneac, C., Rose, J., 2010a. Inorganic manufactured nanoparticles: how their physicochemical properties influence their biological effects in aqueous environments. Nanomedicine 5 (6), 999-1007.

Auffan, M., Pedeutour, M., Rose, J., Masion, A., Ziarelli, F., Borschneck, D., Chaneac, C., Botta, C., Chaurand, P., Labille, J., Bottero, J. Y., 2010b. Structural Degradation at the Surface of a TiO_2-Based Nanomaterial Used in Cosmetics. Environmental Science & Technology 44 (7), 2689-2694.

Bae, T. H., Tak, T. M., 2005. Effect of TiO_2 nanoparticles on fouling mitigation of ultrafiltration membranes for activated sludge filtration. Journal of Membrane Science 249 (1-2), 1-8.

Bagwe, R.P., Yang, C., Hilliard, L.R., Tan, W., 2004. Optimization of dye-doped silica nanoparticles prepared using a reverse microemulsion method. Langmuir 20 (19), 8336-8342.

Baker, J.S., Dudley, L.Y., 1998. Biofouling in membrane systems - a review. Desalination 118 (1-3), 81-90.

Bales, R.C., Li, S., MacGuire, K.M., Yahya, M.T., and Gerba, C.P., 1993. MS-2 and poliovirus transport in porous media: Hydrophobic effects and chemical perturbations. Water Resour. Res. 29, 957-963.

Barksdale, J., 1968. Titanium. The Encyclopedia of the Chemical Elements, Reinhold Book Corporation: Skokie.

Bar-Or, Y. 1990. Hydrophobicity in the aquatic environment. Microbial Cell Surface Hydrophobicity. Ed. by R.J. Doyle and M. Rosenberg. American Society for Microbiology: Washington, D.C.

Barton, SS. 1987. The adsorption of methylene blue by active carbon. Carbon 25 (3), 343-350.

Baun, A., Hartmann, N. B., Grieger, K. D., Hansen, S. F., 2009. Setting the limits for engineered nanoparticles in European surface waters - are current approaches appropriate? Journal of Environmental Monitoring 11 (10), 1774-1781.

Becker, W.C., O'Melia, C.R., Au, K.K., Young, J.S., 2004. Using Oxidants to Enhance Filter Performance. American Water Works Association: Denver.

Benn, T.M., Westerhoff, P.K., 2008. Nanoparticle silver released into water from commercially available sock fabrics. Environmental Science & Technology 42 (11), 4133-4139.

Benn, T., Cavanagh, B., Hristovski, K., Posner, J.D., Westerhoff, P., 2010. The release of nanosilver from consumer products used in the home. Journal of Environmental Quality 39 (6), 1875-1882.

Blaser, S.A., Scheringer, M., MacLeod, M., Hungerbuhler, K., 2008. Estimation of cumulative aquatic exposure and risk due to silver: Contribution of nano-functionalized plastics and textiles. Science of the Total Environment 390 (2-3), 396-409.

Bossi, A., Rinalducci, S., Zolla, L., Antonioli, P., Righetti, P.G., Zapparoli, G., 2007. Effect of tannic acid on Lactobacillus hilgardii analysed by a proteomic approach. Journal of Applied Microbiology 102 (3), 787-795.

Brant, J., Lecoanet, H., Hotze, M., Wiesner, M., 2005. Comparison of electrokinetic properties of colloidal fullerenes (n-C_{60}) formed using two procedures. Environmental Science and Technology 39 (17), 6343-6351.

Brant, J.A., Labille, J., Bottero, J.Y., Wiesner, M.R., 2006. Characterizing the impact of preparation method on fullerene cluster structure and chemistry. Langmuir 22 (8), 3878-3885.

Brar, S. K., Verma, M., Tyagi, R. D., Surampalli, R. Y., 2010. Engineered nanoparticles in wastewater and wastewater sludge - Evidence and impacts. Waste Management 30 (3), 504-520.

Braun, J. H., 1997. Titanium dioxide - A review. Journal of Coatings Technology 69 (868), 59-72.

Brayner, R., Ferrari-Iliou, R., Brivois, N., Djediat, S., Benedetti, M. F., Fievet, F., 2006. Toxicological impact studies based on Escherichia coli bacteria in ultrafine ZnO nanoparticles colloidal medium. Nano Letters 6 (4), 866-870.

Burau, R.G., Zasoski, R.J., 2002. Section 7: Adsorption on soil colloids. Soil and Water Chemistry SSC 102: Course Notes and Graphical Materials – Winter Quarter 2002. University of California, Davis. http://lawr.ucdavis.edu/classes/ssc102/Section7.pdf.

Bystrzejewska-Piotrowska, G., Golimowski, J., Urban, P.L., 2009. Nanoparticles: Their potential toxicity, waste and environmental management. Waste Management 29 (9), 2587-2595.

Carter, D. E., 1995. Oxidation-Reduction Reactions of Metal-Ions. Environmental Health Perspectives 103, 17-19.

Cedervall, T., Lynch, I., Lindman, S., Berggard, T., Thulin, E., Nilsson, H., Dawson, K.A., Linse, S., 2007. Understanding the nanoparticle-protein corona using methods to quantify exchange rates and affinities of proteins for nanoparticles. PNAS 104 (7), 2050-2055.

Chart, H., Smith, H.R., La Rogione, R.M., Woodward, M.J., 2000. An investigation into the pathogenic properties of Escherichia coli strains BLR, BL21, DH5α and EQ1. Journal of Applied Microbiology 89 (6), 1048-1058.

Chang, M.R., Lee, D.J., Lai, J.Y., 2007. Nanoparticles in wastewater from a science-based industrial park – Coagulation using polyaluminum chloride. Journal of Environmental Management 85 (4), 1009-1014.

Chen, K.L. Elimelech, M., 2007. Influence of humic acid on the aggregation kinetics of fullerene (C_{60}) nanoparticles in monovalent and divalent electrolyte solutions. Journal of Colloid and Interface Science 309 (1), 126-134.

Chen, K.L., Elimelech, M., 2008. Interaction of fullerenes (C_{60}) nanoparticles with humic acid and alginate coated silica surfaces: measurements, mechanisms, and environmental implications. Environmental Science and Technology 42 (20), 7607-7614.

Chin, C. J. M., Chen, P. W., Wang, L. J., 2006. Removal of nanoparticles from CMP wastewater by magnetic seeding aggregation. Chemosphere 63 (10), 1809-1813.

Choi, O., Hu, Z.Q., 2008. Size dependent and reactive oxygen species related nanosilver toxicity to nitrifying bacteria. Environmental Science & Technology 42 (12), 4583-4588.

Choi, O. K., Hu, Z. Q., 2009. Nitrification inhibition by silver nanoparticles. Water Science and Technology 59 (9), 1699-1702.

Christian, P., Von der Kammer, F., Baalousha, M., Hofmann, T., 2008. Nanoparticles: structure, properties, preparation and behaviour in environmental media. Ecotoxicology 17 (5), 326-343.

Clouzot, L., Doumenq, P., Vanloot, P., Roche, N., Marrot, B., 2010. Membrane bioreactors for 17 alpha-ethinylestradiol removal. Journal of Membrane Science 362 (1-2), 81-85.

Colvin, V.L. , 2003. The potential environmental impact of engineered nanomaterials. Nature Biotechnology 21 (10), 1166-1170.

Contado, C., Pagnoni, A., 2008. TiO_2 in commercial sunscreen lotion: Flow field-flow fractionation and ICP-AES together for size analysis. Analytical Chemistry 80 (19), 7594-7608.

Crittenden, J.C., Rhodes Trussel, R., Hand, D.W., Howe, K.J., Tchobanoglous, G., 2005. Water Treatment: Principles and Design. 2nd ed. John Wiley & Sons: Hoboken, NJ.

Crosera, M., Bovenzi, M., Maina, G., Adami, G., Zanette, C., Florio, C., Larese, F. F., 2009. Nanoparticle dermal absorption and toxicity: a review of the literature. International Archives of Occupational and Environmental Health 82 (9), 1043-1055.

Dahlberg, C., Millqvist-Fureby, A., Schuleit, M., Furó, I., 2010. Polymer-drug interactions and wetting of solid dispersions. European Journal of Pharmaceutical Sciences 39, 125-133.

Daigger, G.T., Rittmann, B.E., Adham, S.S., Andreottola, G., 2005. Are membrane bioreactors ready for widespread application? Environmental Science and Technology 39, 399A-406A.

Davis, M. L., Cornwell, D. A., 1991. Introduction to Environmental Engineering. 2nd ed. McGraw-Hill: New York.

Demchick, P., Koch, A.L., 1996. The permeability of the wall fabric of Escherichia coli and Bacillus subtilis. Journal of Bacteriology 178 (3), 768-773.

De Silva, V.D.G., Urbain, V., Abeysinghe, R., Rittmann, B.E., 1998. Advanced analysis of membrane-bioreactor performance with aerobic-anoxic cycling. Water Science and Technology 38 (4-5), 505-512.

De Silva, V.D.G., Rittmann, B.E., 2000. Nonsteady-state modeling of multispecies activated sludge process. Water Environment Research 72, 545-553.

Dias, A.M.G.C., Hussain, A., Marcos, A.S., Roque, A.C.A., 2011. A biotechnological perspective on the application of iron oxide magnetic colloids modified with polysaccharides. Biotechnology Advances 29, 142-155.

Dickinson, R.B., 2006. Bacteria: Surface behavior. Encyclopedia of Surface and Colloid Science. Vol. 2. 2nd ed. Ed. by P. Somasundaran. CRC Press.

Diegoli, S., Manciulea, A.L., Begum, S., Jones, I.P., Lead, J.R., Preece, J.A., 2008. Interaction between manufactured gold nanoparticles and naturally occurring organic macromolecules. Science of the Total Environment 402 (1), 51-61.

Dobbs, R.A., Wang, L.P., Govind, R., 1989. Sorption of toxic organic compounds on wastewater solids: correlation with fundamental properties. Environmental Science & Technology 23 (9), 1092-1097.

Domingos, R.F., Tufenkji, N., Wilkinson, K.J., 2009. Aggregation of Titanium Dioxide Nanoparticles: Role of a Fulvic Acid. Environmental Science & Technology 43 (5), 1282-1286.

Doty, R.C., Tshikhudo, T.R., Brust, M., Fernig, D.G., 2005. Extremely stable water-solube Ag nanoparticles. Chemistry of Materials 17 (18), 4630-4635.

Duncan, L.K., Jinschek, J.R., Vikesland, P.J., 2008. C_{60} colloid formation in aqueous systems: effects of preparation method on size, structure, and surface charge. Environmental Science & Technology 42 (1), 173-178.

Eaton, A.D., Clesceri, L.S., Rice, E.W., Greenberg, A.R., 2005. Standard Methods for the Examination of Water and Wastewater. APHA, AWWA, WEF, Baltimore.

Elechiguerra, J.L., Burt, J.L., Morones, J.R., Camacho-Bragado, A., Gao, X., Lara, H.H., Yacaman, M.J., 2005. Interaction of silver nanoparticles with HIV-1. Journal of Nanobiotechnology 3 (6).

Emsley, J., 2001. Nature's Building Blocks: An A-Z Guide to the Elements. Oxford University Press: Oxford.

Esparza-Soto, M. Westerhoff, P.K., 2001. Fluorescence spectroscopy and molecular weight distribution of extracellular polymers from full-scale activated sludge biomass. Water Science and Technology 43 (6), 86-95.

Fabrega, J., Renshaw, J. C., Lead, J. R., 2009. Interactions of Silver Nanoparticles with Pseudomonas putida Biofilms. Environmental Science & Technology 43 (23), 9004-9009.

Fadeel, B., Garcia-Bennett, A.E., 2010. Better safe than sorry: Understanding the toxicological properties of inorganic nanoparticles manufactured for biomedical applications. Advanced Drug Delivery Reviews 62 (3), 362-374.

Farré, M., Perez, S., Gajda-Schrantz, K., Osorio, V., Kantiani, L., Ginebreda, A., Barcelo, D., 2010. First determination of C-60 and C(70) fullerenes and N-methylfulleropyrrolidine C-60 on the suspended material of wastewater effluents by liquid chromatography hybrid quadrupole linear ion trap tandem mass spectrometry. Journal of Hydrology 383 (1-2), 44-51.

Fletcher, M., 1976. Effects of proteins on bacterial attachment to polystyrene. Journal of General Microbiology 94, 400-404.

Fletcher , M., Loeb, G.I., 1979. Influence of substratum characteristics on the attachment of a marine pseudomonad to solid-surfaces. Applied and Environmental Microbiology 37 (1), 67-72.

Fortner, J.D., Lyon, D.Y., Sayes, C.M., Boyd, A.M., Falkner, J.C., Hotze, E.M., Alemany, L.B., Tao, Y.J., Guo, W., Ausman, K.D., Colvin, V.L., Hughes, J.B., 2005. C-60 in water: Nanocrystal formation and microbial response. Environmental Science & Technology 39 (11), 4307-4316.

Furumai, H., Rittmann, B.E., 1992. Advanced modeling of mixed populations of heterotrophs and nitrifiers considering the formation and exchange of soluble microbial products. Water Science and Technology 26 (3-4), 493-502.

Ganesh, R., Smeraldi, J., Hosseini, T., Khatib, L., Olson, B.H., Rosso, D., 2010. Evaluation of nanocopper removal and toxicity in municipal wastewaters. Environmental Science and Technology 44 (20), 7808-7813.

Gerardi, M.H., 2006. Wastewater Bacteria. John Wiley & Sons: Hoboken, New Jersey.

Gottschalk, F.; Sonderer, T.; Scholz, R. W.; Nowack, B., 2009. Modeled Environmental Concentrations of Engineered Nanomaterials (TiO_2, ZnO, Ag, CNT, Fullerenes) for Different Regions. Environmental Science & Technology 43 (24), 9216-9222.

Gottschalk, F., Scholz, R. W., Nowack, B., 2010a. Probabilistic material flow modeling for assessing the environmental exposure to compounds: Methodology and an application to engineered nano-TiO_2 particles. Environmental Modelling & Software 25 (3), 320-332.

Gottschalk, F., Sonderer, T., Scholz, R. W., Nowack, B., 2010b. Possibilities and Limitations of Modeling Environmental Exposure To Engineered Nanomaterials by Probabilistic Material Flow Analysis. Environmental Toxicology and Chemistry 29 (5), 1036-1048.

Gristina, A.G., 1987. Biomaterial-centered infection: Microbial adhesion versus tissue integration. Science 237, 1588-1595.

Guo, H., Wyart, Y., Perot, J., Nauleau, F., Moulin, P., 2010. Application of magnetic nanoparticles for UF membrane integrity monitoring at low-pressure operation. Journal of Membrane Science 350 (1-2), 172-179.

Guzman, K.A.D., Taylor, M.R., Banfield, J.F., 2006. Environmental risks of nanotechnology : national nanotechnology initiative funding, 2000-2004. Environmental Science and Technology, 40 (5), 1401-1407.

Habimana, O., Steenkeste, K., Fontaine-Aupart, M.P., Bellon-Fontaine, M.N., Kulakauskas, S., Briandet, R., 2011. Diffusion of nanoparticles in biofilms is altered by bacterial cell wall hydrophobicity. Applied and Environmental Microbiology 77 (1), 367-368.

Hamadi, F., Latrache, H., Zahir, H., Elghmari, A., Timinouni, M., Ellouali, M., 2007. The relation between Escherichia Coli surface functional groups' composition and their physicochemical properties. Brazilian Journal of Microbiology 39, 10-15.

Handy, R.D. Shaw, B.J., 2007. Toxic effects of nanoparticles and nanomaterials: implications for public health, risk assessment and the public perception of nanotechnology. Health, Risk, and Society 9 (2), 125-144.

Handy, R.D., von der Kammer, F., Lead, J.R., Hasselloy, M., Owen, R., Crane, M., 2008. The ecotoxicology and chemistry of manufactured nanoparticles. Ecotoxicology 17 (4), 287-314.

Holgers, K.M., Ljungh, A., 1999. Cell surface characteristics of microbiological isolates from human percutaneous titanium implants in the head and neck. Biomaterials 20, 1319-1326.

Hou, A., Takamatsu, T., Koshikawa, M.K., Hosomi, M., 2005. Migration of silver, indium, tin, antimony, and bismuth and variations in their chemical fractions on addition to uncontaminated soils. Soil Science 170 (8), 624-639.

Hyung, H., Fortner, J.D., Hughes, J.B., Kim, J.H., 2007. Natural organic matter stabilizes carbon nanotubes in the aqueous phase. Environmental Science and Technology 41 (1), 179-184.

Irvin, R.T., 1990. Hydrophobicity of proteins and bacterial fimbriae. Microbial Cell Surface Hydrophobicity. Ed. by R.J. Doyle and M. Rosenberg. American Society for Microbiology: Washington, D.C.

Jacobsen, B.N., Nyholm, N., Pedersen, B.M., Poulsen, O., Ostfeldt, P., 1993. Removal of organic micropollutants in laboratory activated sludge reactors under various operating conditions: sorption. Water Research 27 (10), 1505-1510.

Jang, N., Ren, X., Cho, J., Kim, I.S., 2006. Steady-state modeling of bio-fouling potentials with respect to the biological kinetics in the submerged membrane bioreactor (SMBR). Journal of Membrane Science 284, 352-360.

Jang, N., Ren, X., Kim, G., Ahn, C., Cho, J., Kim, I.S., 2007. Characteristics of soluble microbial products and extracellular polymeric substances in the membrane bioreactor for water reuse. Desalination 202, 90-98.

Jarvie, H.P., Al-Obaidi, H., King, S.M., Bowes, M.J., Lawrence, M.J., Drake, A.F., Green, M.A., Dobson, P.J., 2009. Fate of silica nanoparticles in simulated primary wastewater treatment. Environmental Science and Technology 43 (22), 8622-8628.

Jassby, D., Chae, S. R., Hendren, Z., Wiesner, M., 2010. Membrane filtration of fullerene nanoparticle suspensions: Effects of derivatization, pressure, electrolyte species and concentration. Journal of Colloid and Interface Science 346 (2), 296-302.

Kaegi, R., Ulrich, A., Sinnet, B., Vonbank, R., Wichser, A., Zuleeg, S., Simmler, H., Brunner, S., Vonmont, H., Burkhardt, M., Boller, M., 2008. Synthetic TiO_2 nanoparticle emission from exterior facades into the aquatic environment. Environmental Pollution 156 (2), 233-239.

Kahru, A., Dubourguier, H. C., 2010. From ecotoxicology to nanoecotoxicology. Toxicology 269 (2-3), 105-119.

Kang, S., Mauter, M. S., Elimelech, M., 2009. Microbial Cytotoxicity of Carbon-Based Nanomaterials: Implications for River Water and Wastewater Effluent. Environmental Science & Technology 43 (7), 2648-2653.

Keller, A. A., Wang, H. T., Zhou, D. X., Lenihan, H. S., Cherr, G., Cardinale, B. J., Miller, R., Ji, Z. X., 2010. Stability and Aggregation of Metal Oxide Nanoparticles in Natural Aqueous Matrices. Environmental Science & Technology 44 (6), 1962-1967.

Kim, B., Park, C.S., Murayama, M., Hochella, M.F., 2010. Discovery and characterization of silver sulfide nanoparticles in final sewage sludge products. Environmental Science and Technology 44 (19), 7509-7514.

Kim, T.D., Shiragami, N., Unno, H., 1995. Development of a model describing virus removal process in an activated-sludge basin. Journal of Chemical Engineering of Japan 28 (3), 257-262.

Kinney, C.A., Furlong, E.T., Zaugg, S.D., Burkhardt, M.R., Werner, S.L., Cahill, J.D., Jorgensen, G.R., 2006. Survey of organic wastewater contaminants in biosolids destined for land application. Environmental Science & Technology 40 (23), 7207-7215.

Kiser, M.A., Westerhoff, P., Benn, T., Wang, Y., Perez-Rivera, J., Hristovski, K., 2009. Titanium nanomaterial removal and release from

wastewater treatment plants. Environmental Science and Technology 43 (17), 6757-6763.

Kiser, M.A., Ryu, H., Jang, H., Hristovski, K., Westerhoff, P., 2010. Biosorption of nanoparticles to heterotrophic wastewater biomass. Water Research 44, 4105-4114.

Kloepfer, J.A., Mielke, R.E., Nadeau, J.L., 2005. Uptake of CdSe and CdSe/ZnS quantum dots into bacteria via purine-dependent mechanisms. Applied and Environmental Microbiology 71 (5), 2548-2557.

Klotz, S.A. 1990. Role of hydrophobic interactions in microbial adhesion to plastics used in medical devices. Microbial Cell Surface Hydrophobicity. Ed. by R.J. Doyle and M. Rosenberg. American Society for Microbiology: Washington, D.C.

Klueh, U., Wagner, V., Kelly, S., Johnson, A., Bryers, J.D., 2000. Efficacy of silver-coated fabric to prevent bacterial colonization and subsequent device-based biofilm formation. Journal of Biomedical Materials Res. Part B: Applied Biomaterials 53, 621-631.

Koeneman, B., Zhang, Y., Westerhoff, P., Chen, Y., Crittenden, J. C., Capco, D. G., 2010. Toxicity and Cellular Responses of Intestinal Cells Exposed to Titanium Dioxide. Cell Biology and Toxicology 26 (3), 225-238.

Labille, J., Feng, J. H., Botta, C., Borschneck, D., Sammut, M., Cabie, M., Auffan, M., Rose, J., Bottero, J. Y., 2010. Aging of TiO_2 nanocomposites used in sunscreen. Dispersion and fate of the degradation products in aqueous environment. Environmental Pollution 158 (12), 3482-3489.

Laspidou, C.S., Rittmann, B.E., 2002a. A unified theory for extracellular polymeric substances, soluble microbial products, and active and inert biomass. Water Research 36 (11), 2711-2720.

Laspidou, C.S., Rittmann, B.E., 2002b. Non-steady state modeling of microbial products and active and inert biomass. Water Research 36 (11), 1983-1992.

Lee, K.C., Rittmann, B.E., Shi, J.C., McAvoy, D., 1998. Advanced steady-state model for the fate of hydrophobic volatile compounds in activated sludge. Water Environment Research 70 (6), 1118-1131.

Lee, S., Kim, K., Shon, H.K., Kim, S.D., Cho, J., 2011. Biotoxicity of nanoparticles: effect of natural organic matter. Journal of Nanoparticle Research 13, 3051-3061.

Leenheer, J. A., Noyes, T. I., Rostad, C. E., Davisson, M. L., 2004. Characterization and origin of polar dissolved organic matter from the Great Salt Lake. Biogeochemistry 69 (1), 125-141.

Leenheer, J. A., Dotson, A., Westerhoff, P., 2007. Dissolved organic nitrogen fractionation. Ann. Environ. Sci. 1, 45-56.

Leenheer, J. A., 2009. Systematic Approaches to Comprehensive Analyses of Natural Organic Matter. Ann. Environ. Sci. 3, 1-130.

Lepock, J.R., Frey, H.E., Inniss, W.E., 1990. Thermal analysis of bacteria by differential scanning calorimetry – Relationship of protein denaturation insitu to maximum growth temperature. Biochimica et Biophysica Acta 1055 (1), 19-26.

Li, B., Logan, B.E., 2004. Bacterial adhesion to glass and metal-oxide surfaces. Colloids and Surfaces B: Biointerfaces 36, 81-90.

Li, S., Ni, L., Sun, C., Wang, L.P., 2004. Influence of organic matter on orthophosphate corrosion inhibition for copper pipe in soft water. Corrosion Science 46 (1), 137-145.

Limbach, L.K., Bereiter, R., Müller, E., Krebs, R., Gälli, R., Stark, W.J., 2008. Removal of oxide nanoparticles in a model wastewater treatment plant: influence of agglomeration and surfactants on clearing efficiency. Environmental Science and Technology 42 (15), 5828-5833.

Lippa, P., Muller, U., Hetzer, B., Wagner, T., 2009. Characterization of nanoparticulate fouling and breakthrough during low-pressure membrane filtration. Desalination and Water Treatment 9 (1-3), 234-240.

Lomer, M. C. E., Thompson, R. P. H., Commisso, J., Keen, C. L., Powell, J. J., 2000. Determination of titanium dioxide in foods using inductively coupled plasma optical emission spectrometry. Analyst 125 (12), 2339-2343.

Lomer, M. C. E., Thompson, R. P. H., Powell, J. J., 2002. Fine and ultrafine particles of the diet: influence on the mucosal immune response and association with Crohn's disease. Proc Nutr Soc 61 (1), 123-130.

Long, T.C., Tajuba, J., Sama, P., Saleh, N., Swartz, C., Parker, J., Hester, S., Lowry, G.V., Veronesi, B., 2007. Nanosize titanium dioxide stimulates reactive oxygen species in brain microglia and damages neurons in vitro. Environmental Health Perspectives 115(11), 1631-1637.

Lovern, S.B., Klaper, R., 2006. Daphnia magna mortality when exposed to titanium dioxide and fullerene (C_{60}) nanoparticles. Environmental Toxicology and Chemistry 25 (4), 1132-1137.

Lowry, G.V., Casman, E.A., 2009. Nanomaterial transport, transformation, and fate in the environment: A risk-based perspective on research needs. Nanomaterials: Risks and Benefits 2, 125-137.

Lyko, S., Al-Halbouni, D., Wintgens, T., Janot, A., Juliane, H., Dott, W., Melin, T., 2007. Polymeric compounds in activated sludge supernatant - characterisation and retention mechanisms at a full-scale municipal membrane bioreactor. Water Research 41 (17), 3894-3902.

Lyon, D.Y., Fortner, J.D., Sayes, C.M., Colvin, V.L., Hughes, J.B., 2005. Bacterial cell association and antimicrobial activity of C_{60} water suspension. Environmental Toxicology and Chemistry 24 (11), 2757-2762.

Lyon, D.Y., Adams, L.K., Falkner, J.C., Alvarez, P.J.J., 2006. Antibacterial activity of fullerene water suspensions: effect of preparation method and particle size. Environmental Science & Technology 40 (14), 4360-4366.

Madigan, M.T., Martinko, J.M., 2006. Brock Biology of Microorganisms. Pearson Prentice Hall: Upper Saddle River, New Jersey.

Maier, R.M., Pepper, I.L., Gerba, C.P., 2000. Environmental Microbiology. Academic Press: San Diego.

Mansoori, G.A., 2005. Principles of Nanotechnology: Molecular-Based Study of Condensed Matter in Small Systems. World Scientific: Hackensack, NJ.

Masters, G.M., Ela, W.P., 2008. Introduction to Environmental Engineering and Science. 3rd ed. Prentice Hall: Upper Saddle River, NJ.

Mattigod, S. V., Fryxell, G. E., Alford, K., Gilmore, T., Parker, K., Serne, J., Engelhard, M., 2005. Functionalized TiO_2 nanoparticles for use for in situ anion immobilization. Environmental Science & Technology 39 (18), 7306-7310.

Mayland, H. F., Florence, A. R., Rosenau, R. C., Lazar, V. A., Turner, H. A., 1975. Soil ingestion by cattle on semiarid range as reflected by titanium analysis of feces. Journal of Range Management 28 (6), 448-452.

Maynard, A.D., 2006. Nanotechnology: Assessing the risks. Nano Today 1 (2), 22-33.

McGraw-Hill, 2011. Online Learning Center Animation: Protein Denaturation. From http://highered.mcgraw-hill.com/sites/0072943696/student_view0/chapter2/animation_protein_denaturation.html.

Meng, F. G., Chae, S. R., Drews, A., Kraume, M., Shin, H. S., Yang, F. L., 2009. Recent advances in membrane bioreactors (MBRs): Membrane fouling and membrane material. Water Research 43 (6), 1489-1512.

Metcalf and Eddy, 2003. Wastewater Engineering: Treatment and Reuse. McGraw Hill: Boston.

Moore, M.N., 2006. Do nanoparticles present ecotoxicological risks for the health of the aquatic environment. Environment International 32 (8), 967-976.

Morimoto, Y., Kobayashi, N., Shinohara, N., Myojo, T., Tanaka, I., Nakanshi, J., 2010. Hazard Assessments of Manufactured Nanomaterials. Journal of Occupational Health 52 (6), 325-334.

Morones, J.R., Elechiguerra, J.L., Camacho, A., Holt, K., Kouri, J.B., Ramirez, J.T., Yacaman, M.J., 2005. The bactericidal effect of silver nanoparticles. Nanotechnology 16 (10), 2346-2353.

Morrow, J. B., Arango, C., Holbrook, R. D., 2010. Association of Quantum Dot Nanoparticles with Pseudomonas aeruginosa Biofilm. Journal of Environmental Quality 39 (6), 1934-1941.

Mueller, N.C., Nowack, B., 2008. Exposure modeling of engineered nanoparticles in the environment. Environmental Science & Technology 42 (12), 4447-4453.

Myers, W. D., Ludden, P. A., Nayigihugu, V., Hess, B. W., 2006. Excretion patterns of titanium dioxide and chromic oxide in duodenal digesta and feces of ewes. Small Ruminant Research 63 (1-2), 135-141.

Namkung, E., Rittmann, B.E., 1986. Soluble microbial products (SMP) formation kinetics by biofilms. Water Research 20, 795-806.

Navarro, E., Baun, A., Behra, R., Hartmann, N.B., Filser, J., Miao, A., Quigg, A., Santschi, P.H., Sigg, L., 2008. Environmental behavior and ecotoxicity of engineered nanoparticles to algae, plants, and fungi. Ecotoxicology 17 (5), 372 – 386.

Nel, A., Xia, T., Madler, L., Li, N., 2006. Toxic potential of materials at the nanolevel. Science 311 (5761), 622-628.

Nohynek, G. J., Lademann, J., Ribaud, C., Roberts, M. S., 2007. Grey goo on the skin? Nanotechnology, cosmetic and sunscreen safety. Critical Reviews in Toxicology 37 (3), 251-277.

Nowack, B., Bucheli, T.D., 2007. Occurrence, behavior and effects of nanoparticles in the environment. Environmental Pollution 150 (1), 5-22.

Nyberg, L., Turco, R. F., Nies, L., 2008. Assessing the impact of nanomaterials on anaerobic microbial communities. Environmental Science & Technology 42 (6), 1938-1943.

Oakes, K.D., Coors, A., Escher, B.I., Fenner, K., Garric, J., Gust, M., Knacker, T., Kuster, A., Kussatz, C., Metcalfe, C.D., Monteiro, S., Moon, T.W., Mennigen, J.A., Parrot, J., Pery, A.R.R., Ramil, M., Roennefahrt, I., Tarazona, J.V., Sanchez-Arguello, P., Ternes, T.A., Trudeau, V.L., Boucard, T., Van Der Kraak, G.J., Servos, M.R., 2010. Environmental risk assessment for the serotonin re-uptake inhibitor fluoxetine: case study using the European risk assessment framework. Integrated Environmental Assessment and Management 6 (S1), 524-539.

Oberdorster, E., 2004. Manufactured nanomaterials (fullerenes, C_{60}) induce oxidative stress in the brain of juvenile largemouth bass. Environmental Health Perspectives 112 (10), 1058-1062.

O'Brien, N., Cummins, E., 2010. Ranking initial environmental and human health risk resulting from environmentally relevant nanomaterials. Journal of Environmental Science and Health Part a-Toxic/Hazardous Substances & Environmental Engineering 45 (8), 992-1007.

Ong, Y.L., Razatos, A., Georgiou, G., Sharma, M.M., 1999. Adhesion forces between E. coli bacteria and biomaterial surfaces. Langmuir 15, 2719-2725.

Oppenheimer, J., Rittmann, B.E., DeCarolis, J., Hirani, Z., Kiser, A., 2010. Investigation of Membrane Bioreactor Effluent Water Quality and Technology. Water Reuse Foundation: Alexandria, VA.

Ouyang, E.M., Wang, W., Long, N., Li, H., 2009. Three-dimensional excitation emission matrix fluorescence spectroscopic characterization of loosely bound and tightly bound extracellular polymeric substances of sludge. Spectroscopy and Spectral Analysis 29 (5), 1313-1318.

Parrott, J., McLaughlin, A., Lapen, D., Topp, E., 2010. Environmental risk assessment of pharmaceuticals. Environmental Risk Assessment and Management from a Landscape Perspective. Ed. by L.A. Kapustka and W.G. Landis. John Wiley & Sons: Hoboken, NJ.

Paul, J.H., Jeffrey, W.H., 1985. Evidence for Separate Adhesion Mechanisms for Hydrophilic and Hydrophobic Surfaces in Vibrio proteolytica. Applied and Environmental Microbiology 50 (2), 431-437.

Popov, A. P., Priezzhev, A. V., Lademann, J., Myllyla, R., 2005. TiO_2 nanoparticles as an effective UV-B radiation skin-protective compound in sunscreens. Journal of Physics D-Applied Physics 38 (15), 2564-2570.

Posner, J.D., 2009. Engineered nanomaterials: Where they go, nobody knows. Nano Today 4 (2), 114-115.

Powell, J. J., Ainley, C. C., Harvey, R. S. J., Mason, I. M., Kendall, M. D., Sankey, E. A., Dhillon, A. P., Thompson, R. P. H., 1996. Characterisation of inorganic microparticles in pigment cells of human gut associated lymphoid tissue. Gut 38 (3), 390-395.

PEN (Project on Emerging Nanotechnologies), 2009. Consumer Products Inventories. From http://www.nanotechproj.org/inventories/consumer

PEN (Project on Emerging Nanotechnologies), 2010. Consumer Products Inventories. From http://www.nanotechproj.org/inventories/consumer

Qiao, R., Roberts, A.P., Mount, A.S., Klaine, S.J., Ke, P.C., 2007. Translocation of C_{60} and its derivatives across a lipid bilayer. Nano Letters 7 (3), 614-619.

Robichaud, C. O., Uyar, A., Darby, M. R., Zucker, L. G., Wiesner, M., 2009. Estimates of Upper Bounds and Trends in Nano-TiO_2 Production As a Basis for Exposure Assessment Environ. Sci. Technol.43 (12), 4227-4233.

Rozada, F., Otero, M., Garcia, A.I., Moran, A., 2007. Applications in fixed-bed systems of adsorbents obtained from sewage sludge and discarded tyres. Dyes and Pigments 72 (1), 47-56.

Rebecca, M., Hsing-Lin, W., Jun, G., Srinivas, I., Gabriel, M., Jennifer, M., Andrew, S.P., Yuping, B., Chun-Chih, W., Zhong, C., Yuan, G., Rashi, I., 2009. Impact of physicochemical properties of engineered fullerenes on key biological responses. Toxicology and Applied Pharmacology 234 (1), 58-67.

Reijnders, L., 2006. Cleaner nanotechnology and hazard reduction of manufactured nanoparticles. Journal of Cleaner Production 14 (2), 124-133.

Rittman, B.E., McCarty, P.L., 2001. Environmental Biotechnology: Principles and Applications. McGraw Hill: New York, NY.

Roco, M.C., 2005. International perspectives on government nanotechnology funding in 2005. Journal of Nanoparticle Research 7 (6), 707-712.

Sabourin, L., Beck, A., Duenk, P.W., Kleywegt, S., Lapen, D.R., Li, H.X., Metcalfe, C.D., Payne, M., Topp, E., 2009. Runoff of pharmaceuticals and personal care products following application of dewatered municipal biosolids to an agricultural field. Science of the Total Environment 407 (16), 4596-4604.

Sayes, C.M., Fortner, J.D., Guo, W., Lyon, D., Boyd, A.M., Ausman, K.D., Tao, Y.J., Sitharaman, B., Wilson, L.J., Hughes, J.B., West, J.L., Colvin, V.L., 2004. The differential cytotoxicity of water-soluble fullerenes. Nano Letters 4 (10), 1881-1887.

Scarano, A., Piattelli, M., Caputi, S., Favero, G.A., Piattelli, A., 2004. Bacterial adhesion on commercially pure titanium and zirconium oxide disks : An in vivo human study. Jour. Periodontol. 75 (2), 292-296.

Schroeder, H. A., Balassa, J. J., Tipton, I. H., 1963. Abnormal trace metals in man - titanium. Journal of Chronic Diseases 16 (1), 55.

Schwab, C., Vogel, R., Gänzle, M.G., 2007. Influence of oligosaccharides on the viability and membrane properties of Lactobacillus reuteri TMW1.106 during freeze-drying. Cryobiology 55, 108-114.

Schwarz, A., Rittmann, B.E., Crawford, G., Klein, A., Daigger, G., 2006. A critical review of the effects of mixed liquor suspended solids on membrane bioreactor operation. Separation Science and Technology 41, 1489-1511.

Scown, T. M., van Aerle, R., Tyler, C. R., 2010. Review: Do engineered nanoparticles pose a significant threat to the aquatic environment? Critical Reviews in Toxicology 40 (7), 653-670.

Shafer, M.M., Overdier, J.T., Armstrong, D.E., 1998. Removal, partitioning, and fate of silver and other metals in wastewater treatment plants and effluent-receiving streams. Environmental Toxicology and Chemistry 17 (4), 630-641.

Sharma, V. K., 2009. Aggregation and toxicity of titanium dioxide nanoparticles in aquatic environment-A Review. Journal of Environmental Science and Health Part a-Toxic/Hazardous Substances & Environmental Engineering 44 (14), 1485-1495.

Sheng, G.P., Zhang, M.L., Yu, H.Q., 2008. Characterization of adsorption properties of extracellular polymeric substances (EPS) extracted from sludge. Colloids and Surfaces B-Biointerfaces 62 (1), 83-90.

Smith, A.H., Zoetendal, E., Mackie, R.I., 2005. Bacterial mechanisms to overcome inhibitory effects of dietary tannins. Microbial Ecology 50 (2), 197-205.

Sondi, I., Salopek-Sondi, B., 2004. Silver nanoparticles as antimicrobial agent: a case study on E. coli as a model for Gram-negative bacteria. Journal of Colloid and Interface Science 275 (1), 177-182.

Song, G. X., Wang, J., Chiu, C. A., Westerhoff, P., 2010. Biogenic Nanoscale Colloids in Wastewater Effluents. Environmental Science & Technology 44 (21), 8216-8222.

Stankus, D.P., Lohse, S.E., Hutchison, J.E., Nason, J.A., 2011. Interactions between natural organic matter and gold nanoparticles stabilized with different organic capping agents. Environmental Science and Technology 45, 3238-3244.

Stone, V., Nowack, B., Baun, A., van den Brink, N., von der Kammer, F., Dusinska, M., Handy, R., Hankin, S., Hassellov, M., Joner, E., Fernandes, T. F., 2010. Nanomaterials for environmental studies: Classification, reference material issues, and strategies for physico-chemical characterisation. Science of the Total Environment 408 (7), 1745-1754.

Unrine, J.M., Tsyusko, O.V., Hunyadi, S.E., Judy, J.D., Bertsch, P.M., 2010. Effects of particle size on chemical speciation and bioavailability of copper to earthworms exposed to copper nanoparticles. Journal of Environment Quality 39 (6), 1942-1953.

USGS, 2010. USGS Mineral Information Survey: Titanium. http://minerals.usgs.gov/minerals/pubs/commodity/titanium

Theron, J., Walker, J. A., Cloete, T. E., 2008. Nanotechnology and water treatment: Applications and emerging opportunities. Critical Reviews in Microbiology 34 (1), 43-69.

The Royal Society and The Royal Academy of Engineering, 2004. Nanoscience and nanotechnologies: opportunities and uncertainties. The Royal Society: London.

Thill, A., Zeyons, O., Spalla, O., Chauvat, F., Rose, J., Auffan, M., Flank, A.M., 2006. Cytotoxicity of CeO2 nanoparticles for Escherichia coli. Physico-chemical insight of the cytotoxicity mechanism. Environmental Science & Technology 40 (19), 6151-6156.

Tiede, K., Boxall, A.B., Wang, X., Gore, D., Tiede, D., Baxter, M., David, H., Tear, S.P., Lewis, J., 2010. Application of hydrodynamic chromatography-ICP-MS to investigate the fate of silver nanoparticles in activated sludge. Journal of Analytical Atomic Spectrometry 25 (7), 1149-1154.

Tiemann, M., 2008. Safeguarding the Nation's drinking water: EPA and congressional actions. CRS Report for Congress RL31294.

Tong, M., Ding, J., Shen, Y., Zhu, P., 2010. Influence of biofilm on the transport of fullerene (C-60) nanoparticles in porous media. Water Research 44 (4, Sp. Iss. SI), 1094-1103.

Unrine, J.M., Tsyusko, O.V., Hunyadi, S.E., Judy, J.D., Bertsch, P.M., 2010. Effects of particle size on chemical speciation and bioavailability of copper to earthworms (Eisenia fetida) exposed to copper nanoparticles. Journal of Environmental Quality 39 (6), 1942-1953.

Upadhyayula, V. K. K., Gadhamshetty, V., 2010. Appreciating the role of carbon nanotube composites in preventing biofouling and promoting biofilms on material surfaces in environmental engineering: A review. Biotechnology Advances 28 (6).

USEPA. 1998. Fate, Transport and Transformation Test Guidelines: OPPTS 835.1110 Activated Sludge Sorption Isotherm. EPA 712-C-98-298. http://fedbbs.access.gpo.gov/library/epa_835-1110.pdf

USEPA, 2009. Targeted National Sewage Sludge Survey Sampling and Analysis Technical Report. http://www.epa.gov/waterscience/biosolids/tnsss-tech.pdf.

USEPA. 2010. Interim Technical Guidance for Assessing Screening Level Environmental Fate and Transport of, and General Population, Consumer, and Environmental Exposure to Nanomaterials. http://www.epa.gov/oppt/exposure/pubs/nanomaterial.pdf

USEPA, 2011. 40 CFR Appendix B to Part 136 - Definition and Procedure for the Determination of the Method Detection Limit - Revision 1.11; US Environmental Protection Agency: Washington, DC.

Vandenberg, G. W., de la Noue, J., 2001. Apparent digestibility comparison in rainbow trout (Oncorhynchus mykiss) assessed using three methods of faeces collection and three digestibility markers. Aquaculture Nutrition 7 (4), 237-245.

Van Loosdrecht, M.C.M., Lyklema, J., Norde, W., Schraa, G., Zehnder, A.J.B., 1987a. The role of bacterial cell wall hydrophobicity in adhesion. Applied and Environmental Microbiology 53 (8), 1893-1897.

Van Loosdrecht, M.C.M., Lyklema, J., Norde, W., Schraa, G., Zehnder, A.J.B., 1987b. Electrophoretic mobility and hydrophobicity as a measure to predict the initial steps of bacterial adhesion. Applied and Environmental Microbiology 53 (8), 1898-1901.

Van Loosdrecht, M.C.M., Norde, W., Lyklema, J., Zehnder, A.J.B., 1990. Hydrophobic and electrostatic parameters in bacterial adhesion. Aquatic Sciences 52 (1), 103-114.

Wang, J.W., Chen, Y.S., Yang, H.C., Chen, X.C., Duan, M.X., Tai, P.C., Sui, S.F., 2003. Ring-like pore structures of SecA: implications for bacterial protein-conducting channels. Proceedings of the National Academy of Sciences of the United States of America 100 (7), 4221-4226.

Wang, L., Govind, R., Dobbs, R.A., 1993. Sorption of toxic organic compounds on wastewater solids: Mechanism and modeling. Environmental Science and Technology 27 (1), 152-158.

Wassall, M.A., Santin, M., Isalberti, C., Cannas, M., Denyer, S.P., 1997. Adhesion of bacteria to stainless steel and silver-coated orthopedic external fixation pins. Journal of Biomedical Materials Research. 36 (3), 325-330.

Water Environment Federation, 2006. Membrane Systems for Wastewater Treatment. McGraw-Hill Books: New York.

Weatherup, R. N., McCracken, K. J., 1998. Comparison of estimates of digestibility of two diets for rainbow trout, Oncorhynchus mykiss (Walbaum), using two markers and two methods of faeces collection. Aquaculture Research 29 (7), 527-533.

Weber, W.J., McGinley, P.M., Katz, L.E., 1992. A distributed reactivity model for sorption by soils and sediments. 1. Conceptual basis and equilibrium assessments. Environmental Science and Technology 26 (10), 1955-1962.

Westerhoff, P., Benn, T., Kiser, A., Herckes, P., Zhang, Y., Crittenden, J.C., Chen, Y., Rittmann, B.E., Dotson, A., 2007. Detection and Fate of Engineered Nanomaterials During Wastewater Treatment, Water Environment Federation Annual Conference (WEFTEC): San Diego, CA.

Westerhoff, P.K., Song, G.X., Hristovski, K., Kiser, M.A., 2011. Occurrence and removal of titanium at full scale wastewater treatment plants: implications for TiO_2 nanomaterials. Journal of Environmental Monitoring 13 (5), 1195-1203.

Wigginton, N.S., de Titta, A., Piccapietra, F., Dobias, J., Nesatyy, V.J., Suter, M.J., Bernier-Latmani, R., 2010. Binding of silver nanoparticles to bacterial proteins depends on surface modifications and inhibits enzymatic activity. Environmental Science and Technology 44 (6), 2163-2168.

Wiesner, M.R., Lowry, G.V., Jones, K.L., Hochella, M.F., Di Giulio, R.T., Casman, E., Bernhardt, E.S., 2009. Decreasing uncertainties in assessing environmental exposure, risk, and ecological implications of nanomaterials. Environmental Science and Technology 43 (17), 7458-6462.

Wingender, J., Neu, T.R., Flemming, H.C., eds., 1999. Microbial Extracellular Polymeric Substances: Characteristics, Structure, and Function. Springer, Berlin.

Wrangstadh, M., Conway, P.L., Kjelleberg, S., 1986. The production of an extracellular polysaccharide during starvation of a marine Pseudomonas sp. And the effect thereof on adhesion. Arch. Microbiol. 145, 220-227.

Xiao, L., Takada, H., Gan, X.H., Miwa, N., 2006. The water-soluble fullerene derivative 'Radical Sponge (R)' exerts cytoprotective action against UVA irradiation but not visible-light-catalyzed cytotoxicity in human skin keratinocytes. Bioorganic and Medicinal Chemistry Letters 16 (6), 1590-1595.

Yamakoshi, Y.N., Yagami, T., Fukuhara, K., Sueyoshi, S., Miyata, N., 1994. Solubilization of fullerenes into water with polyvinylpyrrolidone applicable to biological tests. Journal of the Chemical Society - Chemical Communications 4, 517-518.

Yang, K., Lin, D. H., Xing, B. S., 2009. Interactions of Humic Acid with Nanosized Inorganic Oxides. Langmuir 25 (6), 3571-3576.

Yang, Z., Liu, Z. W., Allaker, R. P., Reip, P., Oxford, J., Ahmad, Z., Ren, G., 2010. A review of nanoparticle functionality and toxicity on the central nervous system. Journal of the Royal Society Interface 7, S411-S422.

Yao, Q, Zhang, H., Wu, J., Shao, L., He, P., 2010. Biosorption of Cr(III) from aqueous solution by freeze-dried activated sludge: Equilibrium, kinetic and thermodynamic studies. Front. Environ. Sci. Engin. China 4 (3), 286-294.

Yin, Y. X., Zhang, X. Q., Graham, J., Luong, L., 2009. Examination of purified single-walled carbon nanotubes on activated sludge process using batch reactors. Journal of Environmental Science and Health Part a-

Toxic/Hazardous Substances & Environmental Engineering 44 (7), 661-665.

Yu, Y.L., Wu, X.M., Li, S.N., Fang, H., Zhan, H.Y., Yu, J.Q., 2006. An exploration of the relationship between adsorption and bioavailability of pesticides in soil to earthworm. Environmental Pollution 141 (3), 428-433.

Zhang, Y., Chen, Y. S., Westerhoff, P., Crittenden, J. C., 2008a. Stability and removal of water soluble CdTe quantum dots in water. Environmental Science & Technology 42 (1), 321-325.

Zhang, Y., Chen, Y. S., Westerhoff, P., Hristovski, K., Crittenden, J. C., 2008b. Stability of commercial metal oxide nanoparticles in water. Water Research 42 (8-9), 2204-2212.

Zhang, Y., Chen, Y., Westerhoff, P., Crittenden, J., 2009. Impact of natural organic matter and divalent cations on the stability of aqueous nanoparticles. Water Research 43, 4249-4257.

Zhang, W., Rittmann, B., Chen, Y., 2011. Size effects on adsorption of hematite nanoparticles on E. coli cells. Environmental Science and Technology 45, 2172-2178.

Zhang, Y., Shen, J., 2007. Enhancement effect of gold nanoparticles on biohydrogen production from artificial wastewater. International Journal of Hydrogen Energy 32 (1), 17-23.

Zhu, Z. J., Carboni, R., Quercio, M. J., Yan, B., Miranda, O. R., Anderton, D. L., Arcaro, K. F., Rotello, V. M., Vachet, R. W., 2010. Surface Properties Dictate Uptake, Distribution, Excretion, and Toxicity of Nanoparticles in Fish. Small 6 (20), 2261-2265.

Ziccardi, L., McArdle, M., Lowney, Y., 2008. The Ecological Effects of Nanomaterials: A Focus on Aquatic Life. Nano 3 (4), 251-255.

Zita, A., Hermansson, M., 1997a. Determination of bacterial cell surface hydrophobicity of single cells in cultures and in wastewater in situ. FEMS Microbiology Letters 152, 299-306.

Zita, A., Hermansson, M., 1997b. Effects of bacterial cell surface structures and hydrophobicity on attachment to activated sludge flocs. Applied and Environmental Microbiology 63 (3), 1168-1170.

APPENDIX A

NANOPARTICLE-BIOMASS BATCH INTERACTION EXPERIMENT

PROTOCOL

Glassware and Matrix Solution Preparation

1. Clean and label all necessary glassware before starting the experiment.

    At the very least, the following materials will be needed:

    a. Sample vials – 20- or 40-mL glass vials for organic (more

        hydrophobic) nanoparticles, like C_{60} or polystyrene, and 15-mL

        plastic centrifuge vials for inorganic (more hydrophilic)

        nanoparticles, like TiO_2 or silver.

    b. 2 1-L Nalgene bottles – one for RAS collection and one for rinsed

        biomass stock.

    c. 1- or 2-L volumetric flask to make the matrix solution and a 1-L

        beaker to hold the matrix solution as samples are made.

    d. Magnetic stir bar for your biomass stock.

2. Make 1-mM $NaHCO_3$ solution. This is the buffer/matrix solution. I

    typically make about 1 to 2 L of the matrix solution, depending on the

    number of samples and controls.

Biomass Stock Preparation

3. Collect return activated sludge (RAS) from the Mesa WWTP. I collect

    RAS in 1-L Nalgene bottles. Immediately after collection, put the bottles

    of RAS in a cooler filled with ice packs ($\sim 4^oC$) and then return to the lab.

    Once in the lab, store the bottles in the 4 ^oC fridge.

4. Within 24 hours, rinse the RAS with the matrix solution:

   a. Allow the solids to settle in the collection bottles. Once settled, decant the WW liquid.

   b. Pour solids into 50-mL plastic centrifuge vials.

   c. Add matrix solution to bring volume up to ~ 40 mL; shake well to completely resuspend solids.

   d. Centrifuge at 2000 F (rcg) for 5 min.

   e. Decant liquid.

   f. Replace decanted volume with fresh matrix solution; shake well to completely resuspend solids.

   g. Repeat steps (d) through (f) for a total of three rinses (three volume changes)

5. Make a biomass suspension by pouring all of the rinsed solids into one bottle and add enough matrix solution to provide the approximate suspended solids concentration you desire. I usually do this in a clean 1-L Nalgene bottle.

6. Measure the TSS and/or COD (whatever properties you need to know) of the biomass suspension.

7. After determining the TSS/COD of the initial rinsed RAS suspension, do the calculations to determine the volumes of biomass stock(s) and nanoparticle suspension you will have to add to each sample to achieve a certain sample total volume with final TSS and nanoparticle concentrations; this is the "sample recipe." Make recipes for controls, too.

For nanoparticle-only controls, replace the biomass stock volume used in the samples with matrix solution and add NP suspension. For biomass-only controls, replace the nanoparticle suspension with matrix solution and add biomass stock.

8. To make biomass stock for experiments, the rinsed biomass suspension must be diluted with matrix solution to achieve a TSS concentration that is approximately the desired TSS concentration in the samples. For example, if samples with a final volume of 15 mL and 800 mg/L TSS are desired, and 14.5 mL of biomass stock (and 0.5 mL of nanoparticle suspension) are to be added to each sample, then try to make the biomass stock around 830 mg/L TSS. If more than one biomass concentration will be used in the experiment, then stocks for each concentration must be prepared.

9. Measure the TSS/COD of the biomass stock(s) following Standard Methods.

10. Store the biomass stock(s) in the 4 ^{o}C fridge until it is time to do the experiment. Try to do the experiment within 24 hours of rinsing the RAS.

NP-Biomass Batch Interaction Experiment

11. Once properties of the biomass stock(s) have been measured, sample recipes have been made, and it is time to do the experiment, put a magnetic stir bar in the biomass stock bottle(s) and put the bottle on a stirring plate. The biomass must be kept completely mixed while being used to make the samples.

12. Arrange labeled vials, a beaker of matrix solution, sonicated nanoparticle suspensions, and biomass stock on the bench space. Try to arrange these components to make adding ingredients simple and to minimize mistakes (adding the wrong volume of ingredient to the wrong vial).

13. Add the determined volume of biomass stock to each sample and biomass-only control vial and the appropriate volume of matrix solution to NP-only control vials.

14. Sonicate (using the bath sonicator) the NP suspension(s).

15. Add determined volume of NP suspension(s) to the sample and control vials.

16. Once everything has been added to the sample and control vials, tightly cap each vial, put all of the vials horizontally into a box, and gently shake the box for a fixed period of time (I usually shake for 3 hours). On the New Brunswick shaker, I usually set the speed to around 30 rpm.

17. Once the shaking is done, set the vials upright on the bench and allow them to settle for 2 hours to ensure good solids separation.

18. Collect the supernatant from each vial and store in clean glass or nalgene vials (again, use glass for hydrophobic NPs like C_{60} and Polystyrene and plastic for metals). If sample supernatants are to be filtered, then I suggest using small vacuum-filter glassware.

19. Store samples in 4 ^{o}C fridge until analysis.

APPENDIX B

FORTRAN CODES FOR WASTEWATER REACTOR MODELS

MBR Fate Model Input Parameters

```
$MBRfparam

  Q0 (L/d)              = 31200,
  S0 (mg CODS/L)        = 250.0,
  Xa0 (mg CODX/L)       = 0.0,
  Xres0 (mg CODX/L)     = 50.0,
  EPS0 (mg CODP/L)      = 0.0,
  UAP0 (mg CODP/L)      = 0.0,
  BAPS0 (mg CODP/L)     = 0.0,
  BAPL0 (mg CODP/L)     = 0.0,
  O20 (mg O2/L)         = 3.0,

  qS (mg CODS/mg CODX-d)        = 10.0,
  qD (mg CODD/mg CODX-d)        = 1.5,
  qBAP (mg CODBAP/mg CODX-d)    = 0.07,
  qUAP (mg CODUAP/mg CODX-d)    = 1.27,
  YS (mgX/mgS)                  = 0.4,
  YP (mgX/mgP)                  = 0.45,
  KBAP (mg CODP/L)              = 85.0,
  KS (mg CODS/L)                = 10.0,
  KD (mgD/L)                    = 0.8,
  KUAP (mg CODP/L)              = 100.0,
  KO (mg O/L)                   = 0.5,
  b (d^-1)                      = 0.1,
  fd                            = 0.8,
  k1 (mg CODP/mg CODS)          = 0.05,
```

```
kEPS (mg CODP/mg CODS)          = 0.18,
khyd (d^-1)                     = 0.17,
xBAPS                           = 0.35,
kLa (d^-1)                      = 2000.0,


V (L)           = 6000,
D (m)           = 5.0,
Thetax (d)      = 30.0,
e               = 0.8,


Si (mg CODS/L)      = 10.0,
Xai (mg CODX/L)     = 2000.0,
Xresi (mg CODX/L)   = 100.0,
EPSi (mg CODP/L)    = 100.0,
UAPi (mg CODP/L)    = 1.0,
BAPSi (mg CODP/L)   = 50.0,
BAPLi (mg CODP/L)   = 50.0,
O2i (mg O2/L)       = 3.0,


SOTE (kg O2/kWh)    = 2.0,
c1s (mg O2/L)       = 8.7,
c1 (mg O2/L)        = 2.0,
beta                = 0.95,
T (C)               = 25.0,


Ci0 (mgC/L)         = 0.000025,
kb (L/g SS-d)       = 430,
Kp (L/g SS)         = 0.9,
Hc (atm-m^3/mol)    = 0.00000000038,
kLac (d^-1)         = 0.1,
xsur                = 0.33,
p1 (atm)            = 1.00,
n_air               = 0.28,
R (kJ/mol-K)        = 8.31,
R_dry (J/kg-K)      = 287.05,
```

```
   ts (s)        = 1.0,
   tdmax (d)     = 1000.0,


$end
```

MBR Fate Model

```
PROGRAM MBRfate

IMPLICIT REAL*8 (a-h,o-z)

REAL*8 Q0,S0,Xa0,Xres0,EPS0,UAP0,BAPS0,BAPL0,ISS,O20, &
qS,qD,qBAP,qUAP,YS,YP,KBAP,KS,KD,KUAP,KO,b,fd,k1,kEPS,khyd,xBAPS,kLa, &
V,d,thetax,e, &
Qw,Qe, &
Si,Xai,Xresi,EPSi,UAPi,BAPSi,BAPLi,O2i, &
ts,td,tdmax, &
S_old,Xa_old,Xres_old,EPS_old,UAP_old,BAPS_old,BAPL_old,O2_old, &
S_new,Xa_new,Xres_new,EPS_new,UAP_new,BAPS_new,BAPL_new,O2_new, &
rs,BAP, &

thetad,thetah, &
Xv,XvSS,Xratio, &
Xv_is,y_theta,X,XSS,Xg,Xkg, &
dXa_dt,dXv_dt,dXSS_dt,dXSS_dt_kg,dXv_dt_biol, &
SWR, &
N,P, &
EffProd,WastProd, &
EQ_COD,EQ_BODL,EQ_BOD5,COD_sum,COD_loading, Rem_COD, &
O2input,O2output,O2uptake,O2uptake_kg, &
SOTE,c1s,c1,beta,T,alpha_KK,FOTE_KK,alpha_C,FOTE_C, &
Power_KK,Power_C, &
Flux_ExtMBR_CFV1,Flux_ExtMBR_CFV1_d,Flux_ExtMBR_CFV3,Flux_ExtMBR_CFV3_d, &
Flux_IntMBR_AF400,Flux_IntMBR_AF400_d, &
AM_ExtMBR_CFV1,AM_ExtMBR_CFV3,AM_IntMBR_AF400, &
```

```
Ci0,kb,kb_mg,Kp,Kp_mg,kLac,xsur,Hc,Hc_LL,p1,p2,n_air,R,R_dry,w,Qa, &
Qa_L,rho_air,Ci,Rem_Ci,Mass_inf,Mass_eff,Mass_was,Mass_vol, &
Mass_aer,Mass_sor,Mass_bio,Mass_sld,Mass_eff_tot,Mass_was_tot, &
Ci_eff,Ci_was,Ci_vol,Ci_aer,Ci_sor,Ci_bio,Ci_sum, &

t0,total_time

INTEGER nt,i

NAMELIST/MBRfparam/ &
Q0,S0,Xa0,EPS0,UAP0,BAPS0,BAPL0,O20, &
qS,qD,qBAP,qUAP,YS,YP,KBAP,KS,KD,KUAP,KO,b,fd,k1,kEPS,khyd,xBAPS,kLa, &
V,d,thetax,e, &
Si,Xai,Xresi,EPSi,UAPi,BAPSi,BAPLi,O2i, &
SOTE,c1s,c1,beta,T, &
Ci0,kb,Kp,kLac,xsur,Hc,p1,n_air,R,R_dry, &
ts,tdmax

! Start counting runtime
t0 = SECNDS(0.0)

! Read input file
OPEN(unit=1, file='MBRfparam.in', status='old')
READ(unit=1, nml=MBRfparam)
CLOSE(1)

! Derived parameters
Xres0 = 0.08*S0
ISS   = 0.05*S0
Qw    = V/thetax
Qe    = Q0 - Qw

! Time stepping
td    = ts / (60*60*24)    ! size of time step in days
nt    = tdmax / td         ! total number of time steps
```

```
! Initialize time-dependent quantities
S_old    = Si
Xa_old   = Xai
Xres_old = Xresi
EPS_old  = EPSi
UAP_old  = UAPi
BAPS_old = BAPSi
BAPL_old = BAPLi
O2_old   = O2i


!!!!!!!!!!!!!!!!!!!!!!!!!!!!!!!!!!!!!!!!!!!!!!!!!!!!!!!!
! Do the time integration of the differential equations !
!!!!!!!!!!!!!!!!!!!!!!!!!!!!!!!!!!!!!!!!!!!!!!!!!!!!!!!!


DO i=1,nt

rs       = qS*S_old/(KS+S_old)
BAP      = BAPS_old + BAPL_old

S_new    = S_old + ( -rs*Xa_old + Q0*S0/V - Qe*S_old/V - Qw*S_old/V ) * td
Xa_new   = Xa_old + ( YS*rs*(1-k1-kEPS)*Xa_old + YP*(qUAP*UAP_old/(KUAP+UAP_old) +
             qBAP*BAP/(KBAP+BAP))*Xa_old - b*Xa_old + Q0*Xa0/V - Qw*Xa_old/V) * td
Xres_new = Xres_old + ( b*(1-fd)*Xa_old + Q0*Xres0/V - Qw*Xres_old/V ) * td
EPS_new  = EPS_old + ( kEPS*rs*Xa_old - khyd*EPS_old + Q0*EPS0/V - Qw*EPS_old/V ) * td
UAP_new  = UAP_old + ( k1*rs*Xa_old - qUAP*UAP_old/(KUAP+UAP_old)*Xa_old + Q0*UAP0/V -
             Qe*UAP_old/V - Qw*UAP_old/V ) * td
BAPS_new = BAPS_old + ( xBAPS*khyd*EPS_old - qBAP*BAPS_old/(KBAP+BAPS_old)*Xa_old +
             Q0*BAPS0/V - Qe*BAPS_old/V - Qw*BAPS_old/V ) * td
BAPL_new = BAPL_old + ( (1-xBAPS)*khyd*EPS_old - qBAP*BAPL_old/(KBAP+BAPL_old)*Xa_old +
             Q0*BAPL0/V - Qw*BAPL_old/V ) * td

S_old    = S_new
Xa_old   = Xa_new
Xres_old = Xres_new
EPS_old  = EPS_new
```

```
UAP_old  = UAP_new
BAPS_old = BAPS_new
BAPL_old = BAPL_new


ENDDO


!!!!!!!!!!!!!!!!!!!!!!!!!!!!!!!!!
! Calculate final output values !
!!!!!!!!!!!!!!!!!!!!!!!!!!!!!!!!!


! System Hydraulic Detention Time
thetad = V/Q0         ! days
thetah = thetad*24    ! hours


! Mixed Liquor Volatile Suspended Solids, MLVSS
Xv   = Xa_new + Xres_new + EPS_new    ! mg CODX/L
XvSS = Xv/1.42                        ! mg VSS/L


! Ratio of Active to Volatile Suspended Solids
Xratio = Xa_new/Xv


! Estimation of Mixed Liquor Suspended Solids, MLSS
Xv_is   = Xv * 10/90             ! Inorganic solids of MLVSS (mg COD_X/L)
y_theta = ISS*thetax/thetad      ! Input inorganic suspended solids (mg COD_X/L)
X       = Xv + Xv_is + y_theta   ! mg COD_X/L
XSS     = X / (0.9*1.42)         ! mg SS/L
Xg      = X / (1000*1.42*0.9)    ! g SS_X/L (assuming VSS = 0.9SS)
Xkg     = Xg / 1000              ! kg SS_X/L


! Solids Loss Rate
dXa_dt       = Xa_new * V/thetaX      ! mg COD_X/d
dXv_dt       = Xv * V/thetax          ! mg COD_X/d
dXSS_dt      = X * V/thetax           ! mg COD_X/d
dXSS_dt_kg   = dXSS_dt / 1000000      ! kg COD_X/d
dXv_dt_biol  = dXv_dt - Q0*Xres0      ! mg COD_X/d
```

216

```
! Sludge Wasting Rate
SWR = Qw*X/1000000     ! kg COD_X/d


! Nutrient Requirements
N = dXv_dt_biol * 0.124/Q0     ! mg N/L
P = dXv_dt_biol * 0.025/Q0     ! mg P/L


! Effluent and Wasted EPS, UAP, and BAP
EffProd  = UAP_new + BAPS_new                          ! mg COD_P/L
WastProd = EPS_new + UAP_new + BAPS_new + BAPL_new     ! mg COD_P/L


! Effluent Quality
EQ_COD      = ISS+ S_new + UAP_new + BAPS_new          ! mg COD/L
EQ_BODL     = S_new + UAP_new + BAPS_new               ! mg BOD_L/L
EQ_BOD5     = 0.68*S_new + 0.14*(UAP_new + BAPS_new    ! mg BOD_5/L
COD_sum     = S0+Xa0+Xres0+EPS0+UAP0+BAPS0+BAPL0       ! mg COD/L
COD_loading = Q0*COD_sum/(1000*V)                      ! kg/m^3/d
Rem_COD     = (1-(EQ_COD/COD_sum))*100                 ! %


! Oxygen Supply Rate Needed
O2input    = Q0*(O20+COD_sum)
     ! mg O2/d
O2output   = (Qe+Qw)*(S_new+UAP_new+BAPS_new) + Qw*(Xa_new+Xres_new+EPS_new+BAPL_new)
     ! mg O2/d
O2uptake   = O2input - O2output
     ! mg O2/d
O2uptake_kg = O2uptake / 1000000
     ! kg O2/d


! Field Oxygen Transfer Efficiency
alpha_KK = EXP(-0.08788*Xg)                                      ! kg O2/kWh
FOTE_KK  = SOTE * 1.035**(T-20) * alpha_KK * (beta*c1s-c1) / 9.2   ! kg O2/kWh
alpha_C  = EXP(-0.046*Xg)                                        ! kg O2/kWh
FOTE_C   = SOTE * 1.035**(T-20) * alpha_C * (beta*c1s-c1) / 9.2    ! kg O2/kWh


! Power Required for Aeration
```

```
Power_KK = O2uptake_kg / (FOTE_KK*24)      ! kW
Power_C  = O2uptake_kg / (FOTE_C*24)       ! kW


! Transmembrane Flux
Flux_ExtMBR_CFV1    = 91.987*Xg**(-0.47)        ! L/m^2-h
Flux_ExtMBR_CFV1_d  = Flux_ExtMBR_CFV1 * 24     ! L/m^2-d
Flux_ExtMBR_CFV3    = 167.63*Xg**(-0.3)         ! L/m^2-h
Flux_ExtMBR_CFV3_d  = Flux_ExtMBR_CFV3 * 24     ! L/m^2-d
Flux_IntMBR_AF400   = 31.85*Xg**(-0.17)         ! L/m^2-h
Flux_IntMBR_AF400_d = Flux_IntMBR_AF400 * 24    ! L/m^2-d


! Minimum Total Membrane Area
AM_ExtMBR_CFV1  = Qe / Flux_ExtMBR_CFV1_d      ! m^2
AM_ExtMBR_CFV3  = Qe / Flux_ExtMBR_CFV3_d      ! m^2
AM_IntMBR_AF400 = Qe / Flux_IntMBR_AF400_d     ! m^2


! Pollutant Fate
Hc_LL      = Hc/(0.082054*293/1000)                        ! L water/L gas
Kp_mg      = Kp/(0.9*1000*1.42)                            ! L/mg COD_P
kb_mg      = kb/(0.9*1000*1.42)                            ! L/mg COD_P-d
p2         = ((p1*101330)+(1000*9.8*d))/101330             ! atm
w          = (8.41*e*Power_KK)/(R*(T+273)*(((p2/p1)**0.283)-1))  ! kg air/s
rho_air    = (p1*101325)/(R_dry*(T+273))                   ! kg/m^3
Qa         = (w/rho_air)*86400                             !m^3/d
Qa_L       = Qa*1000                                       !L/d


Ci    =
(Q0*Ci0)/(Qe+Qw+(xsur*kLac*V)+(Qa_L*Hc_LL)+(Xv*Kp_mg*V/thetax)+(kb_mg*Xa_new*V))
     !mg Ci/L


Rem_Ci        = (1-(Ci/Ci0))*100            ! %
Mass_inf      = Q0*Ci0                      ! mg Ci/d
Mass_eff      = Qe*Ci                       ! mg Ci/d
Mass_was      = Qw*Ci                       ! mg Ci/d
Mass_vol      = (kLac*xsur*V*Ci)            ! mg Ci/d
Mass_aer      = Qa_L*Hc_LL*Ci               ! mg Ci/d
```

```fortran
Mass_sor      = Xv*Kp_mg*Ci*Qw              ! mg Ci/d
Mass_bio      = kb_mg*Xa_new*Ci*V           ! mg Ci/d
Mass_was_tot = (Xv*Kp_mg*Ci*Qw)+Ci*Qw       ! mg Ci/d
Ci_eff        = (Mass_eff/Mass_inf)*100     ! %
Ci_was        = (Mass_was/Mass_inf)*100     ! %
Ci_vol        = (Mass_vol/Mass_inf)*100     ! %
Ci_aer        = (Mass_aer/Mass_inf)*100     ! %
Ci_sor        = (Mass_sor/Mass_inf)*100     ! %
Ci_bio        = (Mass_bio/Mass_inf)*100     ! %


Ci_sum        = Ci_eff+Ci_was+Ci_vol+Ci_aer+Ci_sor+Ci_bio    ! %


!!!!!!!!!!!!!!!!!!!!!!!!!!!
! Write outputs to a file !
!!!!!!!!!!!!!!!!!!!!!!!!!!!
OPEN(unit=1, file='output.txt', status='replace')
WRITE(1,*) S_new
WRITE(1,*) Xa_new
WRITE(1,*) Xres_new
WRITE(1,*) EPS_new
WRITE(1,*) UAP_new
WRITE(1,*) BAPS_new
WRITE(1,*) BAPL_new
WRITE(1,*) BAPS_new+BAPL_new
WRITE(1,*) thetah
WRITE(1,*) Xv
WRITE(1,*) X
WRITE(1,*) Xv/X
WRITE(1,*) ISS
WRITE(1,*) EQ_COD
WRITE(1,*) COD_sum
WRITE(1,*) Rem_COD
WRITE(1,*) dXa_dt
WRITE(1,*) dXv_dt
WRITE(1,*) dXSS_dt
WRITE(1,*) SWR
```

```
WRITE(1,*)  O2input
WRITE(1,*)  O2output
WRITE(1,*)  O2uptake
WRITE(1,*)  FOTE_KK
WRITE(1,*)  alpha_KK
WRITE(1,*)  Power_KK
WRITE(1,*)  Power_KK/Xg
WRITE(1,*)  Q0
WRITE(1,*)  Qe
WRITE(1,*)  Qw
WRITE(1,*)  Qe+Qw
WRITE(1,*)  Ci
WRITE(1,*)  Rem_Ci
WRITE(1,*)  Mass_inf
WRITE(1,*)  Mass_eff
WRITE(1,*)  Mass_was
WRITE(1,*)  Mass_vol
WRITE(1,*)  Mass_aer
WRITE(1,*)  Mass_sor
WRITE(1,*)  Mass_bio
WRITE(1,*)  Mass_was_tot
WRITE(1,*)  Ci_eff
WRITE(1,*)  Ci_was
WRITE(1,*)  Ci_vol
WRITE(1,*)  Ci_aer
WRITE(1,*)  Ci_sor
WRITE(1,*)  Ci_bio
WRITE(1,*)  Ci_sum
WRITE(1,*)  Q0*Ci0
WRITE(1,*)  xsur*kLac*V
WRITE(1,*)  Qa_L*Hc_LL
WRITE(1,*)  Xv*Kp_mg*Qw
WRITE(1,*)  Xv*Kp_mg*V/thetax
WRITE(1,*)  kb_mg*Xa_new*V
WRITE(1,*)  Qa
WRITE(1,*)  Qa_L
```

```fortran
WRITE(1,*) Hc
WRITE(1,*) Hc_LL
WRITE(1,*) w
WRITE(1,*) rho_air
WRITE(1,*) 8.41*e*Power_KK
WRITE(1,*) R*(T+273)*(((p2/p1)**0.283)-1)
WRITE(1,*) p1
WRITE(1,*) p2
WRITE(1,*) p2/p1
WRITE(1,*) (p2/p1)**0.283
WRITE(1,*) ((p2/p1)**0.283)-1
CLOSE(1)

!!!!!!!!!!!!!!!!!!!!!!!!!!!!!!!!!!!!!!!!!!
! Might as well print it to the screen too !
!!!!!!!!!!!!!!!!!!!!!!!!!!!!!!!!!!!!!!!!!!
PRINT*,''
PRINT*,'EQ_COD = ',EQ_COD
PRINT*,'S_new = ',S_new
PRINT*,'UAP_new = ',UAP_new
PRINT*,'BAPS_new = ',BAPS_new
PRINT*,'COD_loading = ',COD_loading
PRINT*,'(COD_sum-EQ_COD)/COD_sum = ',(COD_sum-EQ_COD)/COD_sum
PRINT*,'Xa_new = ',Xa_new
PRINT*,'Xres_new = ',Xres_new
PRINT*,'EPS_new = ',EPS_new
PRINT*,'BAPL_new = ',BAPL_new
PRINT*,'XvSS = ',XvSS
PRINT*,'Xv = ',Xv
PRINT*,'XSS = ',XSS
PRINT*,'X = ',X
PRINT*,'Xv/X = ',Xv/X
PRINT*,'SWR = ',SWR
PRINT*,'O2uptake_kg = ',O2uptake_kg
PRINT*,'FOTE_KK = ',FOTE_KK
PRINT*,'alpha_KK = ',alpha_KK
```

```
PRINT*,'Power_KK = ',Power_KK
PRINT*,'Power_KK/Xg = ',Power_KK/Xg
PRINT*,'Flux_ExtMBR_CFV1_d = ',Flux_ExtMBR_CFV1_d
PRINT*,'Flux_ExtMBR_CFV3_d = ',Flux_ExtMBR_CFV3_d
PRINT*,'Flux_IntMBR_AF400_d = ',Flux_IntMBR_AF400_d
PRINT*,'Flux_IntMBR_AF400 = ',Flux_IntMBR_AF400
PRINT*,'AM_ExtMBR_CFV1 = ',AM_ExtMBR_CFV1
PRINT*,'AM_ExtMBR_CFV3 = ',AM_ExtMBR_CFV3
PRINT*,'AM_IntMBR_AF400 = ',AM_IntMBR_AF400
PRINT*,''

! Get total runtime
total_time = SECNDS(t0)
PRINT*,''
PRINT*,'Total time: ', total_time
PRINT*,''

PAUSE 'All done (press the Enter key)'

END
```

CAS Fate Model Input Parameters

```
$CASfparam

  Q0  (L/d)                = 1000000,
  S0  (mg CODS/L)       = 250.0,
  Xa0  (mg CODX/L)      = 0.0,
  Xres0  (mg CODX/L)    = 50.0,
  EPS0  (mg CODP/L)     = 0.0,
  UAP0  (mg CODP/L)     = 0.0,
  BAPS0  (mg CODP/L)    = 0.0,
  BAPL0  (mg CODP/L)    = 0.0,
  O20  (mg O2/L)        = 3.0,

  qS  (mg CODS/mg CODX-d)      = 10.0,
  qD  (mg CODD/mg CODX-d)      = 1.5,
  qBAP  (mg CODBAP/mg CODX-d)  = 0.07,
  qUAP  (mg CODUAP/mg CODX-d)  = 1.27,
  YS  (mgX/mgS)               = 0.4,
  YP  (mgX/mgP)               = 0.45,
  KBAP  (mg CODP/L)           = 85.0,
  KS  (mg CODS/L)             = 10.0,
  KD  (mgD/L)                 = 0.8,
  KUAP  (mg CODP/L)           = 100.0,
  KO  (mg O/L)                = 0.5,
  b  (d^-1)                   = 0.1,
  fd                          = 0.8,
  k1  (mg CODP/mg CODS)       = 0.05,
  kEPS  (mg CODP/mg CODS)     = 0.18,
  khyd  (d^-1)                = 0.17,
  xBAPS                       = 0.35,
  kLa  (d^-1)                 = 2000.0,

  V  (L)          = 39000,
  D  (m)          = 5.0,
  Thetax  (d)     = 5.0,
```

```
e                  = 0.8,

Xv_eff (mg CODX/L)  = 20,
Xv_rec (mg CODX/L)  = 8000,

Si (mg CODS/L)      = 10.0,
Xai (mg CODX/L)     = 2000.0,
Xresi (mg CODX/L)   = 100.0,
EPSi (mg CODP/L)    = 100.0,
UAPi (mg CODP/L)    = 1.0,
BAPSi (mg CODP/L)   = 50.0,
BAPLi (mg CODP/L)   = 50.0,
O2i (mg O2/L)       = 3.0,
Qwi (L/d)           = 20000,

SOTE (kg O2/kWh)    = 2.0,
c1s (mg O2/L)       = 8.7,
c1 (mg O2/L)        = 2.0,
beta                = 0.95,
T (C)               = 25.0,

Ci0 (mgC/L)         = 0.000025,
kb (L/g SS-d)       = 430,
Kp (L/g SS)         = 0.9,
Hc (atm-m^3/mol)    = 0.00000000038,
kLac (d^-1)         = 0.1,
xsur                = 0.33,
p1 (atm)            = 1.00,
n_air               = 0.28,
R (kJ/mol-K)        = 8.31,
R_dry (J/kg-K)      = 287.05,

ts (s)      = 1.0,
tdmax (d)   = 1000.0,

$end
```

CAS Fate Model

```
PROGRAM CASf

IMPLICIT REAL*8 (a-h,o-z)

REAL*8 Q0,S0,Xa0,Xres0,EPS0,UAP0,BAPS0,BAPL0,ISS,O20, &
qS,qBAP,qUAP,YS,YP,KBAP,KS,KUAP,b,fd,k1,kEPS,khyd,xBAPS, &
V,d,thetax,e, &
Si,Xai,Xresi,EPSi,UAPi,BAPSi,BAPLi,O2i,Qwi, &
ts,td,tdmax, &

S_old,Xa_old,Xres_old,EPS_old,UAP_old,BAPS_old,BAPL_old,Xv_old,Qw_old, Qe_old, &

S_new,Xa_new,Xres_new,EPS_new,UAP_new,BAPS_new,BAPL_new,Xv_new,Qw_new,Qe_new, &
rs,BAP, &

thetad,thetah, &
Xv,Xv_eff,Xv_rec,XvSS,Xratio, &
Xv_is,y_theta,X,XSS,Xg,Xkg, &
dXa_dt,dXv_dt,dXSS_dt,dXSS_dt_kg,dXv_dt_biol, &
SWR, &
N,P, &
EffProd,WastProd, &
EQ_COD,EQ_BODL,EQ_BOD5,COD_sum,COD_loading, Rem_COD, &
O2input,O2output,O2uptake,O2uptake_kg, &
SOTE,c1s,c1,beta,T,alpha_KK,FOTE_KK,alpha_C,FOTE_C, &
Power_KK,Power_C, &

Ci0,kb,kb_mg,Kp,Kp_mg,kLac,xsur,Hc,Hc_LL,p1,p2,n_air,R,R_dry,w,Qa, &
Qa_L,rho_air,Ci,Rem_Ci,Mass_inf,Mass_eff,Mass_was,Mass_vol,Mass_aer,Mass_sor,Mass_bio,
&
Ci_eff,Ci_was,Ci_vol,Ci_aer,Ci_sor,Ci_bio,Ci_sum, &

t0,total_time
```

```
      INTEGER nt,i


      NAMELIST/CASfparam/ &
      Q0,S0,Xa0,Xres0,EPS0,UAP0,BAPS0,BAPL0,O20, &
      qS,qD,qBAP,qUAP,YS,YP,KBAP,KS,KD,KUAP,KO,b,fd,k1,kEPS,khyd,xBAPS,kLa, &
      V,d,thetax,e, &
      Xv_eff,Xv_rec, &
      Si,Xai,Xresi,EPSi,UAPi,BAPSi,BAPLi,O2i,Qwi, &
      SOTE,c1s,c1,beta,T, &
      Ci0,kb,Kp,Hc,kLac,xsur,p1,n_air,R,R_dry, &
      ts,tdmax

      ! Start counting runtime
      t0 = SECNDS(0.0)

      ! Read input file
      OPEN(unit=1, file='CASfparam.in', status='old')
      READ(unit=1, nml=CASfparam)
      CLOSE(1)

      ! Derived parameters
      Xres0 = 0.08*S0
      ISS   = 0.05*S0

      ! Time stepping
      td    = ts / (60*60*24)    ! size of time step in days
      nt    = tdmax / td         ! total number of time steps

      ! Initialize time-dependent quantities
      S_old      = Si
      Xa_old     = Xai
      Xres_old   = Xresi
      EPS_old    = EPSi
      UAP_old    = UAPi
      BAPS_old   = BAPSi
```

226

```
BAPL_old   = BAPLi
O2_old     = O2i
Qw_old     = Qwi


!!!!!!!!!!!!!!!!!!!!!!!!!!!!!!!!!!!!!!!!!!!!!!!!!!!!!
! Do the time integration of the differential equations !
!!!!!!!!!!!!!!!!!!!!!!!!!!!!!!!!!!!!!!!!!!!!!!!!!!!!!

DO i=1,nt

rs        = qS*S_old/(KS+S_old)
BAP       = BAPS_old + BAPL_old
Xv_old    = Xa_old + Xres_old + EPS_old
Qe_old    = Q0 - Qw_old

S_new     = S_old + ( -rs*Xa_old + Q0*S0/V - Qe_old*S_old/V - Qw_old*S_old/V ) * td
Xa_new    = Xa_old + ( YS*rs*(1-k1-kEPS)*Xa_old + YP*(qUAP*UAP_old/(KUAP+UAP_old) +
            qBAP*BAP/(KBAP+BAP))*Xa_old - b*Xa_old + Q0*Xa0/V -
            Qe_old*(Xa_old*Xv_eff/Xv_old)/V - Qw_old*(Xa_old*Xv_rec/Xv_old)/V) * td
Xres_new  = Xres_old + ( b*(1-fd)*Xa_old + Q0*Xres0/V -
            Qe_old*(Xres_old*Xv_eff/Xv_old)/V - Qw_old*(Xres_old*Xv_rec/Xv_old)/V) * td
EPS_new   = EPS_old + ( kEPS*rs*Xa_old - khyd*EPS_old + Q0*EPS0/V -
            Qe_old*(EPS_old*Xv_eff/Xv_old)/V - Qw_old*(EPS_old*Xv_rec/Xv_old)/V) * td
UAP_new   = UAP_old + ( k1*rs*Xa_old - Xa_old*qUAP*UAP_old/(KUAP+UAP_old) + Q0*UAP0/V -
            Qe_old*UAP_old/V - Qw_old*UAP_old/V ) * td
BAPS_new  = BAPS_old + ( xBAPS*khyd*EPS_old - Xa_old*qBAP*BAPS_old/(KBAP+BAPS_old) +
            Q0*BAPS0/V - Qe_old*BAPS_old/V - Qw_old*BAPS_old/V ) * td
BAPL_new  = BAPL_old + ( (1-xBAPS)*khyd*EPS_old - Xa_old*qBAP*BAPL_old/(KBAP+BAPL_old) +
            Q0*BAPL0/V - Qe_old*BAPL_old/V - Qw_old*BAPL_old/V ) * td
Xv_new    = Xa_new + Xres_new + EPS_new
Qw_new    = (Xa_old*V -
            thetax*Qe_old*Xa_old*Xv_eff/Xv_old)/(thetax*Xa_old*Xv_rec/Xv_old)
Qe_new    = Q0-Qw_new

S_old     = S_new
Xa_old    = Xa_new
```

```
Xres_old = Xres_new
EPS_old  = EPS_new
UAP_old  = UAP_new
BAPS_old = BAPS_new
BAPL_old = BAPL_new
Xv_old   = Xv_new
Qw_old   = Qw_new
Qe_old   = Qe_new

ENDDO

!!!!!!!!!!!!!!!!!!!!!!!!!!!!!!!!
! Calculate final output values !
!!!!!!!!!!!!!!!!!!!!!!!!!!!!!!!!

! System Hydraulic Detention Time
thetad = V/Q0         ! days
thetah = thetad*24    ! hours

! Mixed Liquor Volatile Suspended Solids, MLVSS
Xv   = Xv_new    ! mg CODX/L
XvSS = Xv/1.42   ! mg VSS/L

! Ratio of Active to Volatile Suspended Solids
Xratio = Xa_new/Xv

! Estimation of Mixed Liquor Suspended Solids, MLSS
Xv_is   = Xv * 10/90               ! Inorganic solids of MLVSS (mg COD_X/L)
y_theta = ISS*thetax/thetad        ! Input inorganic suspended solids (mg COD_X/L)
X       = Xv + Xv_is + y_theta     ! mg COD_X/L
XSS     = X / (0.9*1.42)           ! mg SS/L
Xg      = X / (1000*1.42*0.9)      ! g SS_X/L (assuming VSS = 0.9SS)
Xkg     = Xg / 1000                ! kg SS_X/L

! Effluent and Recycle Components
Xa_eff   = Xa_new*(Xv_eff/Xv)
```

228

```
Xres_eff = Xa_new*(Xv_eff/Xv)
EPS_eff  = EPS_new*(Xv_eff/Xv)
Xa_rec   = Xa_new*(Xv_rec/Xv)
Xres_rec = Xres_new*(Xv_rec/Xv)
EPS_rec  = EPS_new*(Xv_rec/Xv)

! Solids Loss Rate
dXa_dt      = Xa_new * V/thetax        ! mg COD_X/d
dXv_dt      = Xv * V/thetax            ! mg COD_X/d
dXSS_dt     = X * V/thetax             ! mg COD_X/d
dXSS_dt_kg  = dXSS_dt / 1000000        ! kg COD_X/d
dXv_dt_biol = dXv_dt - Q0*Xres0        ! mg COD_X/d

! Sludge Wasting Rate
SWR = Qw_new*X*(Xv_rec/Xv)/1000000     ! kg COD_X/d

! Nutrient Requirements
N = dXv_dt_biol * 0.124/Q0     ! mg N/L
P = dXv_dt_biol * 0.025/Q0     ! mg P/L

! Effluent and Wasted EPS, UAP, and BAP
EffProd  = (EPS_new*Xv_eff/Xv) + UAP_new + BAPS_new + BAPL_new    ! mg COD_P/L
WastProd = (EPS_new*Xv_eff/Xv) + UAP_new + BAPS_new + BAPL_new    ! mg COD_P/L

! Effluent Quality
EQ_COD      = ISS+ S_new + Xv_eff + UAP_new + BAPS_new + BAPL_new     ! mg COD/L
EQ_BODL     = S_new + Xa_eff + UAP_new + BAPS_new + BAPL_new          ! mg BOD_L/L
EQ_BOD5     = 0.68*S_new + 0.14*(UAP_new + BAPS_new)                  ! mg BOD_5/L
COD_sum     = S0+Xa0+Xres0+EPS0+UAP0+BAPS0+BAPL0+ISS                  ! mg COD/L
COD_loading = Q0*COD_sum/(1000*V)                                    ! kg/m^3/d
Rem_COD     = (1-(EQ_COD/COD_sum))*100                               ! %

! Oxygen Supply Rate Needed
O2input     = Q0*(O20+COD_sum-ISS)                                      ! mg 02/d
O2output    = Qe_new*(S_new+Xv_eff+UAP_new+BAPS_new+BAPL_new) +
              Qw_new*(S_new+Xv_rec+UAP_new+BAPS_new+BAPL_new)    ! mg 02/d
```

229

```
O2uptake     = O2input - O2output                              ! mg O2/d
O2uptake_kg = O2uptake / 1000000                               ! kg O2/d


! Field Oxygen Transfer Efficiency
alpha_KK = EXP(-0.08788*Xg)                                    ! kg O2/kWh
FOTE_KK  = SOTE * 1.035**(T-20) * alpha_KK * (beta*c1s-c1) / 9.2 ! kg O2/kWh
alpha_C  = EXP(-0.046*Xg)                                      ! kg O2/kWh
FOTE_C   = SOTE * 1.035**(T-20) * alpha_C * (beta*c1s-c1) / 9.2  ! kg O2/kWh


! Power Required for Aeration
Power_KK = O2uptake_kg / (FOTE_KK*24)     ! kW
Power_C  = O2uptake_kg / (FOTE_C*24)      ! kW


! Pollutant Fate
Hc_LL        = Hc/(0.082054*293/1000)                          ! L water/L gas
Kp_mg        = Kp/(0.9*1000*1.42)                              ! L/mg COD_P
kb_mg        = kb/(0.9*1000*1.42)                              ! L/mg COD_P-d
p2           = ((p1*101330)+(1000*9.8*d))/101330              ! atm
w            = (29.7*n_air*e*Power_KK)/(R*T*(((p2/p1)**0.283)-1)) ! kg air/s
rho_air      = (p1*101330)/(R_dry*(T+273))                    ! kg/m^3
Qa           = (w/rho_air)*86400                              ! m^3/d
Qa_L         = Qa*1000                                        ! L/d


Ci =
       (Q0*Ci0)/(Qe_new+Qw_new+(xsur*kLac*V)+(Qa_L*Hc_LL)+(Xv_rec*Kp_mg*Qw_new+Xv_eff*Kp
       _mg*Qe_new) +(kb_mg*Xa_new*V))   !mg Ci/L


Rem_Ci       = (1-(Ci/Ci0))*100                                ! %
Mass_inf     = Q0*Ci0                                          ! mg Ci/d
Mass_eff     = Qe_new*Ci                                       ! mg Ci/d
Mass_was     = Qw_new*Ci                                       ! mg Ci/d
Mass_vol     = (kLac*xsur*V*Ci)                                ! mg Ci/d
Mass_aer     = Qa_L*Hc_LL*Ci                                   ! mg Ci/d
Mass_sor     = Xv_rec*Ci*Kp_mg*Qw_new+Xv_eff*Ci*Kp_mg*Qe_new  ! mg Ci/d
Mass_bio     = kb_mg*Xa_new*Ci*V                               ! mg Ci/d
Ci_eff       = (Mass_eff/Mass_inf)*100                         ! %
```

```
Ci_was        = (Mass_was/Mass_inf)*100                              ! %
Ci_vol        = (Mass_vol/Mass_inf)*100                              ! %
Ci_aer        = (Mass_aer/Mass_inf)*100                              ! %
Ci_sor        = (Mass_sor/Mass_inf)*100                              ! %
Ci_bio        = (Mass_bio/Mass_inf)*100                              ! %
Ci_sum        = Ci_eff+Ci_was+Ci_vol+Ci_aer+Ci_sor+Ci_bio           ! %

!!!!!!!!!!!!!!!!!!!!!!!!!!!
! Write outputs to a file !
!!!!!!!!!!!!!!!!!!!!!!!!!!!
OPEN(unit=1, file='output.txt', status='replace')
WRITE(1,*) EQ_COD
WRITE(1,*) S_new
WRITE(1,*) UAP_new
WRITE(1,*) BAPS_new + BAPL_new
WRITE(1,*) COD_loading
WRITE(1,*) Rem_COD
WRITE(1,*) Xa_new
WRITE(1,*) Xres_new
WRITE(1,*) EPS_new
WRITE(1,*) BAPL_new
WRITE(1,*) XvSS
WRITE(1,*) Xv
WRITE(1,*) XSS
WRITE(1,*) X
WRITE(1,*) Xv/X
WRITE(1,*) thetah
WRITE(1,*) SWR
WRITE(1,*) O2uptake_kg
WRITE(1,*) FOTE_KK
WRITE(1,*) alpha_KK
WRITE(1,*) Power_KK
WRITE(1,*) Power_KK/Xg
WRITE(1,*) dXSS_dt
WRITE(1,*) O2input
WRITE(1,*) O2output
```

```
WRITE(1,*) O2uptake
WRITE(1,*) Qe_new
WRITE(1,*) Qw_new
WRITE(1,*) Ci
WRITE(1,*) Rem_Ci
WRITE(1,*) Mass_inf
WRITE(1,*) Mass_eff
WRITE(1,*) Mass_was
WRITE(1,*) Mass_vol
WRITE(1,*) Mass_aer
WRITE(1,*) Mass_sor
WRITE(1,*) Mass_bio
WRITE(1,*) Ci_eff
WRITE(1,*) Ci_was
WRITE(1,*) Ci_vol
WRITE(1,*) Ci_aer
WRITE(1,*) Ci_sor
WRITE(1,*) Ci_bio
WRITE(1,*) Ci_sum
CLOSE(1)

!!!!!!!!!!!!!!!!!!!!!!!!!!!!!!!!!!!!!!!!!
! Might as well print it to the screen too !
!!!!!!!!!!!!!!!!!!!!!!!!!!!!!!!!!!!!!!!!!
PRINT*,''
PRINT*,'EQ_COD = ',EQ_COD
PRINT*,'S_new = ',S_new
PRINT*,'UAP_new = ',UAP_new
PRINT*,'BAPS_new = ',BAPS_new
PRINT*,'COD_loading = ',COD_loading
PRINT*,'(COD_sum-EQ_COD)/COD_sum = ',(COD_sum-EQ_COD)/COD_sum
PRINT*,'Xa_new = ',Xa_new
PRINT*,'Xres_new = ',Xres_new
PRINT*,'EPS_new = ',EPS_new
PRINT*,'BAPL_new = ',BAPL_new
PRINT*,'XvSS = ',XvSS
```

```
PRINT*,'Xv = ',Xv
PRINT*,'XSS = ',XSS
PRINT*,'X = ',X
PRINT*,'Xv/X = ',Xv/X
PRINT*,'SWR = ',SWR
PRINT*,'O2uptake_kg = ',O2uptake_kg
PRINT*,'FOTE_KK = ',FOTE_KK
PRINT*,'alpha_KK = ',alpha_KK
PRINT*,'Power_KK = ',Power_KK
PRINT*,'Power_KK/Xg = ',Power_KK/Xg
PRINT*,''

! Get total runtime
total_time = SECNDS(t0)
PRINT*,''
PRINT*,'Total time: ', total_time
PRINT*,''

PAUSE 'All done (press the Enter key)'

END
```

APPENDIX C

DERIVATIONS OF NANOPARTICLE FATE EQUATIONS

Definitions of Variables and Units

L: length

M_C: mass of contaminant

M_X: mass of volatile suspended solids

T: time

Q: flowrate, L^3/T

C_e: equilibrium contaminant concentration, M_C/L^3

$K_{D,L}$: linear sorption coefficient, L^3/M_X

$K_{D,NL}$: nonlinear sorption coefficient, L^3/M_X

X_V: volatile suspended solids concentration, M_X/L^3

0, e, and w as superscripts: influent, effluent, and waste streams, respectively

General Fate Mechanism Terms and Units

Advection: QC

$$\left[\frac{L^3}{T}\right]\left[\frac{M_C}{L^3}\right]=\left[\frac{M_C}{T}\right]$$
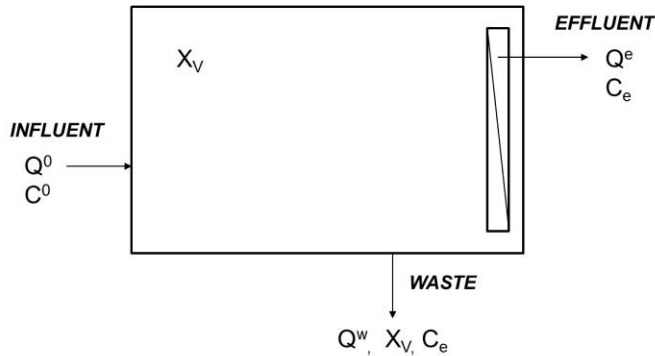
Linear Sorption: $K_{D,L}C_eX_VQ$

$$\left[\frac{L^3}{M_X}\right]\left[\frac{M_C}{L^3}\right]\left[\frac{M_X}{L^3}\right]\left[\frac{L^3}{T}\right]=\left[\frac{M_C}{T}\right]$$

Nonlinear Sorption: $K_{D,NL}C_e^{1/n}X_VQ$

$$\left[\frac{L^3}{M_X}\right]\left[\frac{M_C}{L^3}\right]^{1/n}\left[\frac{M_X}{L^3}\right]\left[\frac{L^3}{T}\right]=\left[\frac{M_C}{T}\right]$$

Fate Model Equations for a Membrane Bioreactor (MBR)

Fate with Linear Sorption

Advection: $Q^0 C_e^0 = Q^e C_e + Q^w C_e$

Sorption: $K_{D,L} C_e^0 X_V^0 Q^0 = K_{D,L} C_e X_V^e Q^e + K_{D,L} C_e X_V^w Q^w$

We assume that the volatile suspended solids (VSS) concentration entering the reactor is negligible ($X_V^0 = 0$). In addition, because solids separation is obtained by membrane separation, we assume perfect removal of VSS from the effluent ($X_V^e = 0$). Finally, because solids are wasted directly from the reactor, the concentration of VSS in the waste stream is the same as the concentration of VSS in the reactor ($X_V^w = X_V$).

With these simplifications, the linear sorption term for an MBR becomes:

$K_{D,L} C_e X_V^w Q^w$

Combining the advection and sorption terms provides a complete fate equation:

$Q^0 C_e^0 = Q^e C_e + Q^w C_e + K_{D,L} C_e X_V^w Q^w$

This equation can be rearranged to solve for C_e, since all other variables should be known:

$$Q^0 C_e^0 = (Q^e + Q^w + K_{D,L} X_V^w Q^w) C_e$$

$$C_e = \frac{Q^0 C_e^0}{Q^e + Q^w + K_{D,L} X_V^w Q^w}$$

In terms of units:

$$\left[\frac{M_C}{L^3}\right] = \frac{\left[\frac{L^3}{T}\right]\left[\frac{M_C}{L^3}\right]}{\left[\frac{L^3}{T}\right] + \left[\frac{L^3}{T}\right] + \left[\frac{L^3}{M_X}\right]\left[\frac{M_X}{L^3}\right]\left[\frac{L^3}{T}\right]}$$

Once C_e is calculated, the mass rate of contaminant (M_C/T) in the effluent stream can be determined by solving the effluent advection term ($Q^e C_e$). Likewise, the mass rate sorbed to solids can be calculated by using C_e to solve the sorption term ($K_{D,L} C_e X_V^w Q^w$).

Fate with Nonlinear Sorption

Advection: The advection terms for this case would be the same as for linear sorption.

Sorption: $K_{D,NL}(C_e^0)^{1/n} X_V^0 Q^0 = K_{D,NL} C_e^{1/n} X_V^e Q^e + K_{D,NL} C_e^{1/n} X_V^w Q^w$

With the same assumptions discussed in the linear sorption scenario for an MBR, the sorption term simplifies to:

$$K_{D,NL} C_e^{1/n} X_V^w Q^w$$

Combining the advection and sorption terms provides a complete fate equation:

$$Q^0 C_e^0 = Q^e C_e + Q^w C_e + K_{D,NL} C_e^{1/n} X_V^w Q^w$$

This equation can be rearranged to solve for C_e as follows:
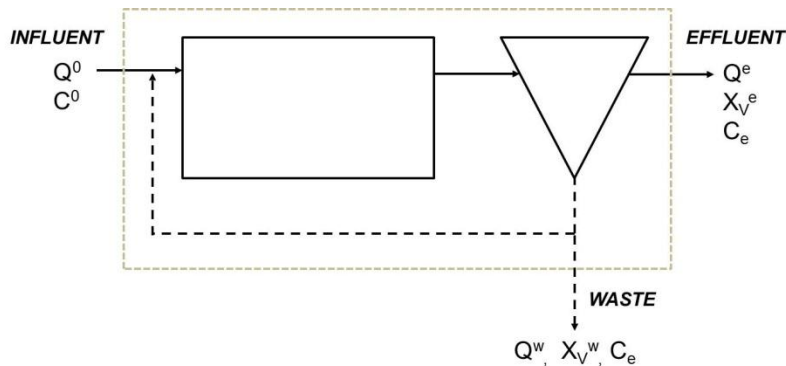
236

$$Q^0 C_e^0 = (Q^e + Q^w) C_e + (K_{D,NL} X_V^w Q^w) C_e^{1/n}$$

$$C_e = \frac{Q^0 C_e^0 - K_{D,NL} C_e^{1/n} X_V^w Q^w}{Q^e + Q^w}$$

In terms of units

$$\left[\frac{M_C}{L^3}\right] = \frac{\left[\dfrac{L^3}{T}\right]\left[\dfrac{M_C}{L^3}\right] - \left[\dfrac{L^3}{M_X}\right]\left[\dfrac{M_C}{L^3}\right]^{1/n}\left[\dfrac{M_X}{L^3}\right]\left[\dfrac{L^3}{T}\right]}{\left[\dfrac{L^3}{T}\right] + \left[\dfrac{L^3}{T}\right]}$$

Fate Model Equations for a Conventional Activated Sludge (CAS) System

Fate with Linear Sorption

Advection: $Q^0 C_e^0 = Q^e C_e + Q^w C_e$

Sorption: $K_{D,L} C_e^0 X_V^0 Q^0 = K_{D,L} C_e X_V^e Q^e + K_{D,L} C_e X_V^w Q^w$

We assume that the volatile suspended solids (VSS) concentration entering the reactor is negligible ($X_V^0 = 0$). In a CAS system, not all solids are removed from suspension in a secondary clarifier, so some solids remain in the effluent stream ($X_V^e \neq 0$). Therefore, the sorption term for a CAS system is as follows:

237

$$K_{D,L}C_eX_V{}^eQ^e + K_{D,L}C_eX_V{}^wQ^w$$

Combining the advection and sorption terms provides a complete fate equation

$$Q^0C_e^0 = Q^eC_e + Q^wC_e + K_{D,L}C_eX_V{}^eQ^e + K_{D,L}C_eX_V{}^wQ^w$$

This equation can be rearranged to solve for C_e, since all other variables should be known.

$$Q^0C_e^0 = (Q^e + Q^w + K_{D,L}X_V{}^eQ^e + K_{D,L}X_V{}^wQ^w)C_e$$

$$C_e = \frac{Q^0C_e^0}{Q^e + Q^w + K_{D,L}X_V^eQ^e + K_{D,L}X_V^wQ^w}$$

In terms of units

$$\left[\frac{M_C}{L^3}\right] = \frac{\left[\frac{L^3}{T}\right]\left[\frac{M_C}{L^3}\right]}{\left[\frac{L^3}{T}\right] + \left[\frac{L^3}{T}\right] + \left[\frac{L^3}{M_X}\right]\left[\frac{M_X}{L^3}\right]\left[\frac{L^3}{T}\right] + \left[\frac{L^3}{M_X}\right]\left[\frac{M_X}{L^3}\right]\left[\frac{L^3}{T}\right]}$$

Once C_e is calculated, the mass rate of contaminant (M_C/T) in the effluent stream can be determined by solving the effluent advection term (Q^eC_e). Likewise, the mass rate sorbed to solids can be calculated by using C_e to solve the sorption term ($K_{D,L}C_eX_V{}^eQ^e + K_{D,L}C_eX_V{}^wQ^w$).

Fate with Nonlinear Sorption

Advection: The advection terms for this case would be the same as for linear sorption.

Sorption: $K_{D,NL}(C_e^0)^{1/n}X_V^0Q^0 = K_{D,NL}C_e^{1/n}X_V{}^eQ^e + K_{D,NL}C_e^{1/n}X_V{}^wQ^w$

With the same assumptions discussed in the linear sorption scenario for a CAS system, the sorption term simplifies to

$$K_{D,NL}C_e^{1/n}X_V{}^eQ^e + K_{D,NL}C_e^{1/n}X_V{}^wQ^w$$

Combining the advection and sorption terms provides a complete fate equation

$$Q^0 C_e^0 = Q^e C_e + Q^w C_e + K_{D,NL} C_e^{1/n} X_V^e Q^e + K_{D,NL} C_e^{1/n} X_V^w Q^w$$

This equation can be rearranged to solve for C_e as follows:

$$Q^0 C_e^0 = (Q^e + Q^w) C_e + (K_{D,NL} X_V^e Q^e + K_{D,NL} X_V^w Q^w) C_e^{1/n}$$

$$C_e = \frac{Q^0 C_e^0 - K_{D,NL} C_e^{1/n} (X_V^e Q^e + X_V^w Q^w)}{Q^e + Q^w}$$

In terms of units

$$\left[\frac{M_C}{L^3}\right] = \frac{\left[\frac{L^3}{T}\right]\left[\frac{M_C}{L^3}\right] - \left[\frac{L^3}{M_X}\right]\left[\frac{M_C}{L^3}\right]^{1/n}\left(\left[\frac{M_X}{L^3}\right]\left[\frac{L^3}{T}\right] + \left[\frac{M_X}{L^3}\right]\left[\frac{L^3}{T}\right]\right)}{\left[\frac{L^3}{T}\right] + \left[\frac{L^3}{T}\right]}$$